Neurophysiology and Electrophysiology of Human and Murine Dental Pulp Stem Cells

Kylie Ellis

BSc, BPsych(Hons)

Discipline of Physiology

School of Medical Sciences

The University of Adelaide

February 2014

A thesis submitted in fulfillment of the requirements for the degree of Doctor of Philosophy

Declaration

I certify that this work contains no material which has been accepted for the award of any other degree or diploma in any university or other tertiary institution and, to the best of my knowledge and belief, contains no material previously published or written by another person, except where due reference has been made in the text. In addition, I certify that no part of this work will, in the future, be used in a submission for any other degree or diploma in any university or other tertiary institution without the prior approval of the University of Adelaide and where applicable, any partner institution responsible for the joint-award of this degree.

I give consent to this copy of my thesis, when deposited in the University Library, being made available for loan and photocopying, subject to the provisions of the Copyright Act 1968.

I also give permission for the digital version of my thesis to be made available on the web, via the University's digital research repository, the Library catalogue and also through web search engines, unless permission has been granted by the University to restrict access for a period of time.

Manuscript accepted for publication 10 February 2014:

Neuronal differentiation of murine dental pulp stem cells in vitro. Stem Cell Research & Therapy, 2014

Kylie Ellis

Date

Acknowledgements

The development and preparation of this thesis has been an extremely challenging yet highly rewarding journey. I have no doubt it would not exist were it not for the intellectual and emotional support of many people around me, some of whom I would now like to take the opportunity to thank.

Firstly to my supervisors David O'Carroll, Simon Koblar and Martin Lewis who helped me tackle an unknown world between academic disciplines with scientific eyes. Thanks also to Keiichi Torimitsu for the opportunity to work in Japan.

To my lab mates across the years, thank you for the laughs, the games and the beers. It's been great to have good friends amongst my colleagues and to count on you for your time, help and extra reagents when need be. I would particularly like to thank my friend and colleague Elizabeth Harford-Wright for keeping me sane throughout the final stages of this journey. Your record timing thesis feedback was invaluable, but insignificant compared to your general support.

My family has always been my biggest cheer squad. Thank you all for believing in me with unwavering support and understanding. I'm proud that you are all now well versed in neurophysiology terms. You must have been listening!

Finally, to my partner JR, you have kept me grounded with a sense of perspective throughout many dire days. Thanks for being wonderfully supportive and reminding me of what everyday life is about when that information was pushed out of my brain to make way for other, stem cell-related things.

Abbreviations

α-MEM	Alpha-Modified Eagles Medium
Ba^{2+}	Barium
BDNF	Brain-Derived Neurotrophic Factor
BMSC	Bone Marrow Stromal Cell
Ca^{2+}	Calcium
ChABC	Chondroitinase ABC
ChAT	Choline Acetyltransferase
Cl^-	Chlorine
CM	Conditioned Medium
CNS	Central Nervous System
CO_2	Carbon Dioxide
CSPG	Chondroitin Sulfate Proteoglycan
Cx43	Connexin 43
DAPI	4',6-diamidino-2-phenylindole
DIV	Days *in vitro*
DMEM	Dulbecco's Modified Eagles Medium
DPSC	Dental Pulp Stem Cell
ECM	Extracellular Matrix
ECoG	Electrocorticography
EEG	Electroencephalography
EM	Electron Microscopy
ER	Epigenetic Reprogramming
ESC	Embryonic Stem Cell
FBS	Fetal Bovine Serum
FES	Functional Electronic Stimulation
FGF	Fibroblast Growth Factor
GAD65/67	Glutamic Acid Decarboxylase 65/67
GAG	Glycosaminoglycan
GFAP	Glial Fibrillary Acidic Protein
H_2O_2	Hydrogen Peroxide
HAS	Hyaluronin Synthase

hDPSC	Human Dental Pulp Stem Cell
hFF	Human Foreskin Fibroblasts
IBMX	3-Isobutyl-1-methylxanthine
IHC	Immunohistochemistry
Interferon-γ	IFN-γ
ITO	Indium Tin Oxide
K^+	Potassium
MAG	Myelin Associated Glycoprotein
MCS	Multi Channel Systems
mDPSC	Murine Dental Pulp Stem Cell
MEA	Microelectrode Array
MMP	Matrix Metalloproteinase
MT	Middle Temporal Area
Na^+	Sodium
NeuN	Neuronal Nuclei
ND	Neuronal Differentiation
NDS	Normal Donkey Serum
NFM	Neurofilament-Medium Chain
NGF	Nerve Growth Factor
NM	Neuronal Maturation
NPC	Neural Progenitor Cell
NSC	Neural Stem Cell
NSPC	Neural Stem/Progenitor Cell
NT-3	Neurotrophin 3
NTT	Nippon Telephone and Telecommunications
Omgp	Oligodendrocyte Myelin Glycoprotein
PBS	Phosphate Buffered Solution
PEI	Poly(ethyleneimine)
PFA	Paraformaldehyde
PLL	Poly-l-lysine
PLO	Poly-l-ornithine
PNN	Perineuronal Net
SD	Standard Deviation
SEM	Standard Error of Noise

SHED	Stem Cells from Human Exfoliated Deciduous Teeth
SiO2	Silicon Oxide
XT-1	Xylotransferase-1
TBI	Traumatic Brain Injury
TEM	Transmission Electron Microscopy
TH	Tyrosine Hydroxylase
TiN	Titanium Nitride
Tn-R	Tenascin-R
TPA	Phorbol 12-myristate 13-acetate
TTX	Tetrodotoxin
V1	Visual Area 1 (visual cortex)
V4	Visual Area 4
V5	Visual Area 5
vGlut2	Vesicular Glutamate Transporter 2
WFA	Wisteria Floribunda Agglutinin

Table of Contents

List of Figures

List of Tables

Abstract

The cortical brain-machine interface has the potential to improve the quality of life for millions of patients with sensory or motor loss, however a range of limitations currently exist that restrict their long term clinical application. Primary amongst these is the low biocompatibility between electrodes and brain tissue. Injury to the central nervous system (CNS) causes a recruitment of inflammatory factors that lead to the long term upregulation of the perineuronal net (PNN) and the development of a glial scar that restrict recovery by forming an inhibitory peri-injury region. We propose that a biological layer of dental pulp stem cells (DPSC) will render the interface more compatible with cortical tissue to allow more efficient signal transduction and promote long-term success. I have approached this interface challenge *in vitro* to determine how DPSC may actively improve the local environment to achieve long-term biocompatibility.

Microelectrode arrays (MEAs) approximate the brain-machine interface *in vitro*. In Chapter 3 I designed and fabricated a novel MEA with design features specific to our research goals. Initial characterisation of these MEAs in comparison with commercial MEAs demonstrated high biocompatibility with cortical cultures, however electrodes had high impedance leading to a low signal-to-noise ratio that ultimately rendered the MEAs unable to detect extracellular electrical activity from the cultured cortical neurons. Future modifications including the addition of electrode polymers on these MEAs will render them more appropriate for *in vitro* use. This directed us to utilise commercial MEAs for subsequent use within the studies of this thesis.

In Chapter 4, human-derived DPSC (hDPSC) were seeded onto commercial MEAs to determine their long-term biocompatibility throughout neuronal differentiation and to assess the development of electrical activity within the developing cultures. DPSC had intrinsically low biocompatibility with MEAs, however long term culture was achieved. Stimulation-induced events were detected in long-term cultures yet no spontaneous activity was measured.

A novel source of DPSC derived from murine incisors (mDPSC) were also characterised for their neuronal potential *in vitro* in Chapter 5. mDPSC developed a neuronal morphology and high expression of neuronal and glial markers identified through immunohistochemical analysis. Differentiated mDPSC networks supported electrophysiology reminiscent of early embryonic development with high expression of L-type voltage-gated Ca^{2+} channels, gap junction proteins and gamma frequency oscillatory activity following neural induction. The ability of mDPSC to

differentiate into neural-like cells supports their future use in a murine model of autologous cell transplantation.

The impact of DPSC on the endogenous inhibition of the brain was also investigated in Chapter 6. It was hypothesised that co-culturing DPSC with dissociated cortical neurons would downregulate the expression of the restrictive PNN around neurons. It was demonstrated that hDPSC co-culture reduced the proportion of neurons that expressed PNN in a time and dose-dependent manner. Moreover, hDPSC conditioned medium also decreased the proportion of PNN-expressing neurons, suggesting that paracrine factors released by the cells may be responsible for this effect.

In conclusion, the present studies have identified a novel ability for DPSC to reduce cortical PNN expression that could improve the long-term efficacy of a brain-machine interface. However, biocompatibility of DPSC with *in vitro* MEAs is low and requires modification to achieve a successful interaction at the interface. Moreover, the neuronal potential of DPSC isolated from murine incisors has been demonstrated for the first time. The multifaceted characteristics of DPSC may present a viable approach to cell-based therapeutics for a range of CNS disorders.

Chapter 1: Introduction

Introduction

Recovery following neurological injury is often limited with traditional treatments such as drugs or physical therapy. There are two major arms of research for alternative therapies aimed at enhancing recovery following damage to the brain. The first is a 'scaffold' approach where biological elements are employed in an effort to stimulate the brain to self-repair through the initiation of localised areas of plasticity. The second approach involves the use of neuroengineered devices to interface with the brain. These can either provide stimulation to areas that have lost natural peripheral input, or be applied to motor centres, where they can monitor neural activity to control external devices such as a computer cursor or prosthetic limb.

Although these two areas of research are seemingly unrelated, their combination could augment traditional drug and physical therapies, as well as enhance the success of either approach alone. On the one hand, a brain-machine interface incurs some inevitable issues of biocompatibility that could be improved through the use of biological scaffold factors, creating a more stable and efficacious interface. On the other, a neuroengineered device could help to direct the establishment of new neural connections induced by the scaffolding molecules. This thesis aims to link these apparently disparate approaches to brain repair by addressing 1) issues of biocompatibility of brain-machine interfaces, and 2) working toward the development of a murine model of autologous stem cell transplantation and considering how stem cells may impact the brain to render an environment more permissive to plastic change and therefore recovery.

1.1 The brain-machine interface

The development of a brain-machine interface suitable for clinical translation has the potential to help the millions of people worldwide that have suffered sensory or motor system damage. The concept of an indirect bridge between the periphery and brain bypasses the need for direct nerve rehabilitation, which has proven to be an extremely challenging goal (Ruff, et al., 2008). There are two potential modes by which brain-machine interfaces can function; 1) to insert electrical signals into the brain and stimulate it directly or 2) to extract information via recording electrodes:

Brain stimulation: This application itself has two alternative aims:

(i) to restore sensory perception by stimulating areas of the brain that no longer receive peripheral information, such as visual or auditory systems damaged by degenerative disease or stroke;

(ii) alternatively, deep brain stimulation can potentially regulate the electrical activity of specific regions of the brain to treat a range of drug-resistant disorders such as tremor and chronic pain.

Brain recording: This approach is primarily aimed at interpreting motor commands from the brain for the control of an external device, be it a computer cursor or prosthetic limb, for patients with a large variety of pathologies.

Both primary applications have achieved encouraging success in experimental animal models and human clinical studies (Chadwick, et al., 2011; Hochberg, et al., 2012; Hochberg, et al., 2006; Serruya, et al., 2002; Simeral, et al., 2011; D. M. Taylor, et al., 2002). However, numerous challenges remain in taking these to a clinically viable product. Among these, issues of implant design and longevity are paramount, relying on a stable and efficient interface between electrode and neuron (Polikov, et al., 2005; Schouenborg, 2011).

The basis of the brain machine interface lies in the implantation of an electrode device that can inject current or record electrical activity from local neuronal populations, creating a direct communication pathway between the brain and an external device or peripheral system. The emergence of this field is a result of the limitations in nerve regeneration after injury, advances in brain mapping, as well as the development of new technologies, creating electrodes of a biologically relevant size to develop enhanced bio-compatibility of these devices (Kipke, et al., 2008; Ruff, et al., 2008; Schouenborg, 2011).

The efficacy of the interface depends primarily on the proximity of an electrode and its target neuron population, which is affected by both the distance and the tissue composition between them (Jackson & Zimmermann, 2012). This is important as there is a natural host tissue response to the implantation of foreign objects that can cause long term alterations in tissue composition such as glial scar formation, that can impede effective signal transmission between the electrode and neurons (Zimmermann & Dours-Zimmermann, 2008). As such, biocompatibility of the electrode implants is arguably the most important limitation to overcome to achieve a successful long-term brain machine interface. Within this introduction, the current state of cortical prosthesis

advancement will be discussed as well as the leading approaches proposed to enhance the efficacy of neuron-electrode interfaces for medical translation. As an illustration of the basic problems, I will first provide a brief overview of the state of cortical visual and motor prostheses, focusing on the important issues of biocompatibility and the interface modifications available to enhance the long-term efficacy of such implants. Visual and motor prostheses present ideal systems to discuss the advancement and challenge of signal transfer interfacing with the cortex in both directions. Both applications have received considerable research effort to address their challenges and are developing a promising future with cortical prosthetics.

1.1.1 Visual prosthesis

1.1.1.1 The human visual system

For effective prosthesis design, it is crucial to understand how natural vision operates in healthy individuals and in those with varying degrees of vision impairment. Vision is a complex hierarchical system that involves signal processing at multiple layers. Briefly, in normal vision, environmental light is focused by the cornea and lens to form an image onto the retina, a sensory layer at the back of the eye (Cohen, 2007). Light-sensitive photoreceptors synapse onto bipolar cells located at the inner retina, which in turn synaptically release glutamate that stimulate ganglion cells at the inner retina. Axons of ganglion cells then exit the eye at the optic disc and transmit action potentials to the cortical visual areas via the optic nerve. The first cortical relay point is at the lateral geniculate nucleus of the thalamus before signals are propagated to the primary visual cortex (V1) and visual association areas. At the level of the retina, individual photoreceptors respond to light information at a particular spatial region, creating a retinotopic map of space which is relayed with high fidelity to cortical area V1. However, the cortex is privileged in that it is also highly organised by visual submodality. Regions of the cortex receive input relating to left or right-eye information, stimulus orientation, direction of motion and also by colour, specific characteristics that have the potential to be utilised by a cortical-based prosthesis (Cohen, 2007).

Visual impairment results from the loss of connectivity at any point along this system and numerous incarnations of visual prostheses have been developed to target the visual system at each level of processing. These have included multiple retinal prosthesis designs, stimulation electrodes for the optic nerve as well as cortical prostheses to target the occipital lobe (V1 and association areas) and the lateral geniculate nucleus of the thalamus (Dobelle, 2000; Dorn, et al.,

2013; Panetsos, et al., 2011; Sun, et al., 2011). Each approaches has its own advantages and disadvantages with respect to treatment of different forms of visual impairment and blindness.

1.1.1.2 Suitable Patients for visual prostheses

Blindness is widely regarded as one of the most devastating of human afflictions. The visual prosthesis available to patients is determined by the level of impairment within the hierarchy of visual processing. Perhaps the best-known approach to artificial vision is the retinal implant, variants of which have been developed worldwide as well as in Australia. The aim of retinal implants is to replace degenerative photoreceptors with a miniature artificial camera coupled to a micro-electrode array (MEA) of stimulating electrodes to interface with intact retinal ganglion cells and thus elicit perception of flashes of light ('phosphenes'). This strategy relies on partial preservation of retinal ganglion cell function, and is therefore targeted at diseases of the eye, particularly retinitis pigmentosa, which involves the progressive degeneration of photoreceptors that cause the loss of vision in no clear spatial pattern and can cause complete vision loss. They have also been proposed for the most common cause of legal blindness in Australia - age-related macular degeneration, which involves the loss of central vision by degeneration of the macula, the area that provides the most detailed central vision (Margalit & Sadda, 2003). However, it is unusual for macular degeneration to lead to complete blindness in patients. It is most likely that sufferers will have difficulty reading or recognising faces but will retain enough peripheral vision to carry out everyday tasks. As such, only late stage sufferers of this disease should qualify for visual prostheses due to the low quality of vision currently provided by the devices (McGie, et al., 2013).

Common blinding diseases, such as glaucoma or diabetic retinopathy, affect other retinal cell types and/or the optic nerve, making the retinal implant unsuitable in any form. Glaucoma is the leading cause of irreversible blindness world-wide, affecting between 1 in 360 and 1 in 1000 individuals (Taylor, et al., 2005) and is caused by a chronic degeneration of the retinal ganglion cells (Glovinsky, et al., 1991) and often leads to complete blindness. Glaucoma is mainly an age-related disease, but is also a frequent cause of childhood blindness. Diabetic retinopathy is the commonest cause of blindness in the working age population, and due to the nature of the pathology, a retinal implant would not be suitable. Most forms of blinding disease in childhood also lead to optic nerve degeneration and thus require a different strategy. Finally, retinal implants are totally unsuitable for treatment of blindness in accidents involving loss of an eye or in

neurological diseases where the problem is not with the eye itself, but damage to the visual pathways of the brain. For example, 50,000 Australians suffer strokes each year, the most frequent form of which (ischemic stroke) damages parts of the primary visual cortex (Islam, et al., 2008). Therefore, the only option currently under investigation for these patients is a prosthesis targeting the visual cortex (Margalit & Sadda, 2003). Even after long-term optic nerve damage, cortical representations for vision remain intact and we can simulate natural sensory information for artificial electrical stimulation at these regions to elicit basic visual perception.

1.1.1.3 Cortical visual prosthesis

A visual prosthesis consists of a camera component that can recognise forms of visual information and relay it to implanted electrodes through a series of electrical stimulation patterns at visual centres of the brain (Figure 1). The patient will learn to interpret those patterns as meaningful visual information. Ideally, signal transfer will be achieved wirelessly to reduce the risk of infection from wires projecting from the skull. Additionally, the system will be lightweight and portable and make use of many stimulating electrodes with high spatial resolution.

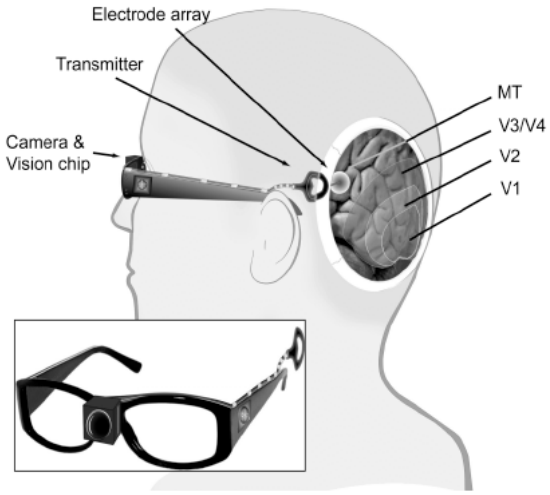

Figure 1.1: Diagram of a cortical visual prosthesis.

A cortical visual prosthesis consists of a camera component most commonly attached to glasses that can transmit signals about the environment to an electrode array positioned at the visual centres of the brain. Patterns of stimulation could potentially encode different information at the level of the cortex, either at a low level (e.g. V1, visual area 1) or at higher orders centres such as the motion-sensitive area MT or pattern-sensitive areas such as the inferotemporal cortex (V4).

There are numerous advantages of targeting the cortex to provide visual input. The cortex is the highest order of processing and has an enlarged area of retinotopic representation that is conceivably easier to target with microstimulation than the retina itself (Cohen, 2007). However, a portion of the central visual field lies in the calcarine sulcus, which is therefore not directly accessible by current surgical techniques (Stensaas, et al., 1974). This area corresponds to the lateral visual fields, which is important for navigation. However, information necessary for navigation could be provided by the stimulation of visual areas distinct from V1, such as the middle temporal area (MT, or V5) that plays a major role in motion perception (Salzman, et al., 1990; C. D. Salzman, et al., 1992). For blind patients, it may be more valuable to gain a sense of these environmental characteristics to aid their negotiation of space and independent living rather than focusing on the fine detail of central vision that the majority of visual prostheses target. Likewise, diseases such as glaucoma that spare central form vision but lose peripheral motion cues could also benefit from such an approach. Research has indeed shown that low amplitude microstimulation of area MT in monkeys affected their direction discrimination. Stimulation of MT neural populations particular to one direction could overcome visual presentation of motion in the opposite direction (Salzman, et al., 1990; C. D. Salzman, et al., 1992) and in another study, could influence their decisions about their own direction of movement (Britten & Van Wezel, 1998). This effect was negatively influenced by increased current amplitude or small changes in electrode amplitude indicating that the directional bias effect is dependent upon the direct activation of a highly localised population of neurons (Salzman, et al., 1992). Nonetheless, simultaneous stimulation of multiple visual zones would be an ideal application for any visual prosthesis.

A number of successful studies have demonstrated that stimulation of the visual cortex can elicit the perception of visual information in human and animals (Bak, et al., 1990; Bradley, et al., 2005; Brindley, 1982; Dobelle, 2000; Dobelle & Mladejovsky, 1974; Schmidt, et al., 1996). These studies were performed using two types of electrodes: surface electrodes and intracortical penetrating electrodes. Each has advantages and disadvantages that illustrate the complexity of the interface challenge.

Surface electrodes

Surface electrode arrays are the least invasive form of cortical implant as they are implanted subdurally to stimulate local neurons without causing physical damage to the brain tissue (Figure 1.2). Early incarnations were employed in breakthrough studies that used 80 large platinum

electrodes that were placed over the pia at the visual cortex and demonstrated that electrical stimulation could elicit the perception of localised flashes of light, or phosphenes, across the patient's visual field (Brindley & Lewin, 1968). It was demonstrated that there was a visuotopic organisation of the visual cortex that varied somewhat between individuals (Brindley & Lewin, 1968; Dobelle, et al., 1979). Later, in brave but ethically contentious work, Dobelle and colleagues (Dobelle, 2000; Kotler, 2002) used a camera mounted to a pair of glasses for visual input. Four blind patients were initially implanted with 64 stimulating electrodes at their visual cortex (Dobelle, et al., 1976; Dobelle, et al., 1979). They described 'seeing' phosphenes at arms length that, even though at basic and slow frame rates, allowed them to negotiate a room and to recognise large lettering. Subjects were implanted for over 20 years during which regular stimulation was applied without infection or other problems (Dobelle, 2000). However, not all results were consistent. Another patient implanted at age 62 who had lost his sight when 5 years old never observed a phosphene over his 20 year implant period. Dobelle hypothesised that even though phosphenes had previously been generated in individuals with long term blindness, the visual prosthesis would produce better results if an individual was previously sighted and that there was a minimal time period between the onset of blindness and cortical stimulation (Dobelle, et al., 1979).

There are two major limitations of cortical surface stimulation for visual prostheses. The first is the increased distance between the electrode and target neurons that lie at inner layers of the cortex. This greater distance increases the degree of charge spread throughout the extracellular space and therefore necessitates a higher stimulation current to affect these cells, which further compounds issues such as heat damage (McCreery & Agnew, 1990). In addition, the resolution of surface electrode stimulation is relatively low, with a two-point discrimination of electrodes at 2-3mm (Dobelle & Mladejovsky, 1974). It is generally accepted that high resolution stimulation is more favourable for producing high resolution image percepts, just as a low resolution computer screen provides much less information to its viewer. However, the columnar organisation of the cortex may allow the effective use of lower resolution stimulation by activating populations of neurons involved with a given task (Albright, et al., 1984; Gilbert & Wiesel, 1989). This population-based stimulation may also be more resistant to signal loss with time as it does not rely on the precise interface between an electrode and neuron that could degenerate. While research using cortical surface stimulation has showed great promise, its progress has halted with the passing of Dobelle and its potential efficacy with more modern processing systems remains unknown.

Intracortical penetrating electrodes

As an alternative to the cortical surface prosthesis, intracortical electrodes were developed, which consist of long, thin needle-like microelectrodes that are physically inserted into the cortical tissue (see Figure 1.2). The advantage of the intracortical stimulation paradigm is that it requires significantly lower stimulus currents to evoke phosphenes (10-20 μA) compared to surface electrodes (1-5 mA) (Cohen, 2007; Dobelle & Mladejovsky, 1974; Tehovnik, 1996). Also, electrodes are typically much smaller and, in theory, can achieve more selective stimulation of smaller populations of neurons down to single cells. To date, few experiments using intracortical stimulation of the visual system have been performed (Bak, et al., 1990; Bradley, et al., 2005; Schmidt, et al., 1996; Shakhnovich, et al., 1982). Of these, one 42 year old blind patient underwent chronic implantation of 38 electrodes for four months at their visual cortex (Schmidt, et al., 1996). It was reported that the patient perceived smaller percepts than that resulting from surface electrodes and that stable stimulation was continued over the implantation period. Another study identified that an inter-electrode spacing of at least 500 μm is required to discriminate two distinct phosphenes (Bak, et al., 1990). However, as a limitation to the long term efficacy of these electrodes, the physical penetration of the cortex can cause injury to the delicate brain tissue that may cause bleeds and possibly seizures (Normann, et al., 1999). Penetrating electrodes may also incur the limitation of a chronic bodily response that will be discussed in more detail below.

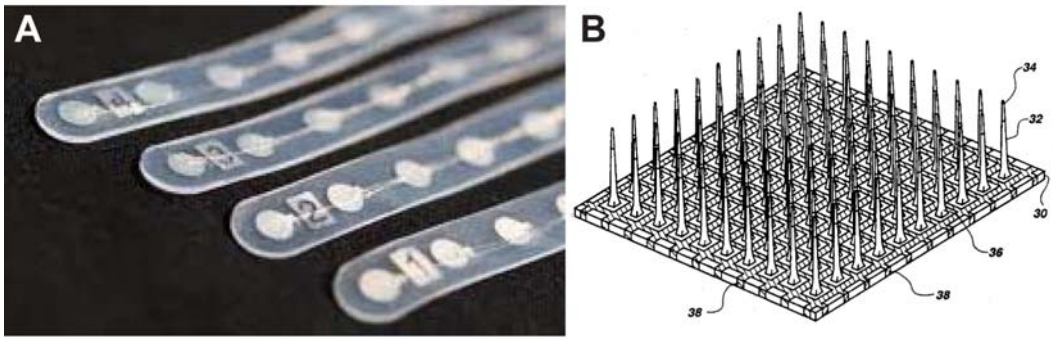

Figure 1.2: A comparison of surface and penetrating electrodes.

A) Example of commercial surface electrodes for cortical implantation (AD-Tech) and B) Schematic diagram of the penetrating Utah array with penetrating electrodes 1.5 mm long (Normann, 1993. Patent 5215088).

Together, these studies illustrate the potential for cortical visual prostheses and identify a trade-off between invasiveness and resolution that will be discussed in more detail below. This electrode balance is not unique to visual prosthetic devices. It is also intrinsic to the second major approach of brain-machine interfaces – that of extracting neural activity patterns, predominantly from the motor cortex, to control the motion of prosthetic devices. Much research has also focused on developing an efficient interface with long term stability for clinical applications. The physiology of the motor system and advances toward a motor prosthesis will be discussed below.

1.1.2 The motor system

The human motor system sends signals that originate at the motor cortex, via the spinal cord to the peripheral muscles to control voluntary movement. Spinal cord injury interrupts the transmission of this signal so that individuals lose voluntary control of their muscles. This can be the result of numerous pathologies, including brain stem stroke, spinal cord injury or the progression of motor neurone disease. There are 2-3 million spinal cord injured individuals worldwide (Wyndaele & Wyndaele, 2006) and for those patients, regaining limb function is a high priority (Anderson, 2004). While there is some hope for the regeneration of spinal tracts with pharmacological manipulation and stem cell treatment, there has also been a strong research focus on using the patient's intact motor cortex to control external devices that may improve their quality of life.

1.1.2.1 Cortical motor prosthesis

A motor prosthesis consists of an electrode array implanted onto the primary motor cortex that detects local field potentials of neuronal populations. These signals are processed in real time to control an external device, often a computer cursor or a prosthetic limb that is distinct from the body. Considerable effort has been invested in demonstrating successful 'mind control' from non-human primates and humans (Carmena, et al., 2003; Donoghue, et al., 2007; Hochberg, et al., 2012; Hochberg, et al., 2006; Jackson & Zimmermann, 2012; Simeral, et al., 2011; Taylor, et al., 2002; Velliste, et al., 2008). Likewise with the visual prosthesis models described previously, there are invasive and non-invasive methods of implementing motor prostheses.

Penetrating electrodes

The majority of animal and human implantation studies have used penetrating electrodes to extract signals from the motor cortex (Hochberg, et al., 2012; Simeral, et al., 2011; Suner, et al., 2005). Like that for visual prostheses, the implants consist of multiple (16-96) long, thin microelectrodes that insert approximately 1.5 mm into the brain parenchyma with the understanding that high spatial resolution is desirable for detecting more precise motor commands (Leuthardt, et al., 2006).

One leading system for motor prostheses is BrainGate, which uses arrays of 96-electrodes to the upper limb representation of the primary motor cortex. This system gained success in allowing an implanted monkey to control a prosthetic arm for grasping and feeding using only its thoughts, and has encouraged the progression to human trials (Zhuang, et al., 2010). The first human tetraplegic patient to receive the BrainGate motor prosthesis was able to operate a two-dimensional computer cursor as well as control the grasping movements of a hand prosthesis (Hochberg, et al., 2006). Subsequent patients who had suffered a brainstem stroke further achieved three-dimensional reaching and grabbing using a prosthetic arm, and one of these patients even learned to control a bottle to drink from with a straw (Hochberg, et al., 2012). Importantly, this prosthesis was implanted in the patient for five years without adverse events. Still, biocompatibility of these invasive implants remains a key issue for their long term success (Ward, et al., 2009).

Non-invasive motor prostheses

Non-invasive techniques are also being developed for recording cortical motor signals such as electroencephalography (EEG) and electrocorticography (ECoG) (Figure 1.3) (Schouenborg, 2011). EEG electrodes sit on the outside of a patient's head and receive low resolution information from motor and other cortical regions. With training, patients can learn to control three-dimensional movement of a computer cursor (McFarland, et al., 2010) and this technique has the potential to assist paralysed patients to control robotic prostheses (Onose, et al., 2012).

Alternatively, ECoG has emerged as a reasonable balance between spatiotemporal resolution, invasiveness and signal stability. ECoG makes use of subdural or epidural electrode grids that record local field potentials at a reasonably high resolution without penetration of the brain.

Numerous human studies with healthy and paralysed individuals have demonstrated their high efficacy for allowing the control of one-, two- and three-dimensional computer cursor movement after only a short learning period and without adverse effects (Leuthardt, et al., 2004; Schalk, et al., 2008; W. Wang, et al., 2013). These studies have been limited to short implantation durations with a maximum of 28 days of recording, however primate studies suggest that signals could be stable for many months (Chao, et al., 2010).

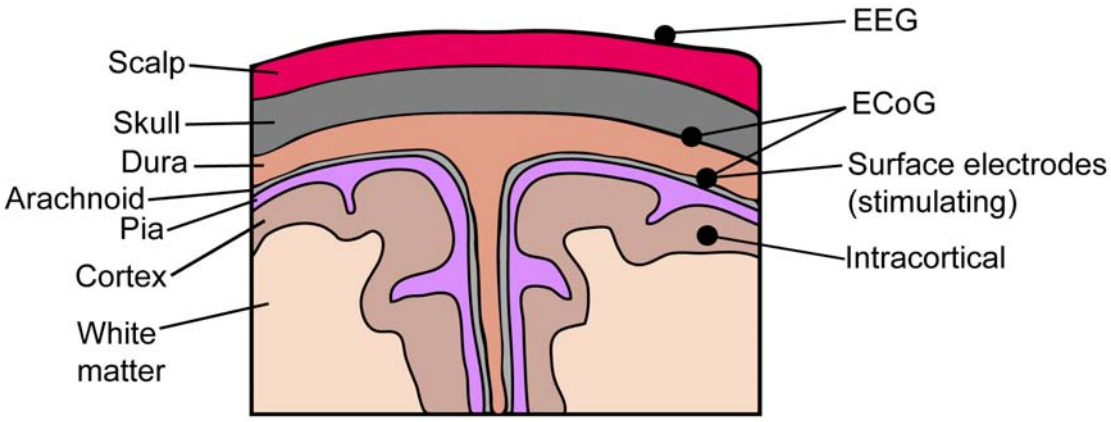

Figure 1.3: Potential sites for prosthesis localisation.

Diagram of the layers of the brain and possible sites for prosthesis implantation. Non-invasive electroencephalography (EEG) records signals from outside of the scalp. Minimally invasive electrocorticography (ECoG) records from planar electrodes at subdural or epidural regions above the motor cortex. Planar surface electrodes stimulate visual cortex and association areas from a subdural position. Intracortical electrodes can stimulate or record electrical activity from within the cortex.

Functional electrical stimulation

A concurrent goal of motor prostheses is to allow spinal cord injured patients to indirectly control their own muscles using brain signals alone. Functional electrical stimulation (FES) involves the stimulation of muscular contractions by electrical activation of motor nerves via surface or implanted electrodes. It is proposed that the benefits of FES on muscle function are maximised when stimulation is coupled with intentional control mechanisms, such as the *thought* to move. Indeed, recent studies have demonstrated the potential of brain-controlled FES to restore wrist movement following temporary peripheral nerve block in monkeys (Moritz, et al., 2008; Pohlmeyer, et al., 2009) and later for voluntary grasping movements (Ethier, et al., 2012). The feasibility of using this system in injured humans has also been tested using a simulated FES

controller (Chadwick, et al., 2011). Notably, the control of FES systems has also been demonstrated using EEG-based methods (Daly, et al., 2009; Muller-Putz, et al., 2005; Pfurtscheller, et al., 2003). The ultimate aim of motor prostheses is to integrate a closed loop system where an individual can control an external device or FES-like system and receive feedback to guide their subsequent responses.

1.2 Functional limitations of the brain machine interface

As mentioned previously, there are functional limitations of an electrode interface with the brain. Biocompatibility is arguably the most influential long term challenge to overcome at the interface, regardless of the type of electrode array used. Other considerations at the interface include infection, heat damage (from the passage of electrical currents) and mechanical stability that all affect the long term efficacy of cortical prostheses. The relative importance of these limitations differs for each prosthesis approach and must be balanced against the signal quality arising from the interface. For example, EEG electrodes do not penetrate the skull and therefore pose little risk of infection and inflammation, however their electrical specificity is low due to the large distance between electrodes and neurons, leading to charge dissipation with a larger population of neurons being involved with the interface. On the other hand, subdural non-penetrating electrodes have increased specificity than EEG but there remains a considerable distance between electrodes and target neurons. For signal input prostheses this necessitates large stimulation currents that can lead to heat damage (McCreery & Agnew, 1990). Additionally, as they are implanted, these electrodes also pose a risk of infection and inflammation. Finally, penetrating electrodes provide the greatest specificity due to close neuronal proximity that reduces the required currents for stimulation and associated heat damage, however they also pose the greatest risk of infection and inflammation (Ward, et al., 2009). Common to all interfaces is the challenge of maintaining long-term mechanical stability and biocompatibility such that neuron-electrode coupling is durable and learned electrical patterns can be sustained clinically.

Biocompatibility of the interface

Electrode implantation inevitably causes a foreign body response from the host, the degree of which depends on the level of electrode invasiveness. The injury associated with insertion of an electrode incites a foreign body response from the host, developing an acute and a chronic inflammatory reaction (Grill, et al., 2009). The acute response to CNS injury is mediated by

activated astrocytes, microglia and extracellular matrix (ECM) components, which have been shown to migrate to the area around the electrode interface. Microglia firstly secrete reactive oxygen species and inflammatory cytokines capable of damage to neurons and also mediate the chronic phase of CNS inflammatory responses. Over time, nearby astrocytes also become activated and form a surrounding sheath over the electrode. This 'glial scar' develops over numerous weeks, becoming thinner but denser and can attach to neural implants more strongly over time (McConnell, et al., 2007; Polikov, et al., 2005; Ward, et al., 2009). As such, there is a developing physical barrier, with high electrical impedance reducing efficient transmission of electrical current between the electrode and cortical tissue. Furthermore, concurrent with the formation of the glial scar, neuronal density within the recording radius of the microelectrodes is reduced (Biran, et al., 2005). The high impedance of the glial scar is inhibitory for neurons, which therefore preferentially extend their neurites away from the electrodes, therefore limiting the direct contact of neuronal elements with the stimulating electrodes (Biran, et al., 2005; R. J. Gilbert, et al., 2005; Szarowski, et al., 2003). The combination of inflammatory scarring and loss of neurons at the electrode interface thus results in a reduction of the high resolution advantages the penetrating electrodes intrinsically provide.

1.2.1 Material modifications of the brain machine interface to improve biocompatibility

Management of the neuron-electrode interface is critical for long term implantation stability. Efforts to minimise the host inflammatory response and promote neuronal survival have utilised numerous methods, including modification of the electrode size and material and using substrate or biological coatings to enhance electrode biocompatibility (Azemi, et al., 2011; Grill, et al., 2009; Purcell, et al., 2009). The bulk of this effort has concentrated on minimising the negative impact of penetrating electrodes on the brain. Less work has focused on modifying the interface of non-penetrating electrodes to make them more efficient and viable so improvement of the surface electrode interface remains a strategy to be addressed.

Electrode modification

Optimisation of electrode material and size has been the focus of much research effort over recent years. The brain naturally moves 10-30 μm as a result of respiration and head movements (Gilletti & Muthuswamy, 2006), which must be accommodated by the electrodes that interface

with it. Penetrating electrodes are routinely made of silicon, the stiffness of which is often cited as a major cause of excessive damage to the cortical tissue (Lee, et al., 2004). Alternative neural electrode materials with greater flexibility, such as polymers like polyimides and parylene, have been proposed and developed to combat this issue (Lee, et al., 2004; Lee, et al., 2004; Takeuchi, et al., 2005). Carbon nanotube electrodes have also been fabricated and have shown early signs of high biocompatibility, making them an interesting avenue for future implant technologies (Li, et al., 2002; Whitten, et al., 2007).

Similarly, electrode size has been modified in an attempt to reduce the host inflammatory response following implantation, with mixed results. Silicon probes with smaller diameter showed an attenuated glial response in the acute stage of implantation. However the chronic encapsulation of the electrode was analogous to that seen with larger electrodes (Szarowski, et al., 2003). Nonetheless, there are limits to electrode material and size modification as their mechanical stability upon implantation and over longer durations of use must be reliable.

Electrode coating substrates

It is conceivable that surface coatings on electrodes could also modify the local microenvironment in the CNS to improve biocompatibility. Numerous types of surface modifications and their impact on the host inflammatory response following implantation of penetrating probes have been investigated. Anti-inflammatory agents have produced an expected reduction in the host response to electrode implantation. Dexamethasone coating on neural electrodes attenuated the microglial, extracellular matrix, and astrocyte reactivity response at one and four weeks post implantation, as well an increasing neuronal survival compared with uncoated probes (Zhong & Bellamkonda, 2007). Electrode coating with another anti-inflammatory agent, alpha-melanocyte stimulating hormone, also reduced microglial and astrocyte immunoreactivity following insertion into the motor cortex of rats (He, et al., 2007). Attenuation of the glial scar will reduce the impedance of an electrode, lowering the current required to stimulate local neurons and the subsequent risk of heat damage in a signal input interface or increase the electrode sensitivity for a signal extraction device.

The presence of a neural adhesion substrate on electrodes can also enhance their biocompatibility upon implantation. Surface immobilisation of L1, a natural molecule from the CNS that promotes neuronal survival and neurite outgrowth, onto neural probes was protective

toward neuronal survival in the immediate vicinity around the implant with no decrease in neural density found compared to healthy tissue. In addition, there was a significantly lower microglial and astrocytic activation measured at 1, 4 and 8 weeks post implantation (Azemi, et al., 2011). Likewise, nanoscale laminin coating of a cortical electrode resulted in an acute increase in microglial immunoreactivity, but a decrease in microglial and astrocyte immunoreactivity compared to untreated electrodes at 4-weeks post implantation, indicating an attenuated glial response (He, et al., 2006). It is proposed that these natural coating substrates may actively promote neurite migration toward the electrode while creating a more biological surface that disguises the foreign implant material.

Cultured probes

Cell-based modifications of electrodes have also been proposed to create a more biological surface to interface with the brain. A cultured probe is a planar electrode array with local populations of neurons cultured over each electrode, which act as intermediates between electrodes and the brain (Rutten, et al., 2001; Rutten, et al., 2003). The concept of the cultured probe is based on the cultured neurons promoting neurite extension from brain, which would in turn allow for a more selective and biocompatible neuron-electrode interface. This system has been developed for use at the retinal interface that more commonly uses planar electrodes but could also be developed to improve the cortical brain machine interface. While its efficacy has not yet been demonstrated in an *in vivo* implantation model it is an interesting avenue for creating a biological interface layer that directly interacts with the brain, particularly for planar electrode prostheses.

Long term efficacy of interface modifications

The proposed interface modifications are likely to have a finite period of action as the biological-based materials inevitably degrade upon implantation *in vivo*. As seen in the studies above, however, it is likely that the modification of the acute inflammatory response may be sufficient to create a more permissive environment for neurons to interact with the implanted electrodes. Long-term modifications may be desirable but not necessary for a successful interface.

1.3 Neuroplasticity

Neuroplasticity is an important element in the successful implementation of neuroprostheses. It has repeatedly been reported that individuals receiving cortical prostheses must undergo a learning phase in order to successfully control an external device in the case of motor prostheses, or to make use of stimulated percepts generated from visual prostheses (Carmena, et al., 2003; Dobelle, 2000; Dobelle & Mladejovsky, 1974; Ganguly, et al., 2011; Taylor, et al., 2002). Learning to use the device can take a variable amount of time and effort between patients and is testament to the brain's intrinsic ability to adapt.

The extent of the brain's ability for neuroplastic change is demonstrated by classic studies of cross-modal sensory substitution, whereby tactile stimulation at various points of the body is perceived as visual information by blind patients (Bach-y-Rita, 2004; Bach-Y-Rita, et al., 1969). Stimulation patterns were applied via vibro- or electro-tactile arrays to the back, thigh, abdomen, fingers, forehead or tongue with sufficient resolution to enable patients to make perceptual judgments such as depth, speed and direction as well as facial recognition, space negotiation and even the ability to bat a rolling ball (Bach-y-Rita, 2004; Bach-Y-Rita, et al., 1969; Bach-y-Rita, et al., 1969; Collins & Bach-y-Rita, 1973; Kaczmarek, et al., 1991; White, et al., 1970). These studies are testament to the brain's intrinsic ability to adapt to limited sensory information available and integrate it into functional, real-world interactions.

It is widely accepted that our capacity for neuroplastic change degreases with age (Colombo, 1982; Hensch, 2005). Accordingly, it is recommended that neuroprostheses would have the most significant benefit for younger individuals who were previously sighted and had lost their vision, hearing or voluntary motor control only recently prior to implantation. Indeed, this has been evidenced in patients with cochlear implants. The cochlear implant stimulates lower order spiral ganglion cells at 22 points across the tonographically organised cochlea, which transmit auditory information to its cortical processing area (Wilson & Dorman, 2008). While adults are able to perceive a broad range of auditory information, including speech and music, the perceptions of children implanted with the auditory prosthesis are far superior (Sharma, et al., 2005; Wilson & Dorman, 2008). This is likely due to the learned component of sensory processing that is achieved throughout childhood. With the maturation of the CNS extracellular matrix (ECM), networks within many areas of the brain become more rigid and resistant to change. Furthermore, following injury such as that sustained with the implantation of electrodes, there is

an upregulation of inhibitory factors within the ECM that impede axon growth and new synaptic connections. Key axon growth inhibitors have been identified and numerous studies have demonstrated how their manipulation can help to reinstate anatomical plasticity and functional recovery following injury (Bradbury, et al., 2002; Caroni & Schwab, 1988; Chen, et al., 2000; Galtrey, et al., 2007; Jones, et al., 2003).

1.3.1 The ECM in the healthy adult CNS

To understand how to modify the adult CNS and enhance the potential for plasticity a greater understanding of the mechanisms in the healthy brain is required. The following section will discuss the role of the ECM in the healthy and damaged adult CNS as well as current methods to reduce its endogenous inhibition.

The ECM is a network of macromolecules that encompasses the extracellular space throughout the CNS and is involved in the development of the stable and mature brain. As well as providing structure and stability to the CNS, components of the ECM can also become inhibitory to neuroplasticity after injury, making it a prime target for interventional therapeutics to enhance recovery. Numerous of these ECM components and approaches to combat them in the injured brain will be discussed throughout this chapter.

The mature ECM network is organised around the linear polysaccharide, hyaluronan, which binds proteoglycans and forms an organisational scaffold to which other ECM molecules and cells bind. Proteoglycans are complex macromolecules found throughout different tissue types in the body. In the CNS, chondroitin sulfate proteoglycans (CSPG) are the most abundant proteoglycans. They are composed of a core protein and glycosaminoglycan (GAG) side chains, the length and number of which vary (Figure 1.4). GAG chains are sulfated polysaccharides made up of two alternating monosaccharide units; uronic acid and either N-acetylgalactosamine or N-acetylglucosamine. While the core proteins of the CSPGs can have direct influences on many functions in the CNS, it is the interactions of the chondroitin sulfate-GAG side chains with other molecules that mediate many of the functions performed by proteoglycans (Bandtlow & Zimmermann, 2000). They contribute to functions such as cell adhesion, receptor binding, growth, migration, barrier formation and interaction with other ECM molecules (for a review see (Bandtlow & Zimmermann, 2000; Ruoslahti, 1996)). It is also these CSPGs that are among the most influential inhibitory molecules in the injured CNS.

1.3.1.1 The lectican family of CSPG

The lectican family constitutes the most abundant CSPG core proteins in the CNS. The family includes aggrecan, versican, neurocan and brevican and is characterised by the N-terminal G1 domain and C-terminal G3 domain, which border a central region at which GAG chains attach (Yamaguchi, 2000) (Figure 1.4). The length of the central binding region, and therefore the number of potential GAG binding sites, varies between family members, from approximately three in brevican up to 100 in aggrecan (Iozzo, 1998). The CSPG core proteins have complex distribution patterns and functional roles that alter during development. For example, brevican is scarce in the embryonic brain but is highly upregulated during early development (Milev, et al., 1998) and, like neurocan, has been shown to be inhibitory to neuronal attachment and neurite outgrowth in *in vitro* studies (Asher, et al., 2000; Yamada, et al., 1997). Aggrecan also has inhibitory effects on cell movement but is believed to be involved with creating cell guidance cues in association with the cell-attractive versican (Perissinotto, et al., 2000).

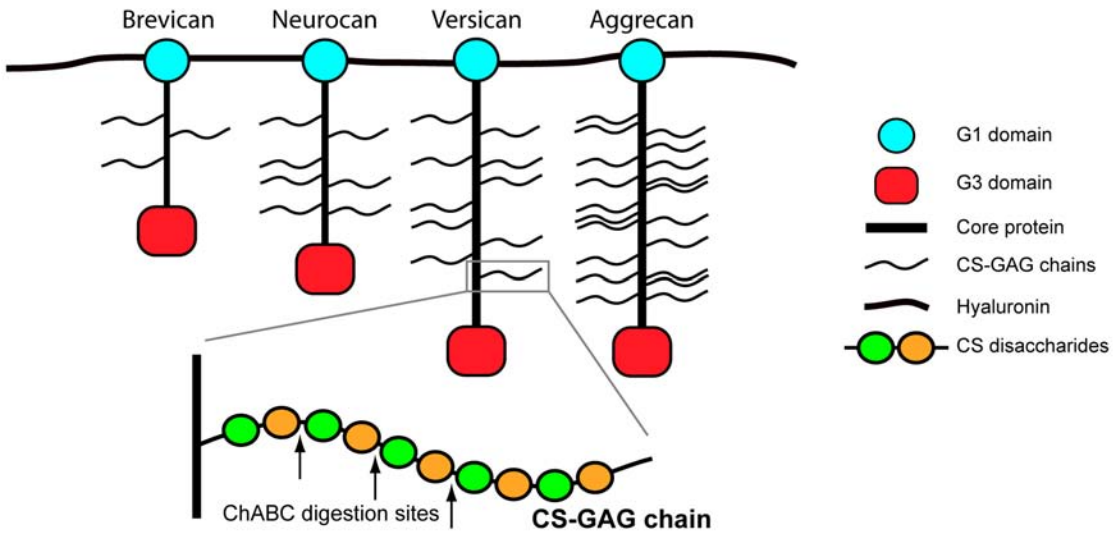

Figure 1.4: Schematic diagram of lectican CSPG structure.

Brevican, neurocan, versican and aggrecan are members of the lectican family of CSPGs. All contain a N-terminal G1 domain, a C-terminal G3 domain and a central GAG-binding core protein. Aggrecan has an additional G2 domain with unknown function. The length of the core protein and therefore the number of GAG-binding sites varies between lecticans. Each GAG side chain consists of a linear polymer of alternating monosaccharide units that binds to the core protein via a serine residue. ChABC treatment removes GAG chains from the core protein by digesting links between monosaccharide units.

1.3.1.2 Other core proteins

Other core proteins can also have differential effects when expressed in association with different cell types and age. Phosphacan (which does not belong to the lectican family but is another common CSPG in the CNS) is inhibitory to neurite outgrowth of neonatal retinal ganglion cells and dorsal root ganglion neurons (Garwood, et al., 1999; Inatani, et al., 2001; Sango, et al., 2003). However, it promotes the outgrowth of embryonic hippocampal and cortical neurites (Garwood, et al., 1999; Maeda & Noda, 1996). Decorin is another interesting small proteoglycan with a single GAG-binding site, which is strongly expressed in the early postnatal rat brain and weakly in the adult brain (Kappler, et al., 1998). In contrast to those proteoglycans listed above, evidence suggests that decorin can inhibit the glial scar reaction following injury when in excess in the adult brain (Logan, et al., 1999).

1.3.2 The perineuronal net (PNN) in the mature CNS

Immediately pericellular to a subset of neurons in the CNS is the perineuronal net (PNN), a layer of dense ECM that surrounds the soma and proximal dendrites of these cells. The PNN is most commonly associated with highly active parvalbumin-positive interneurons (Härtig, et al., 1994) and its putative functions are largely associated with maintaining the structural integrity of neural networks throughout the brain and spinal cord. In the damaged CNS, upregulation of the PNN has been linked to decreased plasticity and limited recovery (Massey, et al., 2006; Yi, et al., 2012). As such, one of the potential targets for inducing plasticity in the CNS is by targeting and degrading the PNN, the mechanisms for doing so have been a recent focus of our laboratory and will be discussed within this thesis.

1.3.2.1 The structure of the PNN

The PNN is composed of common ECM molecules into a highly organised and stable matrix structure. Its major components are hyaluronan, link proteins, CSPGs and tenascin-R (Tn-R) (Figure 1.5). As in the ECM, the backbone of the PNN is formed by linear hyaluronan polymers, which are synthesised and stabilised to the cell surface by a family of enzymes called hyaluronan synthase (HAS)(Carulli, et al., 2006; Galtrey, et al., 2008; Kwok, et al., 2010). CSPGs from the lectican family attach to hyaluronan chains at their N-terminal domain, the bond of which is stabilised by the presence of link proteins and together are crucial for the condensed nature of the PNN (Kwok, et al., 2010). At their C-terminus, up to three CSPGs bind to trimeric Tn-R

(Aspberg, et al., 1997), which completes the stable macromolecular PNN structure (Figure 1.5). Each component of the PNN is integral to its formation and structure, as has been demonstrated by numerous knockout and knock-in models (Carulli, et al., 2010; Kwok, et al., 2010; Weber, et al., 1999).

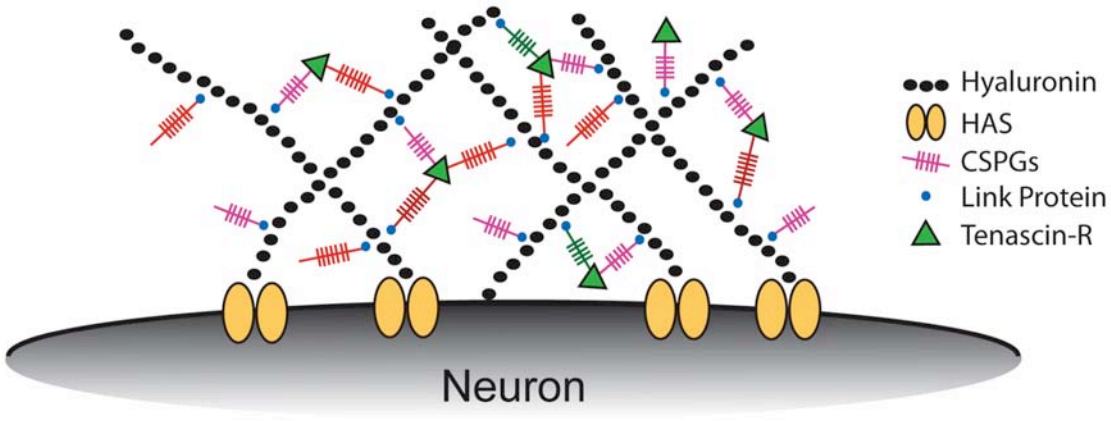

Figure 1.5: Schematic diagram of the perineuronal net structure.

Hyaluronin forms the backbone of the PNN and is synthesised by hyaluronin synthase (HAS) on the neuronal surface. Link proteins bind the N-terminus of CSPGs of the lectican family. Tenascin-R binds up to three CSPGs at their C-terminus to consolidate the rigid PNN lattice structure.

Properties of the particular lectican involved in a PNNs structure may be crucial to its stability and compactness. Among other factors, the length of the central GAG-binding domain of the lectican may affect the degree of cross-linking within the PNN and therefore its density. Indeed, immunohistochemical analysis showed differential distribution of CSPG core proteins in brain and spinal cord sections suggesting that different PNNs contained different CSPGs (Galtrey et al., 2008), which may have functional consequences.

1.3.2.2 The Functional Role of the PNN

There are numerous hypotheses regarding the function of PNNs, primarily based on their distribution of expression and timing of development within the CNS. PNNs are generally observed surrounding highly active parvalbumin-positive GABAergic interneurons, but not slow-firing, burst-firing or regular spiking neurons, suggesting that they may have a role in the activity

of these cells (Härtig, et al., 1994; Härtig, et al., 1999; Morris & Henderson, 2000). It is likely that the negatively charged CS-GAG chains provide a suitable microenvironment to buffer local cations resulting from high spiking activity (J. C. Kwok, et al., 2011). This may be one function of PNNs, however their enzymatic removal does not cause changes in neuronal activity levels as may be expected from this theory (Pizzorusso, et al., 2002).

1.3.2.3 PNN expression reduces plasticity

The primary role of the PNN appears to involve synapse stabilisation and to limit plasticity. The development of the PNN in many brain regions occurs relatively late in postnatal development, which directly coincides with the end of the juvenile critical period (Hockfield, et al., 1990; Lander, et al., 1997; Pizzorusso, et al., 2002). The critical period is a time during which environmental input has the strongest influence of neuronal properties, including their anatomy, physiology and synaptic networks (Hensch, 2005). In rodents, the critical period ends at postnatal day 21-25. For humans, this corresponds to approximately 12-15 years of age, depending on the brain region and physiological system in question (Hensch, 2004). Once the critical period has ended, neuronal networks become much more rigid and do not respond to environmental influences as readily. Proper critical period development is essential for effective motor control and sensory perception later in life, however it is also important that some brain regions, such as the temporal lobes that are involved with memory, do not experience a decrease in plasticity. Furthermore, it is the basic sensory and motor functions that we aim to restore following neurological traumas that have developed a PNN and are resistant to change.

Evidence for the role of the ECM in plasticity was first elegantly demonstrated by Pizzorouso *et. al.* (Pizzorusso, et al., 2002). Following monocular deprivation of young rats during the critical period there is an ocular dominance shift in favour of the non-deprived eye at the expense of the deprived eye. In contrast, monocular deprivation performed in adult animals resulted in little or no plasticity. Incredibly, following enzymatic digestion of the PNN with Chondroitinase ABC (ChABC) in the visual cortex of adult animals, ocular dominance plasticity was restored. By removing the PNN, they had restored neuronal plasticity seen only during the juvenile critical period, suggesting an inhibitory role of the intact PNN in the adult visual cortex.

In later experiments, enzymatic degradation of the PNN in the adult visual cortex coupled with reverse lid suturing rescued visual acuity and dendritic spine density in those animals

(Pizzorusso, et al., 2006), demonstrating that the removal of adult PNN could reverse the effects of long term ocular dominance. A similar study recently reported only modest improvements in visual acuity of the previously deprived eye following binocular exposure in cats (Vorobyov, et al., 2013), which highlights some important distinctions for the capacity of adult plasticity between species. However, the role of PNN-dependent inhibition in the adult nervous system is clear and the potential of its manipulation in restoring plasticity is a promising avenue for therapeutic approaches.

1.3.3 The ECM response to injury

As previously discussed, the ECM has important functions of maintaining homeostasis and synaptic stability in the mature CNS, and may also have an additional protective effect following CNS insult. In response to injury, numerous ECM components are upregulated in concert with proliferating astrocytes, oligodendrocyte progenitor cells and microglia/macrophages that form a glial scar between healthy and necrotic tissue to stop the progression of secondary cellular damage (For a review, see (Rolls, et al., 2009)). The functions of the glial scar become complex beyond the acute phase of injury whereby it also creates a physical and molecular barrier to axon regeneration and plasticity.

1.3.3.1 CSPG-associated inhibition

A key component of the glial scar are proteoglycans, particularly CSPGs, which are upregulated following injury and can undergo changes to their core proteins and sulfation patterns of chondroitin sulfate-GAG side chains (Gilbert, et al., 2005; Properzi, et al., 2003; Properzi, et al., 2005; Wang, et al., 2008). The CSPGs have been shown to remain at an injured site for an extended period of time and are inhibitory to axon growth (Jones, et al., 2003; Silver & Miller, 2004). It has been consistently shown *in vitro* that blockade or degradation of CSPGs promotes neurite outgrowth of numerous neural cell types (McKeon, et al., 1995; Smith-Thomas, et al., 1995). Reports of more specific alterations to lectican expression differ between insults of different nature and at different locations, and may vary between animal models. For example, numerous studies have shown increases in neurocan, versican and brevican associated with the glial scar following spinal cord injury in rodent models. However, these studies report mixed findings regarding changes of aggrecan expression (Andrews, et al.; Jones, et al., 2003; Yi, et al. 2012). After brain injury, there are reports of decreased lectican and PNN expression, even though there is a general increased astroglial scar response (Haddock, et al., 2007; Hobohm, et

al., 2005; Karetko-Sysa, et al.). Localised areas of dense brevican immunoreactivity have been documented in the ipsilaterateral hemisphere five days following middle cerebral artery occlusion, however this was only seen in small areas and was masked when protein was extracted from the whole brain hemisphere (Haddock, et al., 2007). More precise techniques for tissue isolation may therefore be required for assessing localised alterations in lectican expression following stroke. Together, these findings indicate the complex nature of CSPG reactivity in response to CNS injury, which vary according to the region of injury and temporal sequence.

1.3.3.2 Myelin-associated inhibition

Other growth-inhibitory factors have also been identified in the injured CNS. Myelin-derived proteins such as nogo A, myelin associated glycoprotein (MAG) and oligodendrocyte myelin glycoprotein (OMgp) all inhibit axonal growth in addition to scar-related compounds such as CSPGs (Caroni & Schwab, 1988; Chen, et al., 2000; Kottis, et al., 2002; McKerracher, et al., 1994; Mukhopadhyay, et al., 1994). There is a degree of redundancy between this trio which, although structurally diverse, bind to common receptors including NgR1 and PirB (Atwal, et al., 2008; Domeniconi, et al., 2002; Fournier, et al., 2001). There are at least three other myelin-associated inhibitors: Netrin, Sema4D, Ephrin-B3. These factors provide additional potential targets for promoting neural regeneration following injury but their role *in vivo* as inhibitors has not yet been evaluated (Benson, et al., 2005; Löw, et al., 2008; Moreau-Fauvarque, et al., 2003). This family will not be discussed further in this review.

1.3.4 Manipulation of ECM and PNN inhibition to promote plasticity and regeneration

Various therapeutic approaches have attempted to regulate or eliminate the inhibitory factors of the glial scar to promote CNS regeneration after injury (Figure 1.6). As the CNS response to injury consists of a complex cascade of cellular and molecular events it is likely that a multifaceted approach to overcome the endogenous inhibition will yield the most success for brain repair. Furthermore, a number of these approaches may indeed be viable at the brain machine interface to enhance the long term biocompatibility of implanted electrodes.

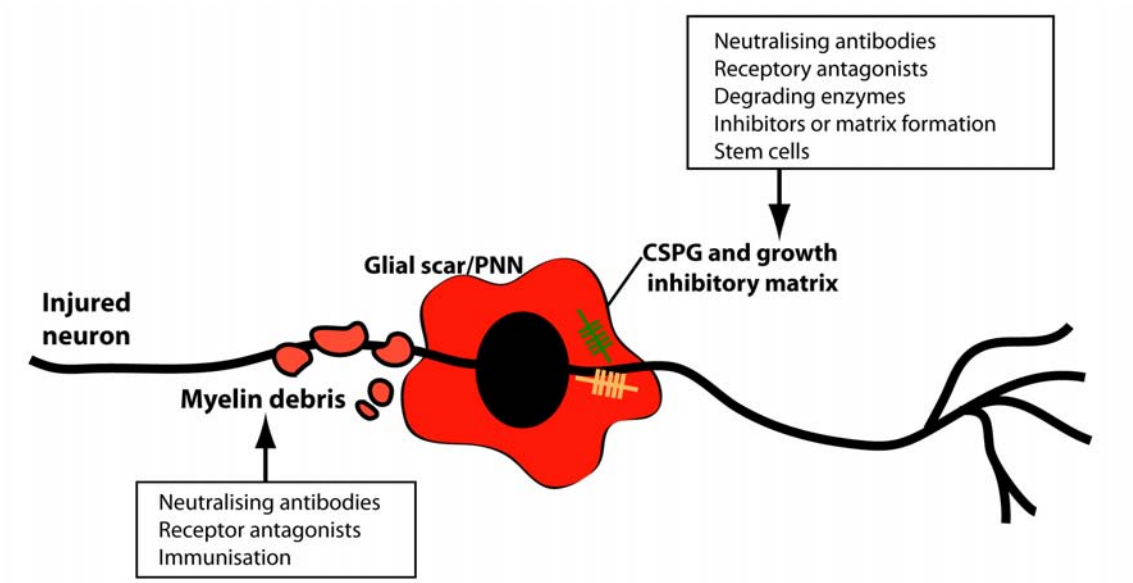

Figure 1.6: Inhibitory components following CNS damage and potential therapeutic interventions.

The major inhibitory components at a CNS injury site include myelin debris and the glial scar, incorporating numerous inhibitory matrix molecules, such as chondroitin sulfate proteoglycans (CSPGs). These factors are potential targets for therapeutic intervention and strategies for their modulation are shown.

1.3.4.1 Degradation of CSGP with Chondroitinase ABC

As we have seen, CSPGs are among the most influential inhibitory molecules in the injured CNS. This makes them a prime target for manipulating the permissiveness of the CNS environment following injury. The cleavage of CS-GAG chains from CSPG core proteins by Chondroitinase ABC (ChABC) has been effective in removing injury-related inhibition in the CNS and promoting anatomical and functional recovery in many injury models in numerous animals: Key studies have shown that acute ChABC administration can promote axonal regeneration and functional recovery following spinal cord injury (Bradbury, et al., 2002) as well as the regeneration of sensory axons across lesions (Shields, et al., 2008; Yick, et al., 2003) and sprouting of damaged axons and dendrites (Barritt, et al., 2006; Garcia-Alias, et al., 2008). The functional reconnection of these sprouting fibers has also been demonstrated. Electrophysiological analysis of receptive fields in the cuneate nucleus following cervical dorsolateral laceration showed an increase in the areas responsive to forelimb stimulation following ChABC treatment, indicating that sprouting afferents were making functional connections (Massey, et al., 2006).

The degree of dendritic plasticity promoted by ChABC was clearly demonstrated in a study of peripheral nerve injury, where the ulnar and median nerves of the forelimb were cut in the adult rat and surgically sutured, either correctly or with reverse contacts. A single injection of ChABC was administered into the ventral horn of the spinal cord after a period of recovery to correct the effects of inaccurate reinnervation. Anatomically, the treatment reduced CSPGs and PNNs, increased sprouting and also improved forelimb function (Galtrey, et al., 2007).

An interesting relationship between inhibition, plasticity and rehabilitation has emerged. Neuroplasticity does not occur as a result of removing inhibition alone, but also requires pro-active environmental influences. As such, ChABC treatment alone in a rodent model produced modest improvements in skilled paw function following experimentally induced spinal cord injury spinal cord injury. However ChABC paired with skilled paw training acted synergistically to allow significant recovery (Garcia-Alias, et al., 2009). Taken together with the anatomical changes following ChABC administration described above, this result indicates that CSPGs inhibit the plastic capacity of the injured spinal cord and that its modification with ChABC allows novel circuit formation.

Central applications of ChABC treatment

A large proportion of the research into ChABC-induced CSPG modification has been performed in animal models of spinal cord injury. However there is also striking evidence for its effectiveness in promoting recovery following brain injury. In addition to the effect of reducing CSPG inhibition on ocular dominance plasticity described earlier, ChABC has also been shown to induce sprouting of undamaged retinal axons into the denervated superior colliculus following a partial retinal injury when administered with BDNF (Tropea, et al., 2003). Functional recovery has also been demonstrated by ChABC administration following stroke. ChABC treatment seven days following middle cerebral artery occlusion of rats increased neuronal immunoreactivity in the peri-infarct area and improved behavioural scores of affected rats (Hill, et al., 2012). Accordingly, while PNN immunoreactivity has been noted to naturally decrease in the lesion epicenter and peri-infarct region in response to stroke, additional CSPG digestion can further promote functional recovery (Hobohm, et al., 2005; Karetko-Sysa, et al.). Another study using aged rats utilised a novel approach to incite plasticity following endothelin-1-induced stroke, whereby ChABC was injected into the cervical spinal cord which induced local CSPG and PNN degradation, collateral

sprouting from the intact corticospinal tract and recovery of forelimb function (Soleman, et al., 2012).

There is also evidence to suggest that ChABC treatment may be an effective strategy to reduce cerebral oedema; a cause of significantly raised intracranial pressure and secondary injury following an initial insult. In a recent study ChABC rapidly reduced oedema in live slices of porcine cortical brain tissue in response to changes in ionic osmotic environments (Elkin, et al.). The translational value of this finding requires further investigation.

From this research, it is evident that there is great potential application for the degradation of the inhibitory PNN following injury. This approach is valid as a direct strategy to induce plasticity and aid self-repair following CNS injury and is also relevant at the brain machine interface through its potential to reduce the negative influences of inflammatory scarring. This is where the two themes of this thesis converge, as 'scaffold' approaches intended to modify local CNS environments and promote neuroplasticity are also highly pertinent to the success of neuroengineered devices, which are themselves employed to overcome interruptions of CNS connectivity. Both challenges face a common set of problems of tissue damage and glial scarring that may be improved by reducing PNN expression in the brain.

1.3.4.2 Limitations to ChABC treatment

While enzymatic degradation of CSPGs with ChABC is the most common form of treatment to modify the endogenous inhibition and has been pivotal in our understanding of the influence of PNNs in the CNS, it may not be the panacea from a clinical therapeutic perspective. Primarily, the lack of specificity of ChABC means it has the ability to degrade CS-GAG chains throughout the ECM, not just at injured areas, so injection methods must be precise. In addition, ChABC is unstable at body temperature and therefore needs to be administered chronically, enhancing the invasive impact of treatment (Lee, et al. 2010). A genetic approach may present a more successful route for ChABC administration in the future. Cafferty *et al*. (Cafferty, et al., 2007) used a transgenic mouse model whose astrocytes expressed ChABC via the GFAP promoter. The results indicated mice experienced better functional recovery following dorsal root crush injury, but not after dorsal hemisection of the spinal cord. Such an approach may present a more specialised and lasting treatment to the modification of injury-based CSPG in the future.

Another limitation of ChABC treatment is its efficacy in promoting regeneration and recovery in clinically relevant injury models. Numerous studies have cited limitations in the degree of functional recovery demonstrated as a result of ChABC administration after contusion spinal cord injury (Iseda et al 2008) and occular dominance deprivation (Vorobyov, et al., 2013) in animal models. This may represent limitations only in particular injury models and animals, or a more general effect. Nonetheless, ChABC has potent effects to reduce inhibitory signals in the CNS and may require administration in combination with other approaches to promote regeneration and induce recovery after injury.

1.3.4.3 Manipulation of CSPGs by alternative mechanisms

While the enzymatic digestion of CSPGs has been the most common approach used to modify inhibitory signals in the injured CNS, numerous alternative approaches to modify CSPG-based inhibition have been investigated.

Decorin

A naturally occurring proteoglycan decorin, has been demonstrated to have antagonist effects against CSPGs in the spinal cord and brain. Decorin is a small leucine rich proteoglycan that is naturally expressed in the embryonic brain but is strongly downregulated during postnatal development (Kappler, et al., 1998). Infusion of decorin following acute injury to the spinal cord and brain has been shown to reduce the formation of a glial scar and specifically reduce the deposition of CSPGs to promote axonal growth across an injury site (Davies, et al., 2004; Logan, et al., 1999). Decorin may also have an effect to desensitise neurons to the inhibitory effects of CSPGs and myelin-associated inhibitors, as has been demonstrated with neurite extension experiments *in vitro* (Minor, et al., 2008). However, the effect of decorin on PNN is yet to be elucidated.

Disruption of GAG chain formation

Interrupting the synthesis of CSPG-GAG chains is another way to potentially reduce inhibition. Xylosyltransferase-1 (XT-1) is an enzyme responsible for the glycosylation of CSPGs (Grimpe & Silver, 2004). A novel DNA enzyme that targets XT-1 function has been shown to reduce CS-GAG chains both *in vitro* and *in vivo* (Grimpe & Silver, 2004; Hurtado, et al., 2008). Following spinal cord injury, XT-1 suppression increased axonal growth and reduced CSPG levels in the

glial scar, which corresponded with an increase in sensorimotor function (Oudega, et al., 2012). In a similar approach, Laabs and colleagues {Laabs, 2007) used short interfering RNA to knock down the level of chondroitin polymerisation factor by 70%. Since this enzyme is critical in the elongation of CS-GAG chains, this reduced the amount of CS produced by astrocytes *in vitro*. These studies are proof of principle that disruption to GAG chain formation can render the injured CNS less inhibitory to nerve recovery.

Interferon-γ (IFN-γ)

Interferon-γ presents another molecular approach to reducing CSPG inhibition. Following contusion injury in the spinal cord of mice, interperitoneal IFN-γ injection facilitated locomotor improvement of animals and serotonergic nerve regeneration. This was likely a result of INF-γ effect to reduce CSPG deposition and increase expression of neurotrophic factors GDNF and IGF-1 at the injury site (Fujiyoshi, et al., 2010).

Antibodies

Other approaches have targeted the activity of the CSPGs rather than interrupting the structure or formation. For instance, antibody blockade of the inhibitory activity of the CSPG NG2 resulted in restored axon regeneration following rat spinal cord injury (Tan, et al., 2006). Furthermore, targeting the receptors that recognise growth-inhibitory factors or the intracellular signals induced by them is also effective at allowing axon regeneration *in vitro* (Borisoff, et al., 2003; Monnier, et al., 2003) and *in vivo* following spinal cord injury (Dergham, et al., 2002; Neumann, et al., 2002).

Modification of myelin associated inhibitors

The major myelin associated inhibitors; MAG, OMgp and Nogo have a high degree of redundancy at the ligand and receptor levels, which makes therapeutic approaches targeting these inhibitors much more complicated. Previous research targeting single molecules in this system have met with little success. MAG knockout mice did not support enhanced axon regeneration in either the optic nerve or the corticospinal tract (Bartsch, et al., 1995). Similarly, OMgp knockout mice failed to demonstrate improved corticospinal axon regeneration following spinal cord injury (Ji, et al., 2008; J. K. Lee, et al., 2010). In contrast, a neutralising antibody against Nogo, IN-1, demonstrated strong positive effects following a range of brain and spinal

cord injury models with increased axonal regeneration, sprouting and plasticity as well as behavioural recovery (Fouad, et al., 2004; Papadopoulos, et al., 2002; Seymour, et al., 2005). However, the effects of Nogo knockout had mixed results on axon regeneration, with the most repeatable result being no effect at all (Kim, et al., 2003; J. K. Lee, et al., 2009; Simonen, et al., 2003; Zheng, et al., 2003). Controversy and confusion therefore still exists regarding Nogo's role in axon regeneration (Filbin, 2003; Zheng, et al., 2006)).

To combat these conflicting results, a triple knockout mouse for MAG, OMgp and Nogo was generated (Cafferty, et al., 2010; J. K. Lee, et al., 2010). Two studies performed by different groups showed synergistic effects of the triple knockout with an increased number of serotonergic axons detected caudal to the injury in a partial spinal cord injury model but unclear results regarding functional regeneration and behavioural recovery between the groups (Cafferty, et al., 2010; Lee, et al., 2010). Efforts to target the common receptors of these ligands have met with mixed results (Lee & Zheng, 2012). As such, evidence is currently lacking for the efficacy of targeting myelin associated inhibition *in vivo*.

Novel immunological approaches have also been attempted to investigate myelin associated inhibitors. Immunised mice were induced to produce endogenous antibodies against proteins present in myelin. Interestingly, these mice supported corticospinal axon regeneration after spinal cord injury (Huang, et al., 1999; Sicotte, et al., 2003). Others have also shown that immunisation against a Nogo-A derived peptide has a neuroprotective effect, mediated by a T-cell response (Hauben, et al., 2001). However, it is uncertain how specific these effects are, as immunisation against non-myelin-associated proteins can produce similar effects. Hence it is unclear to what degree neuroprotection as opposed to regeneration is affected (For a review, see (Lee & Zheng, 2012).

Other members of the ephrin, semaphorin and plexin families of proteins have been identified as potential axon inhibitors following injury. These proteins are mainly known for their role in axon guidance during development and have been shown to be upregulated in the adult CNS following spinal cord injury. Key molecules are eprinB3 (Benson, et al., 2005), ephrinA (Eberhart, et al., 2004), Sema3A (De Winter, et al., 2002; Niclou, et al., 2003), Sema4D (Moreau-Fauvarque, et al., 2003), and Sema5A (Goldberg, et al., 2004). Their role as myelin-associated neurite outgrowth inhibitors is currently being studied with ongoing experiments investigating their role in the regenerative processes *in vivo*.

Neurotrophins

The use of neurotrophins has been another promising avenue for the induction of functional regeneration following CNS injury. Recombinant adenovirus delivery of fibroblast growth factor-2 (FGF-2), nerve growth factor (NGF) and neurotrophin-3 (NT-3) have each induced axonal regeneration in animal models following axonal lesion within the dorsal root (Zhang, et al., 1998) which has lead to recovery of sensory function (Romero, et al., 2001). Whether the positive effects of neurotrophins involve modulation of CSPGs is unknown. Combination therapies using neurotrophins have also been employed with encouraging results, and will be discussed below.

Stem Cells

Many studies have investigated the use of stem cell transplantation following CNS injury to promote nerve regeneration with varied but encouraging results. In the injured spinal cord and brain, numerous stem cell types have successfully aided in the regeneration of axons and functional recovery of movement and neurological deficits (for a review see (Tetzlaff, et al., 2011)), likely by combinatorial mechanisms of cell replacement and the effects of paracrine factors released into the local environment. However, the precise mechanism of repair and regeneration remains unclear (Leong, et al., 2013). Recently, it was demonstrated that conditioned medium from human dental pulp stem cells (hDPSC) could negate the inhibitory effects of cultured CSPGs and MAGs on neurite outgrowth *in vitro* and also aid axon regeneration following complete transection of the spinal cord in rats (Sakai, et al., 2012). Conversely, assessment of bone marrow stromal cell-conditioned medium did not reveal the same effect on modifying neurite growth inhibition. In another study, schwann cell precursors were transplanted following spinal crush injury, which caused a reduction in the surrounding astroglial scar and CSPG expression, suggesting a reduction in inhibition (Agudo, et al., 2008). In Schwann cell precursor-treated animals there was increased axonal growth and sprouting, but no improvement in motor function. Together these findings suggest that some stem and precursor cells may also affect the inhibitory molecules in the injured CNS, likely via the release of neurotrophic factors among other mechanisms.

1.3.4.4 Combination treatments

The endogenous response to CNS injury involves a complex series of events culminating in the maladaptive inhibition of axonal regeneration. However striking the effects of a single treatment have been and may be, it is likely that combination therapies will succeed in restoring functional outcomes to a greater degree than any one alone. Thus far this chapter has outlined some of the research performed to identify many inhibitory factors and approaches to combat them. These also represent a pool of targets and approaches that could potentially be combined for clinical benefit. Indeed, a range of studies have demonstrated the success of combination treatments following CNS damage. Among those, groups have suggested pairing CSPG or myelin-associated inhibition treatments with exercise or skilled motor training following spinal cord injury (Garcia-Alias, et al., 2009; Garcia-Alias & Fawcett, 2012; Jakeman, et al., 2011; Starkey & Schwab, 2012) and with neurotrophin administration (Garcia-Alias, et al., 2011; Massey, et al., 2008). The outcomes of combined motor training with either ChABC or myelin-associated inhibition treatments have been mixed. Various experiments have shown beneficial anatomical and functional outcomes but others have cited no effect, or even deleterious outcomes (Garcia-Alias & Fawcett, 2012; Starkey & Schwab, 2012). These findings suggest that the injury model, training method and temporal sequence employed are important considerations when designing these protocols.

Combination treatments involving neurotrophins have met with more widespread success. The combined treatment of ChABC and NT-3-expressing lentivirus decreased inhibition by CSPGs and increased the innervation of axons by microtransplanted dorsal root ganglion neurons into the denervated adult rat dorsal column nuclei, beyond the immediate region of injury (Massey, et al., 2008). Furthermore, the combined treatment of NT-3 and ChABC increased expression of the NR2D subunit of the NMDA receptor and enhanced axonal sprouting and hindlimb locomotor function following lateral hemisection at T8 in the adult rat more than either treatment alone (Garcia-Alias, et al., 2011). This combined treatment also promoted the reestablishment of a detour pathway of motorneurons around the hemisection.

ChABC has also been combined with cell transplantations in a number of different experimental models. In rats, treatment of a spinal cord contusion injury epicentre with ChABC promoted the migration of transplanted neural stem/progenitor cells and enhanced fiber outgrowth in the lesion (Ikegami, et al., 2005). Furthermore, administration of ChABC at the graft-host tissue interface

has also been shown to improve regeneration and locomotor function when in combination with transplanted schwann cells and olfactory ensheathing glia following spinal cord transection (Fouad, et al., 2005; Vavrek, et al., 2007). This group further demonstrated that the same combination therapy could prevent the deterioration of bladder function following complete spinal cord injury, noting autonomic as well as behavioural recovery (Fouad, et al., 2009). However, improvement of bladder function and locomotion has also been observed following treatment with ChABC alone following spinal cord contusion injury (Caggiano, et al., 2005). In another study, a reduction of infarct volume was noted as a result of ChABC and neural stem/progenitor cell (NSPC) injection following neonatal hypoxic ischemia, compared with NSPC treatment alone, however the effect of ChABC alone was not considered in this study (Sato, et al., 2008). Using bone marrow mesenchymal stem cells in a transection spinal cord injury in the rat, there were modest improvements in numerous measures of anatomical and behavioural function which was increased significantly with the addition of electroacupuncture, which involves the insertion of a needle attached to a trace pulse current that produces electric stimulation (Ding, et al., 2012). This alternate strategy reduced the CSPG and astrocytic immunoreactivity at the site of injury as well as promoting axonal regeneration and locomotor function.

Combining these three major classes of CNS repair strategies, Karimi-Abdolrezaee et al (Karimi-Abdolrezaee, et al., 2010) found that the ChABC administration in concert with intraspinal neural stem/progenitor cell grafts and multiple growth factors promoted functional repair and plasticity of the chronically injured spinal cord following thoracic clip compression. This combined treatment resulted in an increased survival and migration of stem cells into the host parenchyma, enhanced sprouting of both corticospinal tract and serotonergic fibers and improved locomotion. Similarly, enhanced axonal remodeling and locomotor recovery following the combined treatment of neural stem cells, NT-3 and ChABC following hemisection injury in the rat has been reported (Hwang, et al., 2011). These results encourage the synergistic value of combined treatments for CNS repair.

1.4 Modifying the ECM to enhance brain machine interface biocompatibility

With a greater understanding of the molecular CNS response to injury we can potentially propose targeted interventions to minimise inflammation following electrode insertion and promote a more efficient interface between electrodes and neurons. With reduced CSPG and glial encapsulation around electrodes, the repulsive signals for neurons would be minimised, effectively improving

biocompatibility, reducing the distance between the electrode and neuron, and potentially enhancing the success of long term implantation for both penetrating and surface electrodes.

To achieve a more successful interface through modification of the ECM environment any of the interventions discussed have the potential to be utilised, however some are more appropriate to the application than others. Due to its success in promoting functional recovery following spinal cord injury and stroke, ChABC is an obvious treatment to consider at the brain machine interface. Surprisingly, this approach has not been investigated to date. Similarly, many of the other treatments discussed above are still within the developmental stage of understanding and at this stage may not be appropriate for such a challenging application. Furthermore, due to the lacking specificity and short term activity of ChABC a more biological approach may be favourable for neurological applications.

1.4.1 Approaches to improve the brain machine interface

Two approaches that have been investigated previously at the interface are neurotrophin release and treatment with stem cells.

1.4.1 Neurotrophins

In previous research, neurotrophins have been demonstrated to be supportive to neurons when associated with electrodes. The controlled and sustained release of brain-derived neurotrophic factor (BDNF) from doped hydrogels has been shown to promote neural regeneration following spinal cord injury (Jain 2006) and also to increase the spontaneous activity of cultured hippocampal cells on *in vitro* planar microelectrode arrays, indicating its supporting role in neuronal health and activity when in contact with microelectrode materials (Jun, et al., 2008). Secondly, within the auditory system, seeding of the cochlear implant with BDNF-secreting fibroblasts enhanced the survival of target spiral ganglion neurons (Jun, et al., 2008; Rejali, et al., 2007). Neurotrophins have long been known to support neuronal health and present a viable approach to enhancing the neuron-electrode interface. However, it is important to note their effects on the reactive ECM are greatest when in combination with other treatments.

1.4.2 Stem cells

The addition of a stem cell layer on implantable electrodes may improve the brain machine interface in a number of ways. Firstly, it would create a biological layer to conceal the foreign electrode material, which may reduce the host tissue response to implantation. Furthermore, stem cells are known to release a range of paracrine and neurotrophic factors capable of supporting the survival and migration of neurons as well as mitigating the inflammatory response of the CNS due to injury. In support of their use at the brain machine interface, seeding of adipose-derived stromal cells onto biosensor materials involved in prosthetics reduced the host inflammatory response to subcutaneous implantation (Prichard, et al., 2008; Prichard, et al., 2007). At the cortex, seeding of neural progenitor cells (NPC) onto silicon-based neural probes coated with immobilised laminin produced an attenuated glial response than that caused from uncoated probes at 7 days post implantation in murine cortex (Azemi, et al., 2010). They showed that the NPC remained attached to the probe following insertion, overcoming the shear forces from implantation, and remained on or nearby electrodes at 14 days following implantation. Another group implanted neural probes containing a hollow well with a NSC-seeded hydrogel scaffold into rat cortex and demonstrated a reduced early tissue response to implantation with lower astrocyte immunoreactivity and a greater proportion of neurons in the immediate vicinity of probes compared to non-seeded implants (Purcell, et al., 2009). However, by 6 weeks this effect had reversed such that there was enhanced glial encapsulation and lower neuronal immunoreactivity surrounding NSC-seeded probes. The authors propose that the early neuroprotective effect was due to the release of neurotrophic factors from NPCs followed by the degradation of the scaffold and stem cell death. Alternative methods for stem cell delivery are therefore required. To the best of our knowledge, no other stem cell type has been examined for its impact at the brain machine interface to date.

1.4.3 Dental pulp stem cells (DPSC) to modify the brain machine interface

DPSC present an easily accessible population of adult stem cells that could provide a novel cell-based strategy at the brain machine interface to increase biocompatibility and long term implant efficacy. DPSC are a heterogeneous population of cells sourced from the pulp of teeth that can be isolated with minimal invasiveness or ethical complications (Gronthos, et al., 2000). They are neural crest-derived and show dentinogenic as well as neurogenic potential both *in vitro* and *in vivo* (Arthur, et al., 2008; Gronthos, et al., 2011; Leong, et al., 2012). Furthermore, as we saw

above, they also have a distinctive ability to down-regulate CSPG inhibitory activity *in vitro,* to allow neurite extension of ganglion cells, and also to promote axon regeneration following transection of the spinal cord in rats. These properties could be key to reducing the impact of electrode insertion and improving the brain-machine interface.

Close investigation of the properties of DPSC demonstrated that human-derived DPSC (hDPSC) express a variety of trophic factors that promote neuronal survival, proliferation, differentiation and migration (Arthur, et al., 2009; Huang, et al., 2008; Nosrat, et al., 2004; Nosrat, et al., 2001). Their potential for chemo-attraction was demonstrated through hDPSC injection at the trigeminal ganglion of chick embryos, which caused axonal branches to extend away from the rigidly organised trigeminal branching to the site of stem cell injection (Arthur, et al., 2008). This chemo-attraction was achieved by DPSC secretion of chemokines and suggests the potential for DPSC-seeded neural prostheses to promote the migration of host neuronal processes toward electrodes to enhance their electrical coupling. This characteristic could be intensely useful to improve the interface of surface electrodes as well as penetrating electrodes by reducing their distance to target neurons and therefore optimising their electrical coupling as well as reducing the amplitude of current necessary for stimulation or detection.

DPSC have the added advantage of providing support to neurons to overcome the inhibitory effects of CSPGs that are known to be upregulated following CNS damage such as cortical electrode insertion, as described previously (Polikov, et al., 2005; Ward, et al., 2009). It has also been reported that intracortical DPSC injection can enhance functional motor and neurological recovery following rat stroke (Leong, et al., 2012), the mechanisms for which may be through their ability to overcoming CSPG-derived inhibition.

Taken together, the potential of stem cells in a cortical prosthesis interface is four-fold:

i) to create an autologous biological layer more compatible with the cortex

ii) to make synaptic connection with host neurons

iii) to break down the PNN to allow neuroplasticity, and

iv) to produce chemokines to attract neurons toward a prosthesis

In addition, DPSC have the benefit of potential autologous transplantation as well as the ease of accessibility with minimal invasiveness. Unlike neural stem cells or embryonic stem cells derived

from donor tissue, it is conceivable for a patient to have their own DPSC isolated for their own cell-based therapies, which negates the need for immunosuppressants.

1.5 Conclusion and aims

The development of cortical visual and motor prostheses could provide millions of people worldwide with greater autonomy and quality of life. Current limitations of prostheses, however, are largely due to their instability over long term implantation and modifications have therefore been suggested to improve the neuron-electrode interface. The principal aim of brain machine interface modifications is to enhance the electrical coupling between electrodes and their target neurons to achieve a high resolution interface with long term stability. Numerous interface modifications have been discussed based on either material manipulation or electrode surface treatment which all aim to minimise the host tissue response to implantation and maintain a close proximity of neurons to implanted electrodes, whether planar or penetrating. Of the modifications discussed, the treatment of electrodes with dental pulp stem cells presents a multifaceted and feasible solution to improving the interface. They would potentially provide a biological layer capable of producing trophic factors to support neuronal survival and migration toward electrodes, as well as overcoming the inhibitory effects of CSPG upregulation. However, the integration potential of DPSCs with cortical tissue is yet uncharacterised and first needs to be assessed *in vitro* before animal or human implantation with MEAs is attempted. As such, the broad aims of this thesis are to:

1. Investigate the biocompatibility of planar MEAs and their potential for supporting DPSC neuronal differentiation *in vitro*

2. Establish the neuronal potential of DPSC isolated from murine teeth *in vitro* to determine the viability of developing a murine model for autologous cell transplantations

3. To determine the effect of DPSC on the expression of endogenous PNN in cortical tissue *in vitro*

I address these broad aims via three experimental approaches:

In Chapter 3, I explore the characteristics of a purpose-designed and fabricated *in vitro* micro-electrode arrays (MEA) for their biocompatibility with murine cortical cultures and their ability to record electrical activity from the cultures compared with an industry standard model. I show that the novel MEAs have high biocompatibility with cortical cultures, however high impedance of their electrodes results in an inability to record action potentials from the cultures which necessitates the subsequent use of commercial MEAs throughout the thesis. In Chapter 4, I investigate the long-term biocompatibility of neuronally differentiating hDPSC on MEAs to assess the development of electrical activity within the developing cultures. I show that DPSC have intrinsically low biocompatibility with MEAs, however potential stimulus-induced events are identified. In Chapter 5 I develop a murine DPSC model for neuronal differentiation *in vitro* and look at the functional properties of developing neural networks. I show the immature neuronal development of the cells using immunohistochemistry and electrophysiology methods, the properties of which recapitulate early neuroembryonic events. Finally, in Chapter 6 I explore the impact of DPSC on cortical PNN expression *in vitro*. I will demonstrate that hDPSC co-culture reduces the proportion of neurons that express PNN in a time and dose-dependent manner.

Chapter 2: Materials and Methods

2.1 Animal Ethics

All experiments were performed in accordance with the guidelines established by the University of Adelaide Ethics Committee (approval number S-2009-159).

2.2 Cell culture experimental procedures

All culture procedures were performed under sterile conditions within a Class II Biological Safety Cabinet. All equipment was sterilised with 70% ethanol or autoclaved and all solutions were either sterile filtered, autoclaved or obtained sterile. Cultures were incubated in a humidified 37°C incubator (Heraeus HERA Cell 150) with 5% CO_2.

2.2.1 Cell isolation and culture

C57Bl/6 Mouse Cortical Cultures

Primary cortical cultures were established from postnatal day 1 C57 Black pups. Pups were euthanised by decapitation and explants taken from each cortical hemisphere with fine curved forceps. Explants from up to five pups were combined for each experiment. Explants were finely diced with a surgical blade before being exposed to enzymatic *dissociation medium* with 10 µg/mL DNase (BD Bioscience) and 0.15% Trypsin for 20 min. The resulting cell solution was sieved with a 40 µm millipore filter and centrifuged for enzyme removal. Cells were resuspended and plated in Neurobasal medium at a desired concentration. Most cells were plated onto laminin (0.02 mg/mL, Sigma-Aldrich) and poly-l-lysine (PLL, 0.01%, Sigma-Aldrich)-coated coverslips at 15,000 cells/cm^2.

Human DPSC isolation

Human DPSC were previously isolated from the pulp of adult impacted third molars (Figure 2.1). Teeth were opened and their pulp exposed to enzymatic digestion with 3 mg/mL collagenase type I and 4 mg/mL dispase in PBS for incubated at 37°C for 1-2h. The solution was subsequently centrifuged at 200 x g for 5 min and enzymes removed with the supernatant. Remaining cells were cultured in *mesenchymal stem cell solution* (Gronthos, et al., 2011), consisting of α-modified Eagle's Medium (α-MEM, Invitrogen) supplemented with 10% fetal calf

serum, 1x GlutaMAX (Sigma-Aldrich), 50 U/mL penicillin and 50 µg/mL streptomycin (Sigma-Aldrich) and 10 mM L-ascorbate-2-phosphate (Wako). DPSC were allowed to adhere to the plastic flask base (Figure 2.2A). Floating debris could subsequently be removed and a heterogeneous population of DPSC remained. Medium was refreshed every 2-3 days and cultures passaged at 80-90% confluence. DPSC from three individuals were used throughout the following experiments, referred to as H1, H3 and H4, respectively. All were sourced from the healthy third molars of young adults.

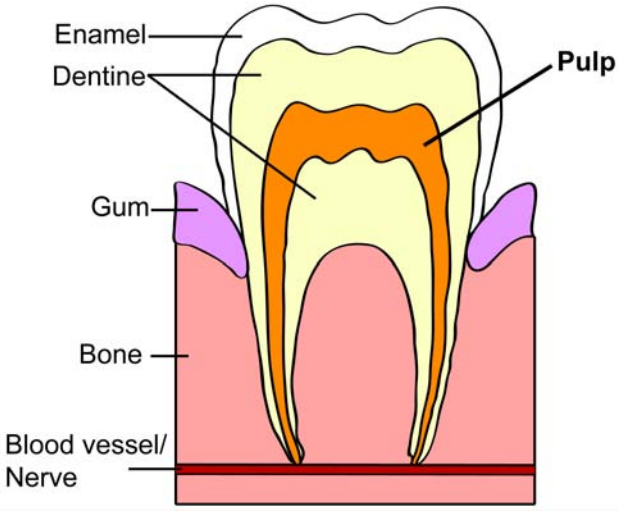

Figure 2.1: Diagram of tooth composition.

Layers of tooth composition including the inner *dental pulp* that contains DSPC.

Murine DPSC isolation

Incisors from adult BALB/c mice were removed and their pulp exposed to enzymatic digestion with 3 mg/mL collagenase type I and 4 mg/mL dispase in PBS for 1-2h. Subsequent techniques were analogous to that performed for human DPSC isolation. Cells were centrifuged at 200g and the supernatant removed before plating in *mesenchymal stem cell solution*. Cells were allowed to adhere to the plastic culture flask so that floating debris could be removed (Figure 2.2B). Medium was refreshed every 2-3 days and cultures passaged at 80-90% confluence.

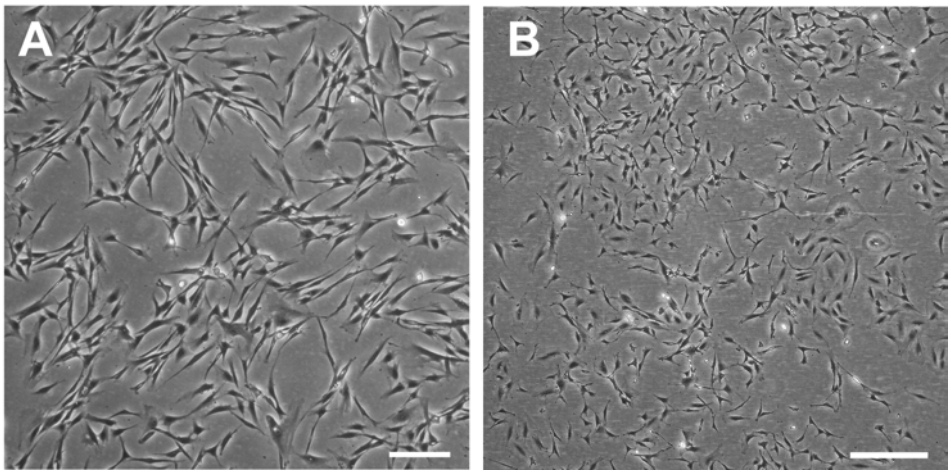

Figure 2.2: Bright field images of undifferentiated DPSC.

A) Undifferentiated hDPSC. B) Undifferentiated mDPSC. Scale bar = 50 µm.

Human Foreskin Fibroblasts (hFF)

Human foreskin fibroblasts were used as a control cell population as they are proliferative cells but do not have stem cell-like characteristics of pluripotency. hFF were maintained in the same mesenchymal stem cell solution as DPSC.

Embryonic stem cell (ESC) culture and neuronal differentiation

Murine ESC were used as a positive control to identify how stem cell-derived neuronal activity would present on MEAs. ESC were underwent *in vitro* neuronal differentiation according to a protocol previously described (Ying, et al., 2003). Briefly, ESCs were maintained in ESC medium containing 10% foetal bovine serum, 2 mM L-Glutamine, 100 µM ß-mercaptoethanol, 1x Leukemia inhibitory factor, 50 U/mL penicillin and 50 µg/mL streptomycin (Sigma) in Dulbecco's modified eagle medium (DMEM). For neuronal differentiation, mESC were dissociated with trypsin and 30-50,000 cells replated onto the electrode region of 0.1% gelatin-coated MEAs in N2B27 medium containing 0.5x N2 and B27 supplements, 50 mg/mL bovine serum albumin, 25 mg/mL insulin, 100µM ß-mercaptoethanol, 1 mM L-Glutamate, 50 U/mL penicillin and 50 µg/mL streptomycin in 50% Neurobasal medium, 50% DMEM/F12. All reagents were sourced from Gibco (Invitrogen) unless otherwise specified.

2.2.2 Cell counts

All cell populations were maintained in uncoated 75 cm^2 plastic flasks. To isolate single cells, culture medium was removed and the cell layer rinsed with phosphate buffered solution (PBS) to remove all traces of serum that contains a trypsin inhibitor. 1 mL 0.1% trypsin was added and the flask gently agitated to detach cells. 10mL culture medium containing serum was subsequently added to cultures to inhibit the activity of trypsin, the cell solution centrifuged at 1500g for 2 min and the supernatant removed. Cells were resuspended in either a *plating medium* (See section 2.2.3) if they were to undergo neuronal differentiation or serum-free PBS if they were to be added as co-cultures to cortical cells. Cell concentration was counted using a haemocytometer (GMBH & Co., Germany) and the desired density of cells plated onto glass coverslips or microelectrode arrays.

2.2.3 DPSC neuronal differentiation

DPSC were seeded onto glass coverslips pre-treated with HCl and coated with adherent substrates laminin (0.02 mg/mL) and poly-l-lysine (PLL) at 20,000 cells/cm^2. Individual coverslips were contained within wells of a 24-well plate. Cells were maintained in basic *plating medium* for 24h containing 1:1 ratio of Dulbecco's modified Eagle's medium (DMEM) and F12 (Invitrogen) supplemented with 2.5% FBS and 50 U/mL penicillin and 50 µg/mL streptomycin. Following 24h in plating medium DPSC underwent neuronal differentiation as previously described (Kiraly, et al., 2009) (See Figure 2.3). Briefly, *epigenetic reprogramming* of the cells was performed with the addition of 10 µM 5-azacytidine, 1 mM dbcAMP and 10 ng/mL beta-fibroblast growth factor (ßFGF) to the basic plating medium for 48h. Cells were then rinsed with PBS and induced with a *neural differentiation* medium containing 250 µM 3-Isobutyl-1-methylxanthine (IBMX), 50 µM forskolin, 1% ITS, 30 nM Phorbol 12-myristate 13-acetate (TPA), 30 ng/mL neurotrophin-3 (NT-3), 10 ng/mL nerve growth factor (NGF), 10 ng/mL FGF-2 in 1:1 DMEM/F12 for 3 days. Finally, cells were rinsed again with PBS before the addition of a *neuronal maturation* medium, which consisted of 1% N2 and B27 supplements (Gibco), 30 ng/mL NT-3, and 1 mM dbcAMP in 1:1 DMEM/F12. All reagents were sourced from Sigma-Aldrich unless otherwise specified.

2.2.3.1 DPSC cell counts

Cell counts of DPSC undergoing neuronal differentiation were performed at days 0, 1, 3, 5, 7, 9 and 11 to determine the rates of proliferation and attrition over the differentiation period. To count

viable DPSC, culture medium was removed and cells gently washed with PBS to remove any floating debris or cells. 100 µL 0.1% trypsin was added to culture wells and cultures gently agitated to detach cells. The cell solution was transferred to a tube and 500 µL mesenchymal stem cell solution containing 10% serum was added. Subsequent washes of culture wells were performed to ensure that all DPSC were removed for counting. Cell density was determined using a haemocytometer. The cell solutions were not spun down with a centrifuge as we could not risk losing cells in the process.

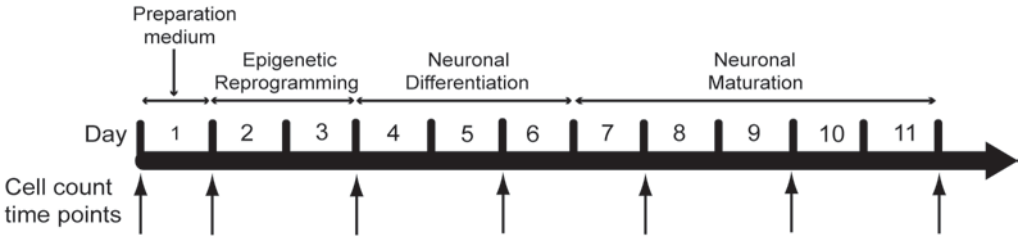

Figure 2.3: Timeline of DPSC neuronal differentiation

Cells underwent an 11-day neuronal induction protocol with successive medium changes through plating, epigenetic reprogramming, neuronal differentiation and neuronal maturation phases. Cell counts were performed at days 0, 1, 3, 5, 7, 9 and 11 to determine cell viability.

2.3 Perineuronal net experimental procedure

2.3.1 DPSC-Cortical cell co-culture

DPSC were added to established cortical cultures originally plated at 15,000 cells/cm^2 after 14 days *in vitro* to determine their impact on endogenous perineuronal net (PNN) expression. A DPSC dose-response experiment was firstly performed where 1000, 2000 or 5000 human or mouse DPSC or hFF (control) were added to cortical cultures for 24h before being fixed for immunohistochemical (IHC) analysis for PNN expression as described below.

The impact of DPSC co-culture duration on cortical PNN expression was also investigated. 4000 cells/cm^2 of either H3 or H4 DPSC or hFF were added to cortical cultures for 24, 48, 72 or 96h before fixing for subsequent IHC analysis for PNN expression. Cortical cultures with no cell additions were also collected at each time point to ensure no baseline time-dependent effects of PNN expression.

Whether DPSC conditioned medium alone was sufficient to incite alterations of cortical PNN expression was then investigated. Experimental cells; either human or mouse DPSC, hFF or no cells were added into MilliCell-CM inserts (Merck Millipore) with 0.4 μm pore holes that kept them separated from cortical cells at day 13 of culture (Figure 2.3). The pores allowed small molecule exchange such that trophic factors released from experimental cells could affect cortical cells without direct contact. Microwell inserts were kept for 24h at which point cortical cultures were collected and underwent IHC analysis for PNN expression. Two experiments were performed using different DPSC experimental cell lines. The first investigated the effect of H1 or M1 DPSC conditioned medium (CM) at 5000 cells/cm^2 and the second, H3 or H4 DPSC CM at 2000 cells/cm^2. All were compared to hFF at the same density or cultures with no cell additions as controls (N=3 each group).

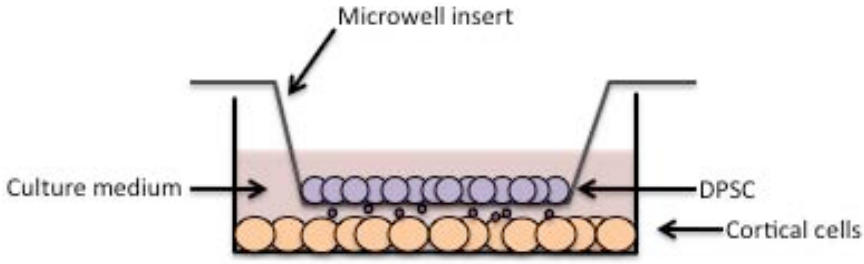

Figure 2.4: Diagram of conditioned media experimental setup.

DPSC (purple) were added to a microwell insert with small 40 μm pores that sat above a layer of established cortical cells (orange). Therefore soluble DPSC trophic factors (dark purple) could diffuse through culture medium and affect cortical cells without direct cell-to-cell contact.

2.3.2 PNN cell counts

Following cortical-DPSC co-culture, the degree of PNN expression was assessed by counting the percentage of NeuN-positive neurons that co-expressed WFA. Approximately 100 NeuN-positive cells were analysed per cortical co-culture by linear sweeps across coverslips as depicted in Figure 2.5. Areas of moderate cell density were primarily targeted to avoid confounding impacts of high or low density on natural PNN expression. All PNN-positive cells were imaged for later analysis.

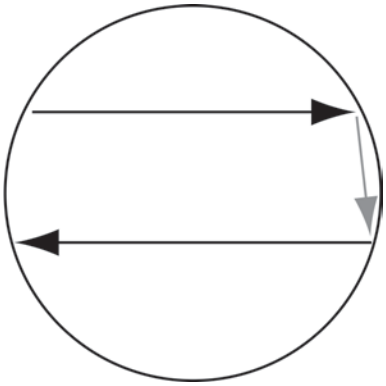

Figure 2.5: Diagram of linear sweeps across a coverslip to measure rates of PNN expression.

Diagram of a coverslip depicting how counts of NeuN-positive neurons with and without co-expression of WFA were measured. To gain a representative and impartial measurement of PNN expression, non-overlapping linear sweeps were taken across different areas of coverslips (black arrows).

2.3.3 ImageJ software analysis

Images of PNN-expressing neurons were analysed using ImageJ software version 1.44o. Images were split into wavelength channels of 'green' (WFA) and 'red' (NeuN) and the WFA channel alone were used for analysis. A threshold of PNN signal intensity was set at 60, between range limits of 0-255, using the RenyiEntropy method to optimise signal detection to PNN regions only and rejecting background signal. A tight region of interest was drawn around the PNN signal area and particle analysis performed to extract a measure of total PNN area and average signal intensity per cell. A measure of total PNN area was calculated based on the average PNN area per cell multiplied by the percentage of NeuN neurons that expressed WFA. This gave a value for total PNN area per 100 cells and could be directly compared across replications and experimental conditions.

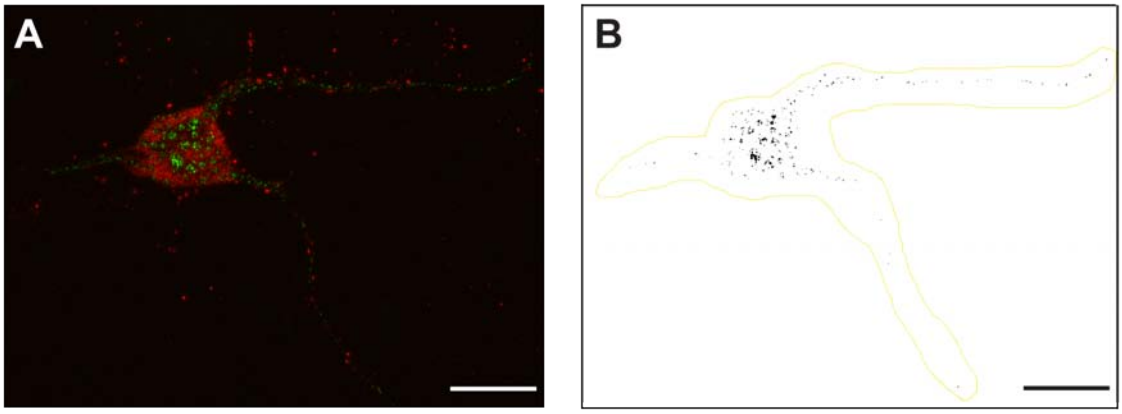

Figure 2.6: Measurement of PNN area and signal intensity.

A) A representative image of a PNN-positive neuron (NeuN-red; WFA-green). B) The WFA signal only is used for analysis. An intensity threshold set at 60 (range 0-255) selects for WFA signal and a tight region of interest drawn around the PNN area before measurements for PNN area and signal intensity are taken. Scale bar = 25 µm.

2.3.4 Perineuronal net data analysis

To compare the distributions of PNN area per cell across conditions, data from three coverslips per condition were collated to form a histogram distribution. Histograms were smoothed using a Savizky-Golay filter, which smooths across area bins while maintaining the shape and height information of distributions. Smoothed histograms were then fitted with log-normal nonlinear regression curves to fit their strong positively skewed shape and compared across experimental conditions with an F-test. The F-test considers the hypothesis that two curves are from the same distribution so a significant F-ratio between curves indicates that they are from different populations, but does not specify how they differ. Based of qualitative assessment of PNN area histogram, two points in the distribution were chosen at which to compare conditions by Chi squared analysis.

2.4 *In vitro* immunohistochemistry

Immunohistochemistry was firstly performed to detect expression of the perineuronal net on mature neurons in C57Bl cortical cultures. Cultures were fixed with 4% paraformaldehyde (PFA) for 20 min then rinsed with PBS three times for five min per wash. Cultures were subsequently permeabilised with 3% H_2O_2 and 10% methanol in PBS for ten min before washing again with fresh PBS three times. Cultures were kept in blocking solution at 4°C overnight which contained 1% bovine serum albumin, 3% horse serum and 3% donkey serum in 0.3% Triton X-100 in PBS

(PBS-Tx). Cultures were then incubated with mouse anti-NeuN (1:200, Invitrogen) and fluorescein-conjugated *Wisteria floribunda agglutinin* (WFA; 1:1000, Vector Laboratories) to detect the perineuronal net. These were diluted in block solution and maintained overnight at 4°C. Cells were again rinsed three times with 0.3% PBS-Tx and incubated with rabbit Alexa555 anti-mouse (1:500, Invitrogen) for one hour at room temperature with gentle shaking. After rinsing, coverslips were removed from culture wells and mounted onto Colourfrost microscope slides (HD Scientific Supplies) with ProLong Gold with 4',6-diamidino-2-phenylindole (DAPI, Invitrogen).

mDPSC were also assessed for their expression of neural protein markers. mDPSC cultures were fixed either undifferentiated or at day 11 of neuronal differentiation with 4% formaldehyde for 20 min. Cells were rinsed then permeabilised with 3% H_2O_2, 10% methanol in PBS for ten min and subsequently washed three times with PBS for five min per wash. Cultures were blocked at 4°C overnight with 1% bovine serum albumin, 3% horse serum and 3% donkey serum in 0.3% Triton X-100 in PBS (PBS-Tx). Cultures were then incubated with primary antibody diluted in block solution overnight at 4°C. Cells were again rinsed three times with 0.3% PBS-Tx and incubated with secondary antibody for one hour at room temperature with gentle shaking. After rinsing, cultures underwent counterstaining or coverslips were removed from wells and mounted onto slides with ProLong Gold with DAPI (Invitrogen). Images were taken with a Leica SP5 scanning confocal microscope and percentage expression of each marker was determined by manual counts of four representative fields of view.

2.4.1 Antibodies

Table 2.1: List of antibodies

Primary Antibodies				
Name	Raised in	Working concentration	Company	Catalogue number
Neuronal nuclei (NeuN)	Mouse	1:200	Invitrogen	MAB377
Wisteria floribunda agglutinin (WFA) - fluorescein conjugated	Plant Lectin	1:1000	Vector Laboratories	FL-1351
Nestin	Rabbit	1:500	Abcam	AB5968
ßIII-tubulin	Mouse	1:500	Millipore	MAB1637
Neurofilament-Medium chain (NFM)	Mouse	1:500	Zymed	13-0700
Glial fibrillary acidic protein (GFAP)	Rabbit	1:1000	Dako	Z0334
S100	Mouse	1:500	Chemicon	MAB079
Connexin 43 (Cx43)	Rabbit	1:1000	Invitrogen	71-0700
Tyrosine Hydroxylase (TH)	Rabbit	1:500	Chemicon	AB152
GAD65/67	Rabbit	1:500	DAKO	AB1511
Choline-Acetyltransferase (ChAT)	Mouse	1:500	Biosensis	R043100
Vesicular Glutamate Transporter2 (vGlut2)	Rabbit	1:500	Synaptic Systems	135403
Secondary Antibodies				
Name	Raided against	Working concentration	Company	Catalogue number
Alexa555	Mouse	1:500	Invitrogen	A31570
Cy3	Rabbit	1:500	Jackson	115-175-146
Cy3-Streptavidin labelled	Biotin	1:500	Vector Laboratories	016-160-084

Non-specific fluorescence was determined by applying each secondary antibody alone, omitting primary antibody.

2.5 Transmission electron microscopy (TEM)

mDPSC were imaged with TEM to gain an understanding of the ultrastructure of undifferentiated cells. To prepare samples, $3x10^6$ undifferentiated mDPSC were liberated with trypsin from two T75 flasks and centrifuged at 2000g for two min. Cells were resuspended in 1.5 mL 1.25% gluteraldehyde and 4% paraformaldehyde (EM fixative) and stored at 4°C for 24 hours. All subsequent preparation was performed in a fume hood. Cells were washed with 4% sucrose in PBS for five min, then post fixed in 2% osmium tetroxide for 45 min. Cells were next dehydrated by serial incubations with 70%, 90%, 95% and 100% ethanol, then incubated in propylene oxide for 20 min. A 1:1 mixture of propylene oxide:resin was applied for one hour then 100% resin, 2x one hour. Cells were then embedded in fresh 100% resin and polymerized at 70°C for 24 hours.

The resin mixture was made of 10 mL Procure 812, 6 mL Araldite 502, 22 mL DDSA and 560 µL DMP-30. Ultrathin sections were taken and imaged on a Philips CM100 TEM.

2.6 Electrophysiology

2.6.1 Whole cell patch clamp analysis

Whole-cell voltage clamp analysis of DPSC was performed at room temperature using a computer-based amplifier (EPC-9, HEKA Electronics, Germany) and PULSE software (HEKA Elektronik, Lambrecht/Pfalz, Germany). Patch pipettes were pulled from borosilicate glass and fire-polished with resistance ranging from 3 to 6 MΩ. Internal pipette solution contained 135 mM Cs-Glutamine, 5mM $CaCl_2$, 5mM $MgCl_2$, 10mM HEPES, 200µM GTP, 5mM ATP, 10mM EGTA and pH adjusted to 7.3 with NaOH. The calculated internal free Ca^{2+} concentration was approximately 100 nM. A standard bath solution with 10 mM $CaCl_2$, 140 mM NaCl, 4 mM CsGlut, 2 mM $MgCl_2$, 10 mM HEPES, adjusted to pH 7.4 was used. Cells with a neuronal morphology with long bipolar or multipolar neurites were targeted. Holding potential was set at -60 mV and 500 ms voltage steps ranging between -40 and 50 mV were applied in 10 mV increments to record membrane currents. Cells were interrogated for evidence of voltage-gated Na^+, Ca^{2+} and K^+ currents as well as sensitivity to 100 nM tetrodotoxin (TTX) and 10 mM Ba^{2+} to block or enhance currents through Na^+ and Ca^{2+} channels, respectively. To record K^+ currents, CsGlut in the internal solution and CsCl in the bath solution were replaced with KGlut and KCl, respectively. Pharmacological agents were introduced through a gravity-fed perfusion system. The capacitance of each cell was measured using automatic capacitance compensation routine of EPC-9 amplifier. Series resistance did not exceed 20 MΩ and was not compensated for.

2.6.2 Neurobiotin and Lucifer yellow injection

2% neurobiotin and 10 µg/mL Lucifer yellow was injected into clustered mDPSC with neuronal morphology by whole cell patch clamp technique. Lucifer yellow, alone, was injected into clustered hDPSC with neuronal morphology. A patch was maintained with the target cells for five minutes to allow the internal pipette solution to diffuse into the patched and surrounding connected cells. Cells were immediately imaged with an epifluorescent microscope to visualize Lucifer yellow and then mDPSC fixed with 4% PFA for 20 min prior to IHC staining with neurobiotin and DAPI. Cultures were washed with PBS, permeabilised with 0.3% PBS-Tx then

counterstained with Cy3-labeled Streptavidin. Cells were imaged on a Zeiss AxioImager Z1 ApoTome microscope.

2.6.3 Microelectrode Arrays

2.6.3.1 MCS MEAs

Commercial MEAs were sourced from Multi Channel Systems (MCS, Reutlingen, Germany). They consisted of 59 active electrodes arranged in an 8 x 8 grid, minus the corner electrodes (Figure 2.7). Electrodes were numbered 1 to 8, horizontally and vertically, such that the top left hand corner position was 11 and the top right 18. Electrode 82 is labeled in Figure 2.x to indicate the numbering system. An additional electrode, e15, was used as an internal reference. Two sizes of MCS MEAs were used. The first had 30 µm diameter titanium nitride (TiN) electrodes (MCS30) with platinum recording pads and interconnects that joined each electrode to its corresponding recording pad. The second batch had 10 µm TiN electrodes (MCS10) with transparent ITO recording pads and interconnects. Both MEAs had an inter-electrode distance of 200 µm.

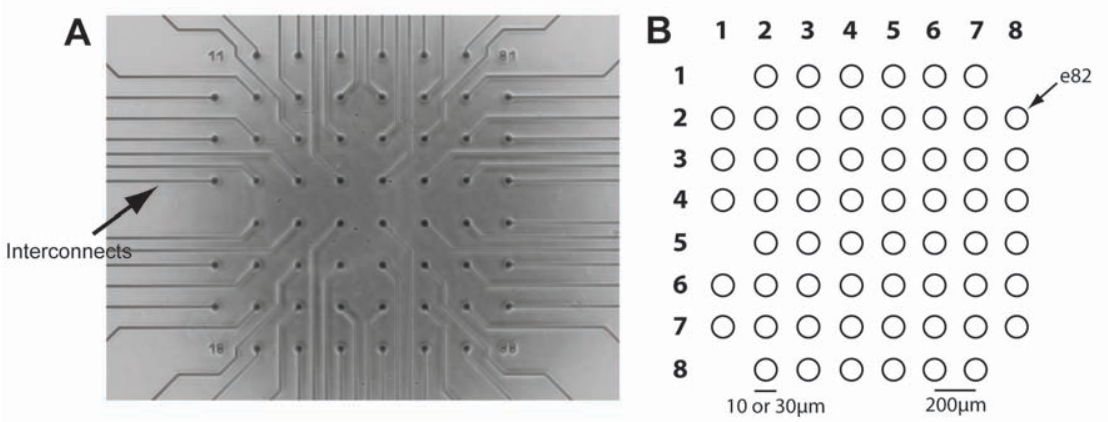

Figure 2.7: The electrode region of the MCS MEA.

A) An image of a MCS30 electrode region showing the electrodes in an 8 x 8 grid arrangement without corner electrodes. Interconnects joining electrodes to recording pads are shown. B) Diagram of MCS MEA electrode region depicting the numbering system. Electrodes were labeled 1-8 horizontally and vertically. Electrodes were numbered with the column number first (eg. Column 8) followed by the row number (eg. Row 2), such as electrode 82, labeled. Two MEA types were used; one with 10 µm electrode diameter and the other with 30 µm electrodes. Each had an inter-electrode spacing of 200 µm.

2.6.3.2 NTT MEAs

Our industrial partner, Nippon Telephone and Telecommunications (NTT) fabricated a novel MEA used as part of this study. A model of the NTT MEA design is shown in Chapter 3; Figure 3.1. A layer of Indium tin oxide (ITO) was deposited onto the silica MEA base and lithographically etched so that only electrodes, pads and interconnects remained (blue regions, Figure 3.1A). ITO was used for its high biocompatibility and transparency. A layer of silicon oxide (SiO_2, red) was deposited over electrodes and recording pads. Finally, a layer of resist was deposited around ITO and SiO_2 regions.

The electrode array consisted of 59 functional electrodes arranged into a three-column grid (Figure 3.1B). Standard electrodes had a diameter of 20 µm, with larger electrodes positioned at the outer corners of the electrode grid 30 µm in diameter. These electrodes were intended for stimulation where a larger electrode size corresponds to lower impedance and less electrical charge loss. Standard inter-electrode distance was 100 µm, up to 400 µm between separated columns. A reference electrode (Figure 3.1C) replaces electrode 15 in the array grid.

2.6.3.3 MEA preparation

MEAs were washed with 0.1% Terg-A-Zyme solution for 4h and rinsed with distilled water six times over 24h. MEAs were then sterilised with 70% ethanol and left to dry under ultraviolet light overnight. A range of coating substrates were applied to the central region of MEAs across different experiments. Most commonly, 50 µL laminin (0.02 mg/mL, Gibco) and poly-l-lysine (PLL, 0.01%, Sigma-Aldrich) solution was applied and allowed to settle for 3h in a humidified incubator to avoid evaporation of the solution. Other substrates used were poly-l-ornithine (PLO, 0.02 mg/mL, Sigma-Aldrich), poly(ethyleneimine) (PEI, 0.05%, Sigma Aldrich) Finally, MEAs were rinsed of excess coating substrate with 3 x PBS washes before plating cells.

2.6.3.4 MEA cell culture

A 20 µL-50 µL droplet containing 20-50,000 cells was added to the electrode region of pre-treated MEAs and kept in a humidified incubator at 37°C with 5% CO_2. mDPSC, hDPSC and cortical cells were used in different experiments. MEAs were sealed with a Teflon membrane lid (MCS) to minimize evaporation and contamination while allowing gas exchange. Cells were allowed to settle for 1h before MEA wells were flooded with either DPSC plating medium or neurobasal medium, depending on the cell type in use. DPSC subsequently underwent neuronal

differentiation as described previously. Half medium changes were made every second day. Cultures were imaged on a Nikon Eclipse inverted microscope to document cell adherence, migration and morphological alterations throughout DPSC differentiation.

2.6.3.5 MEA data acquisition

To record the electrical activity of cultured cells, MEAs were transferred from an incubator to a warmed amplifier stage (MEA1060-Inv with TC02 temperature control, MCS) with pins matching the recording pad layout on MEAs. Cultures were allowed to settle for 30 min to avoid any impact of moving the MEA on its electrical activity. A grounded faraday cage was fitted over the MEA recording system to minimise the impact of environmental noise. MEA cultures were returned to the incubator immediately following data collection.

Signal acquisitions were managed under MC Rack software control (MCS) and sampled at a frequency of 50 Hz. In most cases 3 x 100s recordings were taken on each day of interest. Recording from cortical cells began from day 7 of culture to allow time for cultures to settle and form networks. For DPSC cultures, maturation medium was not applied until day 8 of culture so recordings began from day 9. Electrical activity was assessed a maximum of every 2 days to avoid infection or early cell death due to excess handling and exposure. When available, 10 μM TTX was added to cultures as an end-point to block all Na^+ current and therefore abolish action potentials.

2.6.3.6 MEA electrical stimulation

Two stimulation paradigms were applied to developing DPSC cultures and MEA recordings were taken during the period of stimulation as well as prior to stimulation to determine spontaneous electrical activity. The first voltage stimulation used aimed to promote hDPSC migration toward electrodes and consisted of bipolar pulses lasting 300 μs at each polarity, with amplitude of 200 mV, introduced through seven electrodes simultaneously. A single voltage pulse was applied once per second for three min and repeated three times with five min breaks between stimulations. This stimulation pattern was applied three times daily for three days. Bright field images were taken with a Nikkon Eclipse inverted microscope each day and compared to determine any cell migration.

The second stimulation paradigm was intended to evoke electrical activity from cultured cells. Voltage stimulation was injected by a single electrode by bipolar pulses lasting 300 μs each with an initial amplitude of ±200 mV, increasing my 10 mV increments to 700 mV. Stimulation was

applied twice per second in cultures from day 9 of differentiation and at least every third day or until differentiating cells died.

2.6.3.7 MEA data analysis

MEA data were subsequently analysed offline using Spike2 (v7.09) and Matlab (R2001b) software. A low pass (<4000 Hz) or band pass (250-4000 Hz) filter was applied to all MEA traces prior to analysis. The standard deviation of noise was then calculated for each individual electrode trace and a spike detection threshold set at five times this standard deviation. Only supra-threshold events with a physiologically relevant shape and duration were detected as events according to Spike2 settings and spike shape templates developed and matched to repeating events (template matching requirements; 1:3 width:amplitude ratio, minimum 60% point matches within spike templates, ≥2 matching events to create a template, 20% amplitude change for match). Each event detected was closely scrutinized for reliability. The spike rate, amplitude and duration of differentiated mDPSC events were compared to controls. Only electrodes with two or more events per 100s interval were considered active for analysis purposes.

2.7 Statistical Analysis

All parametric data was assessed using an Analysis of Variance (ANOVA) followed by Tukey's post hoc tests or an unpaired student's t-test (2 groups) with Sidak post hoc analysis. Non-parametric data was analysed by a Kruskall Wallis ANOVA followed by Dunn's multiple comparisons test. Column data is presented as mean ± standard error of mean (SEM). Boxplots represent the first to third quartiles of population distributions with 5-95 percentile whiskers. An alpha value of $p<0.05$ was considered significant.

Chapter 3: Characterisation of a novel microelectrode array design

Statement of Authorship

Title of Chapter

Characterisation of a novel microelectrode array design

Traditional thesis chapter

Kylie M. Ellis (Candidate)

Experimental design, design of novel microelectrode arrays, correspondence with industry partner NTT, performed all experiments, collected, analysed and interpreted all data, wrote manuscript.

I hereby certify that the statement of contribution is accurate

Signed Date

Simon A Koblar (Co-author)

Experimental conceptualisation and design, initiation of industry collaboration, supervision of work, financial support.

I hereby certify that the statement of contribution is accurate and I give permission for the inclusion of the chapter in the thesis.

Signed Date

Martin D. Lewis (Co-author)

Experimental conceptualisation and design, initiation of industry collaboration, supervision of work, financial support.

I hereby certify that the statement of contribution is accurate and I give permission for the inclusion of the chapter in the thesis.

Signed Date

David C. O'Carroll (Co-author)

Experimental conceptualisation and design, initiation of industry collaboration, supervision of work, considerable ongoing concept development, provided expertise for data analysis, financial support, manuscript review.

I hereby certify that the statement of contribution is accurate and I give permission for the inclusion of the chapter in the thesis.

Signed Date

Chapter 3 Context Statement:

This project began with an industrial collaborator, Nippon Telegraph and Telecommunications (NTT, Japan), whose expertise in microelectrode array (MEA) fabrication presented the opportunity to design and develop custom arrays for *in vitro* models of implantation settings. Should the *in vitro* MEAs prove successful for our applications, this partnership was to support the fabrication of other MEAs with possible alternate custom designs. Long-term aims were to develop small planar MEAs suitable for *in vivo* implantation.

I worked with NTT to design and fabricate the MEAs presented in this chapter. The electrode array region was large compared with typical commercial MEAs, which was designed for the potential of monitoring cell migration and integration over the extended distance. The MEAs were compatible with a commercially available system and temperature-controlled mounting stage using materials that had previously been employed successfully at NTT (Nyberg, et al., 2007; Shimada, et al., 2009).

The aim of these NTT MEAs was firstly to approximate cortical neuronal cell chemoattraction and functional integration with dental pulp stem cells. Prior to performing these experiments it was necessary to characterise the properties of the MEAs to ensure they were appropriate for our intended use of detecting cortical and stem cell-derived neuronal electrical activity.

Notably, MEAs used in NTT laboratories typically have their electrodes coated with a PEDOT-PSS [or poly(3,4-ethylenedioxythiophene) poly(styrenesulfonate)] conductive polymer layer that increases the surface area of electrodes. The polymer layer is also considered to be more biocompatible than ITO alone. Unfortunately, we did not have access to the polymer coating process in our Australian laboratory so were forced to approach the technique without it. This was an avenue dedicated to future studies using these arrays, however our collaboration with NTT was interrupted by the earthquake and subsequent nuclear reactor disaster in Japan in 2010, which put financial pressure on NTT and meant that the polymer addition could not be pursued in a reasonable timeline for this study.

The following chapter therefore presents the characterisation of NTT MEAs, considering their biocompatibility and electrical signal detection capacity in their raw state.

3.1 Introduction

Microelectrode arrays (MEAs) provide a valuable tool for detecting electrical activity of cultured cells *in vitro* as well as the potential for monitoring or stimulating electrical activity *in vivo*. *In vitro*, planar MEAs can monitor developing cell cultures over an extended period of time to gain complex network information without damaging cells.

In neuroscience, the primary role of planar MEAs *in vitro* is to detect the impact of pharmacological agents on cultured neurons or to monitor the developing electrical activity of neurally differentiated stem cells (Ban, et al., 2007; Heikkiä, et al., 2009; Illes, et al., 2007; Shimada, et al., 2009). Therefore biocompatibility as well as efficient signal transduction are of primary importance to successful MEA function.

NTT is one of a small number of companies worldwide producing MEAs for research and practical applications. NTT MEAs have been demonstrated to successfully support long term cultures of primary cortical neurons and differentiated neural stem cells to support long term culture with early bursting activity and more mature spontaneous electrical activity (Furukawa, et al., 2013; Shimada, et al., 2009). Our collaboration with NTT has allowed for the design and fabrication of a novel MEA for specific *in vitro* applications. In contrast to the typical MEA design that consists of a single high density grid of electrodes, the electrode array of these novel NTT MEAs contains separated regions of high density electrodes. This electrode design can broaden the potential applications of the arrays as it provides a larger area for electrical monitoring as well as allowing investigation into cell migration of spatially separated cells and their electrical integration.

This study aims to characterise the electrical properties of the newly designed MEA and to determine its biocompatibility with cortical neurons. Biocompatibility in this study is defined as the survival of cell cultures with expected neuronal morphology on MEAs. Other molecular measures of biocompatibility, such as glial cell activation, were not able to be measured due to the damage it would cause the limited NTT MEAs available, but would be a valuable extension of this work. We seek proof of principle that NTT MEAs can be used to monitor the electrical activity of cultured cortical cells to be used for future *in vitro* models.

3.2 Methods

3.2.1 NTT MEA design

Our industrial partner, NTT fabricated the MEAs used in this study. A model of the NTT MEA design is shown in Figure 3.1 and specifications are detailed in Chapter 2 (Section 2.6.3.2). The electrode array consisted of 59 indium tin oxide (ITO) electrodes arranged into a three-column grid (Figure 3.1B). Standard electrodes had a diameter of 20 µm, with larger electrodes positioned at the outer corners of the electrode grid (30 µm in diameter). These electrodes were intended for stimulation as larger electrode sizes incur lower impedance, which improves the transduction of electrical signal. Standard inter-electrode distance was 100 µm, up to 400 µm between separated columns. A reference electrode (Figure 3.1C) replaces electrode 15 in the array grid. In the present study, two MEAs were characterized, NTT1 and NTT2.

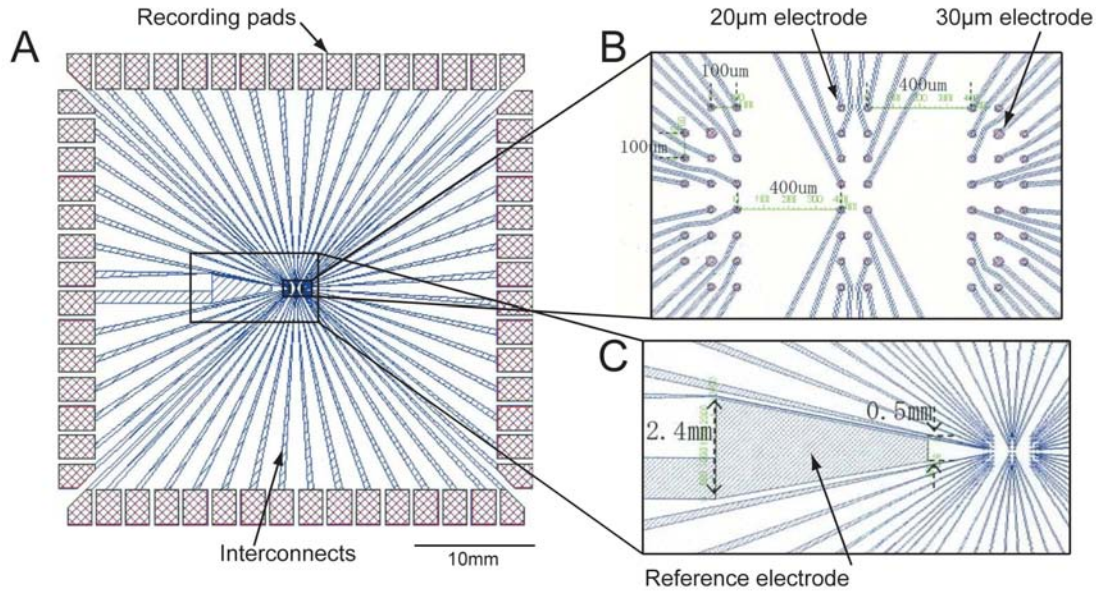

Figure 3.1: Diagram of the NTT MEA design.

A) The scale of the entire MEA. A base coat of ITO composes recording pads, electrode and interconnects (blue) followed by a layer of SiO_2 over recording pads and electrodes. B) The electrode array region of the NTT MEA. C) The reference electrode for electrical scaling.

3.2.2 MultiChannel Systems MEAs

Standard research-quality MEAs sourced from MultiChannel Systems (MCS, Reutlingen, Germany) were compared as control arrays. Two varieties were assessed; the first contained 30 µm diameter titanium nitride (TiN) electrodes (a material that has been widely applied in previous applications (Potter & DeMarse, 2001)) with 30 µm diameter and 200 µm inter-electrode distance, the second had 10 µm TiN electrodes and a 200 µm inter-electrode distance. These MEAs were labelled *MCS 30* and *MCS 10*, respectively. All MEAs were assessed in parallel and handled according to the same methods.

3.2.3 MEA preparation

To promote sterility and cell adhesion MEAs were washed with 0.1% Terg-A-Zyme solution for 4h and rinsed with distilled water six times over 24h. MEAs were then sterilised with 70% ethanol and left to dry under ultraviolet light overnight. 50 µL laminin (0.02 mg/mL) and poly-l-lysine (PLL) (0.01%) solution was subsequently applied to the central electrode region of MEAs and allowed to settle for 3h in a humidified incubator to avoid evaporation of the solution. Finally, MEAs were rinsed of excess coating substrate with 3 x PBS washes.

3.2.4 Murine cortical cultures

Embryonic day 18 C57Bl mice were euthanised by decapitation and cortical explants digested with 10 µg/mL DNase and 0.15% trypsin for 20 min. The resulting cell solution was sieved and centrifuged for enzyme removal. Cells were resuspended in Neurobasal medium and plated at a density of 50,000 cells in a 50 µL droplet to the electrode region of MEAs. Cells were allowed to settle for 1h and MEA wells subsequently flooded with cortical medium, containing Neurobasal medium with 1x B27 and N2 supplements, 1x GlutaMAX, 50 U/mL penicillin, 50 µg/mL streptomycin and 10 ng/mL FGF-2 (mouse). Half medium changes were made every second day. Cultures were imaged on a Nikon Eclipse inverted microscope to document cell adherence, migration and morphological differentiation. Biocompatibility of cultured cortical cells with MEAs was determined visually by measurement of cell adherence and survival as our limited availability of MEAs restricted our ability to measure other forms of biocompatibility such as glial cell activiation.

3.2.5 MEA electrophysiological recording

To assess neuronal responses during different stages of development MEAs were transferred to a mounting stage warmed to 37°C and attached to an amplifier (MultiChannel Systems, Germany). Cultures were allowed to settle for 30 min prior to recording. Three x 100s recordings were taken of each MEA on day 7, 11 and 14 after cell plating with at least 5 min between subsequent recordings to assess neuronal responses during different developmental stages. After control recordings were taken at day 14, 10 μM tetrodotoxin (TTX) was added to cultures to block sodium currents and therefore all electrical activity. 3 x 100s recordings of electrical activity repeated. Electrophysiology traces were analysed offline with Spike2 and MATLAB software.

3.2.6 Offline analysis of electrical activity

First low pass (<4000 Hz), then band pass (250-4000 Hz) filters were applied to preliminary NTT MEA traces to determine the most effective protocol for enhancing the signal-to-noise ratio. Band pass filtering was found to be more effective at removing noise signals so was applied to all electrode traces prior to analysis. A threshold of spike detection was set at five times the standard deviation of noise of each individual electrode using Spike2 7.09 software. Detected events were closely scrutinised for accuracy. Whole-MEA spike rate and the average amplitude of individual spike templates were determined with the use of MATLAB R2001b software.

3.2.7 Statistical analyses

Ungrouped data were analysed by one-way ANOVA followed by Tukey's post hoc tests for multiple comparisons or multiple t-tests with a Sidak post hoc tests. Grouped data were analysed with two-way ANOVA and Tukey's post hoc tests. Non-parametric data was analysed using Kruskal-Wallis tests followed by individual Dunn's multiple comparisons tests. Column graphs are represented as mean ± SEM and boxplots represent the first to third quartiles of population distribution with 5-95 percentile whiskers. Outliers are identified as individual dots.

3.3 Results

3.3.1 NTT-MEA biocompatibility

Cortical cells, comprising a mixture of neurons and glia, were successfully dissociated and plated onto NTT-MEAs. The biocompatibility of the MEAs was high, with cortical cells readily adhering to the laminin and PLL-coated MEA surface for 14 days and, importantly, many remained in direct contact with electrodes. Qualitatively, cells in the vicinity of electrode material appeared similar in health and density to those at other parts of the culture. Furthermore, cortical neural cells were found to proliferate and migrate on the MEAs over time (Figure 3.2). Commercial MCS 30 and MCS 10 MEAs also supported similar long term biocompatibility with cortical neurons (See Figure 3.4).

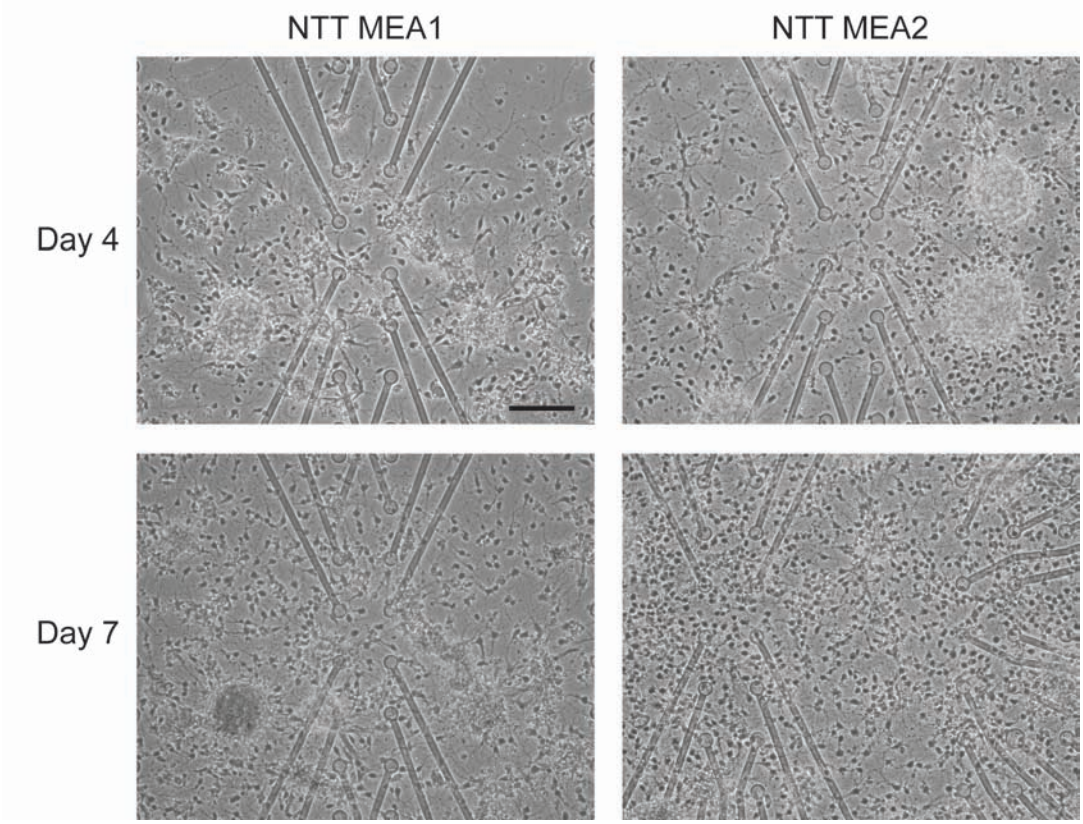

Figure 3.2: Biocompatibility and cortical cell migration on NTT MEAs.

Representative phase contrast images of dissociated cortical cells on two NTT MEAs showing strong adherence, survival and migration between days 4 and 7 of culture. Scale bar = 100 µm.

3.3.2 Cortical electrophysiology

Electrical traces obtained from MEAs first required digital filtering due to large noise artifacts. The spectral power density of 100s raw traces of an NTT MEA revealed a sharp peak at 50 Hz that was consistent across three spatially distinct electrodes on the array (Figure 3.3A). For this reason we experimented with different filters to eliminate the noise artifact (Figure 3.3B). The 'raw' trace shows a clear periodic noise pattern (period 20 ms consistent with 50 Hz electrical interference despite our attempts to ground both the recording apparatus and shielding it with a Faraday cage [see Methods]) that reflects sinusoid noise interference only observed from NTT MEAs and not MCS MEAs. The effectiveness of our band pass filtering (cutoff 250-4000 Hz) is illustrated by third trace in Fig 3.3B. A supathreshold event that was not previously evident in the raw or low pass filtered (<4000 Hz) trace. Henceforth all electrode output was band pass filtered prior to analysis to eliminate this noise artifact.

Having established the high biocompatibility of NTT MEAs and ideal pre-analysis treatment of data, their efficiency in detecting cortical neuronal activity was compared to that of the commonly used MCS MEAs. Phase contrast images of the central region of cortical-MEA cultures 7 days after plating in Figure 3.4 demonstrate that all MEA types were seeded at a similar density and also highlight the differences in electrode size and material. Extracellularly recorded single electrode activity traces taken at days 11 (top trace) and 14 (middle trace) are also depicted and a control recording taken at d14 following 10 μM TTX addition also (bottom trace). Semi-regular bursting activity was observed at day 11 on the MCS 30 (Figure 3.4A) and MCS 10 (Figure 3.4B) MEAs, which is typical of developing neuronal networks (Chiappalone, et al., 2006; James, et al., 2004; Van Pelt, et al., 2004).

By day 14 the individual activity patterns of different recorded cells showed more diversity. On MCS 30 more regular firing was detected but at a lower spike amplitude, whereas on MCS 10, less regular bursting of greater amplitude was evident. Both conditions could represent an alteration in electrode-cell coupling as a result of cell migration or network maturation as described previously in the literature (Chiappalone, et al., 2007). The activity on both MEAs is abolished with the addition of 10 μM TTX (bottom trace). In comparison, it is difficult to determine any clear spiking activity from the NTT MEA electrode traces either before or after TTX application (Figure 3.4C).

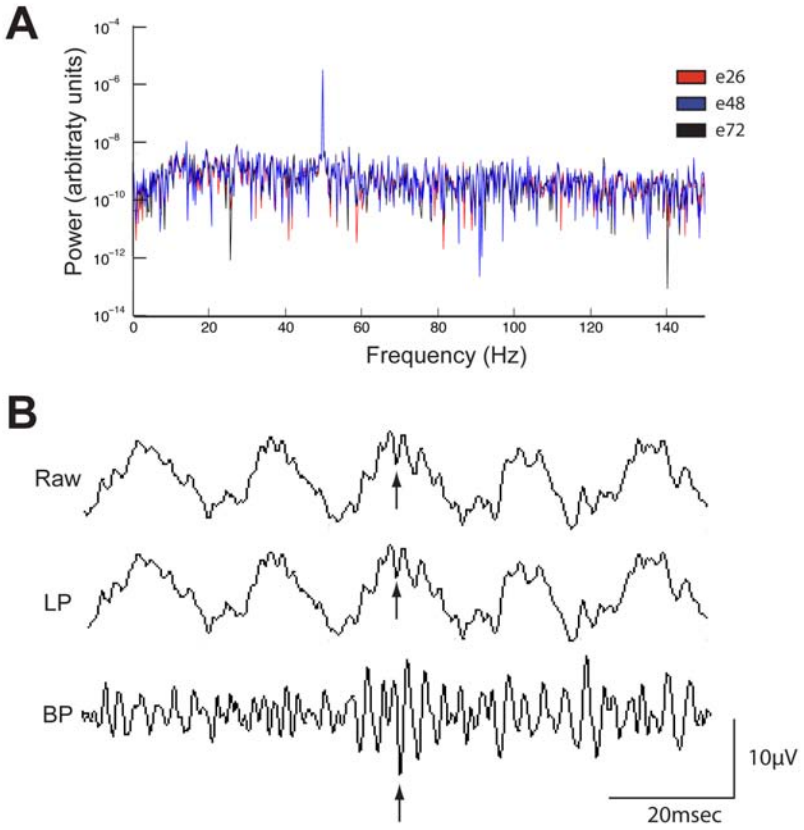

Figure 3.3: Filtering NTT MEA trace data.

A) Spectral power density of three raw NTT MEA electrodes traces (blue, red, black) showing a frequency peak at 50 Hz. B) A representative 100 ms trace from a NTT MEA electrode in its raw form and following low pass (LP, <4000 Hz) and band pass (BP, 250-4000 Hz) filtering. The arrow indicates a suprathreshold event detected by Spike2 analysis in the BP trace that was not detected in the raw or LP filtered states.

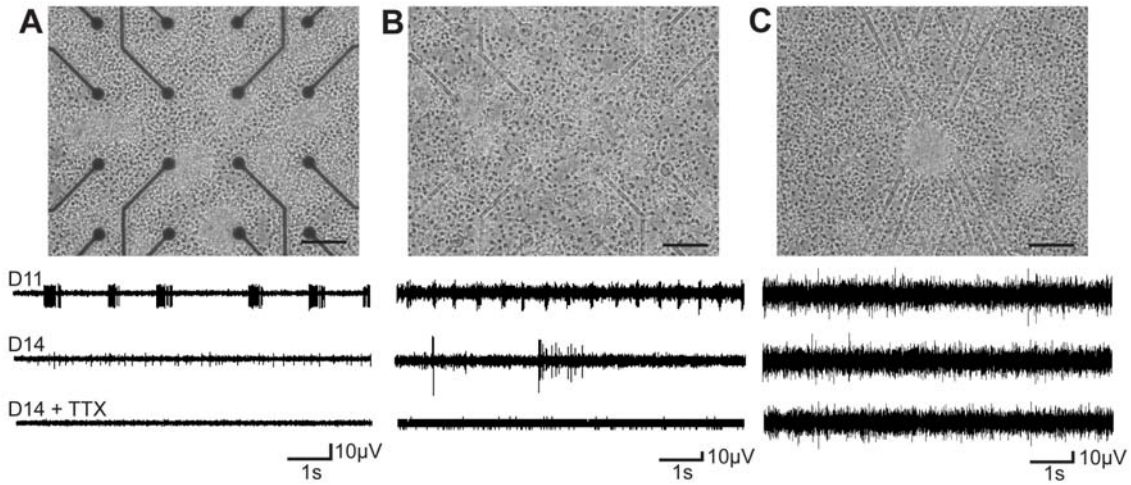

Figure 3.4: Cortical electrical activity detected from three classes of MEAs.

Phase contrast images of the central region of cortical MEA cultures seven days after plating and representative single electrode activity traces at day 11 (top trace), day 14 (middle trace) and at day 14 with 10 μM TTX (bottom trace). A) MCS 30 MEA. B) MCS 10. C) NTT1. Scale bars = 100 μm. Note that voltage scales are not equivalent across conditions.

The single electrode traces in Figure 3.4 identify a distinction between baseline noise levels across the MEA types. Calculations of the standard deviation of noise (SD noise) were taken at day 11 of culture following TTX administration to ensure that spiking activity did not confound the average noise level measured. This confirmed that MCS 30 TiN electrodes has the lowest baseline noise level (SD noise = 1.44 ± 0.01 μV, Figure 3.5), which was significantly higher for the smaller MCS 10 electrode traces (SD noise = 2.52 ± .04 μV, $p<0.0001$), as would be expected considering its higher impedance. However, the baseline noise from NTT MEAs was far greater at 10.35 ± 0.26 μV (NTT1, $p<0.0001$) and 19.53 ± 0.19 μV ($p<0.0001$), which has functional consequences for the threshold at which spike detection is set, and therefore their ability to detect action potentials, particularly the small spikes associated with distant neurons.

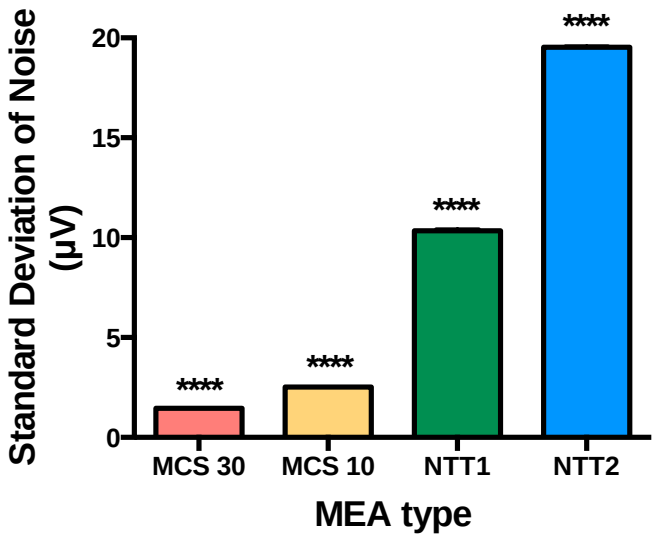

Figure 3.5: Baseline noise of MEAs.

The SD of baseline noise for each MEA type measured across eight electrodes after TTX addition to ensure electrical activity of cultured cells did not influence noise levels. The SD of baseline noise is significantly different between each MEA type (****$p<0.0001$).

As mentioned previously, each NTT MEA contained four electrodes designed for stimulation, which had diameters of 30 μm rather than the normal 20 μm. Since we can both record and simulate via any electrode, this allowed us to further evaluate whether the use of a larger electrode pad would have alleviated the electrode noise due to electrode impedance. However, no difference was found between the SD of noise between 20 μm and 30 μm electrodes on both NTT1 (Figure 3.6A) and NTT2 (Figure 3.6B). However, there was a slight but significant decrease in SD noise measured on MEA NTT1 following TTX administration on 20 μm and 30 μm electrodes ($p<0.001$, Figure 3.6A), suggesting that some of the observed noise may have been due to electrical activity within the culture.

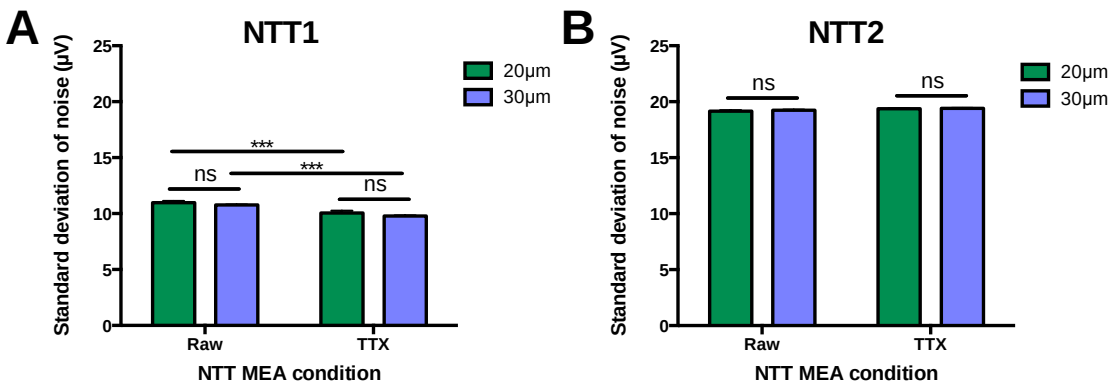

Figure 3.6: Baseline noise of NTT MEA electrodes of different diameters.

No difference in the baseline SD noise measured from electrodes with 20 µm or 30 µm diameter was measured on A) NTT1 or B) NTT2 prior to or following TTX administration. SD noise was slightly but significantly attenuated on 20 µm and 30 µm electrodes following TTX administration on NTT1 ($p<0.001$) but not NTT2. (***$p<0.001$) (n=4 each group).

3.3.4 Spike rate and amplitude

MEA-wide spike rate was greatly reduced in both NTT-MEAs compared to MCS MEAs (Figure 3.7A). The bursting and regular firing of MCS 30 and MCS 10 MEAs accounted for high but variable spike rates of 6368 ± 5956 (n=4 days) and 3178 ± 2005 (n=4 days) within a 100s period, respectively (Figure 3.7A). NTT-MEAs each supported significantly lower spike rates of 62.67 ± 38.40 (NTT1, n=3, $p<0.05$) and 162.5 ± 71.20 (NTT2, n=4), which relates directly to the high threshold of spike detection due to their large baseline noise levels. Spike rate was measured across four days accounting for the high variability of activity measured, particularly on the commercial MEAs with high maximum spike rates.

The average amplitude of each spike template measured from 3 x 100s traces was significantly different between each MEA type ($p<0.0001$, Figure 3.7B) using the automated noise baseline threshold criterion (5 x SD noise). We were able to detect smaller events on MCS 30 than other MEAs with an average of 13.76 ± 6.95 µV ($p<0.0001$, n=143). MCS 10 spikes had a significantly greater average amplitude of 27.34 ± 3.37 µV ($p<0.0001$, n=143). Both measures are within the regular range of extracellularly recorded action potentials. By comparison, the average amplitude of detected events from NTT MEAs were significantly larger at 56.64 ± 2.59 µV (NTT1, $p<0.0001$, n=161) and 100.7 ± 9.82 µV (NTT2, $p<0.0001$, n=182) which are notably large events

from a physiological perspective. This demonstrates the inability of NTT MEAs to detect small or distant action potentials due to the high baseline noise of the electrodes and subsequently high threshold of event detection.

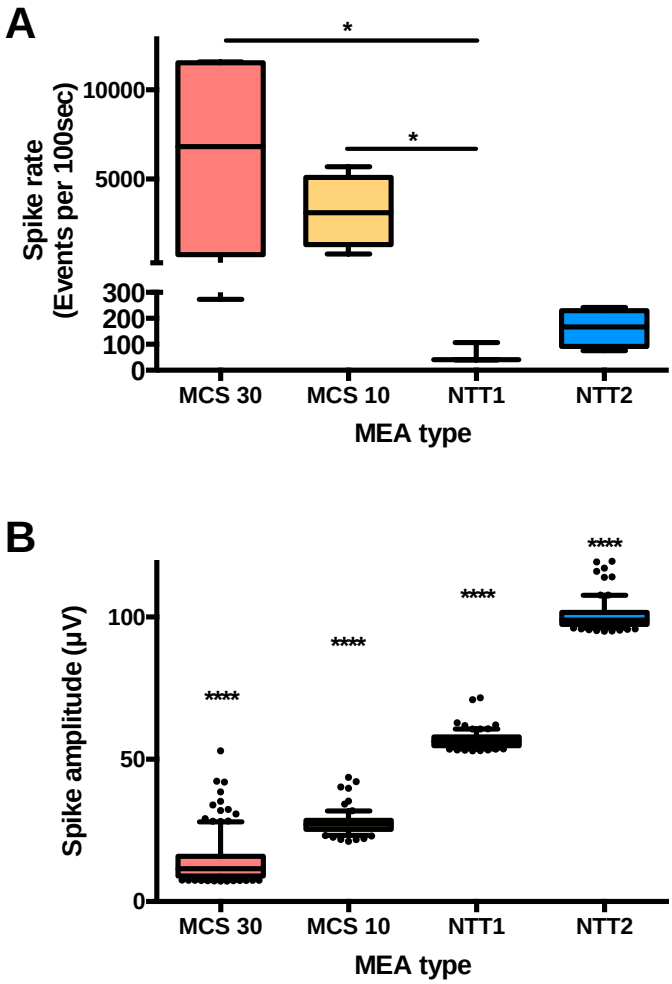

Figure 3.7: Spike rate and amplitude of detected events.

Boxplots with 5-95 percentile whiskers of A) MEA-wide spike rate across three days within a 100s period (n=4) and B) the average amplitude of each spike template measured across 3 x 100s recordings (MCS 30, n=263; MCS 10, n=143; NTT1, n=161, NTT2, n=182) (*p<0.05, ****p<0.0001).

Individual events detected by Spike2 analysis were closely scrutinised for reliability. Interestingly, on commercial MEAs, many electrodes showed high spike rate with some evidence of bursting activity (Figure 3.8A). In contrast, events detected on NTT MEAs often occurred at the same time point on each electrode, creating a vertical alignment of raster points as seen in Figure 3.8B. Closer inspection of these events revealed synchronous noise pattern across all electrodes, three of which are depicted in Figure 3.8C. This demonstrated that the events detected by Spike 2 software in Figure 3.8B were actually rare points of high noise that crossed the threshold of detection rather than array-wide action potentials.

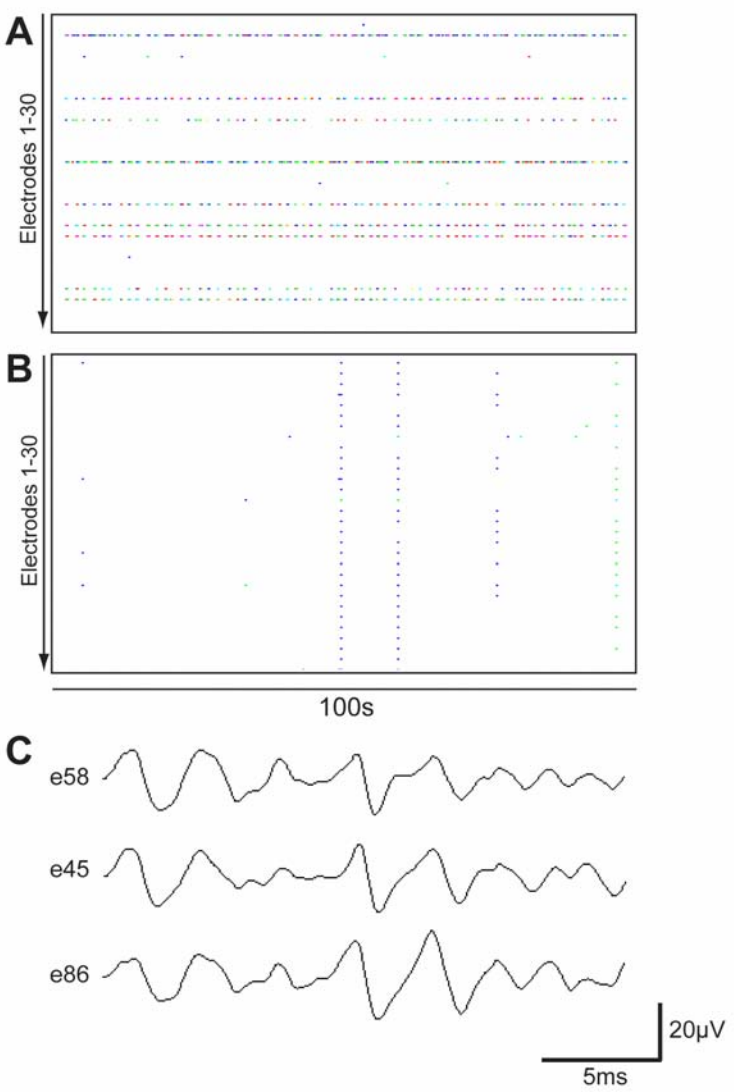

Figure 3.8: Noise pattern synchrony across NTT MEA electrodes.

Raster plot showing timing of detected events from A) MCS 30 and B) NTT1. Colours represent individual spike templates C) Detail from three electrodes showing synchronous noise patterns observed across the entire NTT electrode array.

3.3.5 Effect of TTX on MEA activity

Finally, 10 μM TTX was administered to cortical MEA cultures at day 14 to determine whether detected spikes were real action potentials or electrical artifacts. The high spike rate of MCS 30 and MCS 10 was immediately blocked by TTX administration, falling significantly to a baseline level of approximately 35 spikes per 100s (Figure 3.9A). This reduction was statistically significant for MCS 30 only ($p<0.05$) due to the high variability of spike rate of cultures. However, the effect of spike rate reduction was high for both cultures (MCS 30: Cohen's $d=1.501$; MCS 10: Cohen's $d=2.215$). In contrast, the spike rate of NTT MEAs did not significantly alter following TTX addition, indicating that the events detected were not sodium-dependent action potentials. It is interesting to note that although we measured a slight decrease in the standard deviation of noise on NTT1 following TTX administration in Figure 3.6, which indicated some electrical activity of cultured cells, this did not translate to an alteration in TTX-dependent supra-threshold event detection. Therefore, while there may have been electrical activity of cultured cells, this could not be reliably detected using standard threshold methods based on noise.

The amplitude of detected events following 10 μM TTX administration was also measured. There was a significant reduction of spike amplitude following TTX addition on MCS 30 ($p<0.001$, Figure 3.9B) and MCS 10 ($p<0.0001$), as would be expected due to the abolishment of large action potential spikes. Interestingly, spike amplitude on NTT1 also showed a significant reduction ($p<0.0001$), however event amplitudes remained constant on NTT2.

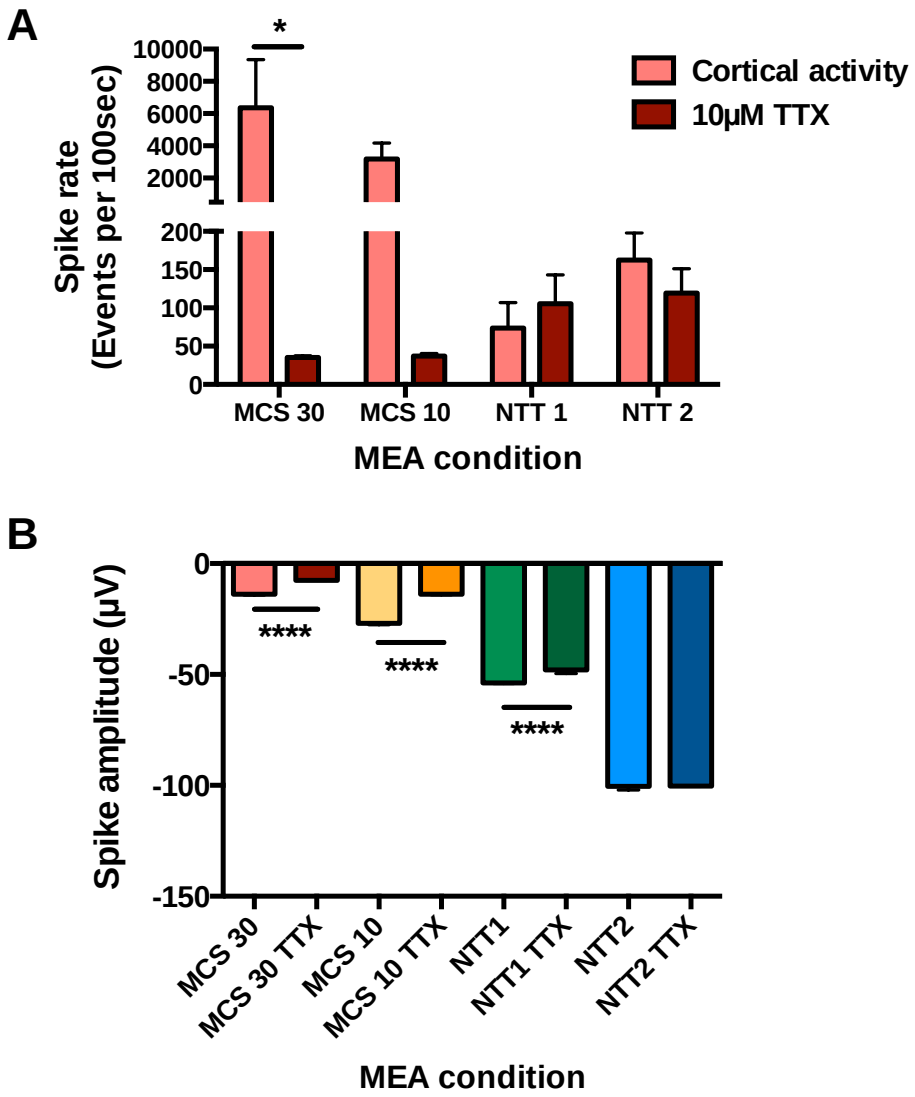

Figure 3.9: Effect of TTX on spike rate and amplitude.

A) 10 µM TTX administration reduces spike rate of MCS 30 and MCS 10 but not NTT MEAs (n=2-4 each group). B) TTX reduces spike amplitude of events detected from MCS 30 (n=263; TTX, n=61), MCS 10 (n=62; TTX, n=59) and NTT1 (n=127; TTX, n=67) MEAs but not the NTT2 MEA (n=105; TTX, n=117) (****p<0.0001).

3.4 Discussion

Characterisation of the novel NTT MEAs with cortical neuronal cultures throughout this chapter has demonstrated a high cell biocompatibility through culture adherence and survival, however it has also identified limitations in terms of their ability to detect the functional activity of cultured neurons. Electrical activity from cortical cultures plated on commercial MEAs was robustly detected whereas the high baseline noise of NTT MEA electrodes obscured the detection of any action potentials present in the culture.

As the NTT MEAs demonstrated good culture adherence and survival and cultures appeared morphologically analogous to those on the commercial MEAs, it is likely that these cortical cells were active at a similar level. However, no spontaneous action potentials or bursting activity was detected as is routinely observed with developing neural networks (Nyberg, et al., 2007; Potter & DeMarse, 2001; Shimada, et al., 2009). The reason for this becomes clear when comparing the spike amplitude of detected action potentials on commercial MEAs with the traces from the NTT MEAs. In most cases, the baseline noise level of NTT MEA traces exceeded the regular action potential amplitudes from commercial MEAs. This indicates that many regular action potentials were likely to be present but undetected due to the high baseline noise level from NTT MEAs.

We must consider the impedance tradeoff when interpreting the signal-to-noise ratio of these electrodes. Generally, a large electrode will have lower impedance than a smaller one, which effectively reduces its baseline noise level. However, the tradeoff occurs as the smaller electrode will measure a larger voltage for the same given current. Practically, this means that at an equal distance from a spiking neuron, a MCS10 electrode will record an event with larger amplitude than a MCS 30 electrode, however it will also incur greater noise associated with the smaller electrode. This could partly explain why such large spikes were detected on MCS 10 in Figure 3.4B. Furthermore, a larger electrode has the ability to detect signals from a greater region simultaneously, provided the signal can be appropriately amplified. As such, the optimal electrode size is a balance between the specificity of a signal versus its strength. It would follow that electrodes of the same material but with differing sizes would incur a proportional difference in baseline noise, as we saw between MCS 10 and MCS 30 electrodes, both made of titanium nitride. However, we unexpectedly measured no distinction in baseline noise between indium tin oxide NTT MEA electrodes with a diameter of 20 µm or 30 µm within the same array. This suggests that electrode material had a far greater role in influencing electrode impedance than their size in this case and the larger electrodes designed for stimulation were not successful in

reducing impedance as was predicted. The TiN material of the MCS arrays acts to increase the active surface area of electrodes by forming a microcollumn surface structure and thereby reducing electrode impedance and noise levels (Stett, et al., 2003; Zhou & Greenberg, 2003) and presents as more successful for signal transduction than ITO alone. However, the addition of other materials, such as polymers, to increase the surface area of ITO electrodes may have a similar effect of reducing impedance at the same time as increasing cell biocompatibility (Nyberg, et al., 2007; Shimada, et al., 2009).

Interestingly, the average noise of the two NTT MEAs sampled in this chapter was quite distinct. While both were significantly higher than commercial MEAs, the NTT2 SD noise was almost twice that of NTT1. This was an unexpected observation considering the MEAs were fabricated with the same specifications and at the same time. They had also undergone identical pre-treatment in the laboratory. In contrast, baseline noise of commercial MCS MEAs was constant across MEAs with the same electrode diameter (data not shown), although there were slight variations between individual electrodes within an array. This may be an inconsistent limitation of the electrode material used for the NTT MEAs and must be noted for future studies. This variation is possibly due to differences in the ITO etching processing and subsequent surface roughness, even though they appear physically identical. It is possible to confirm this through scanning electron microscopic imaging of the surface properties, however our priority has been to maintain the MEAs for further experimentation.

The spike rate and event amplitude measured across MEAs in this study was, in part, a product of baseline noise. MEA-wide spike rate was high for MCS 30 and MCS 10 MEAs as their lower baseline noise allowed for a lower threshold for detection, which in turn allowed a higher proportion of action potentials to be detected. In addition, a lower threshold of detection allowed for spikes with smaller amplitudes to be measured, contributing to the lower average amplitude of events measured from MCS 30 and proportionally larger amplitudes from MCS 10. As a result, a similar upper range of action potential amplitude is detected on both commercial MEAs, however the MCS 30 electrodes detect a greater proportion of lower-amplitude events contributing to overall lower average spike amplitude. In contrast, and as previously discussed, the high baseline noise of NTT MEAs obscured the detection of action potentials, as the threshold for detection was too high as a result. The impact of this is therefore a lower overall spike rate on NTT MEAs. However, those events that do surpass the detection threshold, often noise artifacts, are very large, causing the large average spike amplitude measured in this study. Instinctively, the average amplitude of detected events increased with greater baseline noise levels.

As expected, the detected events and amplitudes of commercial MEAs was reduced to tonic artifact activity rates following TTX administration and levels were similar for both MCS 10 and MCS 30 arrays with a large effect size. There was no such decease in spike rate associated with TTX administration with either NTT-MEA indicating that the detected events were not Na^+-dependent action potentials. However, we did detect a modest decrease in spike amplitude and a decrease in baseline noise on NTT1, but not NTT2, following TTX administration. Accordingly on NTT1, there were the same numbers of detected events, but with lower average amplitude following TTX addition. This is potentially due to the slight reduction in baseline noise also measured following TTX administration on NTT1, which may account for the reduced amplitude of events based on a lower threshold for detection. The baseline noise on NTT2 was considerably larger than that on NTT1 and subsequently the signal-to-noise ratio on this array was likely too low to detect any effects of TTX administration.

Considering array-wide synchronous noise on NTT MEAs

In this chapter, we have demonstrated that the patterns of activity on the different MEA types are distinct, with most detected events on NTT MEAs unreliable artifacts of array-wide synchronous noise. There are a number of ways to interpret this information. Firstly, as there were no key electrodes on NTT MEAs that supported repeatable spiking activity as was seen on commercial MEAs and routinely with developing neuronal networks it is clear that single-cell spiking activity was not being detected. Also, close inspection of the synchronously timed events on NTT MEAs revealed array-wide noise patterns, which cast the reliability of detected events as action potentials into doubt. This seemingly suggests that there were no genuine action potentials detected on NTT MEAs but that they were rather artifacts of noise. Another possible consideration is that characteristics of the array allow strong electrical events to travel across the entire electrode array to create a summed activity level that is reflected on each electrode, albeit at slightly different amplitudes dependent on distance from the activity source. Therefore, while synchronous noise would still exist without cultured cells, the electrical activity of those cells could affect the patterns and amplitude of events seen. Therefore the activity we observe could, in fact, reflect network activity of overlying cortical neurons.

ITO electrodes from NTT are commonly coated with a conductive polymer layer that increases electrode surface area and therefore reduces impedance (Cui, et al., 2001; Ghosh & Inganäs, 2000; Nyberg, et al., 2007). The deposition of this polymer would therefore likely reduce the baseline noise of the NTT MEA electrodes and increase the signal-noise ratio. This is certainly an

avenue for future research to pursue in regards to use of these MEAs. Unfortunately, we did not have the opportunity to assess signal-to-noise ratio improvement through the use of a PEDOT-PSS polymer at this stage of experimentation due to a temporary interruption of collaboration with our industry partner, NTT, in Japan (See context statement).

For the NTT MEAs to be functionally useful as electrical signal detectors, the impedance of electrodes needs to be modified so that signals can be robustly detected. Therefore, for the purposes of further studies toward modeling a cell-machine interface *in vitro* and monitoring the neuronal differentiation of stem cells, the commercially available MCS MEAs provide a more practical device than NTT MEAs without its polymer coating and we will pursue the use of these MEAs for subsequent studies.

Chapter 4: Characterisation of human-derived dental pulp stem cell neural differentiation on microelectrode arrays

Statement of Authorship

Title of Chapter

Characterisation of human-derived dental pulp stem cell neural differentiation on microelectrode arrays

Traditional thesis chapter

Kylie M. Ellis (Candidate)

Experimental design, performed all experiments, collected, analysed and interpreted all data, wrote manuscript.

I hereby certify that the statement of contribution is accurate

Signed Date

Simon A Koblar (Co-author)

Experimental conceptualisation and design, supervision of work, financial support.

I hereby certify that the statement of contribution is accurate and I give permission for the inclusion of the chapter in the thesis.

Signed Date

Martin D. Lewis (Co-author)

Experimental conceptualisation and design, supervision of work, financial support.

I hereby certify that the statement of contribution is accurate and I give permission for the inclusion of the chapter in the thesis.

Signed Date

David C. O'Carroll (Co-author)

Experimental conceptualisation and design, supervision of work, considerable ongoing concept development, provided expertise for data analysis, financial support, manuscript review.

I hereby certify that the statement of contribution is accurate and I give permission for the inclusion of the chapter in the thesis.

Signed Date

Chapter 4 Context Statement:

The original overarching aim of this thesis was to investigate the utility of a DPSC-seeded cortical prosthesis that would, conceptually, improve its long-term biocompatibility and success in its application as a brain-machine interface. As such, the adherence and survival of DPSC on microelectrode arrays (MEAs) *in vitro* and their ability to undergo neuronal differentiation was a primary research question. In the previous chapter we saw that the custom-designed NTT MEAs were supportive of cortical cell adherence and survival, however could not be suitably used for measuring elecrophysiology of those cells due to high electrode impedance. Commercial MEAs were therefore used in this chapter to investigate the survival and differentiation of human DPSC. Not only would this allow us to determine the first stage of conceptual success toward a DPSC-seeded brain-machine interface, but it would also allow us to monitor the development of electrical activity in networks of differentiated hDPSC across many hundreds of cells that lay over the electrode region of an MEA. Previously, electrical recordings have only been taken from individual cells.

Ultimately, we found that the survival of hDPSC on MEAs was unfortunately low. Few cultures survived long enough for neuronal differentiation to occur and therefore meaningful electrical activity was scarcely measured. Of few long-term cultures established, no spontaneous action potentials were measured however artificial stimulation produced action potential-like effects within some differentiated cultures.

Our difficulty in establishing long-term cultures of hDPSC on MEAs led us to consider DPSC from a different species (Chapter 5) and to consider the effects of DPSC within the brain at a more molecular level in future experiments (Chapter 6).

4.1 Introduction

The use of human dental pulp stem cells (hDPSC) in neurological regeneration efforts is becoming an increasingly popular area of research, however we currently know little about the capacity of hDPSC to generate functional neural networks *in vitro* or *in vivo*. The potential of stem cell based therapeutics in neurological regeneration has widespread promise but to implement this clinically a detailed understanding of the properties of these cells and how to manipulate them is required.

Previous work performed in our laboratory and others has demonstrated the neuronal potential of hDPSC. *In vitro*, hDPSC were shown to express a variety of mature neuronal and glial markers and developed voltage-gated sodium and potassium channels following two different neuronal differentiation protocols (Arthur, et al., 2008; Kiraly, et al., 2009). *In vivo*, DPSC have mostly been studied to determine their effects of neural recovery following models of injury such as stroke, corical lesion and spinal cord injury (Leong, et al., 2012; Kiraly, et al., 2011; Sakai, et al., 2012). In a rat model of cerebral ischemia, hDPSCs injected into the striatum and cortex not only expressed mature neuronal and glial markers but also improved functional motor and neurological ability 5 weeks post injury (Leong, et al., 2012). Furthermore, predifferentiation of DPSC may also encourage their survival and maturation following transplantation, as demonstrated with the development of functional ion channels following injection into a cortical stab lesioned rat brain (Kiraly, et al., 2011).

The ability to monitor DPSC neural differentiation and network maturation *in vitro* is valuable for understanding and controlling the cells' development. As seen in Chapter 3, the microelectrode array (MEA) presents us with the opportunity to monitor extracellular electrophysiological recordings of entire neuronal networks in a non-invasive manner, in contrast to the single cell recordings used in previous research (Arthur, et al., 2008; Kiraly, et al., 2009; Potter & DeMarse, 2001). The multi-channel array allows the simultaneous recording of an extended area, which can incorporate thousands of cells to determine patterns of electrical activity across numerous electrodes. It can also input electrical signals from any electrode to stimulate overlaying preparations and characterise the evoked activity of cultures as well as their capacity for learning (Ban, et al., 2007; Jimbo & Kawana, 1992; Shahaf & Marom, 2001). Cultures can be maintained and monitored for weeks to gain information on the maturation properties of developing neurons.

Previous studies have used MEA-based neural differentiations to demonstrate the development of active networks from stem cells. This has been reported from embryonic stem cells,

embryonic-derived neural stem cells and P19 embryonic carcinoma cells (Ban, et al., 2007; Furukawa, et al., 2013; Illes, et al., 2007; Illes, et al., 2009; O'Shaughnessy, et al., 2009; Saito, et al., 2009; Takayama, et al., 2011). However, to the best of our knowledge, the characterisation of the neuronal development of adult stem cells on MEAs has not yet been attempted. Therefore, this study investigates the neuronal differentiation of DPSC cultured on MEAs to assess their biocompatibility in terms of adherence and survival, as well as their long term neuronal maturation.

4.2 Materials and Methods

4.2.1 The microelectrode array

As previously described, MEAs were sourced from Multi Channel Systems, Reutlingen, Germany and were chosen due to their high biocompatibility with cortical cells and good signal-to-noise ratio, as seen in Chapter 3. They consisted of 59 active TiN electrodes arranged in an 8 x 8 grid, minus the corner electrodes (Figure 4.1). Electrodes were numbered 1 to 8, horizontally and vertically, such that the top left hand corner position was 11 and the top right 18. An additional electrode, electrode 15 (e15), was used as an internal reference. Electrode diameter was 30 µm with an inter-electrode distance of 200 µm. Signal acquisitions were managed under MCS software control and sampled at a frequency of 50 Hz.

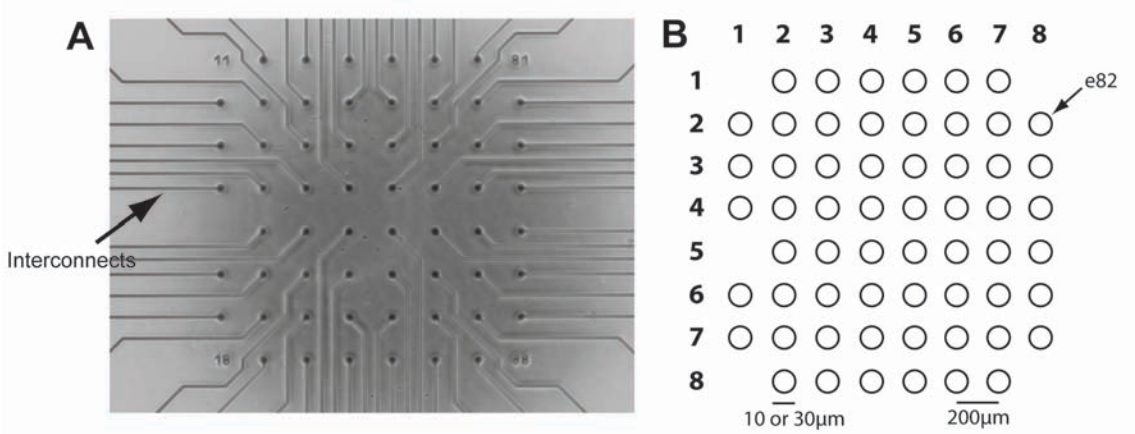

Figure 4.1: The electrode region of the MCS MEA.

A) An image of a MCS30 electrode region showing the electrodes in a 8 x 8 grid arrangement without corner electrodes. Interconnects joining electrodes to recording pads are shown. B) Diagram of MCS MEA electrode region depicting the numbering system. Electrodes were labeled 1-8 horizontally and vertically. Electrodes were numbered with the column number first (eg. Column 8) followed by the row number (eg. Row 2), such as electrode 82, labeled. Two MEA types were used; one with 10 µm electrode diameter and the other with 30 µm electrodes. Each had an inter-electrode spacing of 200 µm.

4.2.2 MEA and coverslip preparation

MEAs were prepared as previously described in Chapter 2 (Section 2.6.3.3). Glass coverslips were treated with 1M hydrochloric acid overnight then subsequently washed with milli-Q water until a litmus test indicated a neutral pH of its solution.

Substrate coatings were then applied to the electrode regions of MEAs or over the whole coverslip and kept overnight at 37℃ in a humidified incubator. Different combinations of the following substrates were applied to achieve maximum cell adherence and differentiation support; laminin (0.02 mg/mL), poly-l-lysine (PLL, 0.01%), poly-l-ornithine (PLO, 0.02 mg/mL) and poly(ethyleneimine) (PEI, 0.05%). MEAs were subsequently washed twice with phosphate buffered saline (PBS) and allowed to dry before applying hDPSCs.

4.2.3 Human dental pulp stem cell isolation and neuronal differentiation

Human DPSC were isolated as described previously in Chapter 2 (Section 2.2.1).

Dissociated DPSC were seeded at 20,000 cells/cm^2 onto glass coverslips. Alternatively, 25-35,000 DPSC were plated over the electrode region of MEAs in a 20 µL droplet and allowed to settle for 1h prior to flooding with *plating medium* containing 1:1 Dulbecco's modified Eagle's medium (DMEM) and F12 supplemented with 2.5% FBS and 50U/mL penicillin and 50 µg/mL streptomycin. Following 24h in plating medium DPSC underwent neuronal differentiation as previously described (Kiraly, et al., 2009). Briefly, *epigenetic reprogramming* of the cells was performed with the addition of 10 µM 5-azacytidine, 1 mM dbcAMP and 10 ng/mL beta-fibroblast growth factor (ßFGF) to the basic plating medium for 48h. Cells were then rinsed with PBS and induced with a *neural differentiation* medium containing 250 µM 3-Isobutyl-1-methylxanthine (IBMX), 50 µM forskolin, 1% ITS, 30 nM Phorbol 12-myristate 13-acetate (TPA), 30 ng/mL neurotrophin-3 (NT-3), 10 ng/mL nerve growth factor (NGF), 10 ng/mL FGF-2 in 1:1 DMEM/F12 for 3 days. Finally, cells were rinsed again with PBS before the addition of a *neuronal maturation* medium, which consisted of 1% N2 and B27, supplements, 30 ng/mL NT-3, and 1 mM dbcAMP in 1:1 DMEM/F12. Differentiating cultures were imaged on a Nikkon inverted microscope at least every three days to document morphological changes.

4.2.4 MEA electrical stimulation

Two stimulation paradigms were applied to developing DPSC cultures and MEA recordings were taken during the period of stimulation as well as prior to stimulation to determine spontaneous electrical activity. The first voltage stimulation used consisted of bipolar pulses lasting 300 µs at each polarity, with amplitude of 200 mV, introduced through seven electrodes simultaneously. A single voltage pulse was applied once per second for three min and repeated three times with five min breaks between stimulations. This stimulation pattern was applied three times daily for

three days. Bright field images were taken with a Nikkon Eclipse inverted microscope each day and compared to determine any cell migration.

The second stimulation paradigm was intended to evoke electrical activity from cultured cells. Voltage stimulation was injected by a single electrode by bipolar pulses lasting 300 µs each with an initial amplitude of ±200 mV, increasing my 10 mV increments to 700 mV. Stimulation was applied twice per second in cultures from day 9 of differentiation and at least every third day or until differentiating cells died.

4.2.5 Whole cell patch clamp recordings

Whole-cell voltage clamp analysis of hDPSC was performed at room temperature using a computer-based amplifier (EPC-9, HEKA Electronics, Germany) and PULSE software (HEKA Elektronik, Lambrecht/Pfalz, Germany). Patch pipettes were pulled from borosilicate glass and fire-polished with resistance ranging from 3 to 6 MΩ. Internal pipette solution contained 135 mM Cs-Glutamine, 5 mM $CaCl_2$, 5 mM $MgCl_2$, 10 mM HEPES, 200 µM GTP, 5 mM ATP, 10 mM EGTA and pH adjusted to 7.3. A standard bath solution with 10 mM $CaCl_2$, 140 mM NaCl, 4 mM CsGlut, 2 mM $MgCl_2$, 10 mM HEPES, adjusted to pH 7.4 was used. Cells with a neuronal morphology were targeted. Holding potential was set at -60 mV and 500 ms voltage steps ranging between -40 and 50 mV were applied in 10 mV increments to record membrane currents. Cells were assessed for evidence of voltage-gated Na^+ currents. The capacitance of each cell was measured using automatic capacitance compensation routine of EPC-9 amplifier. Series resistance did not exceed 20 MΩ and was not compensated for.

4.2.6 Lucifer yellow dye spread

10 µg/mL Lucifer yellow was injected into clustered hDPSC with neuronal morphology by whole cell patch clamp technique. A patch was maintained with the target cell for five minutes to allow the internal pipette solution to diffuse into the patched and surrounding connected cells. Cells were immediately imaged with an epifluorescent microscope to visualise Lucifer yellow.

4.2.7 Offline software analysis

MEA data was analysed using Spike2 and Matlab software. A band pass filter of 250-4000 Hz was applied to all MEA traces prior to analysis. The SD noise was then calculated for each individual electrode trace and a spike detection threshold set at five times this SD. Only supra-threshold events with a physiologically relevant shape and duration were detected as events

according to Spike2 settings and each event detected was closely scrutinized for reliability. The spike rate and amplitude of detected events were compared across the differentiation period. Electrodes with two or more events within a template defined by Spike2 analysis were considered active and also compared across neuronal development of cultures.

4.3 Results

4.3.1 hDPSC neuronal differentiation

hDPSC differentiation on coverslips produced mature neural-like cells up to 48 days of culture. Figure 4.2 shows representative bright field images of differentiating DPSC. Prior to differentiation (Figure 4.2A, day 0) hDPSC cultures consisted of a heterogeneous mix of flat fibroblast-like cells. By day 7 of differentiation many cells developed rounded cell bodies and extended short, thin processes (Figure 4.2B and D) with an underlying layer of large, flat cells. At 24 days of differentiation many DPSC-derived cells retained their rounded phase-bright cell bodies and extended long, complex multiprocesses more reminiscent of mature neurons (Figure 4.2C and E). A large population of cells also retained a large, flat phenotype in resemblance of glial cells. DPSC cultures survived for up to 48 days of differentiation. By this stage cells developed an even more complex multi-processor phenotype and formed intricate patterns of connectivity with neighbouring cells (Figure 4.2F).

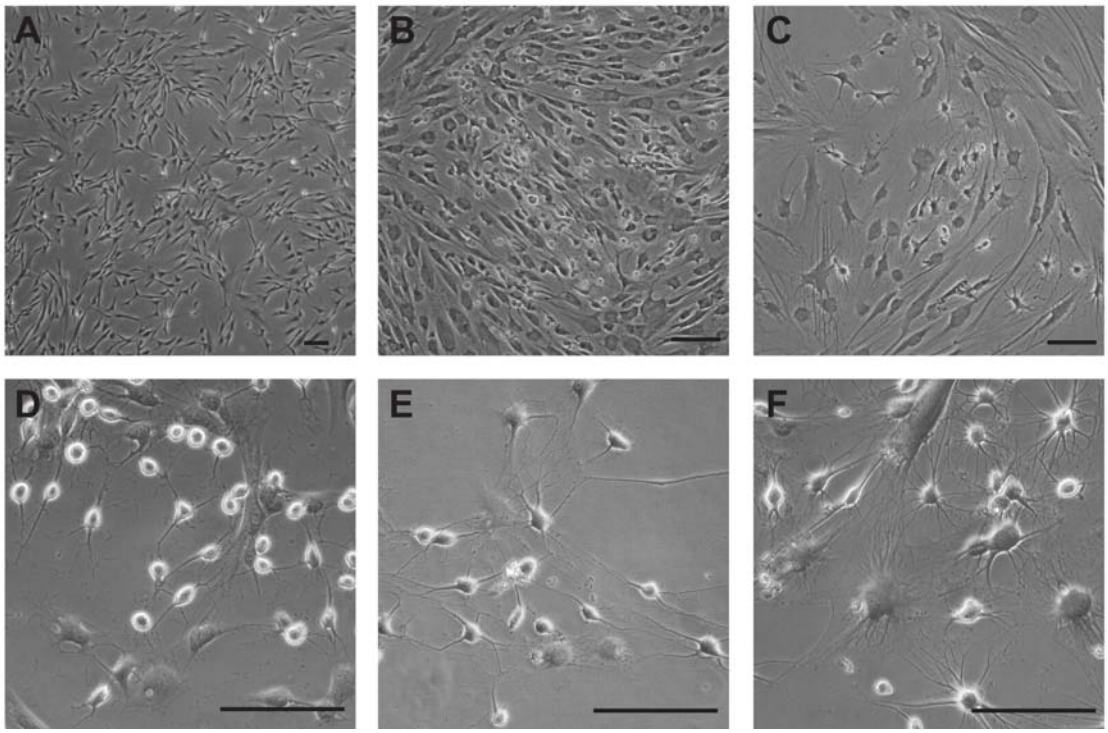

Figure 4.2: DPSC differentiation in culture.

Representative phase contrast images of differentiating hDPSC at day 0 (A), day 7 (B and D), day 24 (C and E) and day 48 (F) of culture. DPSC develop a distinctly neuronal multiprocessor phenotype with increasing maturation time. Scale bars = 200 μm.

4.3.2 Intracellular electrophysiology and network properties of differentiated hDPSC

Whole cell patch clamp analysis of differentiated hDPSC at day 11 revealed the presence of voltage-gated sodium channels in four of six cells tested with neuronal morphology. Figure 4.3A shows representative current traces from one cell in response to voltage steps in the presence of 140 mM Na^+ and the current-voltage relationship of the Na^+ current from the same cell (Figure 4.3B). 500 ms voltage steps were applied from -50 to +50 mV in 10 mV increments.

We noticed that the capacitance of some tightly clustered differentiated hDPSC was high, suggesting that there was charge dissipation occurring across cell membranes. To test this hypothesis, the low molecular weight dye, Lucifer yellow, was injected into a single clustered differentiated hDPSC at day 15 of maturation (Figure 4.3C, arrow). The fluorescent dye spread across the cell membrane to fill the cytoplasm of numerous neighbouring cells and visualised with ultraviolet light (Figure 4.3D)(Vaney, 1991). This indicated that gap junctions or another form of direct cell-to-cell connectivity are present in the developing hDPSC cultures.

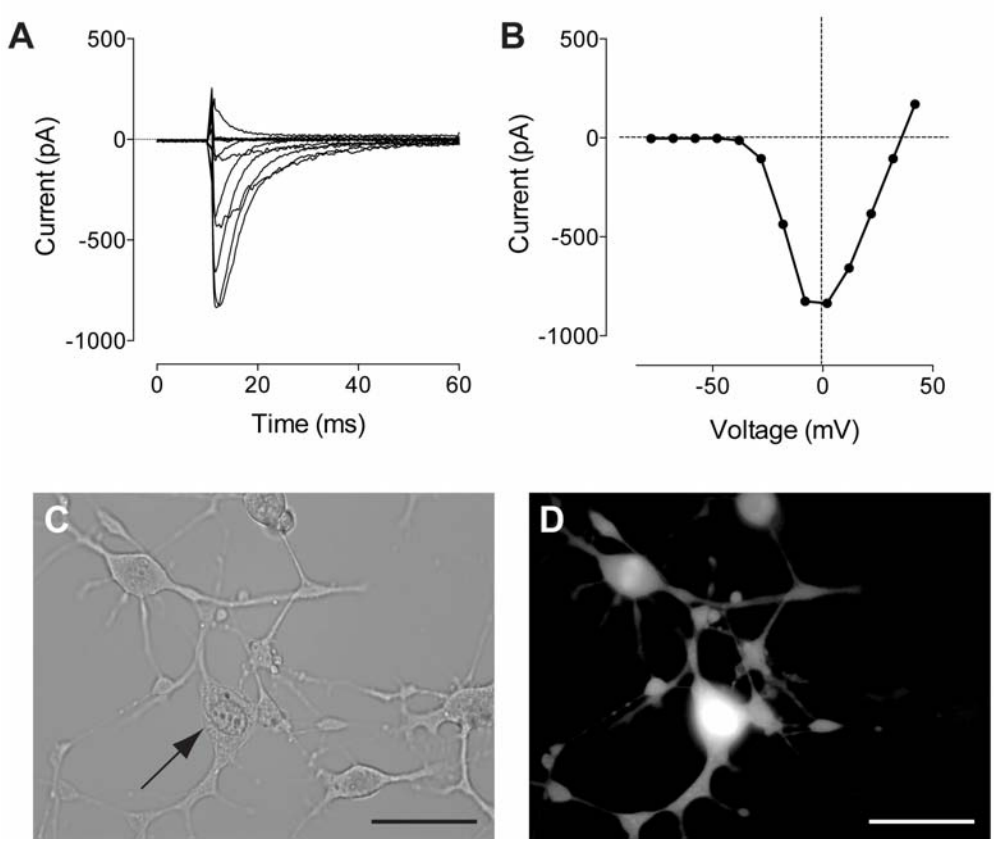

Figure 4.3: Electrophysiology and network properties of differentiated DPSC.

A) Representative whole cell patch clamp recordings of an isolated differentiated DPSC with multiprocessor neuronal morphology showing typical voltage-gated Na^+ current in response to increasing voltage steps. B) The current-voltage relationship of voltage-dependent current of the same cell. C) Bright field image of a differentiated DPSC cluster at day 15 of culture. Lucifer yellow was injected into a single cell (arrow). D) Fluorescent image of Lucifer yellow dye spread across numerous adjacent cells. Scale bars = 25 µm

4.3.2 MEA-hDPSC biocompatibility

Preliminary experiments were performed to determine the most successful substrate coating for the hydrophobic MEA surface to encourage DPSC adherence and differentiation. A combination of 0.05% PEI and 0.02 mg/mL laminin was first trialed based on previous work and the stability of synthetic PEI (Lelong, et al., 1992). Figure 4.4A reveals that the 25,000 hDPSC plated were central and dense one day following plating. By day three, however, almost all cells had migrated away from the electrode region where PEI and laminin were deposited (Figure 4.4B). Cell phenotype was also balled, as their adherence to the MEA surface was low. Stimulation of electrodes closest to the stem cells was attempted over three days to encourage cell migration back toward the electrode region (Figure 4.4C, arrows). Comparison of cell position before and after stimulation indicated that no migration of DPSC occurred over this time and cells had not re-adhered to the MEA surface. DPSC apoptosed by day 5 following plating.

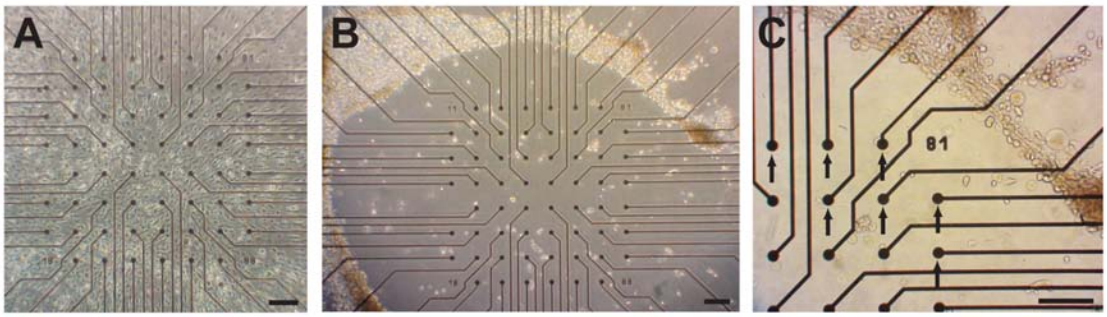

Figure 4.4: Biocompatibility of PEI and laminin on a MEA for DPSC culture

A) DPSC-MEA culture with PEI and laminin coating showing dense and central cell distribution at day 1 of differentiation. B) By day 3 of culture cells had migrated away from the electrode and substrate-coated region of the MEA. C) Higher magnification of MEA culture at day 3 of differentiation. Electrodes closest to DPSC (arrows) were stimulated over 2 days to induce cell migration. Scale bar = 200 μm.

The biocompatibility of MEAs coated with poly-d-lysine and laminin was also considered. Figure 4.5 shows the lack of success of this substrate layer. An initially adherent and healthy hDPSC culture at one day following plating (Figure 4.5A) migrated into a dense aggregation at one corner of the electrode array by day three of culture (Figure 4.5B). This demonstrated the low adherence of cells and unsuccessful biocompatibility of coated MEAs. hDPSC differentiations performed alongside this MEA culture and seeded onto poly-d-lysine and laminin-coated glass coverslips adhered successfully and differentiated until at least day 34 producing complex networks of cells with bipolar and multipolar neuronal-like phenotype (Figure 4.5C and D).

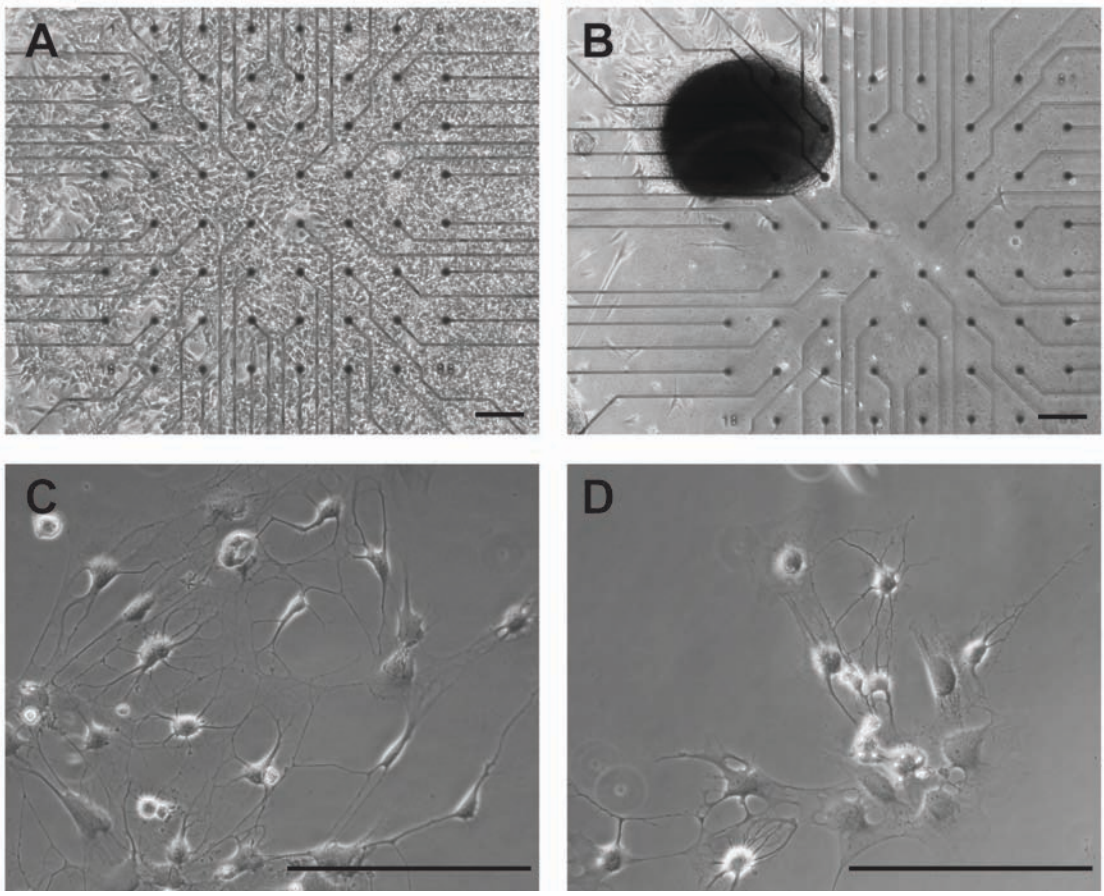

Figure 4.5: Biocompatibility of MEAs coated with poly-d-lysine and laminin.

A) Dense, healthy culture of DPSC one day after plating. B) Complete migration and aggregation of DPSC at day 3 of culture. C) and D) Differentiated DPSC grown simultaneously to MEA cultures on glass coverslips also coated with poly-d-lysine and laminin at day 34 showing healthy multiprocessor and bipolar neural-like cells. Scale bars = 200 µm.

The combination of poly-l-ornithine and laminin was also administered to four MEAs to encourage cell adherence and neuronal differentiation. Cultured hDPSC remained dense and healthy two days following plating at 25,000 cells in a 20 µL droplet (Figure 4.6A). By day 4 hDPSC had undergone cell death or largely migrated away from the electrode region of MEAs. In contrast, parallel DPSC differentiations performed on glass coverslips with the same substrate coating survived for over 34 days in culture and differentiated into a heterogeneous population of neural-like cells (Figure 4.6B). These results suggest that the lack of biocompatibility was MEA-based rather than substrate coating-dependent.

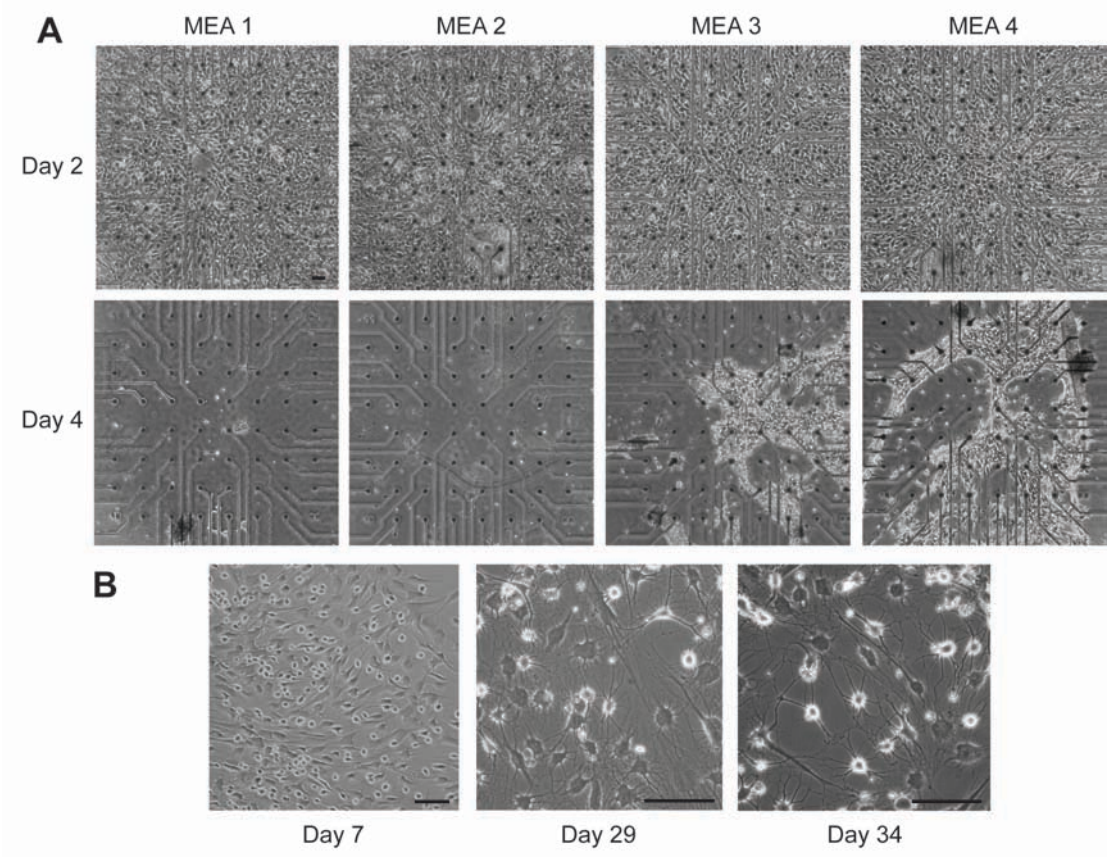

Figure 4.6: Biocompatibility of poly-l-ornithine and laminin on MEAs for DPSC culture

A) Representative bright field images of DPSC-MEA cultures coated with PLO and laminin showing dense and healthy cultures 2 days following plating. By day 4 of differentiation most DPSC had died or migrated away from the MEA electrode region. B) Bright field images of parallel DPSC differentiations performed on glass coverslips showing successful long term differentiation to day 34. Scale bars = 200 µm.

Cell adherence and survival was also compared across MEAs with two different electrode sizes and interconnect material to determine if one may be more conducive to long term DPSC culture. The first had 30 µm TiN electrodes with black platinum interconnects (Figure 4.7A) and had been used for previous studies (n = 3). The second consisted of 10 µm TiN with transparent indium tin oxide interconnects (n = 4). MEAs were coated with laminin only. Following three days of differentiation DPSC on both MEA types showed morphological changes to develop neuronal-like thin processes (Figure 4.7A and B, arrows). However, by day 6 there were no longer any viable DPSC on any MEAs (Figure 4.7C and D).

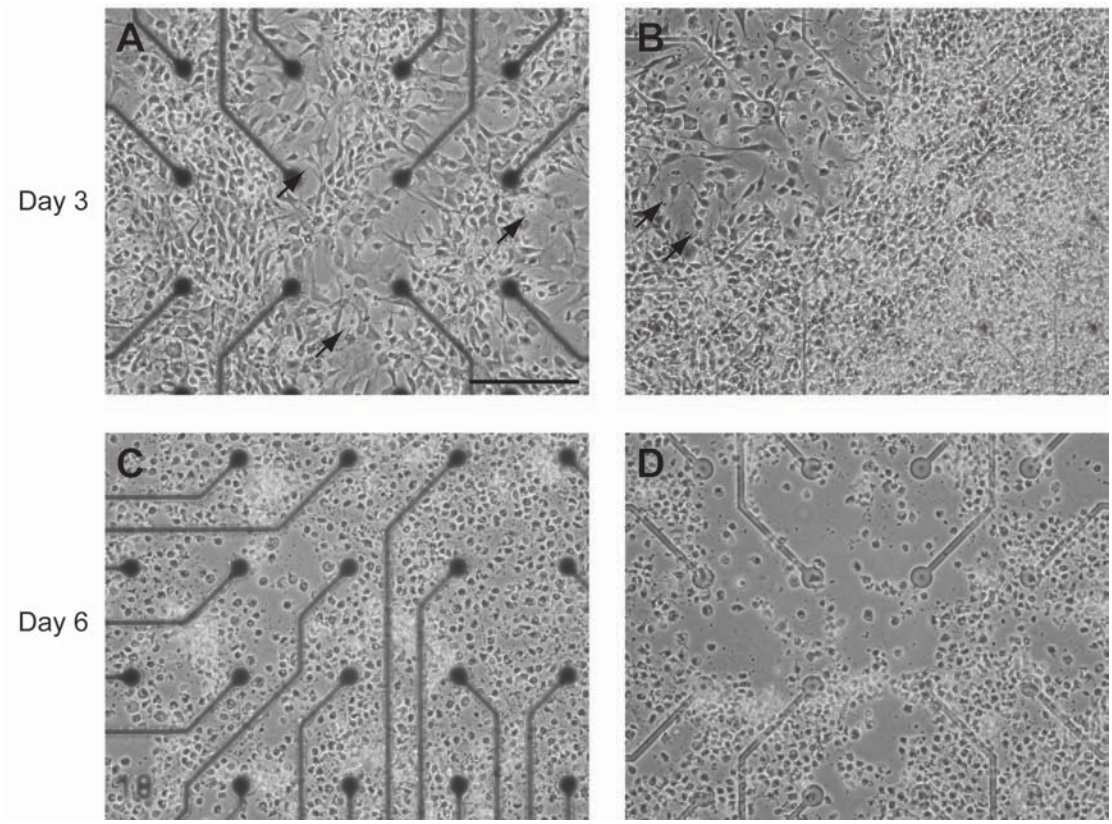

Figure 4.7: Biocompatibility of two MEA types coated with laminin.

hDPSC were seeded and differentiated on MEAs with 30 µm electrodes with platinum interconnect leads (n=3, A and C) or 10 µm electrodes with transparent indium tin oxide leads (n=4, B and D). At day three of differentiation both MEAs supported good hDPSC adherence and some cells with early neuronal-like morphology (arrows). By day six of differentiation all DPSC cultures had stopped with cell death (C and D). Scale bar = 200 µm.

We were able to achieve successful differentiation of one DPSC-MEA culture to day 9. The electrode region of this MEA was coated with poly-l-lysine and laminin. Figure 4.8 demonstrates the development of a neuronal-like morphology of DPSC with many cells developing long, thin multiprocesses. However, four other MEAs assayed in parallel and treated identically did not support DPSC survival past day six of differentiation. This highlights the variability of biocompatibility under equivalent conditions, potentially due to small and unobservable differences in MEA surface conditions.

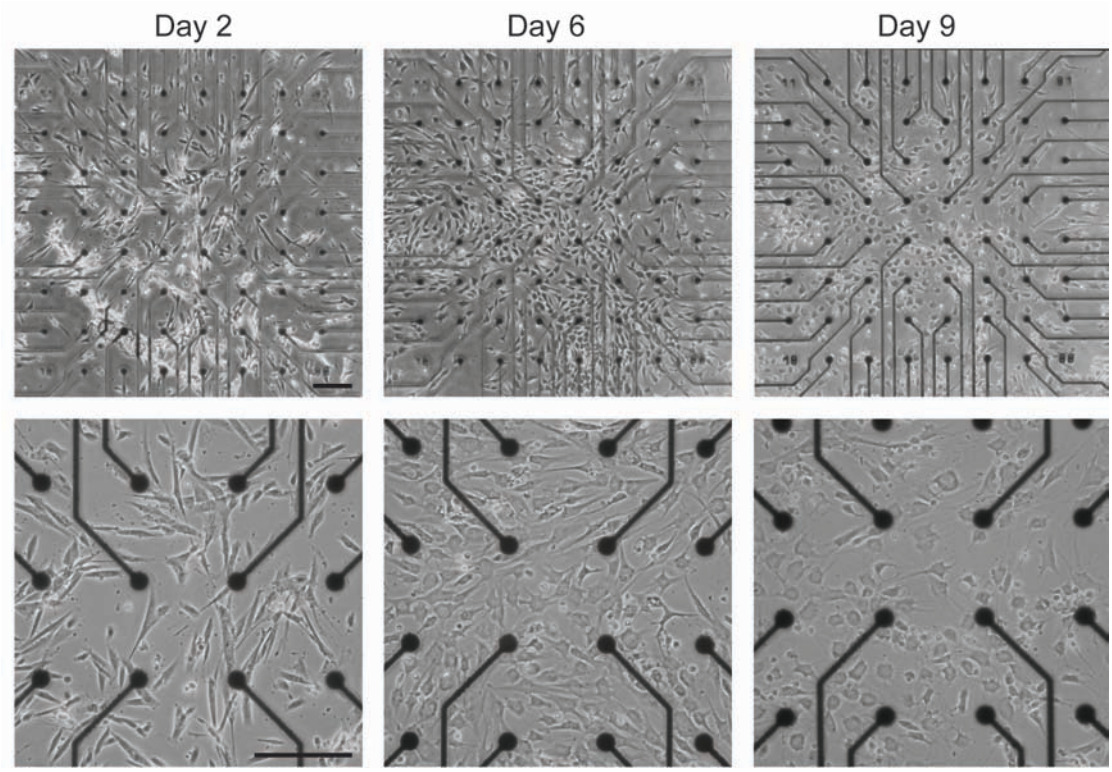

Figure 4.8: Differentiation of DPSC on an MEA.

Bright field images showing the survival and differentiation of hDPSC on an MEA at 2, 6 and 9 days of culture and low and high magnifications. By day 9 many hDPSC-derived cells had neural-like morphology. Scale bar = 200 μm.

4.3.3 Electrophysiology of long term DPSC differentiation on MEAs

One of two platinum MEAs coating with poly-l-lysine and laminin supported successful neuronal differentiation of DPSC until day 27. Figure 4.9A and B shows bright field images of the dense, healthy culture after 15 days of differentiation. Interestingly, the second MEA, treated identically to the first, did not support DPSC adherence in the electrode region and cells died by day two of culture (Figure 4.9C). Figure 4.9D shows that there is a difference in cell phenotype between MEA cultures (Figure 4.9A-C) and parallel hDPSC differentiation cultures on glass coverslips with the same substrate coating. A greater proportion of cells differentiated on glass coverslips than those on MEAs developed a multiprocessor or bipolar neuronal-like phenotype (Figure 4.9D). In addition, electrophysiology recordings were taken at from day 9 of differentiation and throughout the neural maturation period. Measures of spike rate and spike amplitude were compared across development and compared to TTX controls at day 27.

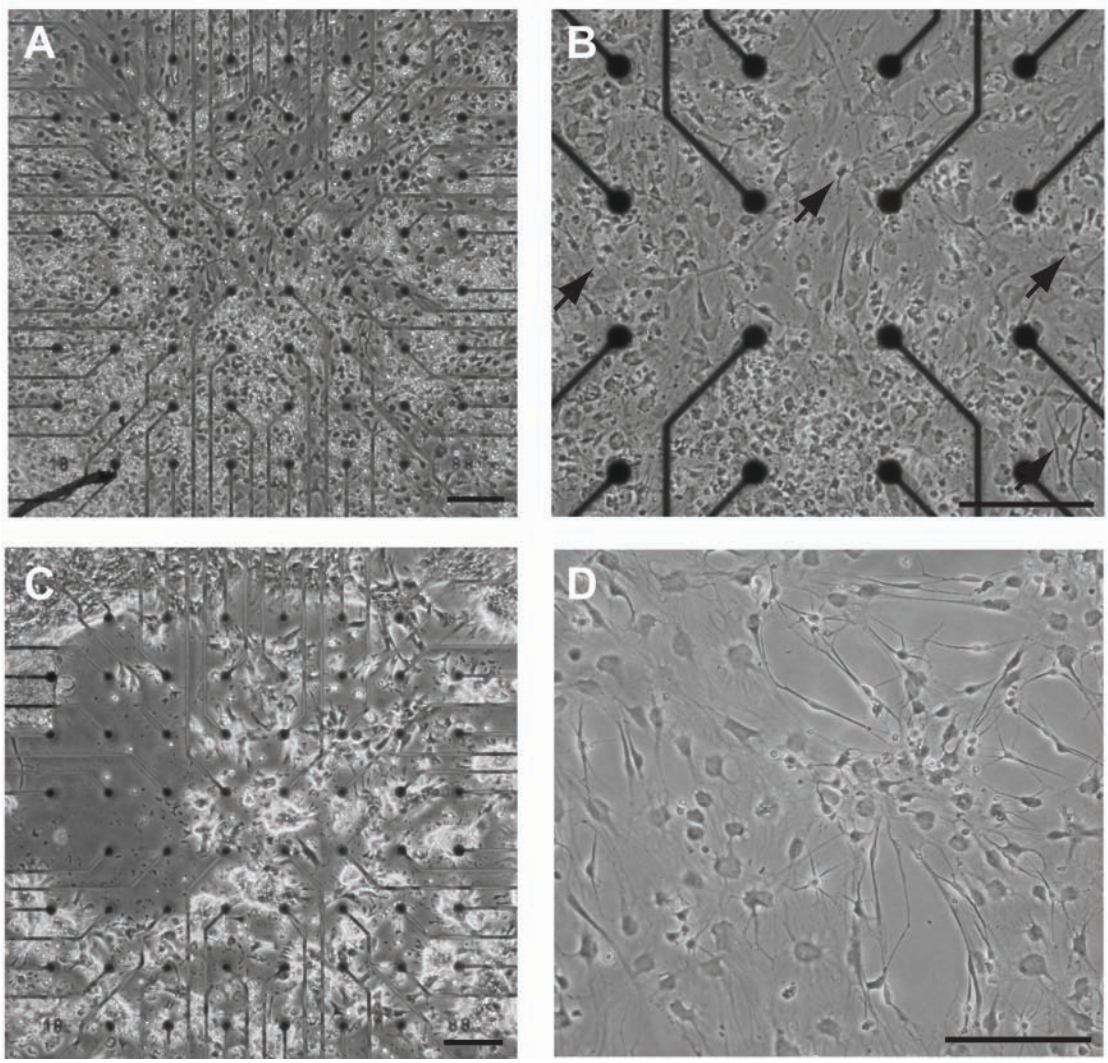

Figure 4.9: Long term differentiation of DPSC on an MEA.

A) Bright field image showing the dense and healthy hDPSC at day 15 of differentiation on a poly-l-lysine and laminin-coated MEA. B) Magnified central region of A) showing the varied morphology of differentiated cells. Some have neural-like long, thin processes (arrows). C) A parallel MEA under identical conditions on day one showing low hDPSC adherence. D) A parallel hDPSC differentiation performed on glass coverslips also coated with poly-l-lysine and laminin at 20 days of culture with many more neuronal-like cells than that seen on MEA cultures. Scale bars = 200 µm.

MEA-wide spike rate was low across the developmental period, ranging between 35-65 events detected over 59 electrodes in a 100s period. Furthermore, spike rate did not show a relationship with culture maturation as would be expected with an increase of electrically active neurons (Figure 4.10A). Instead, it varied daily in a seemingly random manner. In addition, spike amplitude remained stable over the developmental period with all detected events below -8 μV (Figure 4.10B). 'Active' electrodes were deemed those with two or more events within a single spike template. Again, there was no relationship between culture maturation and the number of active electrodes (Figure 4.10C).

We next sought to identify any single electrodes whose spike rate increased during DPSC maturation, indicative of developing electrical activity. One such electrode was identified; electrode 36 (e36). Figure 4.10D shows the increase of spike rate on e36 over the differentiation period, beginning with a modest spike rate of 3 events per 100s and rising from day 15 to 7 events per 100s, which constituted a high single electrode spike rate for this culture. From day 16 spike rate increased up to 22 events at day 27. Furthermore, many spiking events detected were attributed to a common action potential template by Spike2 analysis, suggesting that this was the effect of a single active neuron nearby e36. These events maintained a relatively low spike amplitude of -7.98 ± 0.86 μV, consistent with events detected throughout the MEA.

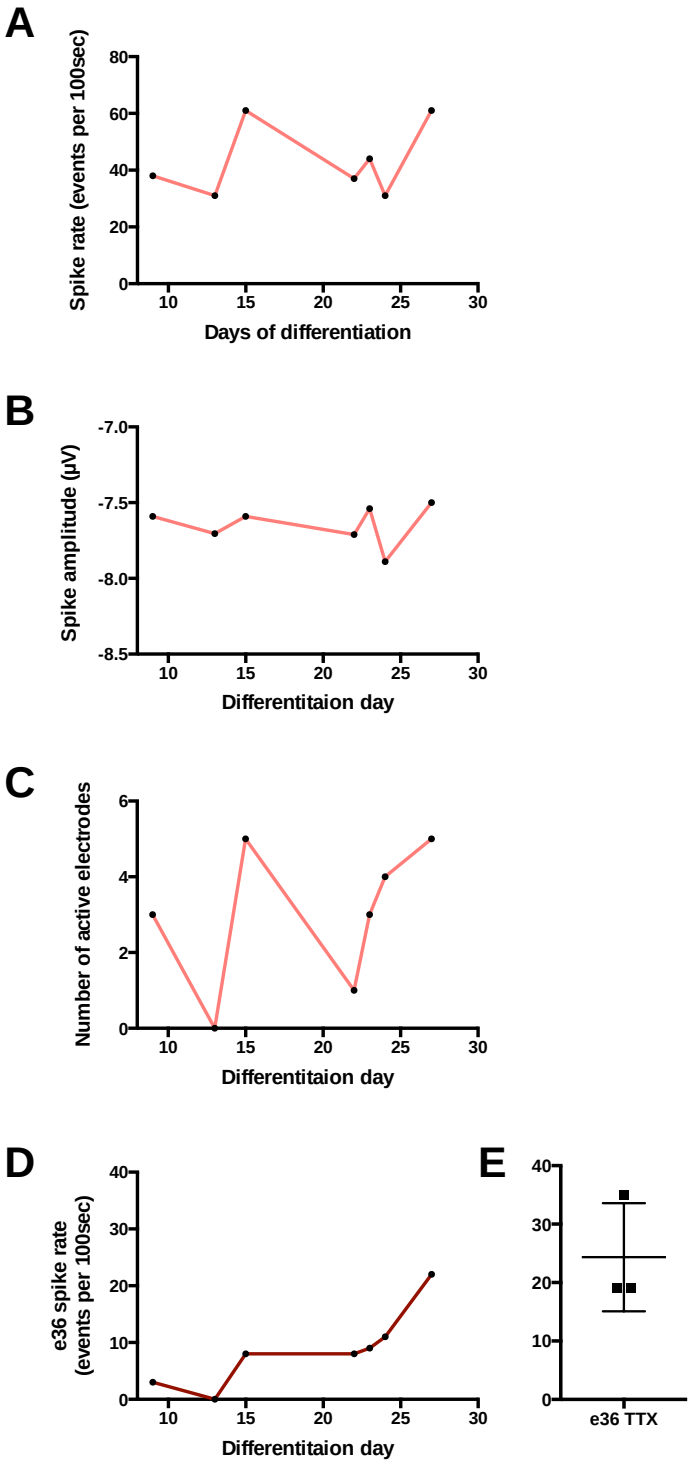

Figure 4.10: Electrophysiology of differentiated DPSC.

Electrophysiology of DPSC differentiated on an MEA measured over 100s recordings from 59 electrodes until differentiation day 27. A) MEA-wide spike rate measured across the differentiation period. B) Average amplitude of detected events. C) Number of 'active' electrodes; those with two or more events detected within a spike template within a 100s period. D) Spike rate of one electrode, e36, over the differentiation period. E) There was no reduction in e36 spike rate following 10 µM TTX administration.

To confirm whether these detected events on e36 and throughout the rest of the MEA were action potentials of developing DPSC-derived neurons or noise artifacts, 10 μM TTX was added to cultures at day 27 to block action potentials. Surprisingly, there was no change in MEA-wide spike rate, spike amplitude or the number of 'active' electrodes following TTX administration (Figure 4.11). Furthermore, the high spike rate of e36 remained unchanged following TTX addition (Figure 4.10E). Together, these finding indicate that the events detected across the long term DPSC MEA culture were artifacts of random noise and not the emergence of action potentials in developing DPSC-derived neurons.

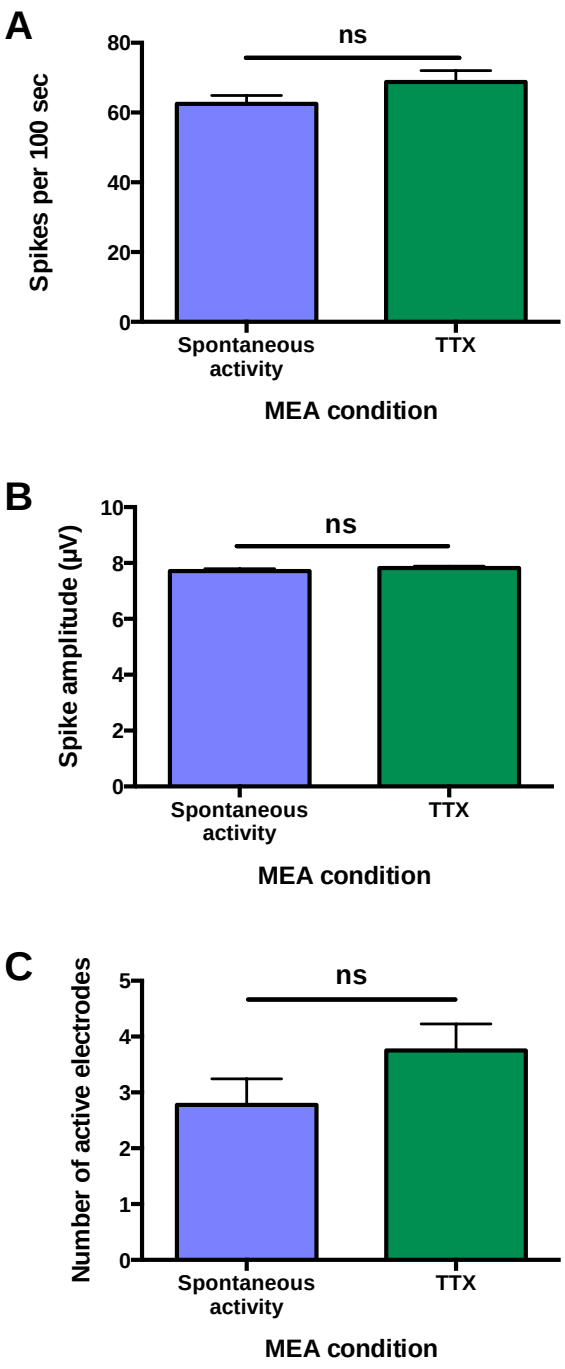

Figure 4.11: Effect of TTX on DPSC electrophysiology.

No difference in A) MEA-wide spike rate, B) detected event amplitude or C) the number of 'active' electrodes following 10 µM TTX addition to differentiated DPSC-MEA culture at day 27 of differentiation. Measurements taken from 12 electrodes across two replicated MEAs in each condition.

We did not observe any TTX-dependent large trace deflections indicative of action potentials from cultured hDPSC, however a negative bias of some electrode traces was noted that may have been influenced by small sub-threshold spikes or large sodium currents of cultured cells causing depolarisation. We assessed the mean noise level of six electrodes from two MEAs without cultured cells to determine the normal ranges of trace voltage bias. All electrodes had a slight positive bias with an average of 9.40 ± 6.10 nV (n=12). This was compared to mean trace signals from MEAs with cultured hDPSC at d15 and d22 of differentiation. There was a significant reduction in the mean voltage of the same electrode traces, at 4.09 ± 4.361 pV (n=24, $p<0.05$, Figure 4.12A), with some producing a negative bias. We also compared traces following TTX administration to determine if the negative voltage bias would be reversed as a result of Na^+ blockade, however we measured a further non-significant decrease in electrode trace voltage from pre-TTX cultures with an average of 0.39 ± 5.16 pV (n=16). As a positive control, we also measured the mean trace voltage from cultures of cortical neurons on the same arrays that had known action potential activity (data from Chapter 3). Even with considerable high amplitude spiking activity, average voltages of 12 electrodes measured remained slightly positive (Figure 4.12B). Following TTX administration, mean electrode voltage increased slightly, most likely due to the abolishment of action potentials and demonstrates what we should expect from active cultures.

There was considerable variation in mean trace voltage between electrodes within the same MEA and in the same hDPSC condition. Nonetheless separation of the electrodes revealed the same trend across each (Figure 4.12C). This data suggests that there is a trend toward more negative electrode traces with cultured cells, independent of the presence of TTX.

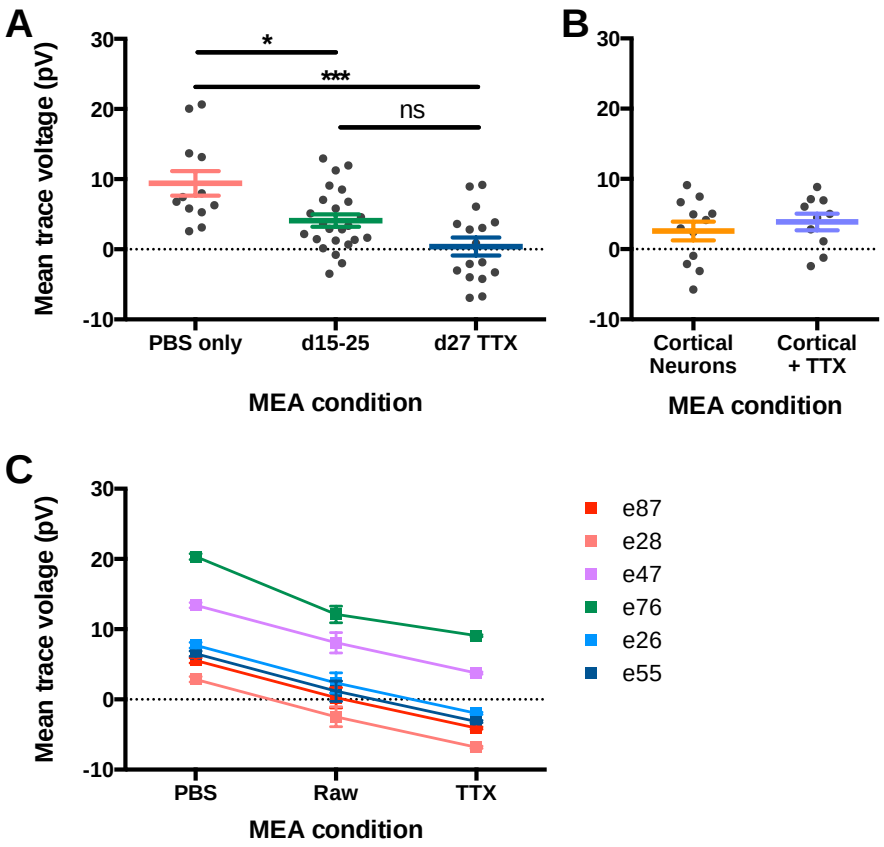

Figure 4.12: The average voltage of electrode traces from MEAs decreases with cultured hDPSC.

Mean voltage of electrode traces from MEAs with differentiated hDPSC prior to and following TTX administration compared with uncultured MEAs. A) Average voltages of electrode traces were significantly more negative when cultured with differentiated hDPSC compared with uncultured MEAs. Electrode trace voltage remained low following TTX administration. B) Average voltages of arrays cultured with cortical cells with known action potentials before and after TTX administration. C) Average electrode trace voltage from each electrode considered in A. Each electrode shows a similar trend of a more negative trace bias when differentiated hDPSC are cultured and a further reduction following TTX addition.

As the MEA is not a supportive surface environment for developing stem cells, investigation of the introduction of pre-differentiated DPSC onto MEAs to monitor their electrical activity occurred. DPSC were pre-differentiated to day 12 on glass coverslips coated with poly-l-lysine and laminin and inverted onto poly-l-lysine and laminin-coated MEA surfaces. Figure 4.13 shows one representative inverted culture immediately following deposition and 24h later. There is a clear breakdown of DPSC-derived neural network health within the electrode region of the MEA with cultures becoming more sparse compared with outer regions (Figure 4.13A and B, respectively).

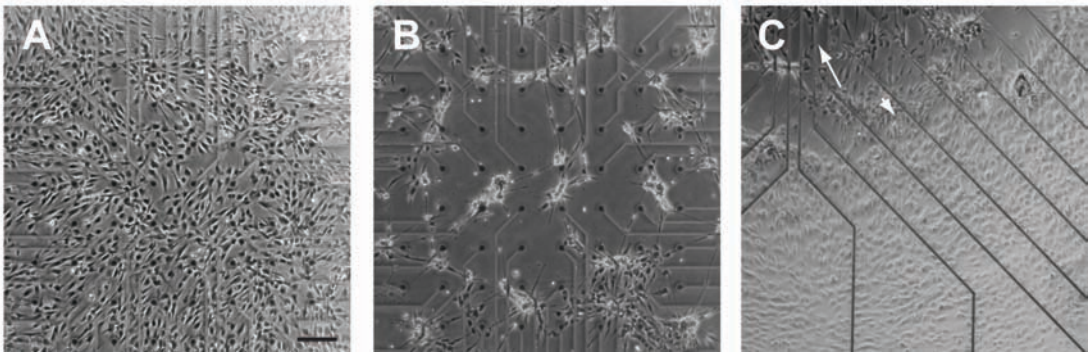

Figure 4.13: Survival of DPSC on inverted coverslip

A) DPSC grown on glass coverslips inverted onto MEAs at day 8 of differentiation. B) Following 24h of inversion most DPSC had apoptosed. C) The health of DPSC cultures 24h after inversion was poor at the electrode region of MEAs (direction of long arrow) but remained dense and healthy at outer regions (short arrow). Scale bar = 200 μm.

4.3.4 Stimulation of differentiated hDPSC cultures

In three hDPSC-MEA cultures that survived through the differentiation period, single-electrode stimulation was introduced in an attempt to incite dormant electrical activity within the developing neural cells. No spontaneous activity was detected on any MEA, however stimulus-induced activity was observed in two of three MEAs from day 9 of differentiation.

It is intrinsically difficult to differentiate spiking activity of electrical artifacts following stimulation in a low spike rate culture so particular care needed to be taken to avoid false detection of action potentials. Stimulation patterns were mirrored in artifact events of adjacent electrodes with large multiphase deflections associated with each stimulation event (eg. e46 and e48, Figure 4.14, orange dots adjacent to the stimulation electrode, red). The amplitude of these events varied in synchrony with the stimulation voltage and overall artifact amplitude generally reduced with increased distance from the stimulation source (eg. e28 and e55, Figure 4.14, blue dots). Nonetheless, the stimulation intensity pattern can be observed in the more distant electrodes sporting artifacts.

In MEA2, the distant electrodes e12 and e13 also supported stimulation-associated events, however these did not distinctly present as artifacts. This was initially due to the amplitude of the events, which did not follow the stimulation pattern intensity seen on other electrodes with artifact events (Figure 4.14). For example, at the onset of stimulation when its voltage is low, the surrounding electrode artifacts are also small, which increase in amplitude as the stimulation voltage also increases. The activity of e12 and e13, however, is strong from the onset of stimulation and remains consistent across the entire stimulation period. The associated e14 trace in Figure 4.14 represents that electrodes closer to the stimulation source did not support the same electrical activity, suggesting that there may be network interconnection between the stimulation source and e12, e13.

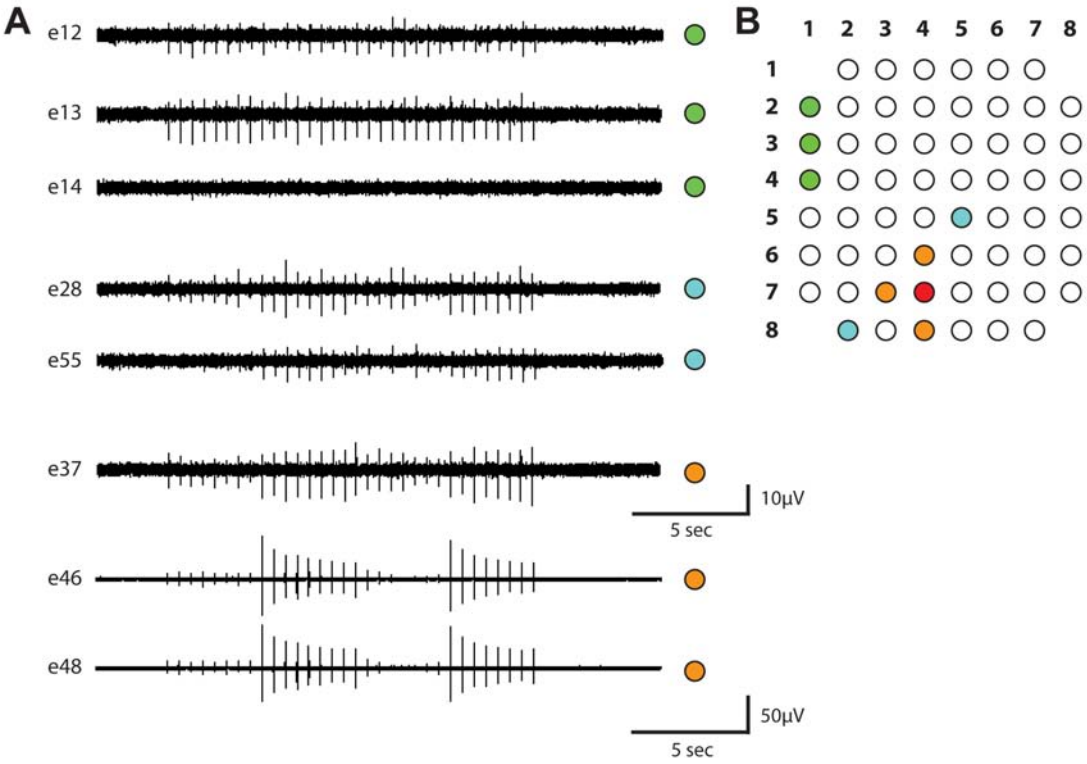

Figure 4.14: Stimulation-induced activity within differentiated DPSC cultures.

Electrical activity and artifacts from differentiated DPSC cultures following stimulation at e47 (red dot). Adjacent electrodes (orange dots) show strong electrical artifacts with amplitude patterns that mirror stimulation voltage (e37, e46, e48). Electrodes that are nearby, but not adjacent to the stimulation source (blue dots, e28, e55) also show stimulation artifacts with amplitudes mirrored from stimulation voltage, however artifacts are at an overall lower amplitude. More distant electrodes generally did not show any electrical artifact (e14). e12 and e13 were the only two distant electrodes that had any stimulation-associated activity. The amplitude of these events, however, was more stable and did not vary with stimulation intensity. B) Schematic representation of electrode distribution of the MEA.

Individual spike event characteristics also varied across these electrodes. Figure 4.15 shows that the electrodes closer to the stimulation source (orange dots) most often have strong negative and positive phases to their artifact event. The positive phase of the artifact is attenuated on electrodes more distant from the stimulation source (blue dots), however it is still prominent. While the spike events on electrodes 12 and 13 have just a short positive and strong negative phase, more representative of an extracellularly recorded action potential. It is worth noting that a small artifact is seen on e14, suggesting that the stimulation is felt across the whole electrode array, and that the response on e12 and e13 was not a regular artifact for the array region. No stimulation-associated activity was detected on e12 or e13 on any subsequent day.

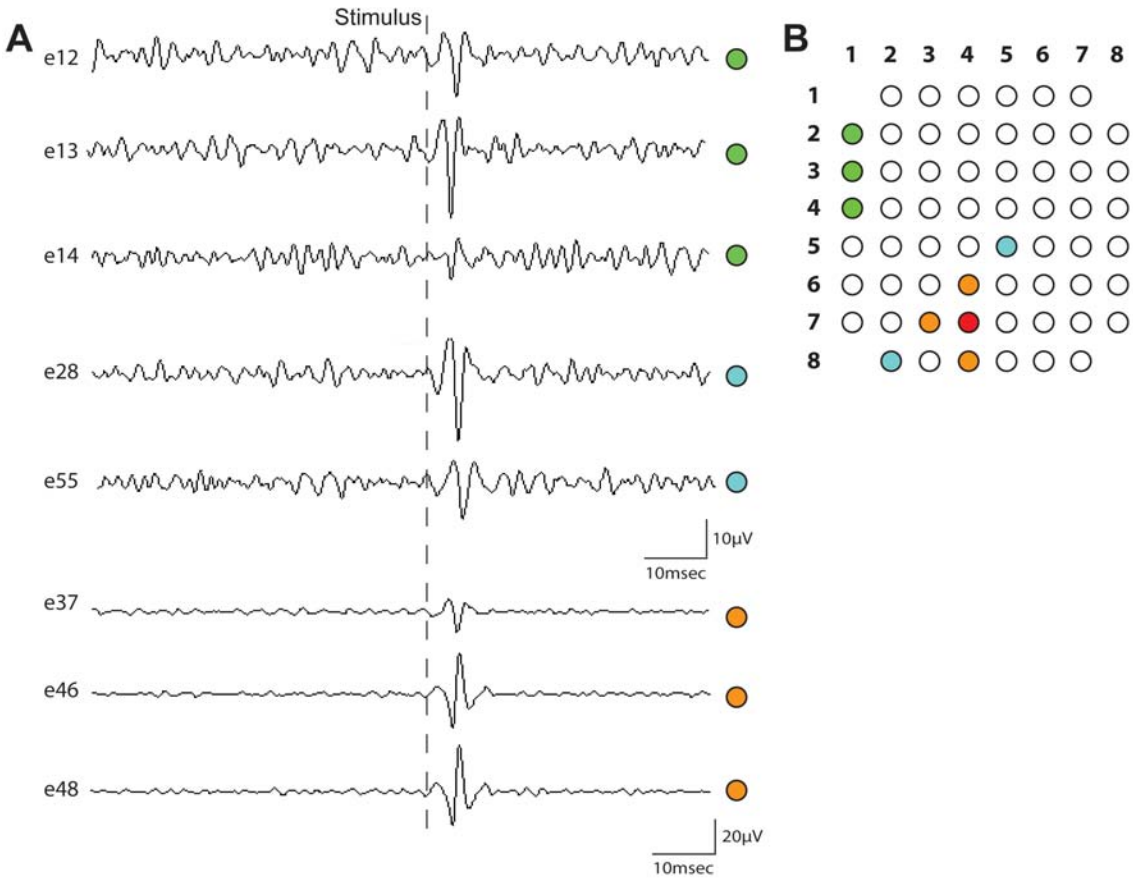

Figure 4.15: A comparison of stimulation-induced events from differentiated DPSC cultures.

A) 100 ms recordings of a single stimulation-evoked event (stimulus at dashed line) compared across 8 electrodes. Electrodes closest to the stimulation source (orange dots) had the largest artifact amplitudes and multiphase shape. Those more distant to the stimulation source (blue dots) had lower artifact amplitudes and an attenuation of the positive phase of the event (not different voltage scale). Distant electrodes (green dots) had variable responses to stimulation. Most showed little or no artifact like that seen of the trace of e14. e12 and e13, however, had large, predominantly negative deflections, reminiscent of action potentials. B) Schematic representation of electrode distribution of the MEA.

4.4 Discussion

This study presents the first characterisation of hDPSC differentiation and electrophysiology on MEAs. We have identified a general biocompatibility challenge to overcome between the stem cells and MEAs, however successful neuronal differentiation was achieved up to 27 days and may have produced stimulation-induced action potentials of DPSC-derived neurons.

In this chapter, five combinations of substrate plating materials on MEAs were trialed, of which one was successful in supporting the adherence and differentiation of hDPSC approximately half of the time. This indicates the inherent difficulty of culturing hDPSC on artificial MEA surfaces, as parallel cultures performed on glass coverslips were much more reliable and stable, surviving and differentiating for over four weeks in some cases. It is possible that the low survival of hDPSC was directly due to their poor attachment to the MEA surface. MEAs are inherently hydrophobic and despite surface pre-treatment with serum and prior cell culture to leave the surfaces more hydrophobic, along with controlled and consistent substrate coatings, this may account for some of the low attachment we observed. Furthermore, while it seemed that some cells did migrate away from the electrode region of MEAs it is likely that poor attachment also contributed to this “cell-free zone”.

Interestingly, hDPSC cultures showed a trend toward initially plating well, with strong adherence and differentiation up to day three of culture. However, beyond this it was unusual for cultures to maintain good adherence to the MEA surface and continue differentiation. In contrast, the results observed in Chapter 3 indicate that cortical neural cultures survived well on MEA surfaces for at least 14 days. They produced MEA-wide network bursting activity to give way to more regular and mature action potentials with time, their success potentially due to the well-developed networks of mature neurons and supportive glial cells. The failure of maintaining long-term DPSC cultures suggests that the limitation lies with performing the neural differentiation of stem cells on the MEA. To combat this issue, pre-differentiation of hDPSC on glass coverslips before inverting them onto MEAs was attempted. While this did not obtain any meaningful electrophysiological information from the cultures, it did provide important insights regarding the biocompatibility of the MEA, whereby the health of cells that were positioned around the electrode region of the MEAs deteriorated quickly, in contrast to those at the outer regions of the MEA that retained a dense network. This suggests, along with the other biocompatibility evidence seen in this study, that there is an inhibitory impact of MEA electrodes toward hDPSC, perhaps due to the more

hydrophobic nature of the surface, despite pre-treatment of the MEAs with serum and previous cell cultures to make them more hydrophilic. It is also possible that there is a small electrical charge in the electrode region of MEAs, providing an inhibitory influence to the cells. According to this finding it applies to immature as well as more mature hDPSC-derived neural cells.

The low survival of hDPSC-MEA cultures was unexpected as previous studies monitoring the neural differentiation of stem cells on MEAs have been successful. Numerous groups have demonstrated the neural differentiation of embryonic stem cells (Illes, et al., 2007; Illes, et al., 2009), neural stem cells (Furukawa, et al., 2013; O'Shaughnessy, et al., 2009) and P19 embryonic carcinoma cells (Takayama, et al., 2011) to develop functional action potentials when grown on MEAs. However, these studies have all used pluripotent embryonic-derived stem cells. To the best of our knowledge, no multipotent adult-derived stem cells have been characterised for their neural differentiation on MEAs to date.

It is worth noting that other groups have also faced limitations of differentiating neural stem cells as monolayers on MEAs, compared with preparing neural cells in neurospheres and replating onto MEAs once differentiation (Illes, et al., 2009). While the monolayer cultures in this study did produce functional action potentials, they did so at a significantly lower rate and had poorer survival. This suggests that the cells need more surrounding supportive factors during differentiation than can be provided on the MEA surface. While it has not been previously performed, neurosphere cultures of hDPSC may be a promising avenue for future work to aid the maturation of the cells.

We were able to overcome nonpermissive state of the MEA surface to achieve long term differentiation of DPSC on numerous occasions, up to 27 days of culture. Cultured cells developed long, thin neurites, reminiscent of neurons. However, the phenotype of cells was noticeably distinct from parallel differentiations performed on glass coverslips, indicating that the MEA had affected their differentiation. DPSC on coverslips produced a high proportion of phase bright multiprocessor and bipolar neuronal-like cells and also a bed of large, flat cells reminiscent of glial cells that interconnected into complex networks. Those on MEAs had more stunted neurites and flatter cell bodies. Few cell morphologies could distinctly be labeled neuronal-like. Furthermore, although coverslip-cultured DPSC developed voltage gated sodium channels from day 11 of differentiation, and have been shown previously to also develop voltage-gated potassium channels (Arthur, et al., 2008; Kiraly, et al., 2009), we did not detect any spontaneous action potentials in the three developing DPSC cultures that survived past 9 days of culture. Small amplitude action potentials are inherently difficult to differentiate from baseline noise levels.

However considering that there was no reduction of spike rate or amplitude following TTX blockade of sodium channel activity we concluded that the events detected were not the result of action potentials of cultured cells. We also identified that electrode traces have a more negative bias when cultured with differentiated hDPSC compared with uncultured MEAs, which suggested that there were depolarisation influences amoungst the cells. This is possibly a result of sodium currents on developing neurons that could cause sub-threshold depolarisations of hDPSC. However, average electrode voltage became more negative following TTX addition, which should not occur according to this hypothesis.

The one electrode in which spontaneous spiking activity did increase over the course of differentiation did not respond to TTX addition. We therefore concluded that these detected events were also electrical artifacts. This presents an underlying confounding issue of long term cell-electrode coupling whereby debris impurities on an electrode can increase noise and crease electrical artifacts such as those detected with electrode 36 from day 15 onward. However, it is also notable that all other electrodes remained free of such artifacts over the 27 days of culture.

While spontaneous activity was not detected in hDPSC-derived neural cultures, it is possible that action potentials were induced by single-electrode voltage stimulation. Electrical artifacts were prominent across electrodes neighbouring the stimulation source and their shape made them clearly identifiable as artifacts. In contrast, events detected at two more distant electrodes were less easily classified as artifacts as their shape more closely resembled action potentials. More convincingly, the amplitude of these distant electrode events remained reasonably constant over the stimulation period rather than varying with stimulation intensity as seen on other electrodes associated with artifacts. However, the instigation of these events occurred in synchrony with the stimulation event and other artifact deflections. We would expect a slight delay in signal transmission over the distance between the stimulation source and the spiking electrodes if synapses were involved. As these were developing neural networks, however, it is possible that cell-to-cell connections were not primarily achieved by synapses, but rather gap junctions that share electrical signals directly, without the slight delay of chemical synaptic connectivity. Indeed we did see evidence of gap junction connectivity throughout differentiated cell clusters with Lucifer yellow dye spread across cell membranes. In this case, cells nearby distant electrodes e12 and e13 could be induced to depolarise in response to activity in electrically coupled cells at the stimulation source. Furthermore, the stimulation-induced activity seen on e13 and e12 were within the amplitude range of physiological action potentials seen from cortical cultures in Chapter 3. It is worthwhile noting that electrical activity on electrode 14, adjacent to e13 but closer to the

stimulation source, did not have the same stimulation-induced events, suggesting that there was some kind of network connection between e13, e12 and the stimulation zone.

The underlying non-permissive surface of MEAs is an important point to consider for their functional application as implantable prostheses in the brain. The immune response to cortical and retinal prostheses has been well documented and we are challenged with a way to render those artificial implants more biologically compatible (Cohen, 2007; Grill, et al., 2009). The introduction of a cultured MEA interface may address this. A biological layer over MEAs may render its implantation environment more permissive to electrical interaction with the device. Furthermore, autologously-derived adult stem cell-derived neurons may enhance the utility of the interface by reducing an immune response, potentially forming functional connections with primary neurons and also attracting target neurons toward the cortical and electrode surface. Many of these properties desired for the biological brain-machine interface could be achieved by a layer of DPSC rather than requiring pre-differentiation and may be a direction for the future *in vivo* implementation.

The results of this chapter clearly demonstrate limitations of MEA biocompatibility for DPSC culture and differentiation. We have demonstrated that these limitations can be largely overcome with simple substrate-coating techniques, however further research is required so long term cultures can be supported more reliably.

Chapter 5: Neurogenic potential of dental pulp stem cells isolated from murine incisors

Authors

Kylie M. Ellis[a,b,e,†], David C. O'Carroll[a,b], Martin D. Lewis[c,e], Grigori Y. Rychkov[b] and Simon A. Koblar[a,d,e]

[a]Adelaide Centre for Neuroscience Research, [b]School of Medical Sciences, [c]School of Molecular and Biomedical Science, [d]School of Medicine, [e]Stroke Research Programme, University of Adelaide, Adelaide, South Australia, Australia.

[†]Corresponding author

Kylie M. Ellis
School of Medical Sciences
University of Adelaide, Adelaide,
SA, Australia 5005
Telephone: +61-88313-7591
e-mail: kylie.ellis@adelaide.edu.au

Statement of Authorship

Title of Chapter

Neurogenic potential of dental pulp stem cells isolated from murine incisors

Manuscript submitted for publication 2013

Kylie M. Ellis

Experimental design, performed all experiments, collected, analysed and interpreted all data, wrote manuscript.

I hereby certify that the statement of contribution is accurate

Signed Date

David C. O'Carroll

Experimental conceptualisation and design, supervision of work, financial support, manuscript review.

I hereby certify that the statement of contribution is accurate and I give permission for the inclusion of the chapter in the thesis.

Signed Date

Martin D. Lewis

Experimental conceptualisation and design, supervision of work, financial support, manuscript review.

I hereby certify that the statement of contribution is accurate and I give permission for the inclusion of the chapter in the thesis.

Signed Date

Grigori Rychkov

Experimental design, provided patch clamp expertise, manuscript review.

I hereby certify that the statement of contribution is accurate and I give permission for the inclusion of the chapter in the thesis.

Signed Date

Simon A. Koblar

Experimental conceptualisation and design, supervision of work, financial support, manuscript review.

I hereby certify that the statement of contribution is accurate and I give permission for the inclusion of the chapter in the thesis.

Signed Date

Chapter 5 Context Statement:

A long-term goal of this line of research is to implant a DPSC-seeded MEA at the cortex in an animal model. As previously mentioned, one of the major benefits of using DPSC therapeutically is the potential of autologous transplantations, which we wanted to mimic in our animal model. We chose mice as a future animal model due to the opportunity of using advanced transgenic technologies in the animals, as well as their DPSC. It was therefore necessary to characterise the properties of murine-derived DPSC (mDPSC), particularly their neuronal potential. This chapter details the neuronal differentiation of mDPSC *in vitro*, focusing on their phenotype as well as electrophysiological properties.

We found for the first time that mDPSC isolated from incisor teeth differentiated successfully to an immature stage of neuronal development, which supports their use in models of autologous transplantations.

This manuscript has been accepted for publication in Stem Cell Research & Therapy (10 February 2014). It has been reformatted to be consistent with this thesis.

Abstract

Interest in the use of Dental Pulp Stem Cells (DPSC) to enhance neurological recovery following stroke and traumatic injury is increasing following successful pre-clinical studies. A murine model of autologous neural stem cell transplantation would be useful for further pre-clinical investigation of the underlying mechanisms. However, while human-derived DPSC have been well characterised, the neurogenic potential of murine DPSC (mDPSC) has been largely neglected. In this study we demonstrate neuronal differentiation of DPSC from murine incisors *in vitro*. mDPSC were cultured under neuroinductive conditions and assessed for neuronal and glial markers and electrophysiological functional maturation. mDPSC developed a neuronal morphology and high expression of neural markers nestin, ßIII-tubulin and GFAP. Neurofilament M and S100 were found in lower abundance. Differentiated cells also expressed protein markers for Schwann cells, cholinergic, GABAergic and glutaminergic neurons, indicating a mixture of central and peripheral nervous system cell types. Intracellular electrophysiological analysis revealed the presence of voltage-gated L-type Ca^{2+} channels in a majority of cells with neuronal morphology. No voltage-gated Na^{+} or K^{+} currents were found and the cultures did not support spontaneous action potentials. Neuronal-like networks expressed the gap junction protein, connexin 43 but this was not associated with dye coupling between adjacent cells after injection of the low-molecular weight tracers Lucifer Yellow or Neurobiotin. This indicated that the connexin proteins were not forming traditional gap junction channels. The data presented support the differentiation of mDPSC into immature neuronal-like networks.

5.1 Introduction

Since their discovery as a source of multipotent adult human stem cells by Gronthos *et al.* (Gronthos, et al., 2000), numerous groups have confirmed the potential of Dental Pulp Stem Cells (DPSC) to differentiate into multiple neural crest-lineage cell types (Arthur, et al., 2008; Karbanová, et al.). Previous studies in our laboratory and others have demonstrated the neural potential of human-derived DPSC (hDPSC) *in vitro* (Arthur, et al., 2008; Kiraly, et al., 2009) and *in vivo* (Arthur, et al., 2009; Kiraly, et al., 2011; Leong, et al., 2012). hDPSC were found to express neural markers following injection into the rat and embryonic chick brain (Kiraly, et al., 2011; Leong, et al., 2012) and also induced endogenous responses through paracrine effects (Arthur, et al., 2009; Huang, et al., 2008; Nosrat, et al., 2004). In the chick embryo, hDPSC induced neuroplasticity of the highly structured trigeminal ganglion (Arthur, et al., 2009) and promoted the recruitment, proliferation and neural differentiation of endogenous precursors in the mouse brain (Huang, et al., 2008). Interestingly, pre-differentiation of hDPSC promoted greater cell survival and neural differentiation following rat cortical lesion (Kiraly, et al., 2011), which could be reflected therapeutically with greater functional recovery.

Given their potential for autologous transplantation and therapeutic applications in dental engineering and neurological disease treatment, the focus to date has been on applications for human-derived DPSC. The cellular and molecular mechanisms underlying recovery in pre-clinical studies of varied animal models of disease are poorly understood. Xenotransplantation is often problematic (i.e. hDPSC injected into rodents) due to immune rejection. The mouse is a fundamentally important animal model in relation to understanding human disease, pre-clinical testing, and transgenic potential to gain better knowledge of mechanisms of action. A murine model of autologous DPSC transplantation would therefore be of great utility.

Like their human counterpart, rodent DPSC show neural crest multipotentiality (Balic, et al., 2010; Balic & Mina, 2010; Guimarães, et al.; Janebodin, et al., 2011). However, a distinction has emerged between DPSC from murine molar and incisor teeth. While they both possess osteo-dentin and adipocyte differentiation potential, erupted murine molars, but not incisors have been found to have chondrocytic potential (Balic, et al., 2010; Balic & Mina, 2010; Janebodin, et al., 2011; Nozaki & Ohura 2011). Janebodin *et al*. (Janebodin, et al., 2011) have described the expression of neuronal, oligodendrocyte and glial markers after *in vitro* differentiation of murine molar DPSC. To the best of our knowledge neural differentiation of incisor mDPSC has not yet

been attempted and could offer an easily accessible source of DPSC for pre-clinical studies. Work by two other groups suggest that rodent incisor DPSC do have neurogenic potential through the successful formation of cells with neuronal-like multipolar morphology that expressed neuronal markers *in vitro* (Sasaki, et al., 2008; Varga, et al., 2013) and the promotion of nerve regeneration *in vivo* using rat incisor DPSC (Sasaki, et al., 2008). Neither study reported electrophysiological properties of the rat DPSC after neuronal differentiation.

Herein we report the *in vitro* neuronal development of DPSC isolated from murine incisors using a neural differentiation methodology found to generate functional neurons from human DPSC (Kiraly, et al., 2009). We found species-specific differences between human and mouse cells and demonstrated that mDPSC develop characteristics suggesting their differentiation into immature neural cells. Unique to our study is the interrogation of the neuronal characteristics of mDPSC-derived cells using electrophysiological methodologies, which is fundamental to understanding neuronal function.

5.2 Materials and Methods

Ethics Statement

Animal ethics was approved by the University of Adelaide Animal Ethics Committee (S-2009-159).

mDPSC isolation and culture

Incisors from adult BalbC mice were removed and their pulp exposed to enzymatic digestion with 3 mg/mL collagenase type 1 and 4 mg/mL dispase in PBS for 1-2h at 37°C with 5% CO_2. The resulting solution was centrifuged at 200 x g for 5 min, the supernatant and enzymes removed and remaining cells cultured in mesenchymal stem cell medium (Gronthos, et al.) containing alpha-MEM supplemented with 10% foetal bovine serum (FBS, Invitrogen), 1x GlutaMAX (Gibco), 100 μM L-ascorbate-2-phosphate (Wako), 50 U/mL penicillin and 50 μg/mL streptomycin (Invitrogen) and dental pulp stem cells were allowed to adhere to the plastic base. Floating debris could subsequently be removed.

mDPSC neuronal differentiation

mDPSC were seeded at 20,000 cells/cm^2 onto laminin (0.02 mg/mL, Gibco) and poly-L-lysine (0.01%) coated glass coverslips and were induced to differentiate based on a protocol previously described (Kiraly, et al., 2009) (Figure 5.1A). Cells were first maintained in *plating* medium containing 1:1 DMEM/F-12 (Gibco) supplemented with 2.5% FBS, 50U/mL penicillin and 50 μg/mL streptomycin for 24h. They then underwent *epigenetic reprogramming* for 48h with the addition of 10 μM 5-azacytidine, 1 mM dbcAMP and 10 ng/mL mouse-specific fibroblast growth factor-2 (FGF-2, ProSpec) to the basic plating medium. Cells were then washed with PBS and induced with a *neural differentiation* medium containing 250 μM 3-Isobutyl-1-methylxanthine (IBMX), 50 μM forskolin, 1% ITS, 30 nM Phorbol 12-myristate 13-acetate (TPA), 30 ng/mL neurotrophin-3 (NT-3, ProSpec), 10 ng/mL mouse-specific nerve growth factor (NGF), 10 ng/mL FGF-2 in 1:1 DMEM/F12 for 3 days. Finally, cells were rinsed again with PBS before the addition of a *neuronal maturation* medium for 3-7 days, which consisted of 1% N2 and B27 supplements (Gibco), 30 ng/mL NT-3, 1mM dbcAMP in 1:1 DMEM/F12. Cell counts were performed by trypan blue exclusion at days 0, 1, 3, 5, 7, 9 and 11 (Figure 5.1A). Three technical replicates were assessed per time point for three differentiation batches. Statistical analysis of cell proliferation

and attrition was performed with one-way analysis of variance with Bonferroni post hoc analysis. Unless otherwise stated, reagents were sourced from Sigma-Aldrich.

Immunohistochemistry

mDPSC cultures were fixed either undifferentiated or at day 11 of neuronal differentiation with 4% formaldehyde for 20 min. Cells were rinsed then permeabilised with 3% H_2O_2, 10% methanol in PBS for ten min and subsequently washed three times with PBS. Due to high background staining of pilot cultures, mDPSC were blocked at 4°C overnight with 1% bovine serum albumin, 3% horse serum and 3% donkey serum in 0.3% Triton X-100 in PBS (PBS-Tx). Cultures were then incubated with primary antibody diluted in block solution overnight at 4°C. Cells were again rinsed three times with 0.3% PBS-Tx and incubated with secondary antibody for one hour at room temperature with gentle shaking. After rinsing, cultures underwent counterstaining or coverslips were removed from wells and mounted onto slides with ProLong Gold with DAPI (Invitrogen). Images were taken with a Leica SP5 scanning confocal microscope and percentage expression of each marker was determined by manual counts of four representative fields of view.

Primary antibodies raised in mouse targeted ßIII tubulin (Millipore), neurofilament – medium chain (NF-M, Zymed) and S100 (Chemicon). Antibodies raised in rabbit targeted nestin (Abcam), GFAP (1:1000, DAKO), connexin43 (Invitrogen), GAD65/67 (Millipore), ChAT (Biosensis) tyrosine hydroxylase (Chemicon) and vGlut2 (Synaptic Systems). Secondary antibodies used were Alexa555 anti-mouse (Invitrogen), donkey Cy3 anti-rabbit (Jackson) and rabbit Cy3-labelled streptavidin (Invitrogen). Non-specific fluorescence was determined by applying each secondary antibody alone, omitting primary antibody and used as a control. Primary and secondary antibodies were used at 1:500 dilution unless otherwise stated.

Intracellular Electrophysiology

Patch Clamp analysis

Whole-cell voltage clamp analysis of mDPSC was performed at room temperature using a computer-based amplifier (EPC-9, HEKA Electronics, Germany) and PULSE software (HEKA Elektronik, Lambrecht/Pfalz, Germany). Patch pipettes were pulled from borosilicate glass and fire-polished with resistance ranging from 3 to 6 MΩ. Internal pipette solution contained 135 mM

Cs-Glutamine, 5 mM $CaCl_2$, 5 mM $MgCl_2$, 10 mM HEPES, 200 µM GTP, 5 mM ATP, 10 mM EGTA and pH adjusted to 7.3 with NaOH. The calculated internal free Ca^{2+} concentration was approximately 100 nM. A standard bath solution with 10 mM $CaCl_2$, 140 mM NaCl, 4 mM CsGlutamine, 2 mM $MgCl_2$ and 10 mM HEPES, adjusted to pH 7.4 was used. Differentiated mDPSC with a neuronal morphology that could be classified as either *isolated* from other cells or *clustered* (Figure 5.4A and 5.4B) were targeted. Holding potential was set at -60 mV and 500 ms voltage steps ranging between -40 and 50 mV were applied in 10 mV increments to record membrane currents. Cells were interrogated for evidence of voltage-gated Na^+, Ca^{2+} and K^+ currents as well as sensitivity to 100 nM tetrodotoxin (TTX) and 10 mM Ba^{2+} to block or enhance currents through Na^+ and Ca^{2+} channels, respectively. To record K^+ currents, CsGlutamine in the internal solution and CsCl in the bath solution were replaced with KGlut and KCl, respectively. Furthermore, L-type Ca^{2+} currents were recorded from undifferentiated and differentiated mDPSC in response to 100 ms voltage ramps from -120 to +120 mV to compare the current amplitude between cell types. Pharmacological agents were introduced through a gravity-fed perfusion system. The capacitance of each cell was measured using automatic capacitance compensation routine of EPC-9 amplifier. Series resistance did not exceed 20 MΩ and was not compensated for.

Neurobiotin and Lucifer yellow injection

2% neurobiotin and 10 µg/mL Lucifer yellow was injected into clustered mDPSC with neuronal morphology by whole cell patch clamp technique. A patch was maintained with the target cell for five minutes to allow the internal pipette solution to diffuse into the patched and surrounding connected cells. Cells were immediately imaged with an epifluorescent microscope to visualize Lucifer yellow and then fixed with 4% PFA for 20 min prior to immunohistochemical staining for neurobiotin. Cultures were washed with PBS, permeabilised with 0.3% PBS-Tx then counterstained with Cy3-labeled Streptavidin. Cells were imaged on a Zeiss AxioImager Z1 ApoTome microscope.

Transmission electron microscopy (TEM)

$3x10^6$ undifferentiated mDPSC were liberated with trypsin from two T75 flasks and centrifuged at 2000g for two min. Cells were resuspended in 1.5mL 1.25% gluteraldehyde and 4% paraformaldehyde (EM fixative) and stored at 4°C for 24 hours. All subsequent preparation was performed in a fume hood. Cells were washed with 4% sucrose in PBS for five min, then post

fixed in 2% osmium tetroxide for 45 min. Cells were next dehydrated by serial incubations with 70%, 90%, 95% and 100% ethanol, then incubated in propylene oxide for 20 min. A 1:1 mixture of propylene oxide:resin was applied for one hour then 100% resin, 2x one hour. Cells were then embedded in fresh 100% resin and polymerized at 70°C for 24 hours. The resin mixture was made of 10 mL Procure 812, 6 mL Araldite 502, 22 mL DDSA and 560 µL DMP-30. Ultrathin sections were taken and imaged on a Philips CM100 TEM.

Microelectrode arrays

Microelectrode arrays (MEAs) and recording stage were supplied by MultiChannel Systems (MCS, Reutlingen, Germany). Each electrode array contained 59 active titanium nitride electrodes arranged in an 8 x 8 grid with the corner electrodes absent and one electrode used as an electrical reference. Electrode diameter was 30 µm with an inter-electrode distance of 200 µm. Signal acquisitions were managed under MCD software control and sampled at a frequency of 50 kHz.

Microelectrode array electrophysiology

mDPSC were seeded onto the centre of microelectrode arrays (n = 12 cultures) in a 40 µL droplet containing 20,000 cells and were kept in a humidified incubator at 37°C with 5% CO_2. MEAs were sealed with a Teflon membrane lid (MCS) to minimize evaporation. The cells were allowed to settle for one hour then flooded with 1mL culture medium. Cultures underwent neuronal induction according to the protocol described above. The external electrophysiology of the cultures was assessed from differentiation day 10. To record from cultures, MEAs were placed in an electrically grounded recording stage and allowed to settle for 30min. Three 100s recordings were taken from all 59 electrodes for each MEA. 10 µM TTX was added to a subset of cultures to inhibit any action potentials (n = 4 cultures). As a positive control, neuronally differentiated murine embryonic stem cells (46C, n = 2 cultures) and cortical neurons (n = 2) were also seeded onto MEAs and assessed for spiking activity (Methods S1). To determine tonic activity of the system, recordings were made with PBS only on MEAs (n = 4). Data were analysed with Spike 2 software.

MEA data analysis

MEA data were subsequently analysed using Spike2 and Matlab software. A low pass filter of 4000Hz was applied to all MEA traces prior to analysis. The standard deviation of noise was then calculated for each individual electrode trace and a spike detection threshold set at five times this standard deviation. Only supra-threshold events with a physiologically relevant shape and duration were detected as events according to Spike2 settings and each event detected was closely scrutinized for reliability. The spike rate, amplitude and duration of differentiated mDPSC events were compared to controls and assessed statistically by one-way ANOVA with Tukey's post hoc analysis. Only electrodes with three or more events per 100s interval were considered active for analysis purposes.

5.3 Results

Undifferentiated DPSC from murine incisors

Cultured mDPSC displayed a heterogeneous phenotype *in vitro.* The cells were adherent and the majority had large nuclei with fibroblast-like soma and projections (Figure 5.1B and 5.1C). A smaller proportion of cells displayed a webbed-like soma (Figure 5.1D). The proliferation of mDPSC appeared rapid with the population doubling in three days. Transmission electron microscopy demonstrated an elaborate ultrastructure of mDPSC with large irregularly shaped nuclei (Figure 5.1E), extensive rough endoplasmic reticula (Figure 5.1F, arrows) and an intricate outer membrane of microvilli-like projections.

Characterisation of mDPSC following neural induction

mDPSC robustly and reproducibly differentiated into neural phenotypes using the described neuronal induction protocol (Figure 5.1A). During the *epigenetic reprogramming* (ER) stage mDPSC developed rounded phase-bright soma with two distinct morphologies; those cells with bipolar processes and cells with multiple processes (Figure 5.1G and 5.1H, arrows). We found that during the plating and ER stages there was a significant increase in cell number from an average at plating of 20,000 cells to 43,000 by the third day of the neuronal induction protocol (Figure 5.1J). Within 24 hours of changing to the *neuronal differentiation* (ND) stage, which includes specific growth factors (FGF, NT-3 and NGF), cAMP and PKC agonists the cells had differentiated into more neuronal-like morphologies. During the ND and neuronal maturation (NM) stages there was marked cell death with numbers stabilising to approximately 23,000 cells by the end of NM. There was a significant change in cellular morphology during NM into three distinct types: rounded and phase-bright soma with multiple long processes (Figure 5.1I, short arrows), smaller phase-bright bipolar cells (long arrow), and large non phase-bright flatter cells with more diffuse multi-processes (arrowheads). Overall the cells matured into a complex neuritic network with approximately two thirds having a neuronal-like morphology.

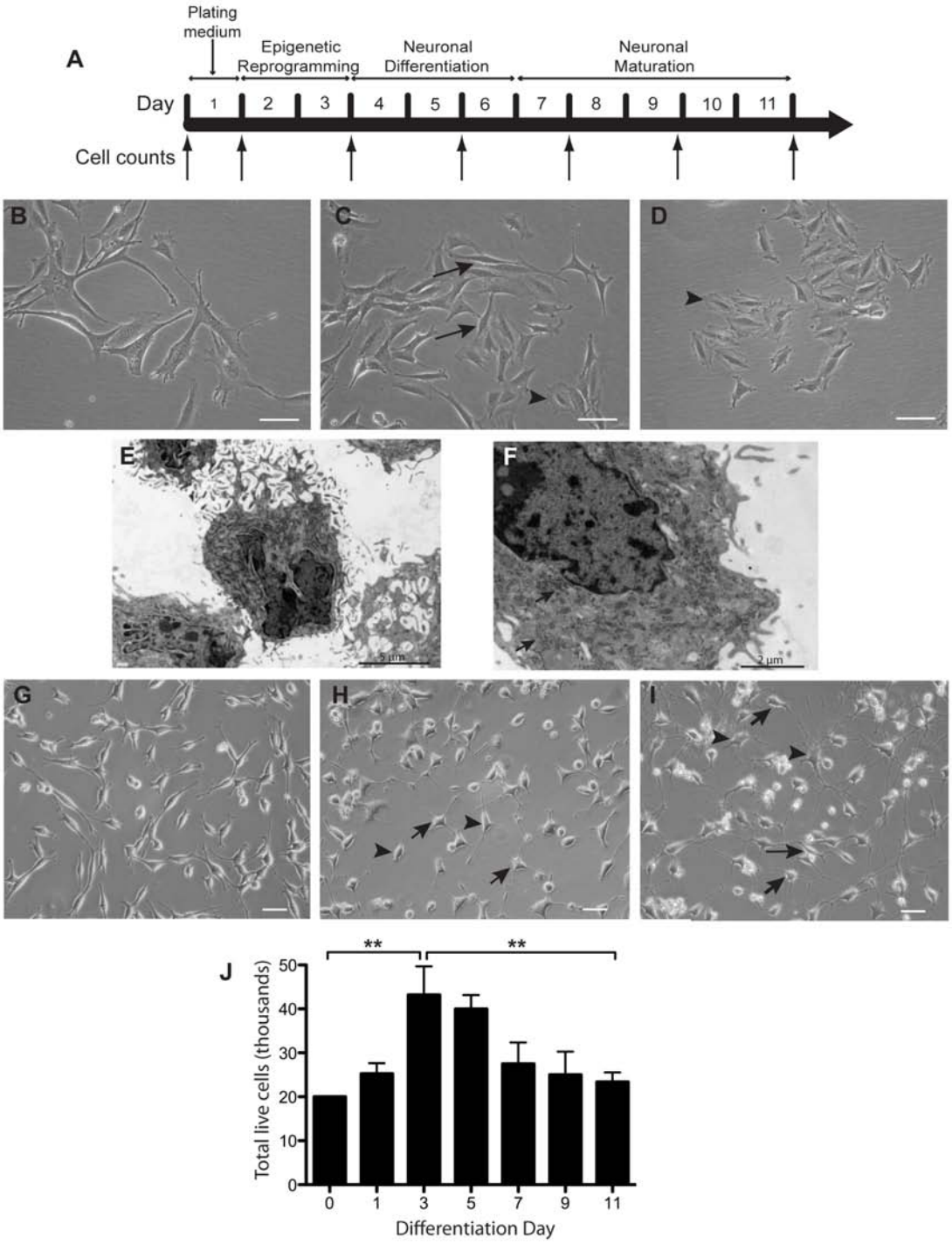
A
Plating medium
Epigenetic Reprogramming
Neuronal Differentiation
Neuronal Maturation
Day
1
2
3
4
5
6
7
8
9
10
11
Cell counts
B
C
D
E
F
G
H
I
J
**
**
Total live cells (thousands)
50
40
30
20
10
0
0
1
3
5
7
9
11
Differentiation Day

Figure 5.1: Timeline, phenotype and survival of differentiating mDPSC.

A) Timeline of neuronal induction protocol with successive medium changes through plating, epigenetic reprogramming, neuronal differentiation and neuronal maturation phases. Cell counts were performed at days 0, 1, 3, 5, 7, 9 and 11 to determine cell viability. B-D) Undifferentiated mDPSC had a fibroblast-like morphology *in vitro*. Some displayed longer processes (B,C arrows) while a smaller population had a webbed soma (C,D arrowheads). E-F) Representative electron micrographs of undifferentiated mDPSC showing a complex ultrastructure with irregularly-shaped nuclei, widespread endoplasmic reticula (arrows) and microvilli-like projections. G-I) Representative bright field images of mDPSC at days 1 (G), 5 (H) and 11 (I) of neuronal differentiation. Cells began to develop short, thin processes by day 5 with bipolar (arrowheads) and multiprocesser (short arrows) morphologies becoming evident. By day 11 mDPSC-derived neural cells had three distinct morphologies; bipolar (long arrow), multiprocessor neural-like cells (arrows) and large, flat multiprocessor glial-like cells (arrowheads). J) Average number of live cells throughout differentiation (n = 3 differentiation batches). Cells showed a high rate of proliferation until day 3 and steadily reduced until significantly less cells were alive at day 11. An average of 23,000 from the original 20,000 plated per well were alive at day 11. Scale bars = 50 μm. **$p<0.01$

At day 11 of induction mDPSC expressed a variety of neuronal and glial proteins. Immunohistochemistry demonstrated the majority of differentiated cells expressed nestin and ßIII tubulin (85% and 79%, respectively; Figure 5.2B and 5.2D). In regards to nestin we found no significant change in expression in comparison to undifferentiated mDPSC with almost all cells expressing this neural precursor protein (Figure 5.2A and 5.2O). ßIII tubulin expression reduced from 97% in undifferentiated mDPSC (Figure 5.2B) to 79% following induction (Figure 5.2D and 5.2O). There was a marked co-expression of nestin and ßIII tubulin in undifferentiated and differentiated mDPSC. Using a mature neuronal marker, NFM (Carden, et al., 1987), expression increased considerably from 2% in the undifferentiated mDPSC up to 20% following induction (Figures 5.2E and 5.2F). GFAP expression was seen in 4% of undifferentiated mDPSC and increased significantly to 94% in differentiated cells (Figures 5.2G and 5.2H). Unexpectedly, the majority of differentiated cells that expressed ßIII-tubulin also co-expressed GFAP (Figure 5.2I-5.2K). To validate this finding of co-expression the same antibodies against ßIII-tubulin and GFAP were used in cultures of primary E19 murine cortical cells and clearly indicated discrete expression of these proteins with respect to their neural cell types (Figure 5.2L-5.2N).

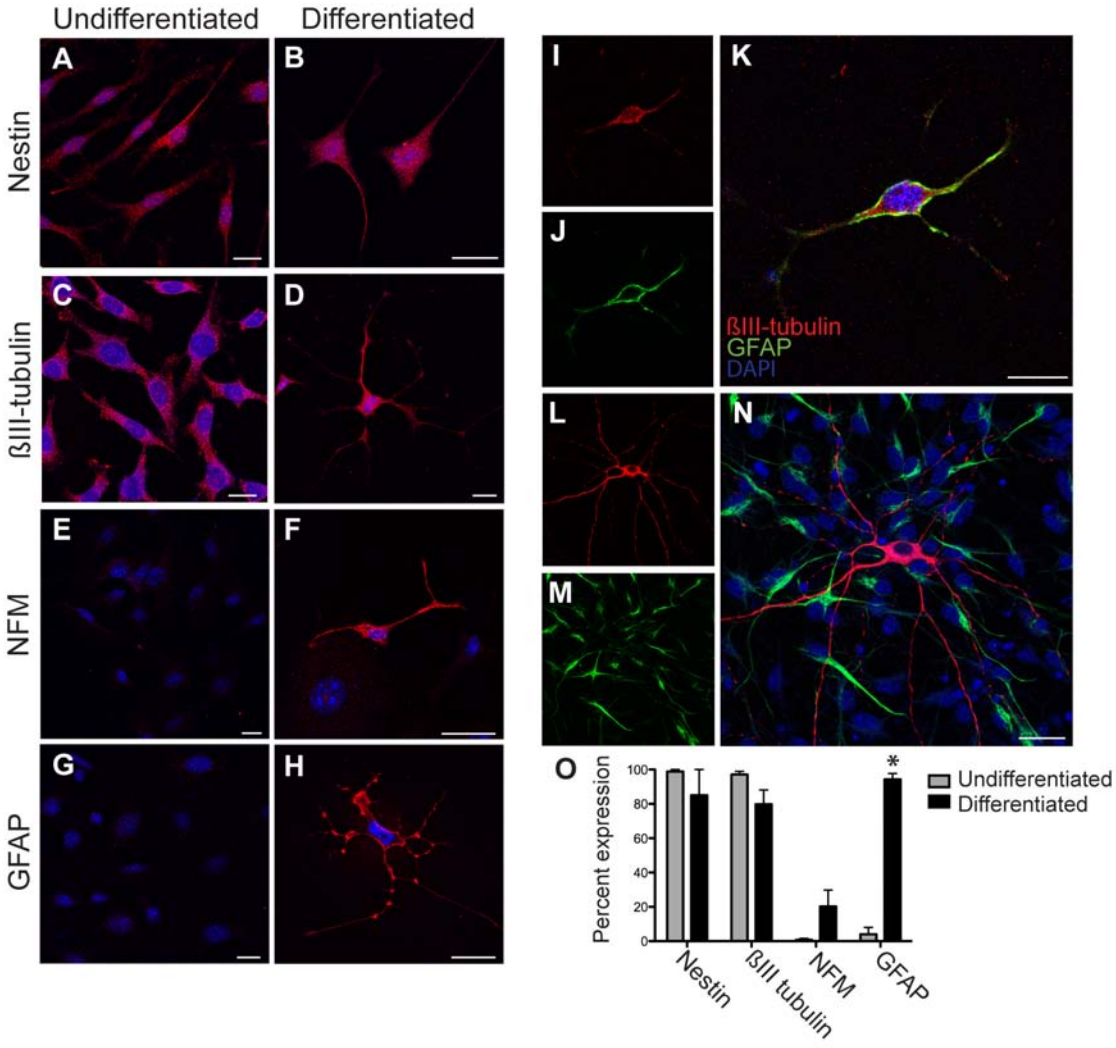

Figure 5.2: Differentiated mDPSC express neuronal and glial markers.

A-H) Representative immunohistochemistry images of undifferentiated mDPSC showing strong expression of nestin and ßIII tubulin but low levels of NFM and GFAP. At day 11 of neuronal differentiation mDPSC retained strong nestin and ßIII tubulin expression (A-D). NFM and GFAP expression was markedly increased following neural induction (E-H). I-K) The majority cells co-expressed ßIII tubulin and GFAP (L-N) Validation of co-expression result using the same ßIII tubulin and GFAP antibodies applied to murine cortical cells, which demonstrates the expected distinction between neurons and glia. O) Quantification of neural IHC. The relative expression of each neural marker before and after differentiation, counted as percent expression per four representative fields of view at 20x magnification. Scale bar = 25 µm. *p<0.05

We next investigated neurally differentiated mDPSC for a range of antigens expressed by mature neural cells to determine whether the expression patterns were consistent with peripheral or central nervous system cell types. We found that 5% of mDPSC at induction day 11 expressed the central and peripheral glial marker, S100, and 87% were positive for acetylcholine specific neurons, ChAT (Figure 5.3A and 5.3B). There was also specific expression of markers for GABAergic (GAD65/67, 5%) and glutaminergic neurons (vGlut2, 15%), but not dopaminergic neurons with a lack of tyrosine hydroxylase immunoreactivity (Figures 5.3C, 5.3D and 5.3E, respectively).

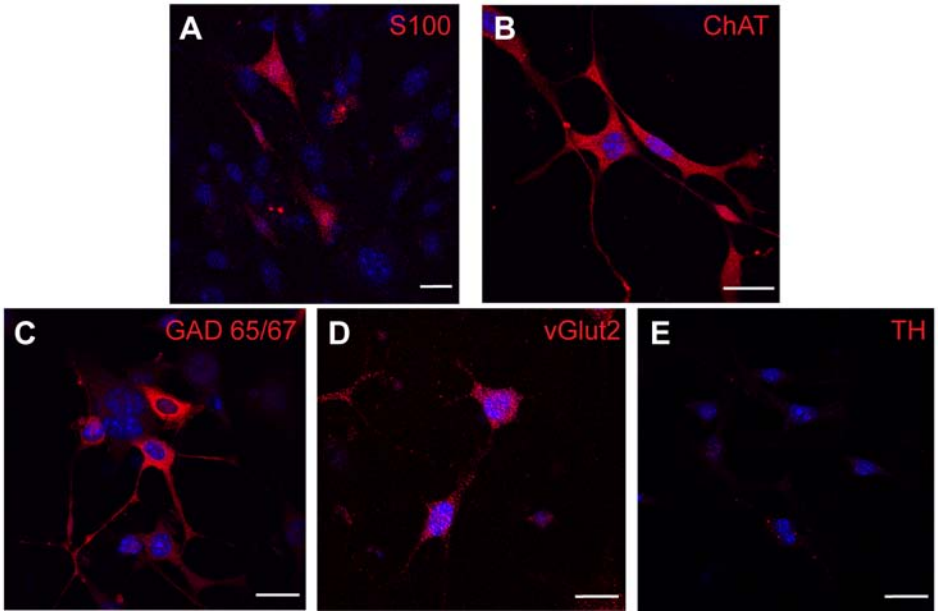

Figure 5.3: Differentiated mDPSC produce central and peripheral nervous system markers.

At day 11 of differentiation mDPSC express central and peripheral nervous system glial marker, S100 (A), and acetylcholine-specific enzyme, ChAT (B). mDPSC also show positive expression of GAD 65/67 (C) and vGlut2 (D) but not TH (E). Scale bar = 25 μm.

Neural network properties of differentiated mDPSC

Differentiated mDPSC demonstrated variable properties indicative of neural networks. Cells were subject to whole cell patch clamp analysis and the results were grouped into neuronal-like cells that were either *isolated* from each other (Figure 5.4B) or *clustered* together (Figure 5.4A). Amplifier-reported capacitance of clustered cells (M = 26.64 ± 12, n = 29 cells) was significantly greater than that of isolated cells (M = 14.32 ± 7.2, n = 12; $p<.01$, Figure 5.4C). However, the reported capacitance of clustered cells was likely a gross underestimation of actual values due the amplifier limitations in compensating for such large current dissipation. Nevertheless, the reported capacitance of isolated cells was accurate and demonstrated the distinction between the classes of differentiated mDPSC.

The nature of cell-cell contacts within clusters was investigated further using immunohistochemistry. Connexin 43 (Cx43), a common gap junction protein, was expressed widely in differentiated (Figure 5.4D) and not undifferentiated mDPSC (Figure 5.4E). Cx43 was more abundantly expressed in cell clusters, as would be expected (Figure 5.4F). We did not find synapsin 1 expression in differentiated cells (data not shown).

To assess the functionality of these gap junctions, Lucifer yellow and neurobiotin tracer dye were injected into a singe cell through a patch pipette and allowed to spread through membrane pores or gap junctions of sufficient size (n = 9 patched cells). Surprisingly, there was no evidence of Lucifer yellow or neurobiotin spread to adjacent cells in differentiated mDPSC cultures indicating that gap junctions were not permeable to small molecules (Figure 5.4G). In contrast, extensive Lucifer yellow dye spread was seen following injection into a single human DPSC after 14 days of the same neuronal differentiation protocol (n = 3 human DPSCs injected, Figure 5.4H and 5.4I). These data indicate a physiological distinction between species.

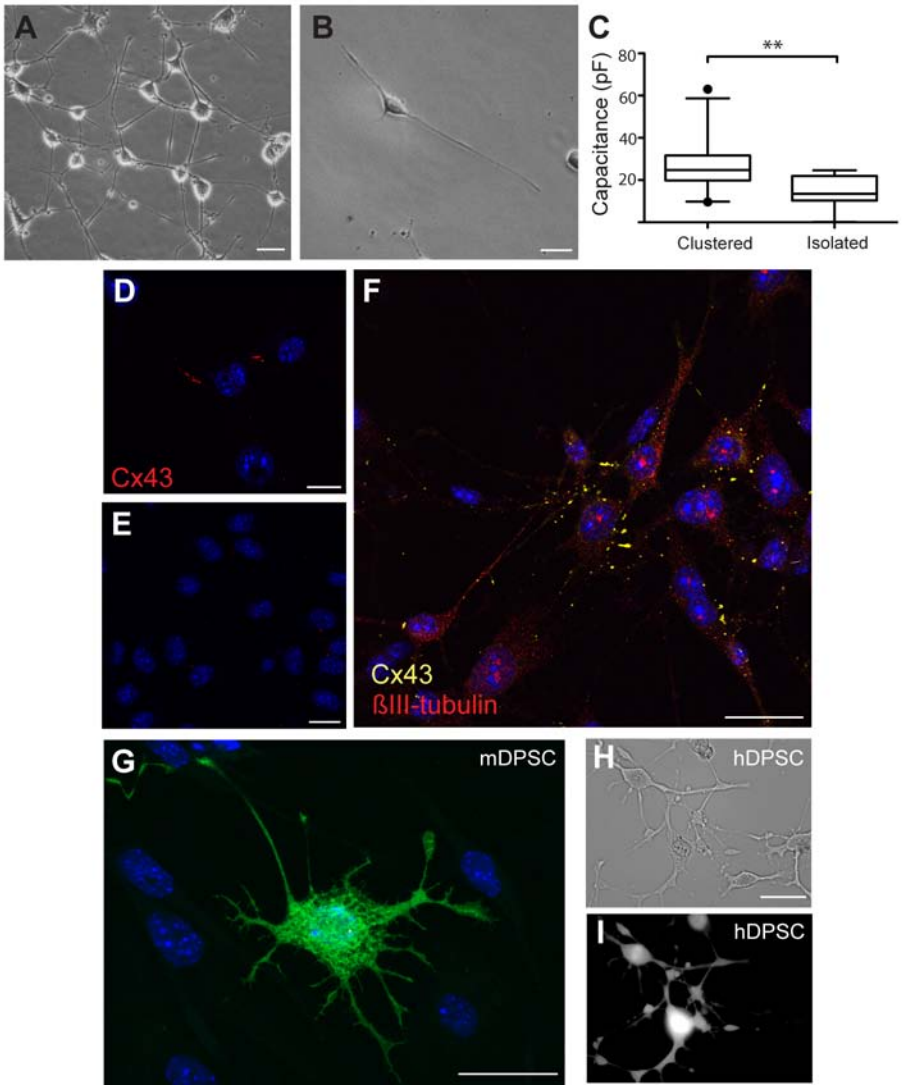

Figure 5.4: Network connectivity of differentiated mDPSC.

Representative images of differentiated mDPSC in a cluster of many cells (A) and as an isolated unit (B). C) Capacitance of clustered cells (n = 23) was significantly greater than isolated cells (n = 9) measured by whole cell patch clamp analysis. IHC shows mDPSC expression of connexin 43 (cx43) in differentiated (D) but not undifferentiated cells (E). F) Cx43 (yellow) is most highly expressed within clusters of ßIII-tubulin (red) positive differentiated mDPSC (iii). G) Image of a clustered mDPSC injected with Lucifer yellow and neurobiotin does not show any dye coupling with adjacent cells. Lucifer yellow injection into a clustered differentiated *human* DPSC does show dye coupling through numerous adjacent cells observed under bright field (H) and ultraviolet light (I). Scale bar = 25 µm. **p<0.01

Differentiated mDPSC express L-type voltage gated Ca^{2+} channels

To determine the presence of neuron-specific ion channels, whole cell patch clamp analysis was performed on undifferentiated mDPSC and mDPSC following neural induction. We found voltage-gated L-type calcium channels in 21 of 27 cells with neuronal-like morphology. Figure 5.5 shows current traces from a representative neuronal-like differentiated cell recorded in response to 500 ms voltage steps in the presence of 10 mM Ca^{2+} (Figure 5.5A) or 10 mM Ba^{2+} (Figure 5.5B) in the bath solution. Figure 5.5C shows current-voltage relationship of the Ca^{2+} current from the same cell. The current amplitude increased more than 2-fold upon Ba^{2+} addition. To normalize the measured currents for variable cell size, the changes in amplitude were expressed as changes in current densities (pA/pF). In contrast, undifferentiated mDPSC produced only small L-type Ca^{2+} currents in response to 100 ms voltage ramps from -120 to +120 mV with an amplitude much lower than that from differentiated mDPSC (Figure 5.5D). No evidence of TTX-sensitive voltage-gated Na^{+} channels (n = 6) or TEA-sensitive K^{+} channels (n = 6) was observed in differentiated cells.

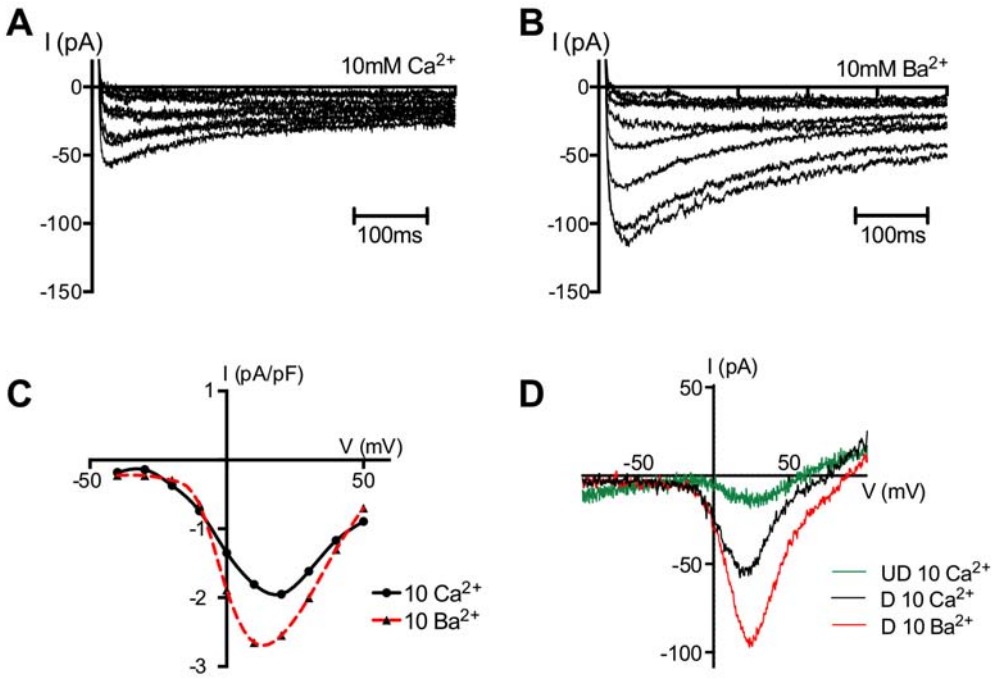

Figure 5.5: Differentiated mDPSC express voltage-gated Ca^{2+} currents.

A) Representative whole cell patch clamp recording of an isolated differentiated mDPSC with multiprocessor neuronal morphology showing typical voltage-gated Ca^{2+} current in response to increasing voltage steps. 500 ms voltage steps of were applied from -50 to +50 mV in 10 mV increments. B) There is a two-fold increase in current amplitude in response to the addition of 10 mM Ba^{2+}. C) The current-voltage relationship of voltage-dependent current from one representative cell with neuronal morphology showing sensitivity to 10 mM Ba^{2+} addition. The amplitude of the current was normalised to cell capacitance. D) Representative L-type Ca^{2+} currents recorded from undifferentiated mDPSC (UD, green) and differentiated DPSC (D, black) in the presence of 10 mM Ca^{2+} and following the addition of Ba^{2+} (D, red), in response to 100 ms voltage ramps from -120 to +120 mV.

Networks of neuronal-like differentiated mDPSC do not demonstrate action potentials

To investigate the network electrophysiology of differentiated mDPSC, cells underwent neuronal induction on MEAs (n = 12 cultures). Each MEA was assessed for extracellular electrical activity between days 10 and 20 with one culture surviving to 34 days. Measurements were taken a maximum of once every two days as increased use led to cell death and infection. Standard noise levels were recorded at 5-8 μV due to the small 30 μm electrodes of MEAs. Numerous spike events were identified in all 12 differentiated mDPSC cultures that satisfied the parameters of an action potential according to predetermined settings of amplitude, duration and shape. Figure 5.6Ai shows a representative single electrode trace from one mDPSC-derived culture at differentiation day 16, such as that seen in Figure 5.6B. It shows one event that passed the spike detection threshold over the four-second period. These events were common across many electrodes and had an average 1ms duration, however they were insensitive to 10 μM TTX administration (n = 4 TTX controls, data not shown). Figure 5.6Aii and 5.6Aiii show representative traces of neuronally differentiated murine embryonic stem cells (mESC) and murine cortical cultures, respectively, which each had larger and more frequent spike events. Average maximum spike rate per 100 sec recording for mDPSC-derived cultures was 2.26 (± 0.751) spikes and was not significantly different from control PBS-only cultures (2.12 ± 0.335, $p>0.05$, Figure 5.6C). Cohen's d demonstrated a small effect size between groups; d = .019 [-0.61,1.01]. Comparatively, the maximum spike rate of differentiated mESC and cortical cultures were both higher at 25.75 ± 17.31 ($p>.05$) and 1028 ± 229 ($p<0.001$) spikes per 100s, respectively. The effect size of each comparison was very large (mESC; d = 2.52 [1.64,3.51]; cortical cells; d = 10.12). Furthermore, as can be seen in Figure 5.6A, event amplitude of mDPSC cultures was far smaller than that of the other cell types. Events from mDPSC cultures had average amplitude of -8.38 ± 1.77 μV, which was not distinguishable from PBS-only cultures (-8.12 ± 0.59 μV, $p>0.05$, d = 0.16 [-1.0,0.68]). By contrast, the average amplitude of mESC events was greater at -12.08 ± 1.1 μV ($p>0.05$, d = 2.52 [1.78,3.33]) and cortical cultures significantly greater at -25.75 ± 8.57 μV ($p<.001$, d = 2.45 [1.82,3.13]) per 100s bin (Figure 5.6D). From these data we conclude that the events observed in mDPSC-derived neural cultures were not spontaneous action potentials.

We recorded oscillatory-like electrical activity over a population of local electrodes on day 32 (n = 1 culture). Each oscillation event lasted approximately 400 ms and occurred up to five times per 100s recording. The epicenter of the oscillations occurred at a single electrode (e13), which had the greatest amplitude of activity (Figure 5.6E). Noise levels between oscillation periods on this electrode (e13) were similar to that of the surrounding electrodes. Numerous other nearby electrodes supported the same oscillatory patterns but with reduced amplitude. Figure 5.6E shows representative traces of one oscillation event from e13, an adjacent electrode, e23, and a distant electrode over 1 mm away, e75, which does not display an obvious oscillatory pattern. The overlay of e13 (black) with adjacent e23 (red) showed that the electrical oscillations from both electrodes were in phase. The power spectral density demonstrated a broad frequency peak at 95 Hz in both e13 and e23 (Figure 5.6F). Interestingly, the control trace from e75 also showed a smaller peak at the same frequency, indicative of weak electrical spread across the entire MEA.

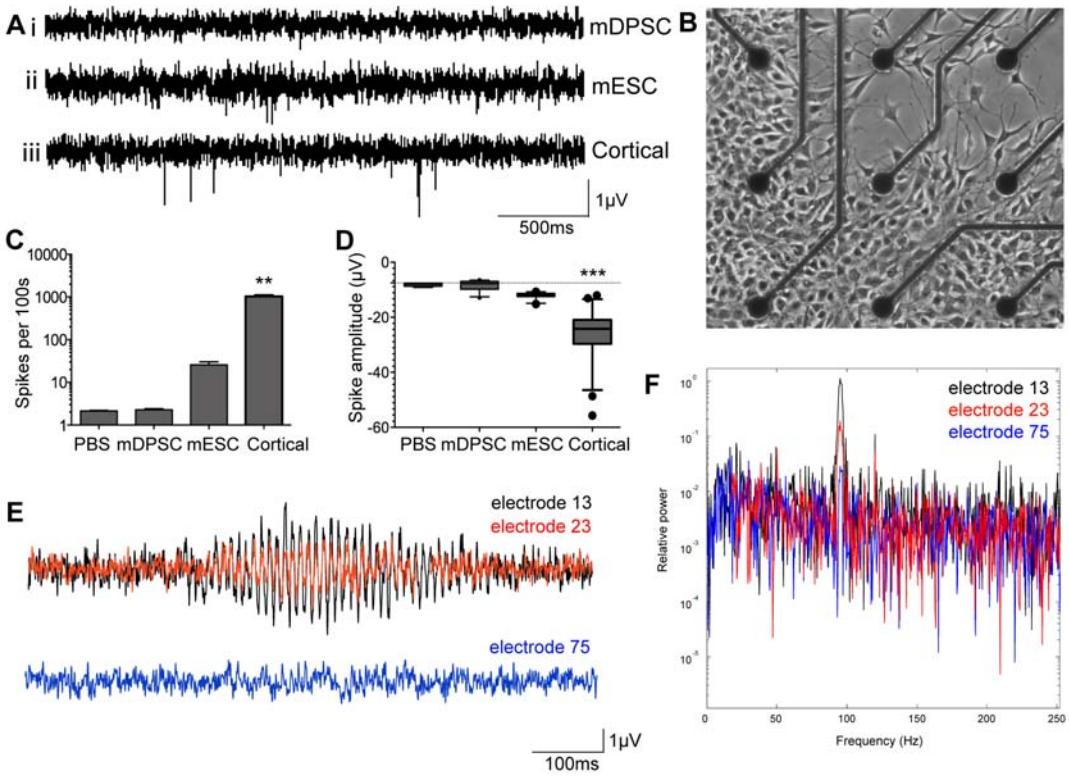

Figure 5.6: Extracellular electrophysiology of differentiated mDPSC.

12 differentiated mDPSC cultures were assayed on MEAs and assessed for network activity. Ai) Differentiated mDPSC cultures exhibited numerous short, low amplitude events that surpassed a threshold of detection. These events were smaller and less numerous than those seen in mESC (Aii) and cortical (Aiii) cultures. B) A representative image of a central region of nine electrodes of a MEA with mDPSC at day 11 of differentiation. Electrode diameter is 30 μm. C) Maximum spike rate of mDPSC events within a 100s bin was significantly lower than mESC and cortical signals and not distinguishable from PBS-only events. D) Boxplots of the mean amplitude of spike events. Spike amplitudes were significantly lower in mDPSC cultures than control mESC or cortical cultures and were not significantly different from PBS-only control traces. E) A representative trace of a single oscillation event observed in an mDPSC MEA culture from day 32 of differentiation. The epicenter of oscillatory activity occurred at electrode 13 (e13, black) and was repeated at numerous adjacent electrodes such as e23 (red) in phasic synchrony. A distant electrode, e75 (ii, blue), did not show any obvious oscillatory activity. F) The spectral power density of oscillatory activity in 6E reveals its broad frequency range peaking at 95 Hz that is consistent across the three representative electrodes seen in E. e13 (red) has the greatest intensity as observed visually followed by e23 and also e75 whose oscillations could not be detected by eye. **p<0.01, ***p<0.0001.

5.4 Discussion

We have shown that DPSC derived from mouse incisors give rise to neural cells. Following neural induction mDPSC expressed neuronal cytoplasmic proteins, neurotransmitter-specific markers, and functional voltage-gated L-type Ca^{2+} channels. The majority of mDPSC developed over time into networks with high gap junction protein expression and did not demonstrate spontaneous action potentials. These data suggest that mDPSC undergo neuronal differentiation *in vitro,* but to a limited maturity with properties more consistent with early neuronal development.

We identified that the majority of undifferentiated mDPSC expressed nestin and ßIII-tubulin which suggests a neurogenic potential. This study, to the best of our knowledge, presents the first evidence of neuronal differentiation of DPSC from murine incisors. Following neural induction mDPSC expressed the more mature neuronal and glial markers NFM and GFAP, respectively. Consistent with other published findings we also observed murine DPSC-derived neural cells co-expressed neuronal and glial markers suggesting these cells were still at an early stage of development (Sakai, et al., 2012). In summary, the immunophenotype of neural cells derived from mDPSC indicated a mixture of central and peripheral nervous system cell types. This was supported by expression of GFAP and S100, a marker of central and peripheral glial cells. In addition we found neuronal-like cells expressed cholinergic, GABAergic and glutaminergic markers. The differentiation of stem cells from human deciduous tooth dental pulp into dopaminergic neuron-like cells *in vitro* has previously been reported (Wang, et al., 2010), indicating the potential for directing the differentiation of DPSC toward a central lineage.

From the neural inductive protocol used throughout these experiments we propose that mDPSC undergo neuronal differentiation *in vitro* but to a limited maturity. This is supported by high expression of a gap junction protein, Cx43, lack of functional Na^+ and K^+ ion channels and a lack of spontaneous action potentials. We found clusters of cellular networks dominated by gap junctions rather than synapse protein expression. *In vivo* nervous system development proceeds from primitive gap junction signaling and later, during maturation, is superseded by synaptic signaling (Dupont, et al., 2006). Cx43, in particular, is involved with neural precursor proliferation, neural differentiation and neurite outgrowth (Bani-Yaghoub, Bechberger, et al., 1999; Bani-Yaghoub, Underhill, et al., 1999; Belliveau, et al., 2006; Todorova, et al., 2008). Moreover, Cx43 blockade decreases the rate of mature neuronal development in the mouse P19 carcinoma cell line, indicating its central role in nervous system maturation (Bani-Yaghoub, Bechberger, et al.,

1999). It is unclear as to what role connexins expressed in mDPSC-derived neural networks retain as we saw no evidence of dye coupling, as would be expected if functional gap junctions were present. Non-channel functions of connexins are also of central importance to neural development. They are involved in cell-to-cell adhesion (Butkevich, et al., 2004) and small molecule release through hemichannels, which is important for functions such as cell migration and neurite outgrowth (Belliveau, et al., 2006; Elias, et al., 2007). In particular, hemichannel-mediated ATP release stimulates Ca^{2+} waves in early neural development, which has been linked with motoneuron, axon and dendritic development (Konur & Ghosh, 2005; Webb & Miller, 2003).

Differentiated mDPSC did not produce spontaneous action potentials or express the ion channels necessary to support them. Rather, we found an abundance of L-type voltage-gated Ca^{2+} channels in differentiated cells, in contrast to low levels of Ca^{2+} currents in undifferentiated mDPSC. Ca^{2+} channels are known to be abundant in developing cortical neurons (Dolmetsch, et al., 2001; Tang, et al., 2003), and calcium transients have been shown to be an important regulator of neurogenesis and neurite extension (Gomez & Spitzer, 1999; Owens & Kriegstein, 1998), often dependent on L-type calcium channel signaling (Tang, et al., 2003). In contrast, human DPSCs reliably developed voltage-gated Na^+ and K^+ currents *vitro* using the same and another differentiation protocol (Arthur, et al., 2008; Kiraly, et al., 2009), highlighting an important distinction between DPSC from different species. We made an isolated interesting observation that in a more mature mDPSC culture there were oscillatory electrical patterns in the gamma frequency range. This suggests the possible development of spontaneous network activity as found *in vivo*. It is well understood that oscillations are central to the development of neural networks during embryogenesis and early postnatal development, however these are typically of a lower beta frequency range (Dupont, et al., 2006; Khazipov & Luhmann, 2006). Gap junctions are intrinsic to sustaining such neural oscillations, as gap junction blockade causes a reduction or cessation of oscillatory activity (Dupont, et al., 2006; Peinado, 2001). Gap junction signalling may be responsible for the oscillations seen in this study but this was not empirically tested. We suggest that these oscillations may demonstrate the emergence of early electrical activity within networks of developing mDPSC. We made multiple attempts to pursue this *in vitro* observation but there were technical difficulties with maintaining these cultures long-term on MEA surfaces.

From the findings presented, it does not seem likely that the cultures would become more mature and develop synapses with longer survival. Rather, alternative methods of neural induction should be considered for more efficient differentiation of mDPSC. Neurosphere generation, for

example, may provide a microenvironment more reminiscent of *in vivo* development to support mature neural differentiation as seen previously with rat incisor and human DPSC (Sasaki, et al., 2008a; Widera, et al., 2007).

In conclusion, we have successfully generated neural cells from murine incisor DPSC to an immature stage of development. Our findings encourage the use of mDPSC to develop mouse models of autologous neural therapeutic transplantations for pre-clinical studies.

Acknowledgements

The authors would like to acknowledge the work by Lauren Sanderman with mouse embryonic stem cells and the patch clamp technical assistance provided by Nathan Scrimgeour.

Supplementary methods (S1)

Murine cortical cultures

C57 Black pups at postnatal day 1 were euthanized by decapitation and cortical explants digested with 10 µg/mL DNase (BD Bioscience) and 0.15% trypsin for 20 min. Resulting cell solution was sieved and centrifuged for enzyme removal. Cells were resuspended and plated in Neurobasal medium containing 1x B27 and N2 supplements, 1x GlutaMAX , 50 U/mL penicillin, 50 µg/mL streptomycin (Sigma) and 10 ng/mL FGF-2 (mouse)(ProSpec) at 15,000 cells/cm^2 onto laminin (0.02 mg/mL) and poly-L-lysine (0.01%) coated glass coverslips or microelectrode array surfaces. Cultures underwent immunohistochemical or electrophysiological analysis as described.

Neuronal differentiation of murine embryonic stem cells (mESC) on microelectrode arrays (MEAs)

mESC were underwent *in vitro* neuronal differentiation according to a protocol previously described (Ying and Smith, 2003). Briefly, mESC were maintained in ESC medium containing 10% foetal bovine serum, 2 mM L-Glutamine, 100 µM ß-mercaptoethanol, 1x Leukemia inhibitory factor, 50 U/mL penicillin and 50 µg/mL streptomycin (Sigma) in Dulbecco's modified eagle medium (DMEM). For neuronal differentiation, mESC were dissociated with trypsin and 3-5x10^4 cells replated onto the electrode region of 0.1% gelatin-coated MEAs in N2B27 medium containing 0.5x N2 and B27 supplements, 50 mg/mL bovine serum albumin, 25 mg/mL insulin, 100 µM ß-mercaptoethanol, 1 mM L-Glutamate, 50 U/mL penicillin and 50 µg/mL streptomycin in 50% Neurobasal medium, 50% DMEM/F12. All reagents were sourced from Gibco unless otherwise specified.

Reference List

Arthur, A., Rychkov, G., Shi, S., Koblar, S. A., & Gronthos, S. (2008). Adult human dental pulp stem cells differentiate toward functionally active neurons under appropriate environmental cues. *Stem Cells, 26*(7), 1787-1795.

Arthur, A., Shi, S., Zannettino, A. C., Fujii, N., Gronthos, S., & Koblar, S. A. (2009). Implanted adult human dental pulp stem cells induce endogenous axon guidance. *Stem Cells, 27*(9), 2229-2237.

Balic, A., Aguila, H. L., Caimano, M. J., Francone, V. P., & Mina, M. (2010). Characterization of stem and progenitor cells in the dental pulp of erupted and unerupted murine molars. *Bone, 46*(6), 1639-1651.

Balic, A., & Mina, M. (2010). Characterization of progenitor cells in pulps of murine incisors. *Journal of Dental Research, 89*(11), 1287-1292.

Bani-Yaghoub, M., Bechberger, J. F., Underhill, T. M., & Naus, C. C. G. (1999). The effects of gap junction blockage on neuronal differentiation of human NTera2/clone D1 cells. *Experimental Neurology, 156*(1), 16-32.

Bani-Yaghoub, M., Underhill, T. M., & Naus, C. C. G. (1999). Gap junction blockage interferes with neuronal and astroglial differentiation of mouse p19 embryonal carcinoma cells. *Developmental Genetics, 24*(1-2), 69-81.

Belliveau, D. J., Bani-Yaghoub, M., McGirr, B., Naus, C. C., & Rushlow, W. J. (2006). Enhanced neurite outgrowth in PC12 cells mediated by connexin hemichannels and ATP. *J Biol Chem, 281*(30), 20920-20931.

Butkevich, E., Hulsmann, S., Wenzel, D., Shirao, T., Duden, R., & Majoul, I. (2004). Drebrin is a novel connexin-43 binding partner that links gap junctions to the submembrane cytoskeleton. *Curr Biol, 14*(8), 650-658.

Carden, M. J., Trojanowski, J. Q., Schlaepfer, W. W., & Lee, V. M. Y. (1987). Two-stage expression of neurofilament polypeptides during rat neurogenesis with early establishment of adult phosphorylation patterns. *Journal of Neuroscience, 7*(11), 3489-3504.

Dolmetsch, R. E., Pajvani, U., Fife, K., Spotts, J. M., & Greenberg, M. E. (2001). Signaling to the nucleus by an L-type calcium channel- calmodulin complex through the MAP kinase pathway. *Science, 294*(5541), 333-339.

Dupont, E., Hanganu, I. L., Kilb, W., Hirsch, S., & Luhmann, H. J. (2006). Rapid developmental switch in the mechanisms driving early cortical columnar networks. *Nature, 439*(7072), 79-83.

Elias, L. A., Wang, D. D., & Kriegstein, A. R. (2007). Gap junction adhesion is necessary for radial migration in the neocortex. *Nature, 448*(7156), 901-907.

Gomez, T. M., & Spitzer, N. C. (1999). In vivo regulation of axon extension and pathfinding by growth-cone calcium transients. *Nature, 397*(6717), 350-355.

Gronthos, S., Arthur, A., Bartold, P. M., & Shi, S. A method to isolate and culture expand human dental pulp stem cells. *Methods Mol Biol, 698*, 107-121.

Gronthos, S., Mankani, M., Brahim, J., Robey, P. G., & Shi, S. (2000). Postnatal human dental pulp stem cells (DPSCs) in vitro and in vivo. *Proc Natl Acad Sci U S A, 97*(25), 13625-13630.

Guimarães, E. T., Cruz, G. S., De Jesus, A. A., Lacerda De Carvalho, A. F., Rogatto, S. R., Pereira, L. D. V., et al. (2011). Mesenchymal and embryonic characteristics of stem cells obtained from mouse dental pulp. *Archives of Oral Biology, 56*(11), 1247-1255.

Huang, A. H., Snyder, B. R., Cheng, P. H., & Chan, A. W. (2008). Putative dental pulp-derived stem/stromal cells promote proliferation and differentiation of endogenous neural cells in the hippocampus of mice. *Stem Cells, 26*(10), 2654-2663.

Janebodin, K., Horst, O. V., Ieronimakis, N., Balasundaram, G., Reesukumal, K., Pratumvinit, B., et al. (2011). Isolation and characterization of neural crest-derived stem cells from dental pulp of neonatal mice. *PLoS One, 6*(11), e27526.

Karaöz, E., Dogan, B. N., Aksoy, A., Gacar, G., Akyüz, S., Ayhan, S., et al. (2010). Isolation and in vitro characterisation of dental pulp stem cells from natal teeth. *Histochem Cell Biol, 133*(1), 95-112.

Karbanová, J., Soukup, T., Suchánek, J., Pytlík, R., Corbeil, D., & Mokry, J. (2011). Characterization of dental pulp stem cells from impacted third molars cultured in low serum-containing medium. *Cells Tissues Organs, 193*(6), 344-365.

Khazipov, R., & Luhmann, H. J. (2006). Early patterns of electrical activity in the developing cerebral cortex of humans and rodents. *Trends Neurosci, 29*(7), 414-418.

Kiraly, M., Kadar, K., Horvathy, D. B., Nardai, P., Racz, G. Z., Lacza, Z., et al. (2011). Integration of neuronally predifferentiated human dental pulp stem cells into rat brain in vivo. *Neurochem Int, 59*(3), 371-381.

Kiraly, M., Porcsalmy, B., Pataki, A., Kadar, K., Jelitai, M., Molnar, B., et al. (2009). Simultaneous PKC and cAMP activation induces differentiation of human dental pulp stem cells into functionally active neurons. *Neurochem Int, 55*(5), 323-332.

Konur, S., & Ghosh, A. (2005). Calcium signaling and the control of dendritic development. *Neuron, 46*(3), 401-405.

Leong, W. K., Henshall, T. L., Arthur, A., Kremer, K. L., Lewis, M. D., Helps, S. C., et al. (2012). Human Adult Dental Pulp Stem Cells Enhance Poststroke Functional Recovery Through Non-Neural Replacement Mechanisms. *Stem Cells Translational Medicine, 1*, 177-187.

Nosrat, I. V., Smith, C. A., Mullally, P., Olson, L., & Nosrat, C. A. (2004). Dental pulp cells provide neurotrophic support for dopaminergic neurons and differentiate into neurons in vitro; implications for tissue engineering and repair in the nervous system. *European Journal of Neuroscience, 19*(9), 2388-2398.

Nozaki, T., & Ohura, K. (2011) Gene expression profile of dental pulp cells during differentiation into an adipocyte lineage. *Journal of Pharmacological Sciences, 115*(3), 354-363.

Owens, D. F., & Kriegstein, A. R. (1998). Patterns of intracellular calcium fluctuation in precursor cells of the neocortical ventricular zone. *Journal of Neuroscience, 18*(14), 5374-5388.

Peinado, A. (2001). Immature neocortical neurons exist as extensive syncitial networks linked by dendrodendritic electrical connections. *J Neurophysiol, 85*(2), 620-629.

Sakai, K., Yamamoto, A., Matsubara, K., Nakamura, S., Naruse, M., Yamagata, M., et al. (2012). Human dental pulp-derived stem cells promote locomotor recovery after complete transection of the rat spinal cord by multiple neuro-regenerative mechanisms. *J Clin Invest, 122*(1), 80-90.

Sasaki, R., Aoki, S., Yamato, M., Uchiyama, H., Wada, K., Okano, T., et al. (2008a). Neurosphere generation from dental pulp of adult rat incisor. *Eur J Neurosci, 27*(3), 538-548.

Sasaki, R., Aoki, S., Yamato, M., Uchiyama, H., Wada, K., Okano, T., et al. (2008b). Tubulation with dental pulp cells promotes facial nerve regeneration in rats. *Tissue Eng Part A, 14*(7), 1141-1147.

Tang, F., Dent, E. W., & Kalil, K. (2003). Spontaneous calcium transients in developing cortical neurons regulate axon outgrowth. *Journal of Neuroscience, 23*(3), 927-936.

Todorova, M. G., Soria, B., & Quesada, I. (2008). Gap junctional intercellular communication is required to maintain embryonic stem cells in a non-differentiated and proliferative state. *Journal of Cellular Physiology, 214*(2), 354-362.

Wang, J., Wang, X., Sun, Z., Yang, H., Shi, S., & Wang, S. (2010). Stem cells from human-exfoliated deciduous teeth can differentiate into dopaminergic neuron-like cells. *Stem Cells Dev, 19*(9), 1375-1383.

Webb, S. E., & Miller, A. L. (2003). Calcium signalling during embryonic development. *Nat Rev Mol Cell Biol, 4*(7), 539-551.

Widera, D., Grimm, W. D., Moebius, J. M., Mikenberg, I., Piechaczek, C., Gassmann, G., et al. (2007). Highly efficient neural differentiation of human somatic stem cells, isolated by minimally invasive periodontal surgery. *Stem Cells Dev, 16*(3), 447-460.

Chapter 6: Dental pulp stem cells downregulate the perineuronal net *in vitro*

Statement of Authorship

Title of Chapter

Dental pulp stem cells downregulate the perineuronal net *in vitro*

Traditional thesis chapter

Kylie M. Ellis

Experimental design, performed all experiments, collected, analysed and interpreted all data, wrote manuscript.

I hereby certify that the statement of contribution is accurate

Signed Date

Martin D. Lewis

Experimental conceptualisation and design, supervision of work, assistance planning data analysis, financial support.

I hereby certify that the statement of contribution is accurate and I give permission for the inclusion of the chapter in the thesis.

Signed Date

David C. O'Carroll

Experimental conceptualisation and design, supervision of work, assistance planning data analysis, financial support.

I hereby certify that the statement of contribution is accurate and I give permission for the inclusion of the chapter in the thesis.

Signed Date

Simon A. Koblar

Experimental conceptualisation and design, supervision of work, assistance planning data analysis, financial support, manuscript review.

I hereby certify that the statement of contribution is accurate and I give permission for the inclusion of the chapter in the thesis.

Signed Date

Chapter 6 Context Statement:

As part of the 'scaffold' approach to brain repair therapy, we sought to understand how DPSC could influence the local microenvironment of the brain to create an environment permissive to plasticity at a brain-machine interface and also in a range of other disorders. In this chapter I investigated whether DPSC can influence the expression of the perineuronal net (PNN), a specialised extracellular matrix that lies around neurons to enhance structural stability. The PNN also has the capacity to limit plasticity after injury (Massey, et al., 2008; Yi, et al., 2012). Previous research has shown that the degradation of the PNN can enhance neural plasticity and functional recovery following neurological damage (Bradbury, et al., 2002; Pizzorusso, et al., 2002).

As shown in previous chapters, both human (Chapter 4) and murine-derived (Chapter 5) DPSC have neurogenic potential *in vitro* – we next wanted to determine their compatibility with cortical tissue and their influence on it at a molecular level. I investigated the expression of the PNN in murine cortical cultures with and without DPSC co-culture and found a dose- and time-dependent decrease in measured PNN. Interestingly, this was achieved from the addition of hDPSC-conditioned medium, suggesting that hDPSC can decrease measured PNN expression through the release of soluble paracrine factors.

This is the first step to understand how DPSC may influence the brain's endogenous inhibition after injury and could present a therapeutic application to improve the brain-machine interface as well as other neurological disorders.

6.1 Introduction

The perineuronal net (PNN) is a specialised form of the extracellular matrix that surrounds the soma and proximal dendrites of predominantly inhibitory interneurons. Its putative roles include the regulation of network stability, ion homeostasis and neuroprotection in the healthy adult central nervous system (CNS) (Wang & Fawcett, 2012). However, the upregulation of many PNN components following insult to the CNS such as spinal cord injury and stroke make it a source of inhibition that can limit functional recovery (Silver & Miller, 2004). Therefore, downregulation of the PNN is a potential treatment target to promote neural regeneration after CNS injury.

In the healthy adult and developing CNS the PNN is vital in the maturation and maintenance of neural networks and its proper function has been implicated in memory, mental health, epilepsy and neuroprotection in Alzheimer's disease (Berretta, 2012; Gogolla, et al., 2009; Khler, et al., 2011; McRae, et al., 2012; Miyata, et al., 2007; Morawski, et al., 2010; Quirk, et al., 2010). Its formation directly coincides with the end of the 'critical period', a time during early postnatal development where environmental input has the strongest influence on neuronal properties and synaptic networks (Hensch, 2004; Hockfield, et al., 1990). Once the critical period ends and the PNN becomes established, neuronal networks become stable and do not respond to environmental influences as readily (Pizzorusso, et al., 2002). Furthermore, the downregulation of the adult PNN can reinstate juvenile-like plasticity in the brain and spinal cord (Carulli, et al., 2010; Pizzorusso, et al., 2006). These findings implicate the PNN in the control of synaptic plasticity (For a review see (Wang & Fawcett, 2012)).

Structurally, the PNN consists of a highly organised matrix of macromolecules. The backbone is composed of linear hyaluronan polymer chains, which are attached to the neuron cell surface by a family of enzymes called hyaluronin synthase (HAS) (Carulli, et al., 2006; Galtrey, et al., 2008; Kwok, et al., 2010). Hyaluronin binds the N-terminus end of chondroitin sulfate proteoglycans (CSPGs) through stabilising link proteins (Kwok, et al., 2010). At their C-terminus, up to three CSPGs bind to trimeric Tn-R (Aspberg, et al., 1997), which completes the stable macromolecular PNN structure.

Following CNS trauma, PNN components, particularly CSPGs, are upregulated by reactive astrocytes and oligodendrocytes as part of the glial scar, forming a dense and restrictive layer around neurons (Jones, et al., 2003; McKeon, et al., 1999). CSPGs are a major family of axon growth inhibitors that form a barrier to regeneration and synaptic plasticity. Numerous groups have shown that the degradation of glycosaminoglycan (GAG) side chains on CSPGs by the

bacterial enzyme Chondroitinase ABC (ChABC) can promote axonal regeneration and functional recovery following spinal cord injury in rodents *in vivo* (Bradbury, et al., 2002; Garcia-Alias, et al., 2009). Furthermore, intracerebral ChABC administration can also promote anatomical and behavioural improvements following stroke in rats (Hill, et al., 2012; Soleman, et al., 2012). Together these studies indicate that the removal of restrictive CSPGs and PNN matrix restores the ability of neurons to alter their synaptic connections to promote regeneration following injury.

Cellular-based therapy is a viable and promising avenue as a multifaceted therapeutic strategy to overcome CNS damage and promote functional recovery. Over the last decade a variety of stem cell types, including human neural stem cells (Cummings, et al., 2005; Toda, et al., 2001; Zhang, et al., 2003), embryonic stem cell-derivatives (Erceg, et al., 2010; Erdö, et al., 2003; Hoehn, et al., 2002; Kumagai, et al., 2009) and adult bone marrow stromal cells (BMSCs) (Chen, et al., 2001; Cizkova, et al., 2006; Hofstetter, et al., 2002) have been transplanted into the injured spinal cord or stroke-affected brain of rodents and their neuroregenerative properties assessed (Leong, et al., 2013). These studies have demonstrated that engraftment of stem cells can promote functional recovery to varying degrees through both cell-replacement and paracrine effects. However, the usefulness of these therapies also relies on the availability and accessibility of the cells.

Recently, the affinity of stem cells from adult teeth to repair the CNS following damage has been identified and presents an easily accessible source of multipotent stem cells with minimal invasiveness or ethical complications. The dental pulp stem cells (DPSC) have mesenchymal stem cell-like properties of self-renewal (Gronthos, et al., 2000) and as well as showing dentinogenic and neurogenic potential (Arthur, et al., 2008; Gronthos, et al., 2000; Kiraly, et al., 2009). Additionally, they express a variety of trophic factors that promote neuronal survival, proliferation, differentiation and migration (Arthur, et al., 2009; Huang, et al., 2008; Nosrat, et al., 2004; Nosrat, et al., 2001). Furthermore, their trophic support through conditioned medium to ganglion neurons helps to overcome inhibitory signals from co-cultured CSPGs *in vitro* to reinstate healthy neurite outgrowth (Sakai, et al., 2012). *In vivo*, Sakai *et al* (Sakai, et al., 2012) recently demonstrated that stem cells from human exfoliated deciduous teeth (SHED), which have properties very similar to adult DPSC, could promote regeneration of transected spinal cord axons through the inhibition of multiple axon growth inhibition signals by paracrine mechanisms.

Recently, transplanted human DPSC has also been demonstrated to enhance functional recovery following stroke in the rat brain (Leong, et al., 2012). The precise mechanisms for recovery following DPSC transplantation is unknown, however is postulated to be via non neural

replacement effects as only a low rate of DPSC survival and neural differentiation was observed to survive at 4 weeks following injection. It may be that hDPSC actively reduce inhibitory signals in injured tissue, such as the PNN, allowing neuroplasticity and promoting anatomical and functional recovery. To the best of our knowledge, no such stem cell mechanism of action with respect to PNN induced increased neuroplasticity in the stroke brain has been investigated. Murine DPSC, like their human counterparts, have neurogenic potential *in vitro* (Janebodin, et al., 2011) but it remains unclear as to how they may differ from other mammalian species. As such, investigation of murine DPSC in a mouse model of autologous cell transplantation following stroke would provide further insights into mechanisms of action in this paradigm.

As DPSC are known to overcome the inhibitory effects of CSPGs *in vitro* and aid neurological recovery following injury *in vivo*, is it possible that their effect is through the manipulation of the PNN. A greater understanding of the mechanisms of DPSC-enhanced recovery could aid in more efficient delivery of cell-based therapy in the future. Therefore, the aim of the current study was to investigate whether DPSC co-culture downregulated the expression of the PNN in cortical neuronal cultures. We hypothesise that DPSC may downregulate PNN expression in a dose and temporal-dependent manner *in vitro*.

6.2 Methods

6.2.1 Murine cortical cultures

Primary cortical cultures were established from postnatal day 1 C57 Black pups. Briefly, pups were euthanised by decapitation and cortical explants digested with 10µg/mL DNase and 0.15% trypsin for 20 min. Resulting cell solution was sieved with a 40 µm millipore and centrifuged for cellular debris. Cells were resuspended and plated in Neurobasal medium containing 1x B27 and N2 supplements, 1x GlutaMAX , 50 U/mL penicillin, 50 µg/mL streptomycin and 10 ng/mL FGF-2 (mouse) at 15,000 cells/cm^2 onto laminin (0.02 mg/mL) and poly-L-lysine (0.01%) coated acid-treated glass coverslips. Cultures were maintained for up to 21 days with a half-medium change every second day.

6.2.2 Dental pulp stem cell isolation and culture

Human DPSC were isolated from adult impacted third molars as previously described and stored in liquid nitrogen (Gronthos, et al., 2000). DPSC from three healthy young adult donors were used, labelled H1, H3 and H4, respectively. Murine DPSC were previously isolated from adult BalbC incisors as previously described (Kremer et al. *in preparation*). One mDPSC labelled M1 was used in the study, which had been derived from BalbC incisor teeth.

Both human DPSC and foreskin fibroblasts (hFF), and murine DPSC were maintained in alpha-modified Eagle's medium supplemented with 10% foetal bovine serum, 100 µM L-ascorbic acid 2-phosphate, 1x GlutaMAX, 100 U/mL penicillin and 100 µg/mL streptomycin at 37 ℃ in 5% CO2, as previously described (Gronthos, et al., 2000). Cells were dissociated with 0.15% trypsin, resuspended in PBS and immediately added to cortical cultures at a desired concentration. Cell viability was determined by trypan blue exclusion assay as described previously.

6.2.3 PNN development assay

To determine the time required for cortical cultures to develop a quantifiable PNN *in vitro*, cultures were established as described above and fixed after 7, 14 or 21 days *in vitro* (DIV). They were subsequently assessed for PNN-expression by immunohistochemistry staining for the PNN marker *Wisteria Floribunda* agglutinin (WFA,1:1000). PNN expression patterns were compared across three time points (duplicated).

6.2.4 DPSC dose assay

Cortical cultures were established as described above and 1000, 2000 or 5000 DPSC or hFF per cm^2 were added after 13 DIV (all at least duplicated). Co-cultures were maintained for 24h and fixed for immunohistochemical (IHC) analysis of PNN expression as described below.

6.2.5 Conditioned media assay

Cortical cultures were established and maintained as described above. After 13 DIV 2000 cells/cm^2 of H3, H4 DPSC or hFF were added into microwell™ inserts (Merck Millipore) with 0.4 µm pore holes that kept them separated from cortical cells (N=3). The pores allowed small molecule exchange such that trophic factors released from experimental cells could affect cortical cells without direct contact. Microwell inserts were kept for 24h at which point cortical cultures were collected and underwent IHC analysis for PNN expression. Cortical cultures with microwell inserts but without cell additions were compared as a control (N=3).

6.2.6 Duration assay

Cortical cultures were maintained as described previously. 4000 cells/cm^2 of either H3 DPSC, H4 DPSC or hFF were added to cortical cultures and fixed with 4% paraformaldehyde after 24, 48, 72 or 96h to determine duration effects of DPSC co-culture (N=3 each group). Control cortical cultures with no cell additions were also collected at each time point to ensure no baseline time-dependent effects in PNN expression. All cultures were analysed by IHC as described below.

6.2.7 Immunohistochemistry

Cortical co-cultures were fixed with 4% paraformaldehyde for 20 min. Cells were rinsed then permeabilised with 3% H_2O_2, 10% methanol in PBS for 10 min and subsequently washed three times with PBS for five min per wash. Cultures were blocked at 4°C overnight with 1% bovine serum albumin, 3% horse serum and 3% donkey serum in 0.3% Triton X-100 in PBS (PBS-Tx). Cultures were then incubated with mouse anti-NeuN (1:200) and fluoroscein-conjugated WFA (1:1000) diluted in block solution overnight at 4°C. Cells were again rinsed three times with 0.3% PBS-Tx and incubated with rabbit Alexa555 anti-mouse (1:500) for one hour at room temperature with gentle shaking. After rinsing, coverslips were removed from culture wells and mounted onto slides with ProLong Gold with DAPI. Representative images were taken with a Leica SP5 scanning confocal microscope or Zeiss ApoTome.

6.2.8 Cell counts

Cortical co-cultures were assessed for PNN expression by counting the percentage of NeuN-positive neurons that co-expressed WFA. Approximately 100 NeuN-positive cells were analysed per cortical co-culture by linear sweeps across the coverslip and all PNN-positive cells were imaged for later analysis.

6.2.9 ImageJ software analysis

Images of PNN-expressing neurons were analysed using ImageJ software. Images were split into wavelength channels and the WFA channel alone was used for analysis. A threshold of PNN signal intensity was set at 60, between range limits of 0-255, using the RenyiEntropy method to optimise signal detection to PNN regions only and rejecting background signal. The region of interest was drawn around the PNN signal area and particle analysis performed to extract a measure of total PNN area and average signal intensity per cell. A measure of total PNN area was calculated based on the average PNN area per cell multiplied by the percentage of NeuN neurons that expressed PNN. This gave a value for total PNN area per 100 cells and could be directly compared across replications and experimental conditions.

6.2.10 Statistical analysis

Grouped data were analysed using two-way ANOVA followed by a Tukey's post hoc tests for multiple comparisons. Ungrouped data (conditioned media experiments) were analysed by one-way ANOVA with Tukey's post hoc correction for multiple comparisons. Data was displayed as mean ± SEM. An alpha-value of 0.05 was deemed significant in all experiments.

To compare the distributions of PNN area per cell across conditions, data from three coverslips per condition were collated to form a histogram distribution. Histograms were smoothed using a Savizky-Golay filter. Smoothed histograms were then fitted with log-normal nonlinear regression curves to fit their strong positively skewed shape and qualitatively compared across experimental conditions. Cumulative histograms counted the cumulative number of neurons with increasing PNN area. The proportion of cells with small (15th percentile), medium (50th percentile) and large (90th percentile) PNN areas was compared by Chi-square analysis across cell types and dosage conditions.

6.3 Results

6.3.1 Characterisation of PNN cellular development *in vitro*

WFA was found to be expressed in murine cortical cultures, indicative of the development of PNN structure from 7 DIV, which became more pronounced by days 14 and 21 (Figure 6.1). After 7 DIV cortical PNN expression was sparse and weak. However, by 14 DIV PNN expression was strongly upregulated and more closely and densely associated with cell soma and proximal dendrites. PNN expression was also strong at 21 DIV, however parallel cultures appeared to be more variable. As cortical cultures expressed robust and reproducible PNN expression at 14 DIV this time point was chosen for subsequent experimentation.

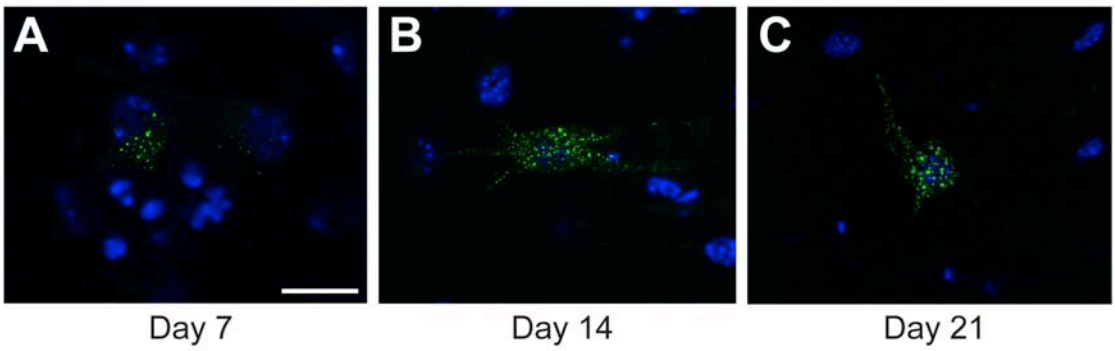

Figure 6.1: PNN development in cortical cultures.

PNN expression (green) was apparent from day 7 *in vitro* (A) and became more apparent, closer and denser in relation to neurons by days 14 (B) and 21 (C) *in vitro*. Green - WFA expression; Blue – DAPI. Scale bar = 25 µm

Within cortical neural cultures we found a wide-breath of PNN levels of expression at a cellular level. Figure 6.2 shows representative images of NeuN-positive cells that co-expressed either low, moderate or strong PNN. Analysis of PNN expression area per cell demonstrated a skewed distribution wherein the majority of neurons expressed a small to moderate level of PNN and a minority of neurons expressed larger PNN areas, creating a long positively skew tail (Figure 6.2D).

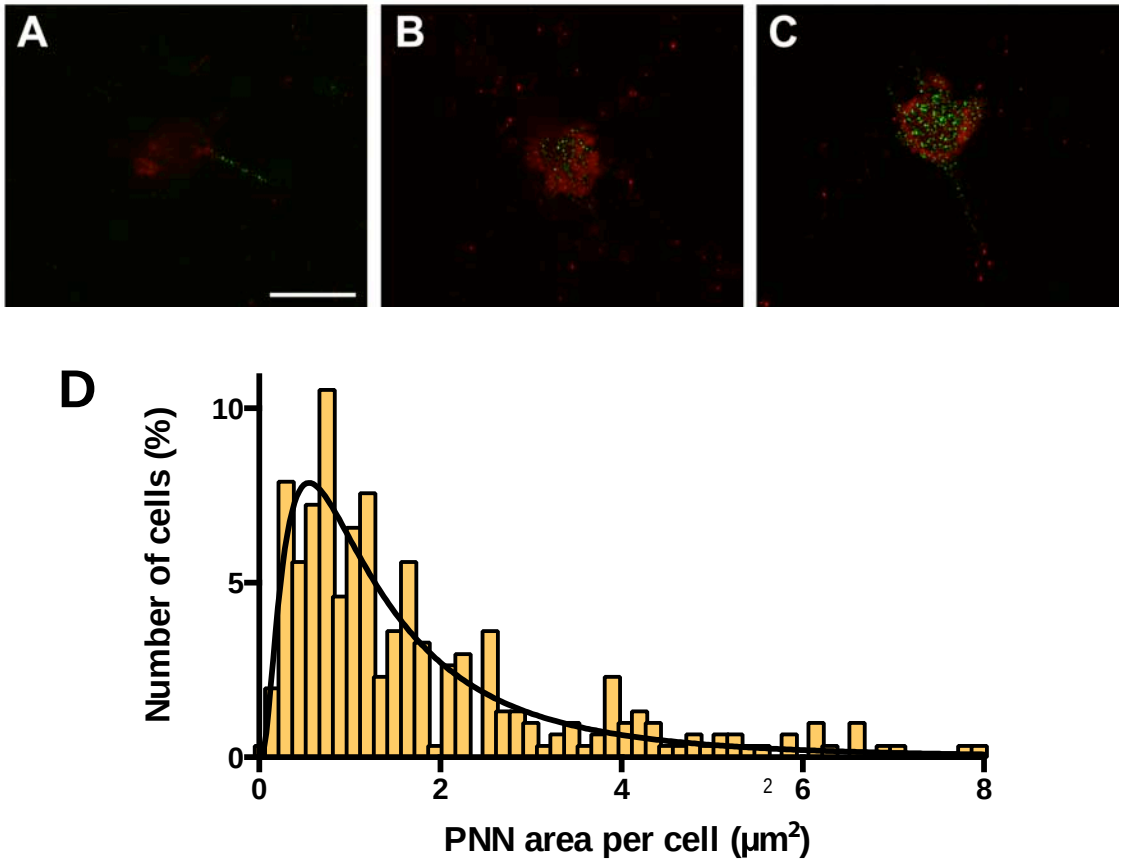

Figure 6.2: Range and distribution of neuronal PNN expression area per cell

Representative images demonstrating the range of PNN cellular expression (WFA, green) from low area (A) to moderate (B) and large area (C) around NeuN-positive neurons (red). The distribution of PNN area per cell from untreated control cultures at 14 DIV (D). Scale bar = 25 µm.

6.3.2 DPSC treatment downregulates PNN expression in a dose-dependent manner

14 DIV was identified as a reproducible time point for assaying PNN expression. Therefore, human or murine DPSC were added to cortical cultures at day 13 for 24h to characterise their effect on PNN expression compared with hFF control cells and cultures with no cell additions. We found that following 24h human DPSC co-culture the percentage of NeuN-positive cells that were co-localised with WFA expression was reduced in a dose-dependent manner (Figure 6.3A). The effect of mDPSC co-culture was less clear. The addition of 1000 murine and human DPSC/cm^2 resulted in a modest decrease in the percentage of WFA-positive cells compared with control cultures with no cell additions but was not significantly reduced from hFF-treated controls. The effect at 2000 and 5000 cells/cm^2 co-culture was stronger for hDPSC with approximately 14% and 10% fewer NeuN neurons co-localised with WFA expression than in hFF-treated controls, respectively. No effect in the percentage of neurons co-localised with WFA expression was observed with 2000 or 5000 mDPSC/cm^2 treatment. This accounted for an overall cell type effect ($p<0.01$), and a dose-dependent effect ($p<0.05$), whereby increasing concentrations of hDPSC treatment downregulated PNN expression. We found no effect of mDPSC and hFF treatment compared to untreated controls.

Each neuron with associated WFA-expression counted was further analysed for its area of PNN. Total measured PNN area was unaltered following 1000 cells/cm^2 co-culture with any cell type (Figure 6.3B). There was a non-significant trend for a cell type effect ($p=0.051$), indicating that hDPSC treatment only caused a reduction in PNN area in a dose-dependent manner. Consistent with our previous results, there was no effect of mDPSC or hFF treatment.

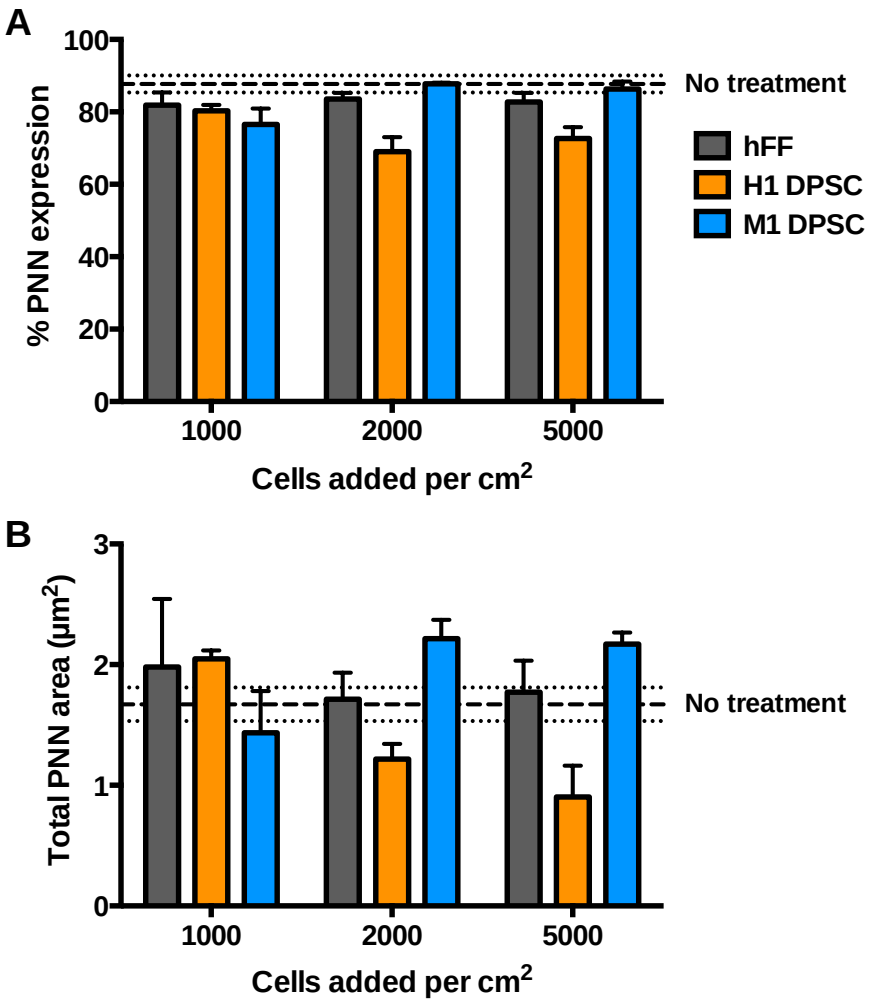

Figure 6.3: DPSC treatment downregulated PNN expression in a dose-dependent manner.

A) The percentage of NeuN-positive neurons that co-localised with WFA expression. hDPSC treatment caused a reduction in PNN expression compared to hFF treated controls in a dose-dependent manner (cell type effect, $p<0.05$). mDPSC treatment had no effect. B) Total PNN area decreased with increased hDPSC dosage. The 'no treatment' lines demonstrate the mean and SEM of total area of PNN per cell without any DPSC addition. N= at least 3 replicates per treatment group.

PNN expression was analysed in a more detailed manner to derive further understanding of treatment effects. The distributions of measured PNN area per cell were fitted by log-normal nonlinear regression and compared between conditions to characterise DPSC treatment effect on PNN expression. This analysis focused on the distribution of neuronal PNN expression in different treatment conditions. At 1000 and 2000 cells/cm^2 hDPSC treatments the distribution of neuronal PNN area expression were similar (Figure 6.4A and B). However, murine DPSC treatment at 2000 cells/cm^2 diverged (Figure 6.4B). At the highest cell treatment of 5000 cells/cm^2 there was a strong divergence in human and murine DSSC treatment in comparison to hFF, though in opposite directions. Following the highest hDPSC treatment a larger proportion of neurons demonstrated smaller PNN areas of expression (peak left shift) with a converse smaller proportion of neurons with larger PNN expression as shown by an attenuated tail in comparison to hFF treatment (Figure 6.4C). mDPSC treatments at 2000 and 5000 cells/cm^2 demonstrated fewer neurons with smaller PNN expression areas and a greater proportion of neurons with larger PNN expression areas in comparison to hFF treatments.

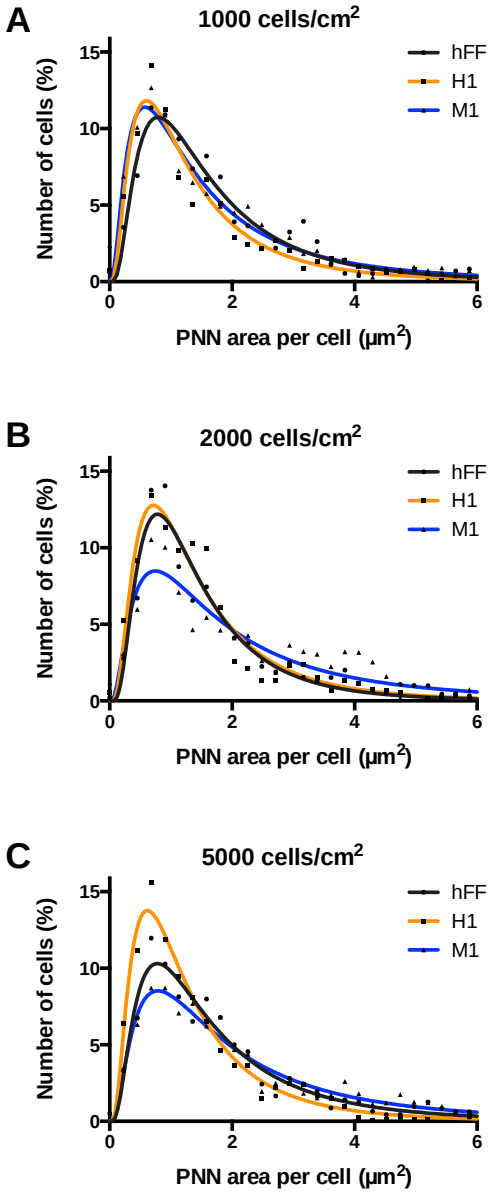

Figure 6.4: Distributions of PNN area per cell following human and murine DPSC treatment.

Percentage histograms of measured PNN area per cell fitted with log-normal nonlinear regression curves at each co-culture dosage. A) PNN areas were similar across all treatment conditions at 1000 cells/cm^2 dosage. B) PNN expression was similar following 200 cells/cm^2 hDPSC and hFF treatment. mDPSC treatment resulted in fewer cells with small PNN areas (lower peak) and a greater proportion with large areas (higher tail) compared with hFF-treated controls. C) 5000 hDPSC/cm^2 treatment increased the proportion of neurons with small PNN area compared to hFF controls. mDPSC treatment reduced the proportion of neurons with small PNN areas.

Cumulative histograms demonstrated the proportion of neurons with increasing PNN area. The proportion of neurons with 'small', 'medium' and 'large' PNN areas were compared to the standard distribution from hFF treatment. A 'large' PNN area was considered to be at and above the 90th percentile of PNN area distribution of hFF treatment (hFF-90%, Figure 6.5). 'Medium' PNN areas were at the 50th percentile and 'small' areas at or below the 15th percentile of hFF treatment. Statistical analysis was then performed to investigate the difference in cell type and dosage treatment effects (Table 6.1). In summary, we found that human DPSC treatment significantly downregulated PNN expression at higher cell doses in comparison to hFF treatment and mDPSC treatment significantly increased PNN expression.

To dissect DPSC treatment effects in detail see Figure 6.5 and Table 6.1. Following 1000 DPSC/cm^2 treatment, there was little difference between the relative proportions of PNN areas compared to hFF controls (Figure 6.5A). However, hDPSC treatment resulted in a greater proportion of neurons with large PNN areas (χ^2=7.42, p<0.01; Table 6.1). At 2000 hDPSC/cm^2 treatment did not produce any significant changes in the proportion of neurons with small (χ^2=0.33, p>0.05), medium (χ^2=1.48, p>0.05) or large (χ^2=2.55, p>0.05) PNN areas (Figure 6.5B). However, treatment with mDPSC at this dosage resulted in significantly fewer neurons with medium-sized PNN areas (hFF-50%; χ^2=4.18, p<0.05).

There was a significant effect of 5000 human and murine DPSC/cm^2 treatment on PNN expression. hDPSC treatment caused a left-shift of the cumulative histogram curve, indicative of a greater proportion of cells with smaller PNN areas (Figure 6.5C). There were significantly fewer neurons with medium sized (χ^2=7.19, p<0.01) and large PNNs (χ^2=4.11, p<0.05; Table 6.1), together accounting for an overall reduction in PNN expression. In contrast, mDPSC treatment at this dosage caused a right-shift of the curve, indicating more cells had larger PNN areas. As seen with 2000 cells/cm^2 treatment, there were significantly fewer neurons with medium-sized PNN areas (χ^2=29.86, p<0.001).

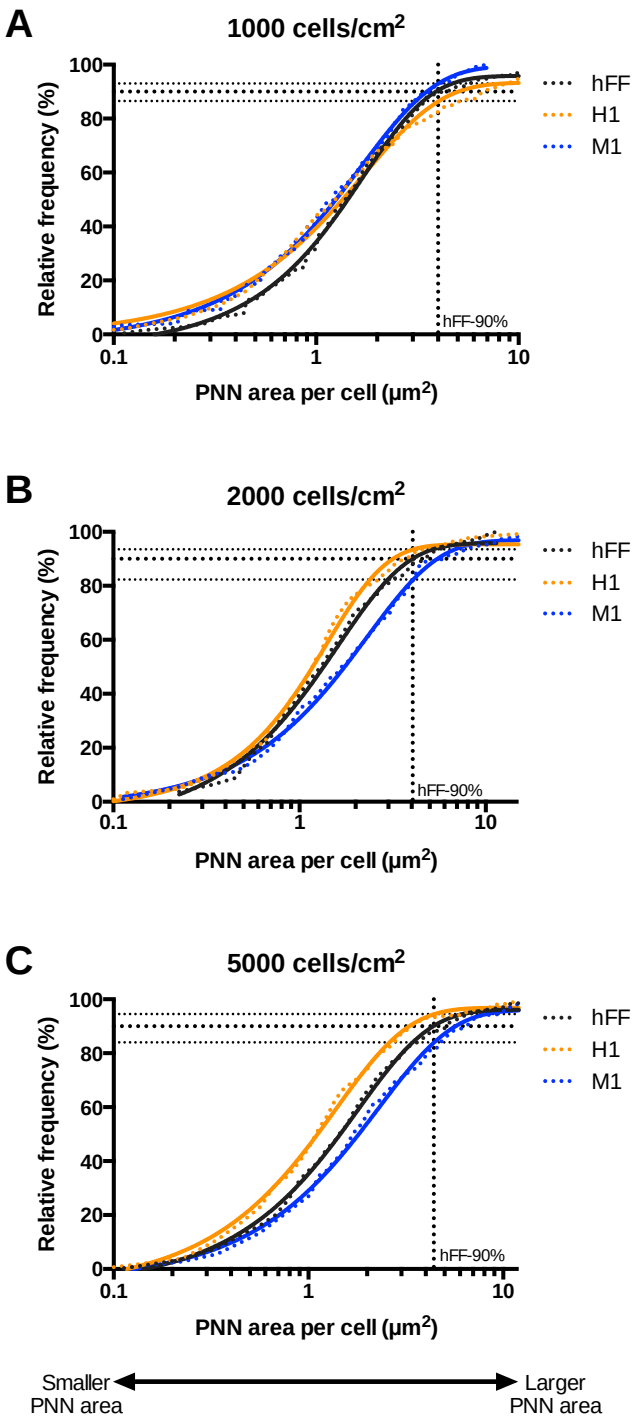

Figure 6.5: Cumulative histograms of PNN area per cell distributions.

A) There was little effect of 1000 DPSC/cm^2 treatment on PNN area distribution. B) 2000 mDPSC treatment resulted in a right-shift of the distribution, which indicates a greater proportion of cells had large PNN areas. C) 5000 hDPSC/cm^2 treatment resulted in a greater proportion of neurons with small PNN areas (left shift). There was also a more pronounced right-shift due to mDPSC treatment. Vertical gridlines show the PNN area at the 90th percentile of the hFF treatment distribution (hFF-90%).

A

Cell number	1000								
PNN area size	Small			Medium			Large		
Distribution	HFF	H1	M1	HFF	H1	M1	HFF	H1	M1
Percentile	*15*	22	22	*50*	53.5	56.5	*90*	85	93
χ^2		1.56	2.81		0.32	1.41		7.42	0.64
p		ns	ns		ns	ns		<0.01	ns
		-	-		-	-		**	-

B

Cell number	2000								
PNN area size	Small			Medium			Large		
Distribution	HFF	H1	M1	HFF	H1	M1	HFF	H1	M1
Percentile	*15*	17.5	14	*50*	56.5	40	*90*	94.5	85
χ^2		0.33	1.33		1.48	4.18		2.55	1.97
p		ns	ns		ns	<0.05		ns	ns
		-	-		-	*		-	-

C

Cell number	5000								
PNN area size	Small			Medium			Large		
Distribution	HFF	H1	M1	HFF	H1	M1	HFF	H1	M1
Percentile	*15*	21	12.5	*50*	61.5	42	*90*	95	85
χ^2		3.58	0.63		7.19	29.86		4.11	3.07
p		ns	ns		<0.01	<0.001		<0.05	ns
		-	-		**	***		*	-

Table 6.1: DPSC treatment effects on the proportion of neurons with *small*, *medium* and *large* PNN areas.

Chi-squared analysis of the proportion of DPSC-treated neurons with small PNN areas (15th percentile of hFF area distribution), medium (hFF-50%) or large PNN (hFF-90%) areas following dosage of A) 1000 cells/cm^2, B) 2000 cells/cm^2 and 5000 human or murine DPSC/cm^2. (*p<0.05, **p<0.01, ***p<0.001)

6.3.3 hDPSC downregulation of PNN expression is consistent for multiple donors

The previous results investigated the treatment effect from one human donor, H1, on PNN expression so to understand if this result was consistent amongst other donors we examined H3 and H4 DPSCs. We found a significant downregulation of the percentage of neurons with PNN expression at higher DPSC treatment doses with H4 in comparison to hFF treatment ($p<0.05$; Figure 6.6A).

A significant overall cell type effect ($p<0.05$) of total PNN area per 100 cells was also evident (Figure 6.6B) in comparison to hFF treatment with increasing cell dose. There was a 60% downregulation in average PNN area per 100 cells with 2000 H4 DPSC/cm^2 treatment. At 5000 DPSC/cm^2 treatment H3 and H4 donors demonstrated similar downregulation in overall measured PNN area at approximately 30% in comparison to hFF treatment.

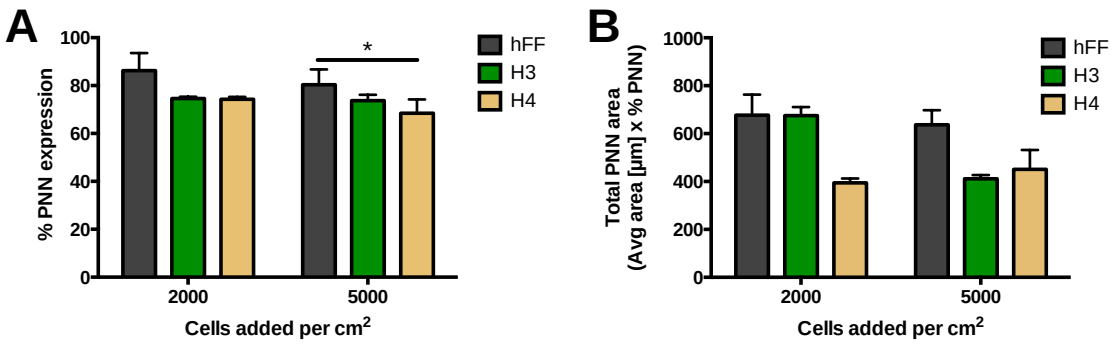

Figure 6.6: DPSC treatment using two other donors downregulated PNN expression.

A) There was an overall cell type effect of H3 and H4 DPSC co-culture in reducing the percentage of NeuN-positive cells that expressed a PNN. B) There was an overall cell type effect ($p<0.05$) of H3 and H4 DPSC co-culture in reducing total cortical PNN area. (*$p<0.05$)

We previously found with H1 treatment more detailed statistical analysis demonstrated interesting results not evident from total PNN expression analysis. Using the same analysis to compare the distribution of PNN area per neuron, 2000 cells/cm^2 H4 DPSC treatment resulted in a greater proportion of cells with small PNN areas than hFF treated cultures (Figure 6.7A). 5000 cells/cm^2 treatment with H3 and H4 DPSC caused a more pronounced downregulation in the area of PNN expression on neurons (Figure 6.7B).

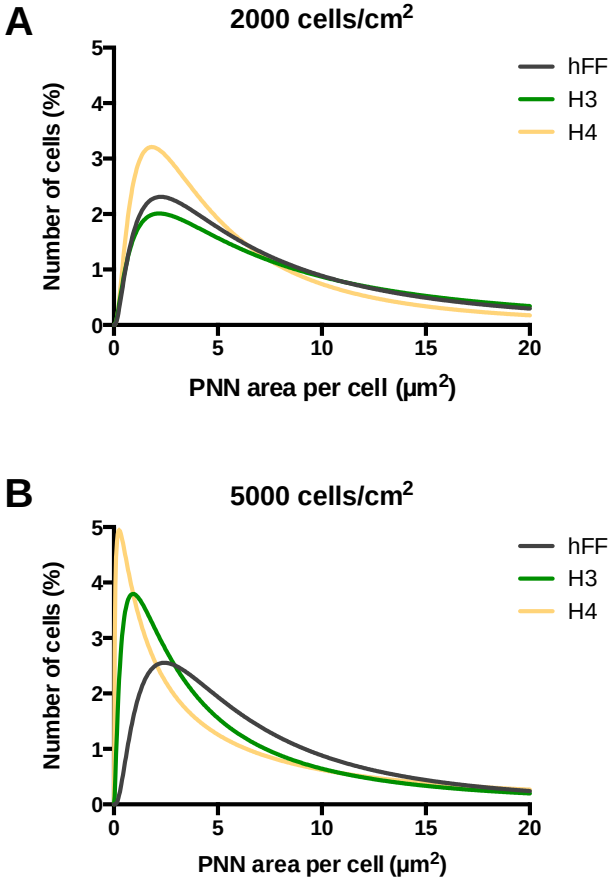

Figure 6.7: H3 and H4 DPSC treatment results in divergent PNN expression in comparison to hFF.

A) 2000 cells/cm^2 H4 DPSC treatment caused a downregulation of PNN area per neuron whereas H3 DPSC treatment had little effect. B) Following 5000 cells/cm^2 treatment with both H3 and H4 produced a greater proportion of cells with small PNN areas.

Cumulative histograms were compared across conditions at the 15th, 50th and 90th percentiles of hFF PNN area distributions to indicate the proportion of neurons with 'small', 'medium and 'large' PNN areas following DPSC treatment as previously analysed using H1 DPSC. At 2000 H4 DPSC/cm^2 treatment there was a left-shift of the entire curve (Figure 6.8A). There were significantly more neurons with small (χ^2=5.01, p<0.05) and medium (χ^2=11.35, p<0.001) PNN areas and fewer with large areas (χ^2=7.02, p<0.01; Table 6.2A). At 5000 DPSC/cm^2 treatment H3 DPSC treatment resulted in a greater proportion of neurons with small (χ^2=10.37, p<0.01) and medium (χ^2=9.56, p<0.01) PNN areas (Table 6.2B), but no difference in the proportion with large PNN areas (χ^2=2.23, p>0.05; Figure 6.8B). H4 DPSC treatment at this dosage resulted in a greater proportion neurons with small PNN areas (χ^2=9.68, p<0.01), however there was no effect on the proportion of medium or large PNN areas compared to hFF control cultures. hFF-treatment curves were consistent across the two doses. In summary, there was a significant downregulation of PNN expression using two other DPSC donors treatments, which suggested this is an activity pertaining to hDPSC from varied donors.

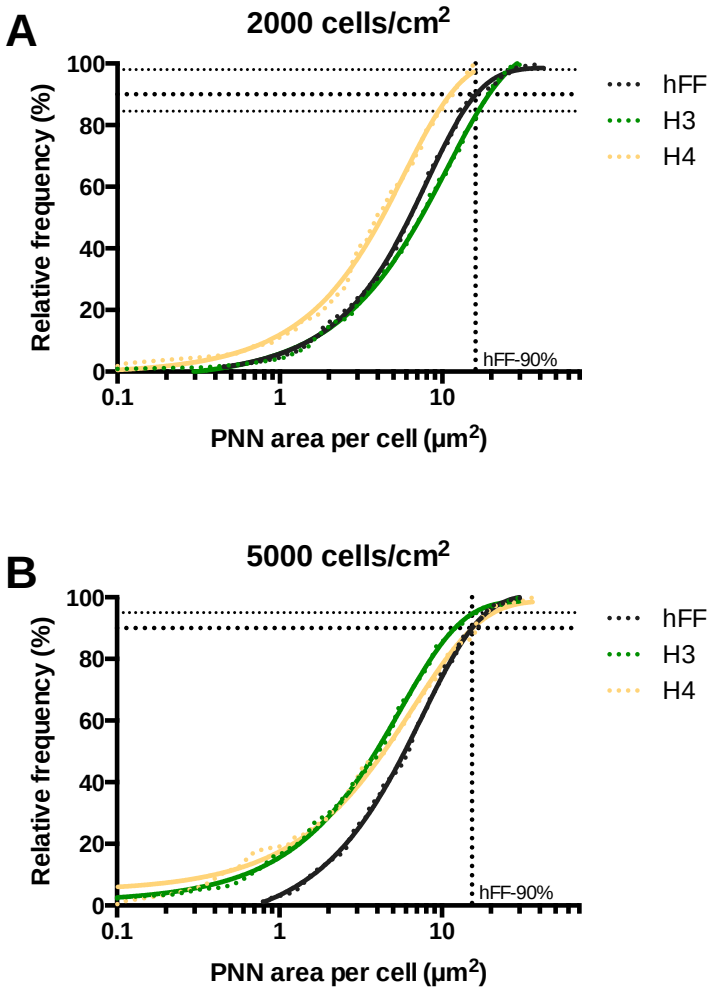

Figure 6.8: H3 and H4 DPSC treatment increases the proportion of neurons with small PNN areas.

Cumulative histograms of PNN area per cell. A) An overall left-shift of the 2000 H4 DPSC treatment curve indicated a greater proportion of neurons with small PNN areas. B) Both H3 and H4 DPSC treatment caused a caused a greater proportion of neurons with small PNN areas compared with hFF controls. Vertical gridlines show the PNN area at the hFF-90%.

A

Cell number	2000								
PNN area size	Small			Medium			Large		
Distribution	HFF	H3	H4	HFF	H3	H4	HFF	H3	H4
Percentile	*15*	15	26	*50*	44	69	*90*	84.5	98
χ^2		0.25	5.01		0.98	11.35		2.23	7.02
p		ns	<0.05		ns	<0.001		ns	<0.01
		-	*		-	***		-	**

B

Cell number	5000								
PNN area size	Small			Medium			Large		
Distribution	HFF	H3	H4	HFF	H3	H4	HFF	H3	H4
Percentile	*15*	30	30	*50*	66.5	60	*90*	95	90
χ^2		10.37	9.68		9.56	3.08		1.8	0
p		<0.01	<0.01		<0.01	ns		ns	ns
		**	**		**	-		-	-

Table 6.2: H3 and H4 donor DPSC treatment significantly downregulates PNN expression.

Chi-squared analysis of the proportion of DPSC-treated neurons with 'small', 'medium' and 'large' PNN areas corresponding to the 15th, 50th and 90th percentile of the hFF PNN area distribution following A) 2000 and B) 5000 cells/cm^2 H3 and H4 DPSC treatment.

6.3.4 Effects of DPSC conditioned medium on cortical PNN expression

Preliminary experiments were performed to investigate whether conditioned medium (CM) from DPSC contained the activity to downregulate PNN expression. hDPSC CM from two donors (H3 and H4) were compared to hFF CM or cultures with no cell treatment. We found a significant downregulation in PNN expression following 24h H4 DPSC CM treatment in comparison to hFF treatment (Figure 6.9). There was downregulation in PNN expression with H3 DPSC treatment but this did not reach statistical significance.

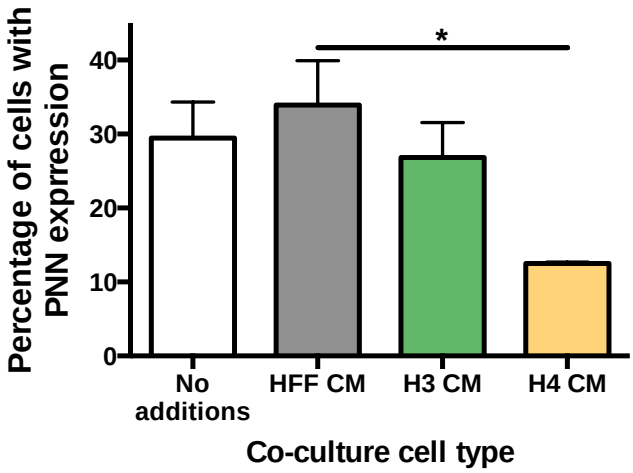

Figure 6.9: hDPSC conditioned medium downregulates PNN expression.

A statistically significant reduction in PNN expression was found following H4 treatment as compared to hFF and H3 treatment (N=3, *p<0.05).

6.3.5 hDPSC downregulate PNN expression in a time-dependent manner

DPSC-dependent PNN downregulation was found to be enhanced with increasing duration of treatment. Total PNN cellular expression was significantly downregulated across 24 to 96 hour treatment durations (Figure 6.10). 96h duration of hDPSC treatment demonstrated the peak of H4 DPSC effect on PNN expression with a significant 22% reduction in comparison to hFF ($p<0.001$) treatment and also 14% lower than H3 donor treatment ($p<0.05$). There did appear to be a difference between duration of treatment effect between different DPSC donors.

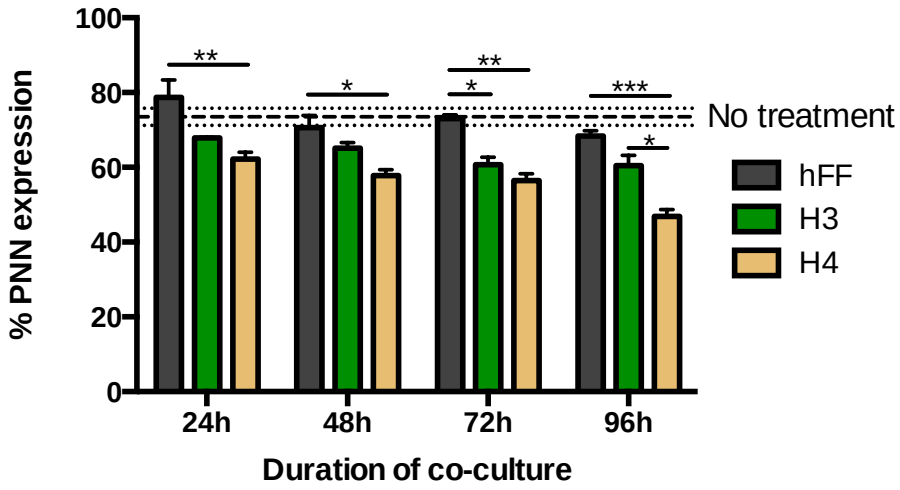

Figure 6.10: PNN downregulation increased with longer hDPSC treatment.

There was an overall time-dependent effect of DPSC-mediated PNN downregulation ($p<0.001$). H4 DPSC caused more potent effects than H3. (*$p<0.05$, **$p<0.01$, ***$p<0.001$).

6.4 Discussion

The data in this study convincingly demonstrated the paracrine activity of DPSC to downregulate PNN expression in a dose and time-dependent manner in a number of human donors and across mammalian species. We used a stringent method to analyse the precise effects of DPSC-cortical co-culture to reveal not only a reduction in the proportion of NeuN-positive neurons that were surrounded by a PNN, but also a reduction in the measured PNN area around those neurons. Previous studies have reported a positive effect of DPSC cell transplantation *in vivo* for functional recovery following stroke and spinal cord injury (Leong, et al., 2012; Sakai, et al., 2012; Sugiyama, et al., 2011) and these results suggests that one way they may incite this effect is through a breakdown of the inhibitory PNN around neurons.

We suggest that DPSC present a new and promising biological reagent for future CNS therapeutics. Their mesenchymal stem cell-like properties of self-renewal and multipotentiality along with ease of accessibility make them a viable stem cell source for autologous transplantation (Gronthos, et al., 2000). Other stem cell varieties such as neural stem cells, bone marrow stromal cells and embryonic-derived cells have all demonstrated sound anatomical and functional improvements after neural damage (Andres, et al., 2011; Daadi, et al., 2009; Hofstetter, et al., 2002; Ikegame, et al., 2011; Kumagai, et al., 2009) but have limitations when considering ease of accessibility. Moreover, DPSC are derived from adults and therefore do not encounter the moral issues associated with many stem cell-based therapeutics.

We have shown that DPSC co-culture causes a downregulation in cortical PNN expression *in vitro*; an effect that we postulate will decrease molecular inhibition in the CNS after injury to allow greater neuroplasticity and recovery. Neuroplasticity involves the alteration of synaptic connectivity in response to environmental cues. Therefore a reduction of PNN allows neurons to respond to new directive cues toward recovery. For example, Garcia-Alias *et al*. (Garcia-Alias, et al., 2009) demonstrated that PNN degradation in the spinal cord with ChABC improved hindlimb motor function, but that ChABC treatment paired with specialised motor training resulted in a synergistic enhancement of motor recovery. In this way, DPSC treatment may create a molecular environment primed for rehabilitation.

The finding that hDPSC co-culture caused a graded reduction in overall cortical PNN expression is in contrast to the global degradation seen following ChABC treatment (Miyata, et al., 2005). This could be considered an advantage to the non-specific effects of ChABC treatment *in vivo*. There was a dose-dependent effect of DPSC downregulation in PNN expression, which was

stronger at higher cell doses. Following 5000 H1 DPSC/cm^2 treatment there were fewer neurons with 'large' PNNs and a corresponding 2-fold reduction in overall PNN area compared to attenuated effects at lower treatment densities. H3 and H4 DPSC treatment also resulted in a dose-dependent downregulation in PNN area, however the proportion of large PNN neurons did not change following treatment at the higher dosage. Rather, they affected neurons with more moderate-sized PNNs to increase the proportion of cells with small PNNs. In contrast, ChABC treatment degrades PNN expression almost entirely across all neurons (Miyata, et al., 2005). We would suggest that hDPSC treatment could present a more controlled and sustained method of PNN modification *in vivo*.

Notably, there was also a duration effect of hDPSC co-culture on cortical PNN expression. We measured an extra 15% reduction in the proportion of NeuN-positive cells that co-expressed WFA between 24h and 96h H4 DPSC co-culture treatment. For H3 DPSC there was a smaller but still significant extra 7.5% reduction in percentage PNN expression between the two time points. We did not determine DPSC proliferation at these different treatment durations and so it is difficult to determine whether the PNN reduction effect was a result of duration itself or indirectly due to a higher dosage effect. Nonetheless, this is an important finding that should be considered when factoring the effect of a cell-based treatment as opposed to a molecular approach that may not be as stable and long-lasting. In addition, it suggests that the survival rate of transplanted cells may have a functional effect on outcomes.

In relation to species differences we found a more robust downregulation of PNN expression with human DPSC treatment as compared to murine. To the best of our knowledge, no study has reported the use of mDPSC *in vivo* for neural therapies or has modeled them *in vitro*. It is clear, however, that murine and human DPSC differ in some key aspects. Most significantly from a neural perspective, hDPSC readily differentiate into mature functional neurons whereas mDPSC were limited in their functional electrophysiological maturity (See Chapter 4). This may translate into altered neuronal compatibility. The different species' DPSC also have modest variations in cell surface markers and it is unknown whether mDPSC also express the neurotrophic factors as human DPSC (Balic & Mina, 2010; Gronthos, et al., 2000; Guimarães, et al.). Overall, this highlights important species differences between DPSC that must be considered in future research.

It remains to be elucidated what paracrine activity is responsible for the DPSC downregulation of the PNN. Previous work has demonstrated that hDPSC-conditioned medium can annul the inhibitory effects of co-cultured CSPGs to reinstate neurite outgrowth of ganglion neurons *in vitro*

(Sakai, et al., 2012). This suggests that hDPSC can interrupt the inhibitory effect of CSPGs, and therefore PNNs, by paracrine factors. It has been well established that hDPSC express a range of neurotrophic factors, including GDNF, BDNF and CNTF at levels far greater than that of skin-derived fibroblasts or BMSC (Sakai, et al., 2012) and these may have a role to play in decreasing cortical inhibition. The ability of neurotrophins to enhance anatomical and functional recovery following CNS injury has been previously demonstrated (Romero, et al., 2001; Y. Zhang, et al., 1998), however Sakai *et al*. (Sakai, et al., 2012) suggest that neurotrophins alone were insufficient to overcome CSPG-mediated neurite outgrowth suppression and instead attributed DPSC-mediated effects to be a result of currently unidentified factors.

The factors that contribute to this reduction in the PNN is currently unknown, however there are several possible mechanisms by which this could occur. Firstly, soluble factors released by DPSC could reduce the production of PNN components. Secondly, DPSC-related factors could be preventing PNN molecules from forming the macromolecular complexes. Finally, these factors may actively degrade CSPGs in the PNNs in a similar fashion to ChABC. Considering the short period of DPSC co-culture required to demonstrate a reduction in PNN expression, it is more likely that factors actively degrade aspects of the PNN, rather than preventing their formation. It would be useful to investigate the neurite length of cortical neurons with and without DPSC treatment to determine if this might be a mechanism of action. If the soluble factors secreted by DPSC are degrading CSPGs in the culture, it would be expected that neurite length of cortical neurons would be increased due to a lack of inhibition surrounding them.

In conclusion, the present study demonstrated for the first time that hDPSC from three individual donors downregulated PNN expression in a paracrine, dose and time-dependent manner. DPSC-mediated PNN downregulation is a possible mode of action for functional recovery observed following rodent stroke (Leong, et al., 2012; Sugiyama, et al., 2011). DPSC treatment may be a viable therapy to enhance neuroplasticity and functional recovery in a broad range of neurological diseases.

Chapter 7: Discussion

In this thesis I have demonstrated the neurogenic potential of human and mouse-derived dental pulp stem cells in *vitro* and their potential impact on CNS plasticity through modification of PNN expression. I have identified limitations of the biocompatibility of DPSC on MEAs, although long-term culture might still be achieved with optimization of polymer-based supportive surfaces. Taken together, the data presented in this thesis has identified a potential mode of action for DPSC-mediated recovery following CNS injury and future potential strategies to improve the neuron-electrode interface for cortical prostheses.

7.1 Neuronal differentiation of DPSC *in vitro*

Throughout Chapters 4 and 6 I characterised the neurogenic potential of human and murine-derived DPSC, respectively. The ability for hDPSC to form neuronal-like cells *in vitro* and *in vivo* has been previously reported (Arthur, et al., 2008; Kiraly, et al., 2011; Kiraly, et al., 2009; Leong, et al., 2012), however to the best of our knowledge, this is the first evidence of incisor-derived mDPSC neuronal differentiation. The findings presented in this thesis demonstrate that mDPSC differentiated to an early stage of neuronal development, expressing both pan-neuronal and glial markers concurrently and also developed strong expression of connexins throughout neural networks. These neural networks of differentiated mDPSC developed electrical oscillation activity in a gamma frequency range but did not support spontaneous action potentials when grown on MEAs.

7.1.1 Advantages of murine-derived DPSC

There are several advantages of using murine-derived DPSC in experimental models. Firstly, there is the opportunity to use advanced transgenic technologies available in this mammalian model. Using gene knockout lines it is possible to focus on the contribution of individual genes to DPSC characteristics. DPSC are a naturally heterogeneous population of cells and it is likely that only a subpopulation have neurological potential (Gronthos, et al., 2000). The results in this thesis demonstrate that neuronal differentiation of DPSC *in vitro* produces a range of cell types. These include neuronal- and glial-like cells, in addition to a subpopulation that do not survive the differentiation period, consistent with prior literature regarding hDPSC (Kiraly, et al., 2009). Utilising genetic knockout mouse lines may provide an opportunity to identify a biomarker for neural potential within the DPSC population. Identification of the specific population with

neurogenic potential is important for future neurological treatments, as it has the potential to improve the survival and efficacy of DPSC when injected *in vivo*.

In addition, the availability of mDPSC also presents the opportunity to model autologous cell transplantations in a range of neurological disease mouse models. Ultimately, the aim of DPSC treatment in the CNS is to use an individual's own cells for their personalised therapy, negating the need for immunosuppressants. However, current models for DPSC transplantation most often use human-derived DPSC within rodent models for disease (De Almeida, et al., 2011; Inoue, et al., 2013; Kiraly, et al., 2011; Leong, et al., 2012; Sakai, et al., 2012). While it is necessary to investigate the potential of human-derived cells in *in vivo* models, it is also important to understand the utility of autologous cell-based treatments.

7.1.2 Disparate characteristics of DPSC from different species

My work has identified distinctions between human and mouse-derived DPSC characteristics. Firstly, each expressed different ion channels following neuronal differentiation. While hDPSC developed functional voltage-gated sodium channels (Chapter 5; Figure 5) indicative of more mature neurons from day 11 of differentiation, and have been reported to express potassium channels at a similar stage of development (Arthur, et al., 2008; Kiraly, et al., 2009), mDPSC expressed neither of these currents, both of which are necessary for synaptic transmission. Rather, I found that mDPSC expressed voltage-gated calcium channels, which are more typical of neurons at an early developmental stage (Dolmetsch, et al., 2001; Tang, et al., 2003).

Neural network properties were also distinct between DPSC derived from human and mouse. In hDPSC-derived cultures there was high interconnectivity between cells as evidenced by the low molecular weight dye spread throughout numerous adjacent cells. Conversely, in mDPSC differentiated cultures, while there was high expression of gap junction protein, connexin 43, and high capacitance of clustered cells, no Lucifer yellow or neurobiotin dye spread was observed. Nonetheless, mDPSC cultures showed electrical connectivity through common oscillatory activity observed over numerous MEA electrodes, potentially involving hundreds of differentiated cells and indicating that gap junctions were active in supporting electrical spread. Gap junctions have a central role in the developing brain, proving a rapid mode of electrical communication between early neuronal networks (Dupont, et al., 2006), as well as supporting cell migration, proliferation, differentiation, neurite outgrowth and the organisation of columnar structures within the immature brain (Bani-Yaghoub, Bechberger, et al., 1999; Bani-Yaghoub, Underhill, et al., 1999; Hormuzdi, et al., 2004; Todorova, et al., 2008). Taken together, this evidence suggests that mDPSC

undergo neuronal differentiation but to a limited maturity using the differentiation protocol presented here. In contrast, the results of this study demonstrated that hDPSC can differentiate to form mature neurons with functional ion channels and more mature neuronal immunoreactivity, a finding that is consistent with the literature (Arthur, et al., 2008; Kiraly, et al., 2009). The limited maturity of mDPSC neuronal cells may be a product of the culturing method that could be improved with an alternative induction strategy. Neurosphere-based culture methods present one potential approach to provide the necessary support to developing neural stem cells and could be a viable method for DPSC induction in the future. Regardless, it is important to note the key distinctions between DPSC from different species when aiming to compare them directly.

7.2 DPSC may induce neuroplasticity – downregulation of PNN

In Chapter 6, I demonstrated the ability of hDPSC to reduce PNN expression of cortical tissue in a dose- and time-dependent manner. A major putative function of PNN is its maintenance of neural network stability and control of synaptic plasticity. Previous studies have demonstrated how the application of hDPSC can enhance functional recovery following stroke and SCI (Leong, et al., 2012; Sakai, et al., 2012; Sugiyama, et al., 2011), however the mechanisms for this effect have been unclear. My findings suggest that one mode of action may be via the breakdown of the inhibitory PNN around neurons, which could increase the potential for neuroplasticity, a principal mode of recovery following CNS damage. Notably, I found that this effect was consistent for hDPSC isolated from three individuals, indicating that it is a common characteristic of this stem cell type. Furthermore, conditioned medium from hDPSC also caused a reduction in the proportion of neurons expressing PNN, indicating that this effect may be a result of soluble paracrine factors released by the DPSC. In contrast, co-culture of DPSC isolated from murine incisors did not appear to robustly down-regulate PNN expression of cortical tissue, which may present a distinction between the species' DPSC or that only one mDPSC cell population was used. These data lead to further possible investigations to look at other mDPSC populations from C57/Bl6, for example, and also other stem cell populations such as neural and embryonic.

I also demonstrated a dose and time dependent effect of DPSC co-culture on PNN degradation, which has a functional impact for *in vivo* treatments. According to these findings, survival of the cells following implantation is critical to achieving a maximal effect of reduced PNN expression. Notably, stem cell survival is generally low following CNS transplantation, however may vary depending on the disease model. In stroke, for example, survival rates following transplantation

into the stroke brain are often low (Chu, et al., 2004; Hicks, et al., 2009; Leong, et al., 2012; Takahashi, et al., 2008), however more variable rates of up to 30% have been reported following implanted into the injured spinal cord (Sakai, et al., 2012). Regardless of this variation, even low stem cell survival has been linked to considerable improvements in functional outcomes in numerous CNS damage models. It is possible that a major aspect of DPSC-mediated CNS recovery can be achieved without their large numbers of cells surviving long-term, even though a dose-dependent response may enhance this activity.

The molecular mechanism underlying hDPSC-mediated breakdown of cortical PNN is unknown. There have been numerous reports that the therapeutic value of DPSC may not be the result of differentiation of the stem cells, but rather the indirect effect of trophic or other factors secreted by them. This was demonstrated recently by Sakai et al. (Sakai, et al., 2012) who revealed that DPSC-conditioned media assisted ganglion neurons overcome the inhibitory signals from co-cultured CSPGs to achieve greater neurite extension *in vitro*. In addition, blockade of neurotrophins BDNF and NGF abolished the neuroprotective effect of DPSC in an *in vitro* model of Parkinson's Disease. Furthermore, reports of low DPSC survival could not account for the functional improvement observed following injection into the rat brain post-stroke, leading the authors to deduce that the cells were having a non-neural replacement effect to improve recovery (Huang, et al., 2008; Leong, et al., 2012). Together, these studies suggest that DPSC may exert their neuroplastic effect through the release of paracrine factors that affect neurons indirectly. It has been widely reported that both human- and monkey-derived DPSC release neurotrophic factors such as BDNF, CNTF, NGF, NT-3, VEGF and GDNF which are supportive of neural tissue and enhance recovery (De Almeida, et al., 2011; Huang, et al., 2008; Sakai, et al., 2012; Sugiyama, et al., 2011). However, it has been suggested that the benefits generated following DPSC treatment is unlikely be explained by the influence of neurotrophic factors alone (Sakai, et al., 2012). Rather, unidentified factors are proposed to have an additional impact. Identification of these factors could further promote more directed and controlled approaches to CNS recovery using cell-based therapy.

Another possible molecular mechanism for DPSC-mediated PNN degradation is through the action of matrix metalloproteases (MMPs) that are involved in the degradation of the ECM in the CNS. MMPs are a family of proteolytic enzymes with complex functions involved with both CNS injury and repair mechanisms. Numerous MMPs perform enzymatic cleavage of lectican core proteins present in PNNs and the glial scar and the promotion of neuroplasticity (Hsu, et al., 2006). Furthermore, numerous stem and progenitor cells have been demonstrated to improve

axon regeneration and neurite outgrowth through MMP-dependent mechanisms (Heine, et al., 2004; Pastrana, et al., 2006; Zhang, et al., 2007). Olfactory ensheathing cells and NSC were found to secrete MMP-2 in *in vitro* models of axonal regeneration, suggesting that DPSC may also affect the PNN through MMP-mediated mechanisms (Heine, et al., 2004; Pastrana, et al., 2006). However, direct treatment with MMP at sites of injury can be complex as they are also involved with detrimental outcomes that have limited their implementation in neuro-rehabilitation strategies. For example, following SCI contusion injury there is an acute upregulation of numerous MMPs, including MMP-9 and MMP-12, which have been correlated with increased inflammation and lowered blood spinal cord barrier integrity (Noble, et al., 2002; Wells, et al., 2003). The acute blockade of MMP activity after SCI has been shown to improve recovery (Noble, et al., 2002), however its prolonged blockade reverses this effect (Hsu, et al., 2006). An advantage of stem cell-based therapy potentially lies in the cells' ability to adapt to changing environments to alter the paracrine support they provide.

7.3 The therapeutic potential of DPSC at the BMI and beyond

DPSC compatibility with the CNS

My findings as discussed above all have relevance to the proposed application of DPSC at the BMI. Firstly, in Chapter 6 I demonstrated the compatibility of hDPSC and cortical tissue in co-cultures surviving for at least four days. This period would likely be extended without experimental interruption. Notably, DPSC continued to proliferate during the cortical co-culture period regardless of being maintained in serum-free cortical medium as seen in Chapter 5. This observation has significant application at the BMI, suggesting high compatibility between the cell populations and the potential effectiveness of a DPSC layer to provide a more biocompatible surface than that of electrode material. This could effectively reduce the issue of a host tissue response to electrode insertion as seen previously with a NSC layer on a neural probe (Azemi, et al., 2010). However, it remains to be determined if the health of neural tissue may influence this biocompatibility at the interface, as the presence of necrotic tissue is a likely influence on low DPSC survival *in vivo* discussed above.

Influence of DPSC on the PNN at the interface

The ability of DPSC to reduce PNN expression is highly advantageous at the neuron-electrode interface. Following CNS injury there is a general increase of CSPG as part of the glial scar and PNN upregulation, which is restrictive to neural plasticity and therefore learning and recovery. To the best of our knowledge, the PNN response to electrode insertion in the cortex has not yet been described, however the development of the glial scar has been well documented and an associated upregulation of PNN would be expected (Polikov, et al., 2005; Ward, et al., 2009). As such, the presence of DPSC at the cortical BMI provides the opportunity to break down part of the natural inhibition present following electrode insertion. Lower levels of inhibition at the interface would potentially allow a heightened ability for neural cells to undergo plasticity in response to new cues, which would allow a user to adapt and learn to use a cortical prosthesis more efficiently.

It is not yet clear how pervasive the molecular effect of DPSC treatment may be in the CNS. Following previous reports that DPSC conditioned medium can support neurons to overcome the inhibitory effects of CSPGs *in vitro*, it is also possible that DPSC at the neuron-electrode interface may provide sufficient trophic support to overcome the effects of the glial scar. Effectively, this would render the electrode interface less repulsive to neuronal growth and therefore enhance electrical coupling between the neuron and electrode.

DPSC-electrode biocompatibility

The current limitation of the proposed DPSC-mediated BMI is the biocompatibility of electrode material with DPSC. In Chapter 4 I demonstrated that hDPSC did not survive well on MEA surfaces despite being modified with numerous substrates to promote cell attachment and neuronal differentiation. It was common for DPSC to seed onto MEAs successfully for a short period of time. Following the onset of neuronal induction, however, the health of DPSC was challenged and most cells either detached from the MEA surface or underwent spontaneous cell death. This contrasts with simultaneous DPSC differentiations performed with analogous conditions on glass coverslips that survived and differentiated beyond a month in culture. Considering the limitations of performing neural differentiations on MEA surfaces, the transfer of pre-differentiated DSPC onto MEAs was trialed with cultured coverslip inversions. This experiment highlighted the unsupportive environment of the electrode region of MEAs as the

DPSC-derived neuronal cells that were inverted at this region showed a rapid decline in health with high cell death compared to cells at the outer regions of the MEA.

Neuronal differentiation of hDPSC on MEAs was investigated firstly in an effort to understand the neurogenic potential of the cells. DPSC electrophysiology has previously been investigated *in vitro*, but their network properties and spontaneous activity have not been reported (Arthur, et al., 2008; Kiraly, et al., 2009). In addition, it has been suggested that pre-differentiation of hDPSC can enhance their survival and integration into the brain following transplantation, which could be a useful strategy for enhancing electrical coupling at the interface (Kiraly, et al., 2011). However, as the differentiation of DPSC was not supported on MEAs, it may be a more robust strategy to apply undifferentiated cells that may be less susceptible to the material challenges of cortical prosthesis electrodes.

Surprisingly, the biocompatibility of neural cells with MEAs was even greater than that of differentiating DPSC. In chapter 3 I detailed the successful survival of murine cortical cultures on three different types of MEAs for at least 14 days. The electrode material of each MEA was distinct and had a strong effect on the signals recorded from the cultured neurons. The titanium nitride (MCS10 and MCS30) electrodes on commercial MEAs were most successful at providing a high signal-to-noise ratio capable of recording electrical activity from cultured cells. Electrodes on NTT MEAs were made of ITO, which produced considerably higher noise that masked the electrical activity of cultured neurons. The performance of these MEAs would be improved through a polymer coating to increase surface area and therefore decrease impedance, however this modification was not available at the time of experimentation (Furukawa, et al., 2013; Shimada, et al., 2009). This finding highlights the impact of electrode material and size at the cortical interface for the quality of signal transfer. Thus, polymers may be necessary to coat planar electrodes before stem cell treatment and subsequent insertion at the cortex to both increase biocompatibility to DPSC as well as reducing impedance.

7.4 The advantage of dental pulp stem cells for neural therapeutics

Stem cells present a viable biological strategy to improve functional outcome following CNS damage from varied causes. Numerous stem cell types other than DPSC also display properties that may be supportive to CNS repair and recovery, however most also lack some key characteristics important to the success of DPSC. Neural stem cells (NSC) are one population that, like DPSC, produce trophic factors and have been found to be supportive to the health of

neurons. Indeed, seeding of neural probes with neural stem cells has resulted in improved tissue response to the implantation (Azemi, et al., 2010; Purcell, et al., 2009). However, the feasibility of the cells is also an important consideration for their eventual clinical implementation. Unlike NSC that are isolated from brain tissue, DPSC are easily accessible and provide an individual with the opportunity to use their own cells for their own personalised treatments. This may remove the need for immunosuppressants following transplantation, which can be the source of a range of additional issues.

Other stem cells have similarly been considered for CNS therapies. Bone marrow stromal cell (BMSC) implantation has successfully improved recovery following SCI and has been shown to be neuroprotective in models of Alzheimer's disease and Parkinson's disease (Hellmann 2006, Lu 2005). However, in a direct comparison, BMSC had a much less potent effect of rescuing neurite extension when cultured with CSPG (Sakai, et al., 2012). This suggests that the ability of these cells to affect the biocompatibility of a BMI and to improve neuroplasticity in other CNS applications is potentially inferior to that of DPSC. In animal models of stroke, many different types of multi and pluripotent stem cells have been investigated (Leong, et al., 2013) and the approach remains uncertain at this point in time. Ultimately, controlled trials will need to compare the stem cell types to determine the superiority of any one for particular CNS therapies.

7.5 Future directions

The research presented in my thesis serve as proof of principle that DPSC can influence the inhibitory environment of the damaged CNS and may provide a viable therapeutic strategy to improve long term efficacy of an implanted cortical prosthesis. Additionally, I have demonstrated that DPSC can decrease the PNN expression of healthy cortical tissue, although future work is required to identify the presumed enzyme underlying this activity and whether it underlies enhanced neurological outcome in models of CNS damage *in vivo*. It would also be of benefit to utilise genetic modification of mice to identify a neural stem cell biomarker of DPSC to generate an enriched population with neurogenic potential.

Finally, much more research is required to implement a DPSC layer to interface a cortical prosthesis to promote long-term biocompatibility. The long-term interaction of undifferentiated DPSC on electrode arrays must firstly be identified with a range of electrode materials and coating substrates. Following successful achievement of DSPC-electrode coupling, models of

neural probe cortical insertion could be trialed to determine the impact of DPSC at the BMI *in vivo*.

7.6 Conclusion

My research has identified a novel ability for human-derived DPSC to downregulate PNN expression in cortical tissue that could improve the long-term efficacy of a BMI. Coupled with their high biocompatibility with cortical tissue, neurogenic potential, chemoattraction properties and their ability to provide trophic support to neurons, DPSC may present a multifaceted approach to neural cell-based therapeutics for a range of CNS disorders. Furthermore, characterisation of the neurogenic potential of murine incisor-derived DSPC suggests that this cell type may be a useful murine model to investigate autologous transplantation and the mechanisms of action using the power of murine transgenesis.

Reference List

Agudo, M., Woodhoo, A., Webber, D., Mirsky, R., Jessen, K. R., & McMahon, S. B. (2008). Schwann cell precursors transplanted into the injured spinal cord multiply, integrate and are permissive for axon growth. *GLIA, 56*(12), 1263-1270.

Albright, T. D., Desimone, R., & Gross, C. G. (1984). Columnar organization of directionally selective cells in visual area MT of the Macaque. *Journal of Neurophysiology, 51*(1), 16-31.

Anderson, K. D. (2004). Targeting recovery: Priorities of the spinal cord-injured population. *Journal of Neurotrauma, 21*(10), 1371-1383.

Andres, R. H., Horie, N., Slikker, W., Keren-Gill, H., Zhan, K., Sun, G., et al. (2011). Human neural stem cells enhance structural plasticity and axonal transport in the ischaemic brain. *Brain, 134*(6), 1777-1789.

Andrews, E. M., Richards, R. J., Yin, F. Q., Viapiano, M. S., & Jakeman, L. B. (2012). Alterations in chondroitin sulfate proteoglycan expression occur both at and far from the site of spinal contusion injury. *Experimental Neurology, 235*(1), 174-187.

Arthur, A., Rychkov, G., Shi, S., Koblar, S. A., & Gronthos, S. (2008). Adult human dental pulp stem cells differentiate toward functionally active neurons under appropriate environmental cues. *Stem Cells, 26*(7), 1787-1795.

Arthur, A., Shi, S., Zannettino, A. C., Fujii, N., Gronthos, S., & Koblar, S. A. (2009). Implanted adult human dental pulp stem cells induce endogenous axon guidance. *Stem Cells, 27*(9), 2229-2237.

Asher, R. A., Morgenstern, D. A., Fidler, P. S., Adcock, K. H., Oohira, A., Braistead, J. E., et al. (2000). Neurocan is upregulated in injured brain and in cytokine-treated astrocytes. *Journal of Neuroscience, 20*(7), 2427-2438.

Aspberg, A., Miura, R., Bourdoulous, S., Shimonaka, M., Heinegard, D., Schachner, M., et al. (1997). The C-type lectin domains of lecticans, a family of aggregating chondroitin sulfate proteoglycans, bind tenascin-R by protein-protein interactions independent of carbohydrate moiety. *Proceedings of the National Academy of Sciences of the United States of America, 94*(19), 10116-10121.

Atwal, J. K., Pinkston-Gosse, J., Syken, J., Stawicki, S., Wu, Y., Shatz, C., et al. (2008). PirB is a functional receptor for myelin inhibitors of axonal regeneration. *Science, 322*(5903), 967-970.

Azemi, E., Gobbel, G. T., & Cui, X. T. (2010). Seeding neural progenitor cells on silicon-based neural probes: Laboratory investigation. *Journal of Neurosurgery, 113*(3), 673-681.

Azemi, E., Lagenaur, C. F., & Cui, X. T. (2011). The surface immobilization of the neural adhesion molecule L1 on neural probes and its effect on neuronal density and gliosis at the probe/tissue interface. *Biomaterials, 32*(3), 681-692.

Bach-y-Rita, P. (2004). Tactile sensory substitution studies, *Annals of the New York Academy of Sciences* (Vol. 1013, pp. 83-91).

Bach-Y-Rita, P., Collins, C. C., Saunders, F. A., White, B., & Scadden, L. (1969). Vision substitution by tactile image projection [18]. *Nature, 221*(5184), 963-964.

Bach-y-Rita, P., Collins, C. C., White, B., Saunders, F. A., Scadden, L., & Blomberg, R. (1969). A tactile vision substitution system. *American journal of optometry and archives of American Academy of Optometry, 46*(2), 109-111.

Bak, M., Girvin, J. P., Hambrecht, F. T., Kufta, C. V., Loeb, G. E., & Schmidt, E. M. (1990). Communication: Visual sensations produced by intracortical microstimulation of the human occipital cortex. *Medical and Biological Engineering and Computing, 28*(3), 257-259.

Balic, A., Aguila, H. L., Caimano, M. J., Francone, V. P., & Mina, M. (2010). Characterization of stem and progenitor cells in the dental pulp of erupted and unerupted murine molars. *Bone, 46*(6), 1639-1651.

Balic, A., & Mina, M. (2010). Characterization of progenitor cells in pulps of murine incisors. *Journal of Dental Research, 89*(11), 1287-1292.

Ban, J., Bonifazi, P., Pinato, G., Broccard, F. D., Studer, L., Torre, V., et al. (2007). Embryonic stem cell-derived neurons form functional networks in vitro. *Stem Cells, 25*(3), 738-749.

Bandtlow, C. E., & Zimmermann, D. R. (2000). Proteoglycans in the developing brain: New conceptual insights for old proteins. *Physiological Reviews, 80*(4), 1267-1290.

Bani-Yaghoub, M., Bechberger, J. F., Underhill, T. M., & Naus, C. C. G. (1999). The effects of gap junction blockage on neuronal differentiation of human NTera2/clone D1 cells. *Experimental Neurology, 156*(1), 16-32.

Bani-Yaghoub, M., Underhill, T. M., & Naus, C. C. G. (1999). Gap junction blockage interferes with neuronal and astroglial differentiation of mouse p19 embryonal carcinoma cells. *Developmental Genetics, 24*(1-2), 69-81.

Barritt, A. W., Davies, M., Marchand, F., Hartley, R., Grist, J., Yip, P., et al. (2006). Chondroitinase ABC promotes sprouting of intact and injured spinal systems after spinal cord injury. *Journal of Neuroscience, 26*(42), 10856-10867.

Bartsch, U., Bandtlow, C. E., Schnell, L., Bartsch, S., Spillmann, A. A., Rubin, B. P., et al. (1995). Lack of evidence that myelin-associated glycoprotein is a major inhibitor of axonal regeneration in the CNS. *Neuron, 15*(6), 1375-1381.

Belliveau, D. J., Bani-Yaghoub, M., McGirr, B., Naus, C. C., & Rushlow, W. J. (2006). Enhanced neurite outgrowth in PC12 cells mediated by connexin hemichannels and ATP. *J Biol Chem, 281*(30), 20920-20931.

Benson, M. D., Romero, M. I., Lush, M. E., Lu, Q. R., Henkemeyer, M., & Parada, L. F. (2005). Ephrin-B3 is a myelin-based inhibitor of neurite outgrowth. *Proceedings of the National Academy of Sciences of the United States of America, 102*(30), 10694-10699.

Berretta, S. (2012). Extracellular matrix abnormalities in schizophrenia. *Neuropharmacology, 62*(3), 1584-1597.

Biran, R., Martin, D. C., & Tresco, P. A. (2005). Neuronal cell loss accompanies the brain tissue response to chronically implanted silicon microelectrode arrays. *Experimental Neurology, 195*(1), 115-126.

Borisoff, J. F., Chan, C. C. M., Hiebert, G. W., Oschipok, L., Robertson, G. S., Zamboni, R., et al. (2003). Suppression of Rho-kinase activity promotes axonal growth on inhibitory CNS substrates. *Molecular and Cellular Neuroscience, 22*(3), 405-416.

Bradbury, E. J., Moon, L. D. F., Popat, R. J., King, V. R., Bennett, G. S., Patel, P. N., et al. (2002). Chondroitinase ABC promotes functional recovery after spinal cord injury. *Nature, 416*(6881), 636-640.

Bradley, D. C., Troyk, P. R., Berg, J. A., Bak, M., Cogan, S., Erickson, R., et al. (2005). Visuotopic mapping through a multichannel stimulating implant in primate V1. *Journal of Neurophysiology, 93*(3), 1659-1670.

Brindley, G. S. (1982). Effects of electrical stimulation of the visual cortex. *Human Neurobiology, 1*(4), 281-283.

Brindley, G. S., & Lewin, W. S. (1968). The sensations produced by electrical stimulation of the visual cortex. *Journal of Physiology, 196*(2), 479-493.

Britten, K. H., & Van Wezel, R. J. A. (1998). Electrical microstimulation of cortical area MST biases heading perception in monkeys. *Nature Neuroscience, 1*(1), 59-63.

Butkevich, E., Hulsmann, S., Wenzel, D., Shirao, T., Duden, R., & Majoul, I. (2004). Drebrin is a novel connexin-43 binding partner that links gap junctions to the submembrane cytoskeleton. *Curr Biol, 14*(8), 650-658.

Cafferty, W. B. J., Duffy, P., Huebner, E., & Strittmatter, S. M. (2010). MAG and OMgp synergize with Nogo-A to restrict axonal growth and neurological recovery after spinal cord trauma. *Journal of Neuroscience, 30*(20), 6825-6837.

Cafferty, W. B. J., Yang, S. H., Duffy, P. J., Li, S., & Strittmatter, S. M. (2007). Functional axonal regeneration through astrocytic scar genetically modified to digest chondroitin sulfate proteoglycans. *Journal of Neuroscience, 27*(9), 2176-2185.

Caggiano, A. O., Zimber, M. P., Ganguly, A., Blight, A. R., & Gruskin, E. A. (2005). Chondroitinase ABCI improves locomotion and bladder function following contusion injury of the rat spinal cord. *Journal of Neurotrauma, 22*(2), 226-239.

Carden, M. J., Trojanowski, J. Q., Schlaepfer, W. W., & Lee, V. M. Y. (1987). Two-stage expression of neurofilament polypeptides during rat neurogenesis with early establishment of adult phosphorylation patterns. *Journal of Neuroscience, 7*(11), 3489-3504.

Carmena, J. M., Lebedev, M. A., Crist, R. E., O'Doherty, J. E., Santucci, D. M., Dimitrov, D. F., et al. (2003). Learning to control a brain-machine interface for reaching and grasping by primates. *PLoS Biology, 1*(2).

Caroni, P., & Schwab, M. E. (1988). Antibody against myelin associated inhibitor of neurite growth neutralizes nonpermissive substrate properties of CNS white matter. *Neuron, 1*(1), 85-96.

Carulli, D., Pizzorusso, T., Kwok, J. C. F., Putignano, E., Poli, A., Forostyak, S., et al. (2010). Animals lacking link protein have attenuated perineuronal nets and persistent plasticity. *Brain, 133*(8), 2331-2347.

Carulli, D., Rhodes, K. E., Brown, D. J., Bonnert, T. P., Pollack, S. J., Oliver, K., et al. (2006). Composition of perineuronal nets in the adult rat cerebellum and the cellular origin of their components. *Journal of Comparative Neurology, 494*(4), 559-577.

Chadwick, E. K., Blana, D., Simeral, J. D., Lambrecht, J., Kim, S. P., Cornwell, A. S., et al. (2011). Continuous neuronal ensemble control of simulated arm reaching by a human with tetraplegia. *Journal of Neural Engineering, 8*(3).

Chao, Z. C., Nagasaka, Y., & Fujii, N. (2010). Long-term asynchronous decoding of arm motion using electrocorticographic signals in monkeys. *Frontiers in neuroengineering, 3*.

Chen, J., Li, Y., Wang, L., Lu, M., Zhang, X., & Chopp, M. (2001). Therapeutic benefit of intracerebral transplantation of bone marrow stromal cells after cerebral ischemia in rats. *Journal of the Neurological Sciences, 189*(1-2), 49-57.

Chen, J., Li, Y., Wang, L., Zhang, Z., Lu, D., Lu, M., et al. (2001). Therapeutic benefit of intravenous administration of bone marrow stromal cells after cerebral ischemia in rats. *Stroke, 32*(4), 1005-1011.

Chen, M. S., Huber, A. B., Van Der Haar, M. E. D., Frank, M., Schnell, L., Spillmann, A. A., et al. (2000). Nogo-A is a myelin-associated neurite outgrowth inhibitor and an antigen for monoclonal antibody IN-1. *Nature, 403*(6768), 434-439.

Chiappalone, M., Bove, M., Vato, A., Tedesco, M., & Martinoia, S. (2006). Dissociated cortical networks show spontaneously correlated activity patterns during in vitro development. *Brain Research, 1093*(1), 41-53.

Chiappalone, M., Vato, A., Berdondini, L., Koudelka-Hep, M., & Martinoia, S. (2007). Network dynamics and synchronous activity in cultured cortical neurons. *International Journal of Neural Systems, 17*(2), 87-103.

Chu, K., Kim, M., Park, K. I., Jeong, S. W., Park, H. K., Jung, K. H., et al. (2004). Human neural stem cells improve sensorimotor deficits in the adult rat brain with experimental focal ischemia. *Brain Research, 1016*(2), 145-153.

Cizkova, D., Rosocha, J., Vanick√Ω, I., Jergova, S., & Cizek, M. (2006). Transplants of human mesenchymal stem cells improve functional recovery after spinal cord injury in the rat. *Cellular and Molecular Neurobiology, 26*(7-8), 1167-1180.

Cohen, E. D. (2007). Prosthetic interfaces with the visual system: Biological issues. *Journal of Neural Engineering, 4*(2), R14-R31.

Collins, C. C., & Bach-y-Rita, P. (1973). Transmission of pictorial information through the skin. *Advances in biological and medical physics, 14*, 285-315.

Colombo, J. (1982). The critical period concept: research, methodology, and theoretical issues. *Psychological Bulletin, 91*(2), 260.

Cui, X., Lee, V. A., Raphael, Y., Wiler, J. A., Hetke, J. F., Anderson, D. J., et al. (2001). Surface modification of neural recording electrodes with conducting polymer/biomolecule blends. *Journal of Biomedical Materials Research, 56*(2), 261-272.

Cummings, B. J., Uchida, N., Tamaki, S. J., Salazar, D. L., Hooshmand, M., Summers, R., et al. (2005). Human neural stem cells differentiate and promote locomotor recovery in spinal cord-injured mice. *Proceedings of the National Academy of Sciences of the United States of America, 102*(39), 14069-14074.

Daadi, M. M., Davis, A. S., Arac, A., Li, Z., Maag, A. L., Bhatnagar, R., et al. (2009). Human Neural Stem Cell Grafts Modify Microglial Response and Enhance Axonal Sprouting in Neonatal Hypoxic-Ischemic Brain Injury. *Stroke, 41*(3), 516-523.

Daly, J. J., Cheng, R., Rogers, J., Litinas, K., Hrovat, K., & Dohring, M. (2009). Feasibility of a new application of noninvasive brain computer interface (BCI): A case study of training for recovery of volitional motor control after stroke. *Journal of Neurologic Physical Therapy, 33*(4), 203-211.

Davies, J. E., Tang, X., Denning, J. W., Archibald, S. J., & Davies, S. J. A. (2004). Decorin suppresses neurocan, brevican, phosphacan and NG2 expression and promotes axon growth across adult rat spinal cord injuries. *European Journal of Neuroscience, 19*(5), 1226-1242.

De Almeida, F. M., Marques, S. A., Ramalho, B. D. S., Rodrigues, R. F., Cadilhe, D. V., Furtado, D., et al. (2011). Human dental pulp cells: A new source of cell therapy in a mouse model of compressive spinal cord injury. *Journal of Neurotrauma, 28*(9), 1939-1949.

De Winter, F., Oudega, M., Lankhorst, A. J., Hamers, F. P., Blits, B., Ruitenberg, M. J., et al. (2002). Injury-induced class 3 semaphorin expression in the rat spinal cord. *Experimental Neurology, 175*(1), 61-75.

Dergham, P., Ellezam, B., Essagian, C., Avedissian, H., Lubell, W. D., & McKerracher, L. (2002). Rho signaling pathway targeted to promote spinal cord repair. *Journal of Neuroscience, 22*(15), 6570-6577.

Ding, Y., Yan, Q., Ruan, J. W., Zhang, Y. Q., Li, W. J., Zeng, X., et al. (2012). Electroacupuncture promotes the differentiation of transplanted bone marrow mesenchymal stem cells overexpressing TrkC into neuron-like cells in transected spinal cord of rats. *Cell Transplantation, 22*(1), 65-86.

Dobelle, W. H. (2000). Artificial vision for the blind by connecting a television camera to the visual cortex. *ASAIO Journal, 46*(1), 3-9.

Dobelle, W. H., & Mladejovsky, M. G. (1974). Phosphenes produced by electrical stimulation of human occipital cortex, and their application to the development of a prosthesis for the blind. *Journal of Physiology, 243*(2), 553-576.

Dobelle, W. H., Mladejovsky, M. G., Evans, J. R., Roberts, T. S., & Girvin, J. P. (1976). 'Braille' reading by a blind volunteer by visual cortex stimulation. *Nature, 259*(5539), 111-112.

Dobelle, W. H., Quest, D. O., Antunes, J. L., Roberts, T. S., & Girvin, J. P. (1979). Artificial vision for the blind by electrical stimulation of the visual cortex. *Neurosurgery, 5*(4), 521-527.

Dolmetsch, R. E., Pajvani, U., Fife, K., Spotts, J. M., & Greenberg, M. E. (2001). Signaling to the nucleus by an L-type calcium channel- calmodulin complex through the MAP kinase pathway. *Science, 294*(5541), 333-339.

Domeniconi, M., Cao, Z., Spencer, T., Sivasankaran, R., Wang, K. C., Nikulina, E., et al. (2002). Myelin-associated glycoprotein interacts with the Nogo66 receptor to inhibit neurite outgrowth. *Neuron, 35*(2), 283-290.

Donoghue, J. P., Nurmikko, A., Black, M., & Hochberg, L. R. (2007). Assistive technology and robotic control using motor cortex ensemble-based neural interface systems in humans with tetraplegia. *Journal of Physiology, 579*(3), 603-611.

Dorn, J. D., Ahuja, A. K., Caspi, A., Da Cruz, L., Dagnelie, G., Sahel, J. A., et al. (2013). The detection of motion by blind subjects with the epiretinal 60-electrode (Argus II) retinal prosthesis. *JAMA Ophthalmology, 131*(2), 183-189.

Dupont, E., Hanganu, I. L., Kilb, W., Hirsch, S., & Luhmann, H. J. (2006). Rapid developmental switch in the mechanisms driving early cortical columnar networks. *Nature, 439*(7072), 79-83.

Eberhart, J., Barr, J., O'Connell, S., Flagg, A., Swartz, M. E., Cramer, K. S., et al. (2004). Ephrin-A5 Exerts Positive or Inhibitory Effects on Distinct Subsets of EphA4-Positive Motor Neurons. *Journal of Neuroscience, 24*(5), 1070-1078.

Elias, L. A., Wang, D. D., & Kriegstein, A. R. (2007). Gap junction adhesion is necessary for radial migration in the neocortex. *Nature, 448*(7156), 901-907.

Elkin, B. S., Shaik, M. A., & Morrison Iii, B. (2011). Chondroitinase ABC reduces brain tissue swelling in vitro. *Journal of Neurotrauma, 28*(11), 2277-2285.

Erceg, S., Ronaghi, M., Oria, M., Roselló, M. G., Aragó, M. A. P., Lopez, M. G., et al. (2010). Transplanted oligodendrocytes and motoneuron progenitors generated from human embryonic stem cells promote locomotor recovery after spinal cord transection. *Stem Cells, 28*(9), 1541-1549.

Erdö, F., Buhrle, C., Blunk, J., Hoehn, M., Xia, Y., Fleischmann, B., et al. (2003). Host-dependent tumorigenesis of embryonic stem cell transplantation in experimental stroke. *Journal of Cerebral Blood Flow and Metabolism, 23*(7), 780-785.

Ethier, C., Oby, E. R., Bauman, M. J., & Miller, L. E. (2012). Restoration of grasp following paralysis through brain-controlled stimulation of muscles. *Nature, 485*(7398), 368-371.

Filbin, M. T. (2003). Myelin-associated inhibitors of axonal regeneration in the adult mammalian CNS. *Nature Reviews Neuroscience, 4*(9), 703-713.

Fouad, K., Klusman, I., & Schwab, M. E. (2004). Regenerating corticospinal fibers in the Marmoset (Callitrix jacchus) after spinal cord lesion and treatment with the anti-Nogo-A antibody IN-1. *European Journal of Neuroscience, 20*(9), 2479-2482.

Fouad, K., Pearse, D. D., Tetzlaff, W., & Vavrek, R. (2009). Transplantation and repair: Combined cell implantation and chondroitinase delivery prevents deterioration of bladder function in rats with complete spinal cord injury. *Spinal Cord, 47*(10), 727-732.

Fouad, K., Schnell, L., Bunge, M. B., Schwab, M. E., Liebscher, T., & Pearse, D. D. (2005). Combining Schwann cell bridges and olfactory-ensheathing glia grafts with chondroitinase promotes locomotor recovery after complete transection of the spinal cord. *Journal of Neuroscience, 25*(5), 1169-1178.

Fournier, A. E., GrandPre, T., & Strittmatter, S. M. (2001). Identification of a receptor mediating Nogo-66 inhibition of axonal regeneration. *Nature, 409*(6818), 341-346.

Fujiyoshi, T., Kubo, T., Chan, C. C. M., Koda, M., Okawa, A., Takahashi, K., et al. (2010). Interferon-γ decreases chondroitin sulfate proteoglycan expression and enhances hindlimb function after spinal cord injury in mice. *Journal of Neurotrauma, 27*(12), 2283-2294.

Furukawa, Y., Shimada, A., Kato, K., Iwata, H., & Torimitsu, K. (2013). Monitoring neural stem cell differentiation using PEDOT-PSS based MEA. *Biochimica et Biophysica Acta - General Subjects*.

Galtrey, C. M., Asher, R. A., Nothias, F., & Fawcett, J. W. (2007). Promoting plasticity in the spinal cord with chondroitinase improves functional recovery after peripheral nerve repair. *Brain, 130*(4), 926-939.

Galtrey, C. M., Kwok, J. C. F., Carulli, D., Rhodes, K. E., & Fawcett, J. W. (2008). Distribution and synthesis of extracellular matrix proteoglycans, hyaluronan, link proteins and tenascin-R in the rat spinal cord. *European Journal of Neuroscience, 27*(6), 1373-1390.

Ganguly, K., Dimitrov, D. F., Wallis, J. D., & Carmena, J. M. (2011). Reversible large-scale modification of cortical networks during neuroprosthetic control. *Nature Neuroscience, 14*(5), 662-669.

Garcia-Alias, G., Barkhuysen, S., Buckle, M., & Fawcett, J. W. (2009). Chondroitinase ABC treatment opens a window of opportunity for task-specific rehabilitation. *Nature Neuroscience, 12*(9), 1145-1151.

Garcia-Alias, G., & Fawcett, J. W. (2012). Training and anti-CSPG combination therapy for spinal cord injury. *Experimental Neurology, 235*(1), 26-32.

Garcia-Alias, G., Lin, R., Akrimi, S. F., Story, D., Bradbury, E. J., & Fawcett, J. W. (2008). Therapeutic time window for the application of chondroitinase ABC after spinal cord injury. *Experimental Neurology, 210*(2), 331-338.

Garcia-Alias, G., Petrosyan, H. A., Schnell, L., Horner, P. J., Bowers, W. J., Mendell, L. M., et al. (2011). Chondroitinase ABC Combined with Neurotrophin NT-3 Secretion and NR2D Expression Promotes Axonal Plasticity and Functional Recovery in Rats with Lateral Hemisection of the Spinal Cord. *Journal of Neuroscience, 31*(49), 17788-17799.

Garwood, J., Schnädelbach, O., Clement, A., Schütte, K., Bach, A., & Faissner, A. (1999). DSD-1-proteoglycan is the mouse homolog of phosphacan and displays opposing effects on neurite outgrowth dependent on neuronal lineage. *Journal of Neuroscience, 19*(10), 3888-3899.

Ghosh, S., & Inganäs, O. (2000). Electrochemical characterization of poly(3,4-ethylene dioxythiophene) based conducting hydrogel networks. *Journal of the Electrochemical Society, 147*(5), 1872-1877.

Gilbert, C. D., & Wiesel, T. N. (1989). Columnar specificity of intrinsic horizontal and corticocortical connections in cat visual cortex. *Journal of Neuroscience, 9*(7), 2432-2422.

Gilbert, R. J., McKeon, R. J., Darr, A., Calabro, A., Hascall, V. C., & Bellamkonda, R. V. (2005). CS-4, 6 is differentially upregulated in glial scar and is a potent inhibitor of neurite extension. *Molecular and Cellular Neuroscience, 29*(4), 545-558.

Gilletti, A., & Muthuswamy, J. (2006). Brain micromotion around implants in the rodent somatosensory cortex. *Journal of Neural Engineering, 3*(3), 189-195.

Glovinsky, Y., Quigley, H. A., & Dunkelberger, G. R. (1991). Retinal ganglion cell loss is size dependent in experimental glaucoma. *Invest Ophthalmol Vis Sci, 32*(3), 484-491.

Gogolla, N., Caroni, P., Lüthi, A., & Herry, C. (2009). Perineuronal nets protect fear memories from erasure. *Science, 325*(5945), 1258-1261.

Goldberg, J. L., Vargas, M. E., Wang, J. T., Mandemakers, W., Oster, S. F., Sretavan, D. W., et al. (2004). An oligodendrocyte lineage-specific semaphorin, sema5A, inhibits axon growth by retinal ganglion cells. *Journal of Neuroscience, 24*(21), 4989-4999.

Gomez, T. M., & Spitzer, N. C. (1999). In vivo regulation of axon extension and pathfinding by growth-cone calcium transients. *Nature, 397*(6717), 350-355.

Grill, W. M., Norman, S. E., & Bellamkonda, R. V. (2009). Implanted neural interfaces: Biochallenges and engineered solutions, *Annual Review of Biomedical Engineering* (Vol. 11, pp. 1-24).

Grimpe, B., & Silver, J. (2004). A Novel DNA Enzyme Reduces Glycosaminoglycan Chains in the Glial Scar and Allows Microtransplanted Dorsal Root Ganglia Axons to Regenerate beyond Lesions in the Spinal Cord. *Journal of Neuroscience, 24*(6), 1393-1397.

Gronthos, S., Arthur, A., Bartold, P. M., & Shi, S. A method to isolate and culture expand human dental pulp stem cells. *Methods Mol Biol, 698*, 107-121.

Gronthos, S., Arthur, A., Bartold, P. M., & Shi, S. (2011). A method to isolate and culture expand human dental pulp stem cells. *Methods Mol Biol, 698*, 107-121.

Gronthos, S., Mankani, M., Brahim, J., Robey, P. G., & Shi, S. (2000). Postnatal human dental pulp stem cells (DPSCs) in vitro and in vivo. *Proc Natl Acad Sci U S A, 97*(25), 13625-13630.

Guimarães, E. T., Cruz, G. S., De Jesus, A. A., Lacerda De Carvalho, A. F., Rogatto, S. R., Pereira, L. D. V., et al. (2011). Mesenchymal and embryonic characteristics of stem cells obtained from mouse dental pulp. *Archives of Oral Biology, 56*(11), 1247-1255.

Haddock, G., Cross, A. K., Allan, S., Sharrack, B., Callaghan, J., Bunning, R. A. D., et al. (2007). Brevican and phosphacan expression and localization following transient middle cerebral artery occlusion in the rat. *Biochemical Society Transactions, 35*(4), 692-694.

Härtig, W., Brauer, K., Bigl, V., & Brückner, G. (1994). Chondroitin sulfate proteoglycan-immunoreactivity of lectin-labeled perineuronal nets around parvalbumin-containing neurons. *Brain Res, 635*(1-2), 307-311.

Härtig, W., Derouiche, A., Welt, K., Brauer, K., Grosche, J., Mader, M., et al. (1999). Cortical neurons immunoreactive for the potassium channel Kv3.1b subunit are predominantly surrounded by perineuronal nets presumed as a buffering system for cations. *Brain Res, 842*(1), 15-29.

Hauben, E., Ibarra, A., Mizrahi, T., Barouch, R., Agranov, E., & Schwartz, M. (2001). Vaccination with a Nogo-A-derived peptide after incomplete spinal-cord injury promotes recovery via a T-cell-mediated neuroprotective response: Comparison with other myelin antigens. *Proceedings of the National Academy of Sciences of the United States of America, 98*(26), 15173-15178.

He, W., McConnell, G. C., & Bellamkonda, R. V. (2006). Nanoscale laminin coating modulates cortical scarring response around implanted silicon microelectrode arrays. *Journal of Neural Engineering, 3*(4).

He, W., McConnell, G. C., Schneider, T. M., & Bellamkonda, R. V. (2007). A novel anti-inflammatory surface for neural electrodes. *Advanced Materials, 19*(21), 3529-3533.

Heikkiä, T. J., Yla-Outinen, L., Tanskanen, J. M. A., Lappalainen, R. S., Skottman, H., Suuronen, R., et al. (2009). Human embryonic stem cell-derived neuronal cells form spontaneously active neuronal networks in vitro. *Experimental Neurology, 218*(1), 109-116.

Heine, W., Conant, K., Griffin, J. W., & Höke, A. (2004). Transplanted neural stem cells promote axonal regeneration through chronically denervated peripheral nerves. *Experimental Neurology, 189*(2), 231-240.

Hensch, T. K. (2004). Critical period regulation, *Annual Review of Neuroscience* (Vol. 27, pp. 549-579).

Hensch, T. K. (2005). Critical period plasticity in local cortical circuits. *Nature Reviews Neuroscience, 6*(11), 877-888.

Hicks, A. U., Lappalainen, R. S., Narkilahti, S., Suuronen, R., Corbett, D., Sivenius, J., et al. (2009). Transplantation of human embryonic stem cell-derived neural precursor cells and enriched environment after cortical stroke in rats: Cell survival and functional recovery. *European Journal of Neuroscience, 29*(3), 562-574.

Hill, J. J., Jin, K., Mao, X. O., Xie, L., & Greenberg, D. A. (2012). Intracerebral chondroitinase ABC and heparan sulfate proteoglycan glypican improve outcome from chronic stroke in rats. *Proceedings of the National Academy of Sciences of the United States of America, 109*(23), 9155-9160.

Hobohm, C., Günther, A., Grosche, J., Roßner, S., Schneider, D., & Brückner, G. (2005). Decomposition and long-lasting downregulation of extracellular matrix in perineuronal nets induced by focal cerebral ischemia in rats. *Journal of Neuroscience Research, 80*(4), 539-548.

Hochberg, L. R., Bacher, D., Jarosiewicz, B., Masse, N. Y., Simeral, J. D., Vogel, J., et al. (2012). Reach and grasp by people with tetraplegia using a neurally controlled robotic arm. *Nature, 485*(7398), 372-375.

Hochberg, L. R., Serruya, M. D., Friehs, G. M., Mukand, J. A., Saleh, M., Caplan, A. H., et al. (2006). Neuronal ensemble control of prosthetic devices by a human with tetraplegia. *Nature, 442*(7099), 164-171.

Hockfield, S., Kalb, R. G., Zaremba, S., & Fryer, H. (1990). Expression of neural proteoglycans correlates with the acquisition of mature neuronal properties in the mammalian brain. *Cold Spring Harbor Symposia on Quantitative Biology, 55*, 505-514.

Hoehn, M., Küstermann, E., Blunk, J., Wiedermann, D., Trapp, T., Wecker, S., et al. (2002). Monitoring of implanted stem cell migration in vivo: A highly resolved in vivo magnetic resonance imaging investigation of experimental stroke in rat. *Proceedings of the National Academy of Sciences of the United States of America, 99*(25), 16267-16272.

Hofstetter, C. P., Schwarz, E. J., Hess, D., Widenfalk, J., El Manira, A., Prockop, D. J., et al. (2002). Marrow stromal cells form guiding strands in the injured spinal cord and promote recovery. *Proceedings of the National Academy of Sciences of the United States of America, 99*(4), 2199-2204.

Hormuzdi, S. G., Filippov, M. A., Mitropoulou, G., Monyer, H., & Bruzzone, R. (2004). Electrical synapses: A dynamic signaling system that shapes the activity of neuronal networks. *Biochimica et Biophysica Acta - Biomembranes, 1662*(1-2), 113-137.

Hsu, J. Y. C., McKeon, R., Goussev, S., Werb, Z., Lee, J. U., Trivedi, A., et al. (2006). Matrix metalloproteinase-2 facilitates wound healing events that promote functional recovery after spinal cord injury. *Journal of Neuroscience, 26*(39), 9841-9850.

Huang, A. H., Snyder, B. R., Cheng, P. H., & Chan, A. W. (2008). Putative dental pulp-derived stem/stromal cells promote proliferation and differentiation of endogenous neural cells in the hippocampus of mice. *Stem Cells, 26*(10), 2654-2663.

Huang, D. W., McKerracher, L., Braun, P. E., & David, S. (1999). A therapeutic vaccine approach to stimulate axon regeneration in the adult mammalian spinal cord. *Neuron, 24*(3), 639-647.

Hurtado, A., Podinin, H., Oudega, M., & Grimpe, B. (2008). Deoxyribozyme-mediated knockdown of xylosyltransferase-1 mRNA promotes axon growth in the adult rat spinal cord. *Brain, 131*(10), 2596-2605.

Hwang, D. H., Kim, H. M., Kang, Y. M., Joo, I. S., Cho, C. S., Yoon, B. W., et al. (2011). Combination of multifaceted strategies to maximize the therapeutic benefits of neural stem cell transplantation for spinal cord repair. *Cell Transplantation, 20*(9), 1361-1379.

Ikegame, Y., Yamashita, K., Hayashi, S. I., Mizuno, H., Tawada, M., You, F., et al. (2011). Comparison of mesenchymal stem cells from adipose tissue and bone marrow for ischemic stroke therapy. *Cytotherapy, 13*(6), 675-685.

Ikegami, T., Nakamura, M., Yamane, J., Katoh, H., Okada, S., Iwanami, A., et al. (2005). Chondroitinase ABC combined with neural stem/progenitor cell transplantation enhances graft cell migration and outgrowth of growth-associated protein-43-positive fibers after rat spinal cord injury. *European Journal of Neuroscience, 22*(12), 3036-3046.

Illes, S., Fleischer, W., Siebler, M., Hartung, H. P., & Dihné, M. (2007). Development and pharmacological modulation of embryonic stem cell-derived neuronal network activity. *Experimental Neurology, 207*(1), 171-176.

Illes, S., Theiss, S., Hartung, H. P., Siebler, M., & Dihné, M. (2009). Niche-dependent development of functional neuronal networks from embryonic stem cell-derived neural populations. *BMC Neuroscience, 10*.

Inatani, M., Honjo, M., Otori, Y., Oohira, A., Kido, N., Tano, Y., et al. (2001). Inhibitory effects of neurocan and phosphacan on neurite outgrowth from retinal ganglion cells in culture. *Investigative Ophthalmology and Visual Science, 42*(8), 1930-1938.

Inoue, T., Sugiyama, M., Hattori, H., Wakita, H., Wakabayashi, T., & Ueda, M. (2013). Stem cells from human exfoliated deciduous tooth-derived conditioned medium enhance recovery of focal cerebral ischemia in rats. *Tissue Engineering - Part A, 19*(1-2), 24-29.

Iozzo, R. V. (1998). Matrix proteoglycans: From molecular design to cellular function, *Annual Review of Biochemistry* (Vol. 67, pp. 609-652).

Islam, M. S., Anderson, C. S., Hankey, G. J., Hardie, K., Carter, K., Broadhurst, R., et al. (2008). Trends in incidence and outcome of stroke in Perth, Western Australia during 1989 to 2001: The Perth Community Stroke Study. *Stroke, 39*(3), 776-782.

Jackson, A., & Zimmermann, J. B. (2012). Neural interfaces for the brain and spinal cord - Restoring motor function. *Nature Reviews Neurology, 8*(12), 690-699.

Jakeman, L. B., Hoschouer, E. L., & Basso, D. M. (2011). Injured mice at the gym: Review, results and considerations for combining chondroitinase and locomotor exercise to enhance recovery after spinal cord injury. *Brain Research Bulletin, 84*(4-5), 317-326.

James, C. D., Spence, A. J. H., Dowell-Mesfin, N. M., Hussain, R. J., Smith, K. L., Craighead, H. G., et al. (2004). Extracellular recordings from patterned neuronal networks using planar microelectrode arrays. *IEEE Transactions on Biomedical Engineering, 51*(9), 1640-1648.

Janebodin, K., Horst, O. V., Ieronimakis, N., Balasundaram, G., Reesukumal, K., Pratumvinit, B., et al. (2011). Isolation and characterization of neural crest-derived stem cells from dental pulp of neonatal mice. *PLoS One, 6*(11), e27526.

Ji, B., Case, L. C., Liu, K., Shao, Z., Lee, X., Yang, Z., et al. (2008). Assessment of functional recovery and axonal sprouting in oligodendrocyte-myelin glycoprotein (OMgp) null mice after spinal cord injury. *Molecular and Cellular Neuroscience, 39*(2), 258-267.

Jimbo, Y., & Kawana, A. (1992). Electrical stimulation and recording from cultured neurons using a planar electrode array. *Bioelectrochemistry and Bioenergetics, 29*(2), 193-204.

Jones, L. L., Margolis, R. U., & Tuszynski, M. H. (2003). The chondroitin sulfate proteoglycans neurocan, brevican, phosphacan, and versican are differentially regulated following spinal cord injury. *Experimental Neurology, 182*(2), 399-411.

Jun, S. B., Hynd, M. R., Dowell-Mesfin, N. M., Al-Kofahi, Y., Roysam, B., Shain, W., et al. (2008). Modulation of cultured neural networks using neurotrophin release from hydrogel-coated microelectrode arrays. *Journal of Neural Engineering, 5*(2), 203-213.

Kaczmarek, K. A., Webster, J. G., Bach-y-Rita, P., & Tompkins, W. J. (1991). Electrotactile and vibrotactile displays for sensory substitution systems. *IEEE Transactions on Biomedical Engineering, 38*(1), 1-16.

Kappler, J., Stichel, C. C., Gleichmann, M., Gillen, C., Junghans, U., Kresse, H., et al. (1998). Developmental regulation of decorin expression in postnatal rat brain. *Brain Research, 793*(1-2), 328-332.

Karbanová, J., Soukup, T., Suchánek, J., Pytlík, R., Corbeil, D., & Mokry, J. (2011). Characterization of dental pulp stem cells from impacted third molars cultured in low serum-containing medium. *Cells Tissues Organs, 193*(6), 344-365.

Karetko-Sysa, M., Skangiel-Kramska, J., & Nowicka, D. (2011). Disturbance of perineuronal nets in the perilesional area after photothrombosis is not associated with neuronal death. *Experimental Neurology, 231*(1), 113-126.

Karimi-Abdolrezaee, S., Eftekharpour, E., Wang, J., Schut, D., & Fehlings, M. G. (2010). Synergistic effects of transplanted adult neural stem/progenitor cells, chondroitinase, and growth factors promote functional repair and plasticity of the chronically injured spinal cord. *Journal of Neuroscience, 30*(5), 1657-1676.

Khazipov, R., & Luhmann, H. J. (2006). Early patterns of electrical activity in the developing cerebral cortex of humans and rodents. *Trends Neurosci, 29*(7), 414-418.

Khler, A. K., Djurovic, S., Rimol, L. M., Brown, A. A., Athanasiu, L., Jnsson, E. G., et al. (2011). Candidate gene analysis of the human natural killer-1 carbohydrate pathway and perineuronal nets in schizophrenia: B3GAT2 Is associated with disease risk and cortical surface area. *Biological Psychiatry, 69*(1), 90-96.

Kim, J. E., Li, S., GrandPre, T., Qiu, D., & Strittmatter, S. M. (2003). Axon regeneration in young adult mice lacking Nogo-A/B. *Neuron, 38*(2), 187-199.

Kipke, D. R., Shain, W., Buzsuki, G., Fetz, E., Henderson, J. M., Hetke, J. F., et al. (2008). Advanced neurotechnologies for chronic neural interfaces: New horizons and clinical opportunities. *Journal of Neuroscience, 28*(46), 11830-11838.

Kiraly, M., Kadar, K., Horvathy, D. B., Nardai, P., Racz, G. Z., Lacza, Z., et al. (2011). Integration of neuronally predifferentiated human dental pulp stem cells into rat brain in vivo. *Neurochem Int, 59*(3), 371-381.

Kiraly, M., Porcsalmy, B., Pataki, A., Kadar, K., Jelitai, M., Molnar, B., et al. (2009). Simultaneous PKC and cAMP activation induces differentiation of human dental pulp stem cells into functionally active neurons. *Neurochem Int, 55*(5), 323-332.

Konur, S., & Ghosh, A. (2005). Calcium signaling and the control of dendritic development. *Neuron, 46*(3), 401-405.

Kotler, S. (2002). Vision Quest A half century of artificial-sight research has succeeded. And now this blind man can see. Behind the bionic-eye breakthrough. *WIRED-SAN FRANCISCO-, 10*(9), 94-94.

Kottis, V., Thibault, P., Mikol, D., Xiao, Z. C., Zhang, R., Dergham, P., et al. (2002). Oligodendrocyte-myelin glycoprotein (OMgp) is an inhibitor of neurite outgrowth. *Journal of Neurochemistry, 82*(6), 1566-1569.

Kumagai, G., Okada, Y., Yamane, J., Nagoshi, N., Kitamura, K., Mukaino, M., et al. (2009). Roles of ES cell-derived gliogenic neural stem/progenitor cells in functional recovery after spinal cord injury. *PLoS One, 4*(11).

Kwok, J. C., Dick, G., Wang, D., & Fawcett, J. W. (2011). Extracellular matrix and perineuronal nets in CNS repair. *Developmental Neurobiology, 71*(11), 1073-1089.

Kwok, J. C. F., Carulli, D., & Fawcett, J. W. (2010). In vitro modeling of perineuronal nets: Hyaluronan synthase and link protein are necessary for their formation and integrity. *Journal of Neurochemistry, 114*(5), 1447-1459.

Lander, C., Kind, P., Maleski, M., & Hockfield, S. (1997). A family of activity-dependent neuronal cell-surface chondroitin sulfate proteoglycans in cat visual cortex. *Journal of Neuroscience, 17*(6), 1928-1939.

Lee, H., McKeon, R. J., & Bellamkonda, R. V. Sustained delivery of thermostabilized chABC enhances axonal sprouting and functional recovery after spinal cord injury. *Proceedings of the National Academy of Sciences of the United States of America, 107*(8), 3340-3345.

Lee, J. K., Chan, A. F., Luu, S. M., Zhu, Y., Ho, C., Tessier-Lavigne, M., et al. (2009). Reassessment of corticospinal tract regeneration in Nogo-deficient mice. *Journal of Neuroscience, 29*(27), 8649-8654.

Lee, J. K., Geoffroy, C. G., Chan, A. F., Tolentino, K. E., Crawford, M. J., Leal, M. A., et al. (2010). Assessing Spinal Axon Regeneration and Sprouting in Nogo-, MAG-, and OMgp-Deficient Mice. *Neuron, 66*(5), 663-670.

Lee, J. K., & Zheng, B. (2012). Role of myelin-associated inhibitors in axonal repair after spinal cord injury. *Experimental Neurology, 235*(1), 33-42.

Lee, K., Singh, A., He, J., Massia, S., Kim, B., & Raupp, G. (2004). Polyimide based neural implants with stiffness improvement. *Sensors and Actuators, B: Chemical, 102*(1), 67-72.

Lee, K. K., He, J., Singh, A., Massia, S., Ehteshami, G., Kim, B., et al. (2004). Polyimide-based intracortical neural implant with improved structural stiffness. *Journal of Micromechanics and Microengineering, 14*(1), 32-37.

Lelong, I. H., Petegnief, V., & Rebel, G. (1992). Neuronal cells mature faster on polyethyleneimine coated plates than on polylysine coated plates. *Journal of Neuroscience Research, 32*(4), 562-568.

Leong, W. K., Henshall, T. L., Arthur, A., Kremer, K. L., Lewis, M. D., Helps, S. C., et al. (2012). Human Adult Dental Pulp Stem Cells Enhance Poststroke Functional Recovery Through Non-Neural Replacement Mechanisms. *Stem Cells Translational Medicine, 1*, 177-187.

Leong, W. K., Lewis, M. D., & Koblar, S. A. (2013). Concise review: Preclinical studies on human cell-based therapy in rodent ischemic stroke models: Where are we now after a decade? *Stem Cells, 31*(6), 1040-1043.

Leuthardt, E. C., Schalk, G., Moran, D., & Ojemann, J. G. (2006). The emerging world of motor neuroprosthetics: a neurosurgical perspective. *Neurosurgery, 59*(1), 1-14.

Leuthardt, E. C., Schalk, G., Wolpaw, J. R., Ojemann, J. G., & Moran, D. W. (2004). A brain-computer interface using electrocorticographic signals in humans. *Journal of Neural Engineering, 1*(2), 63-71.

Li, J., Cassell, A., Delzeit, L., Han, J., & Meyyappan, M. (2002). Novel three-dimensional electrodes: Electrochemical properties of carbon nanotube ensembles. *Journal of Physical Chemistry B, 106*(36), 9299-9305.

Logan, A., Baird, A., & Berry, M. (1999). Decorin attenuates gliotic scar formation in the rat cerebral hemisphere. *Experimental Neurology, 159*(2), 504-510.

Löw, K., Culbertson, M., Bradke, F., Tessier-Lavigne, M., & Tuszynski, M. H. (2008). Netrin-1 is a novel myelin-associated inhibitor to axon growth. *Journal of Neuroscience, 28*(5), 1099-1108.

Maeda, N., & Noda, M. (1996). 6B4 proteoglycan/phosphacan is a repulsive substratum but promotes morphological differentiation of cortical neurons. *Development, 122*(2), 647-658.

Margalit, E., & Sadda, S. R. (2003). Retinal and Optic Nerve Diseases. *Artificial Organs, 27*(11), 963-974.

Massey, J. M., Amps, J., Viapiano, M. S., Matthews, R. T., Wagoner, M. R., Whitaker, C. M., et al. (2008). Increased chondroitin sulfate proteoglycan expression in denervated brainstem targets following spinal cord injury creates a barrier to axonal regeneration overcome by chondroitinase ABC and neurotrophin-3. *Experimental Neurology, 209*(2), 426-445.

Massey, J. M., Hubscher, C. H., Wagoner, M. R., Decker, J. A., Amps, J., Silver, J., et al. (2006). Chondroitinase ABC digestion of the perineuronal net promotes functional collateral sprouting in the cuneate nucleus after cervical spinal cord injury. *Journal of Neuroscience, 26*(16), 4406-4414.

McConnell, G. C., Schneider, T. M., Owens, D. J., & Bellamkonda, R. V. (2007). Extraction force and cortical tissue reaction of silicon microelectrode arrays implanted in the rat brain. *IEEE Transactions on Biomedical Engineering, 54*(6), 1097-1107.

McCreery, D. B., & Agnew, W. F. (1990). *Neuronal and axonal injury during functional electrical stimulation; A review of the possible mechanisms.* Paper presented at the Proceedings of the Annual Conference on Engineering in Medicine and Biology.

McFarland, D. J., Sarnacki, W. A., & Wolpaw, J. R. (2010). Electroencephalographic (EEG) control of three-dimensional movement. *Journal of Neural Engineering, 7*(3).

McGie, S. C., Nagai, M. K., & Artinian-Shaheen, T. (2013). Clinical ethical concerns in the implantation of brain-machine interfaces: Part II: Specific clinical and technical issues affecting ethical soundness. *IEEE Pulse, 4*(2), 32-37.

McKeon, R. J., Hoke, A., & Silver, J. (1995). Injury-induced proteoglycans inhibit the potential for laminin-mediated axon growth on astrocytic scars. *Experimental Neurology, 136*(1), 32-43.

McKeon, R. J., Jurynec, M. J., & Buck, C. R. (1999). The chondroitin sulfate proteoglycans neurocan and phosphacan are expressed by reactive astrocytes in the chronic CNS glial scar. *Journal of Neuroscience, 19*(24), 10778-10788.

McKerracher, L., David, S., Jackson, D. L., Kottis, V., Dunn, R. J., & Braun, P. E. (1994). Identification of myelin-associated glycoprotein as a major myelin-derived inhibitor of neurite growth. *Neuron, 13*(4), 805-811.

McRae, P. A., Baranov, E., Rogers, S. L., & Porter, B. E. (2012). Persistent decrease in multiple components of the perineuronal net following status epilepticus. *European Journal of Neuroscience, 36*(11), 3471-3482.

Milev, P., Maurel, P., Chiba, A., Mevissen, M., Popp, S., Yamaguchi, Y., et al. (1998). Differential regulation of expression of hyaluronan-binding proteoglycans in developing brain: Aggrecan, versican, neurocan, and brevican. *Biochemical and Biophysical Research Communications, 247*(2), 207-212.

Minor, K., Tang, X., Kahrilas, G., Archibald, S. J., Davies, J. E., & Davies, S. J. (2008). Decorin promotes robust axon growth on inhibitory CSPGs and myelin via a direct effect on neurons. *Neurobiology of Disease, 32*(1), 88-95.

Miyata, S., Nishimura, Y., Hayashi, N., & Oohira, A. (2005). Construction of perineuronal net-like structure by cortical neurons in culture. *Neuroscience, 136*(1), 95-104.

Miyata, S., Nishimura, Y., & Nakashima, T. (2007). Perineuronal nets protect against amyloid Œ≤-protein neurotoxicity in cultured cortical neurons. *Brain Research, 1150*(1), 200-206.

Monnier, P. P., Sierra, A., Schwab, J. M., Henke-Fahle, S., & Mueller, B. K. (2003). The Rho/ROCK pathway mediates neurite growth-inhibitory activity associated with the chondroitin sulfate proteoglycans of the CNS glial scar. *Molecular and Cellular Neuroscience, 22*(3), 319-330.

Morawski, M., Brückner, G., Jäger, C., Seeger, G., & Arendt, T. (2010). Neurons associated with aggrecan-based perineuronal nets are protected against tau pathology in subcortical regions in Alzheimer's disease. *Neuroscience, 169*(3), 1347-1363.

Moreau-Fauvarque, C., Kumanogoh, A., Camand, E., Jaillard, C., Barbin, G., Boquet, I., et al. (2003). The transmembrane semaphorin Sema4D/CD100, an inhibitor of axonal growth, is expressed on oligodendrocytes and upregulated after CNS lesion. *Journal of Neuroscience, 23*(27), 9229-9239.

Moritz, C. T., Perlmutter, S. I., & Fetz, E. E. (2008). Direct control of paralysed muscles by cortical neurons. *Nature, 456*(7222), 639-642.

Morris, N. P., & Henderson, Z. (2000). Perineuronal nets ensheath fast spiking, parvalbumin-immunoreactive neurons in the medial septum/diagonal band complex. *European Journal of Neuroscience, 12*(3), 828-838.

Mukhopadhyay, G., Doherty, P., Walsh, F. S., Crocker, P. R., & Filbin, M. T. (1994). A novel role for myelin-associated glycoprotein as an inhibitor of axonal regeneration. *Neuron, 13*(3), 757-767.

Muller-Putz, G. R., Scherer, R., Pfurtscheller, G., & Rupp, R. (2005). EEG-based neuroprosthesis control: A step towards clinical practice. *Neuroscience Letters, 382*(1-2), 169-174.

Neumann, S., Bradke, F., Tessier-Lavigne, M., & Basbaum, A. I. (2002). Regeneration of sensory axons within the injured spinal cord induced by intraganglionic cAMP elevation. *Neuron, 34*(6), 885-893.

Niclou, S. P., Franssen, E. H. P., Ehlert, E. M. E., Taniguchi, M., & Verhaagen, J. (2003). Meningeal cell-derived semaphorin 3A inhibits neurite outgrowth. *Molecular and Cellular Neuroscience, 24*(4), 902-912.

Noble, L. J., Donovan, F., Igarashi, T., Goussev, S., & Werb, Z. (2002). Matrix metalloproteinases limit functional recovery after spinal cord injury by modulation of early vascular events. *Journal of Neuroscience, 22*(17), 7526-7535.

Normann, R. A., Maynard, E. M., Rousche, P. J., & Warren, D. J. (1999). A neural interface for a cortical vision prosthesis. *Vision Research, 39*(15), 2577-2587.

Nosrat, I. V., Smith, C. A., Mullally, P., Olson, L., & Nosrat, C. A. (2004). Dental pulp cells provide neurotrophic support for dopaminergic neurons and differentiate into neurons in vitro; implications for tissue engineering and repair in the nervous system. *European Journal of Neuroscience, 19*(9), 2388-2398.

Nosrat, I. V., Widenfalk, J., Olson, L., & Nosrat, C. A. (2001). Dental pulp cells produce neurotrophic factors, interact with trigeminal neurons in vitro, and rescue motoneurons after spinal cord injury. *Developmental Biology, 238*(1), 120-132.

Nozaki, T., & Ohura, K. (2011). Gene expression profile of dental pulp cells during differentiation into an adipocyte lineage. *Journal of Pharmacological Sciences, 115*(3), 354-363.

Nyberg, T., Shimada, A., & Torimitsu, K. (2007). Ion conducting polymer microelectrodes for interfacing with neural networks. *Journal of Neuroscience Methods, 160*(1), 16-25.

O'Shaughnessy, T. J., Liu, J. L., & Ma, W. (2009). Passaged neural stem cell-derived neuronal networks for a portable biosensor. *Biosensors and Bioelectronics, 24*(8), 2365-2370.

Onose, G., Grozea, C., Anghelescu, A., Daia, C., Sinescu, C. J., Ciurea, A. V., et al. (2012). On the feasibility of using motor imagery EEG-based brain-computer interface in chronic tetraplegics for assistive robotic arm control: A clinical test and long-term post-trial follow-up. *Spinal Cord, 50*(8), 599-608.

Oudega, M., Chao, O. Y., Avison, D. L., Bronson, R. T., Buchser, W. J., Hurtado, A., et al. (2012). Systemic administration of a deoxyribozyme to xylosyltransferase-1 mRNA promotes recovery after a spinal cord contusion injury. *Experimental Neurology, 237*(1), 170-179.

Owens, D. F., & Kriegstein, A. R. (1998). Patterns of intracellular calcium fluctuation in precursor cells of the neocortical ventricular zone. *Journal of Neuroscience, 18*(14), 5374-5388.

Panetsos, F., Sanchez-Jimenez, A., Cerio, E. D., Diaz-Guemes, I., & Sanchez, F. M. (2011). Consistent phosphenes generated by electrical microstimulation of the visual thalamus. An experimental approach for thalamic visual neuroprostheses. *Frontiers in Neuroscience*(JUL).

Papadopoulos, C. M., Tsai, S. Y., Alsbiei, T., O'Brien, T. E., Schwab, M. E., & Kartje, G. L. (2002). Functional recovery and neuroanatomical plasticity following middle cerebral artery occlusion and IN-1 antibody treatment in the adult rat. *Annals of Neurology, 51*(4), 433-441.

Pastrana, E., Moreno-Flores, M. T., Gurzov, E. N., Avila, J., Wandosell, F., & Diaz-Nido, J. (2006). Genes associated with adult axon regeneration promoted by olfactory ensheathing cells: A new role for matrix metalloproteinase 2. *Journal of Neuroscience, 26*(20), 5347-5359.

Peinado, A. (2001). Immature neocortical neurons exist as extensive syncitial networks linked by dendrodendritic electrical connections. *J Neurophysiol, 85*(2), 620-629.

Perissinotto, D., Iacopetti, P., Bellina, I., Doliana, R., Colombatti, A., Pettway, Z., et al. (2000). Avian neural crest cell migration is diversely regulated by the two major hyaluronan-binding proteoglycans PG-M/versican and aggrecan. *Development, 127*(13), 2823-2842.

Pfurtscheller, G., Muller, G. R., Pfurtscheller, J., Gerner, H. J., & Rupp, R. (2003). 'Thought' - Control of functional electrical stimulation to restore hand grasp in a patient with tetraplegia. *Neuroscience Letters, 351*(1), 33-36.

Pizzorusso, T., Medini, P., Berardi, N., Chierzi, S., Fawcett, J. W., & Maffei, L. (2002). Reactivation of ocular dominance plasticity in the adult visual cortex. *Science, 298*(5596), 1248-1251.

Pizzorusso, T., Medini, P., Landi, S., Baldini, S., Berardi, N., & Maffei, L. (2006). Structural and functional recovery from early monocular deprivation in adult rats. *Proceedings of the National Academy of Sciences of the United States of America, 103*(22), 8517-8522.

Pohlmeyer, E. A., Oby, E. R., Perreault, E. J., Solla, S. A., Kilgore, K. L., Kirsch, R. F., et al. (2009). Toward the restoration of hand use to a paralyzed monkey: Brain-controlled functional electrical stimulation of forearm muscles. *PLoS One, 4*(6).

Polikov, V. S., Tresco, P. A., & Reichert, W. M. (2005). Response of brain tissue to chronically implanted neural electrodes. *Journal of Neuroscience Methods, 148*(1), 1-18.

Potter, S. M., & DeMarse, T. B. (2001). A new approach to neural cell culture for long-term studies. *Journal of Neuroscience Methods, 110*(1-2), 17-24.

Prichard, H. L., Reichert, W., & Klitzman, B. (2008). IFATS collection: Adipose-derived stromal cells improve the foreign body response. *Stem Cells, 26*(10), 2691-2695.

Prichard, H. L., Reichert, W. M., & Klitzman, B. (2007). Adult adipose-derived stem cell attachment to biomaterials. *Biomaterials, 28*(6), 936-946.

Properzi, F., Asher, R., & Fawcett, J. (2003). Chondroitin sulphate proteoglycans in the central nervous system: changes and synthesis after injury. *Biochemical Society Transactions, 31*(2), 335-336.

Properzi, F., Carulli, D., Asher, R. A., Muir, E., Camargo, L. M., Van Kuppevelt, T. H., et al. (2005). Chondroitin 6-sulphate synthesis is up-regulated in injured CNS, induced by injury-related cytokines and enhanced in axon growth inhibitory glia. *European Journal of Neuroscience, 21*(2), 378-390.

Purcell, E. K., Seymour, J. P., Yandamuri, S., & Kipke, D. R. (2009). In vivo evaluation of a neural stem cell-seeded prosthesis. *Journal of Neural Engineering, 6*(2), 026005.

Quirk, G. J., Paré, D., Richardson, R., Herry, C., Monfils, M. H., Schiller, D., et al. (2010). Erasing fear memories with extinction training. *Journal of Neuroscience, 30*(45), 14993-14997.

Rejali, D., Lee, V. A., Abrashkin, K. A., Humayun, N., Swiderski, D. L., & Raphael, Y. (2007). Cochlear implants and ex vivo BDNF gene therapy protect spiral ganglion neurons. *Hearing Research, 228*(1-2), 180-187.

Rolls, A., Shechter, R., & Schwartz, M. (2009). The bright side of the glial scar in CNS repair. *Nature Reviews Neuroscience, 10*(3), 235-241.

Romero, M. I., Rangappa, N., Garry, M. G., & Smith, G. M. (2001). Functional regeneration of chronically injured sensory afferents into adult spinal cord after neurotrophin gene therapy. *Journal of Neuroscience, 21*(21), 8408-8416.

Ruff, R. L., McKerracher, L., & Selzer, M. E. (2008). Repair and neurorehabilitation strategies for spinal cord injury, *Annals of the New York Academy of Sciences* (Vol. 1142, pp. 1-20).

Ruoslahti, E. (1996). Brain extracellular matrix. *Glycobiology, 6*(5), 489-492.

Rutten, W., Mouveroux, J. M., Buitenweg, J., Heida, C., Ruardij, T., Marani, E., et al. (2001). Neuroelectronic interfacing with cultured multielectrode arrays toward a cultured probe. *Proceedings of the IEEE, 89*(7), 1013-1029.

Rutten, W. L. C., Ruardij, T. G., & Van Pelt, J. (2003). *Neural networks on 'cultured probe' micro electrode arrays: Network confinement and activity patterns.* Paper presented at the Proceedings of the Atlantic Symposium on Computational Biology and Genome Information Systems and Technolgoy, CBGIST 2001.

Saito, A., Takayama, Y., Moriguchi, H., Kotani, K., & Jimbo, Y. (2009). *Developmental effects of low frequency magnetic fields on P19-derived neuronal cells.* Paper presented at the Proceedings of the 31st Annual International Conference of the IEEE Engineering in Medicine and Biology Society: Engineering the Future of Biomedicine, EMBC 2009.

Sakai, K., Yamamoto, A., Matsubara, K., Nakamura, S., Naruse, M., Yamagata, M., et al. (2012). Human dental pulp-derived stem cells promote locomotor recovery after complete transection of the rat spinal cord by multiple neuro-regenerative mechanisms. *J Clin Invest, 122*(1), 80-90.

Salzman, C. D., Britten, K. H., & Newsome, W. T. (1990). Cortical microstimulation influences perceptual judgements of motion direction. *Nature, 346*(6280), 174-177.

Salzman, C. D., Murasugi, C. M., Britten, K. H., & Newsome, W. T. (1992). Microstimulation in visual area MT: Effects on direction discrimination performance. *Journal of Neuroscience, 12*(6), 2331-2355.

Salzman, C. D., Murasugi, C. M., Britten, K. H., & Newsome, W. T. (1992). Microstimulation in visual area MT: effects on direction discrimination performance. *The Journal of Neuroscience, 12*(6), 2331-2355.

Sango, K., Oohira, A., Ajiki, K., Tokashiki, A., Horie, M., & Kawano, H. (2003). Phosphacan and neurocan are repulsive substrata for adhesion and neurite extension of adult rat dorsal root ganglion neurons in vitro. *Experimental Neurology, 182*(1), 1-11.

Sasaki, R., Aoki, S., Yamato, M., Uchiyama, H., Wada, K., Okano, T., et al. (2008a). Neurosphere generation from dental pulp of adult rat incisor. *Eur J Neurosci, 27*(3), 538-548.

Sasaki, R., Aoki, S., Yamato, M., Uchiyama, H., Wada, K., Okano, T., et al. (2008b). Tubulation with dental pulp cells promotes facial nerve regeneration in rats. *Tissue Eng Part A, 14*(7), 1141-1147.

Sato, Y., Nakanishi, K., Hayakawa, M., Kakizawa, H., Saito, A., Kuroda, Y., et al. (2008). Reduction of brain injury in neonatal hypoxic-ischemic rats by intracerebroventricular injection of neural stem/progenitor cells together with chondroitinase ABC. *Reproductive Sciences, 15*(6), 613-620.

Schalk, G., Miller, K. J., Anderson, N. R., Wilson, J. A., Smyth, M. D., Ojemann, J. G., et al. (2008). Two-dimensional movement control using electrocorticographic signals in humans. *Journal of Neural Engineering, 5*(1), 75-84.

Schmidt, E. M., Bak, M. J., Hambrecht, F. T., Kufta, C. V., O'Rourke, D. K., & Vallabhanath, P. (1996). Feasibility of a visual prosthesis for the blind based on intracortical microstimulation of the visual cortex. *Brain, 119*(2), 507-522.

Schouenborg, J. (2011). Biocompatible multichannel electrodes for long-term neurophysiological studies and clinical therapy-Novel concepts and design, *Progress in Brain Research* (Vol. 194, pp. 61-70).

Serruya, M. D., Hatsopoulos, N. G., Paninski, L., Fellows, M. R., & Donoghue, J. P. (2002). Instant neural control of a movement signal. *Nature, 416*(6877), 141-142.

Seymour, A. B., Andrews, E. M., Tsai, S. Y., Markus, T. M., Bollnow, M. R., Brenneman, M. M., et al. (2005). Delayed treatment with monoclonal antibody IN-1 1 week after stroke results in recovery of function and corticorubral plasticity in adult rats. *Journal of Cerebral Blood Flow and Metabolism, 25*(10), 1366-1375.

Shahaf, G., & Marom, S. (2001). Learning in networks of cortical neurons. *Journal of Neuroscience, 21*(22), 8782-8788.

Shakhnovich, A. R., Ogleznev, K., Abakumova, L., Tishchenko, L. S., & Razumovskii, A. E. (1982). Phosphene formation during electrical stimulation of the visual cortex. *Human physiology, 8*(1), 34-39.

Sharma, A., Dorman, M. F., & Kral, A. (2005). The influence of a sensitive period on central auditory development in children with unilateral and bilateral cochlear implants. *Hearing Research, 203*(1-2), 134-143.

Shields, L. B. E., Zhang, Y. P., Burke, D. A., Gray, R., & Shields, C. B. (2008). Benefit of chondroitinase ABC on sensory axon regeneration in a laceration model of spinal cord injury in the rat. *Surgical Neurology, 69*(6), 568-577.

Shimada, A., Kasai, N., Furukawa, Y., Nyberg, T., & Torimitsu, K. (2009). Neural signal transmission measurements with a conductive polymer microelectrode array. *IEEJ Transactions on Electronics, Information and Systems, 129*(2), 267-271+210.

Sicotte, M., Tsatas, O., Jeong, S. Y., Cai, C. Q., He, Z., & David, S. (2003). Immunization with myelin or recombinant Nogo-66/MAG in alum promotes axon regeneration and sprouting after corticospinal tract lesions in the spinal cord. *Molecular and Cellular Neuroscience, 23*(2), 251-263.

Silver, J., & Miller, J. H. (2004). Regeneration beyond the glial scar. *Nature Reviews Neuroscience, 5*(2), 146-156.

Simeral, J. D., Kim, S. P., Black, M. J., Donoghue, J. P., & Hochberg, L. R. (2011). Neural control of cursor trajectory and click by a human with tetraplegia 1000 days after implant of an intracortical microelectrode array. *Journal of Neural Engineering, 8*(2).

Simonen, M., Pedersen, V., Weinmann, O., Schnell, L., Buss, A., Ledermann, B., et al. (2003). Systemic deletion of the myelin-associated outgrowth inhibitor Nogo-A improves regenerative and plastic responses after spinal cord injury. *Neuron, 38*(2), 201-211.

Smith-Thomas, L. C., Stevens, J., Fok-Seang, J., Faissner, A., Rogers, J. H., & Fawcett, J. W. (1995). Increased axon regeneration in astrocytes grown in the presence of proteoglycan synthesis inhibitors. *Journal of Cell Science, 108*(3), 1307-1315.

Soleman, S., Yip, P. K., Duricki, D. A., & Moon, L. D. F. (2012). Delayed treatment with chondroitinase ABC promotes sensorimotor recovery and plasticity after stroke in aged rats. *Brain, 135*(4), 1210-1223.

Starkey, M. L., & Schwab, M. E. (2012). Anti-Nogo-A and training: Can one plus one equal three? *Experimental Neurology, 235*(1), 53-61.

Stensaas, S. S., Eddington, D. K., & Dobelle, W. H. (1974). The topography and variability of the primary visual cortex in man. *Journal of Neurosurgery, 40*(6), 747-755.

Stett, A., Egert, U., Guenther, E., Hofmann, F., Meyer, T., Nisch, W., et al. (2003). Biological application of microelectrode arrays in drug discovery and basic research. *Analytical and Bioanalytical Chemistry, 377*(3), 486-495.

Sugiyama, M., Iohara, K., Wakita, H., Hattori, H., Ueda, M., Matsushita, K., et al. (2011). Dental pulp-derived CD31(-)/CD146(-) side population stem/progenitor cells enhance recovery of focal cerebral ischemia in rats. *Tissue Eng Part A, 17*(9-10), 1303-1311.

Sun, J., Lu, Y., Cao, P., Li, X., Cai, C., Chai, X., et al. (2011). Spatiotemporal properties of multipeaked electrically evoked potentials elicited by penetrative optic nerve stimulation in rabbits. *Investigative Ophthalmology and Visual Science, 52*(1), 146-154.

Suner, S., Fellows, M. R., Vargas-Irwin, C., Nakata, G. K., & Donoghue, J. P. (2005). Reliability of signals from a chronically implanted, silicon-based electrode array in non-human primate primary motor cortex. *IEEE Transactions on Neural Systems and Rehabilitation Engineering, 13*(4), 524-541.

Szarowski, D., Andersen, M., Retterer, S., Spence, A., Isaacson, M., Craighead, H., et al. (2003). Brain responses to micro-machined silicon devices. *Brain Research, 983*(1), 23-35.

Takahashi, K., Yasuhara, T., Shingo, T., Muraoka, K., Kameda, M., Takeuchi, A., et al. (2008). Embryonic neural stem cells transplanted in middle cerebral artery occlusion model of rats demonstrated potent therapeutic effects, compared to adult neural stem cells. *Brain Research, 1234*, 172-182.

Takayama, Y., Saito, A., Moriguchi, H., Kotani, K., & Jimbo, Y. (2011). Ensemble recording of electrical activity in neurons derived from P19 embryonal carcinoma cells. *Electronics and Communications in Japan, 94*(4), 8-16.

Takeuchi, S., Ziegler, D., Yoshida, Y., Mabuchi, K., & Suzuki, T. (2005). Parylene flexible neural probes integrated with microfluidic channels. *Lab on a Chip - Miniaturisation for Chemistry and Biology, 5*(5), 519-523.

Tan, A. M., Colletti, M., Rorai, A. T., Skene, J. H. P., & Levine, J. M. (2006). Antibodies against the NG2 proteoglycan promote the regeneration of sensory axons within the dorsal columns of the spinal cord. *Journal of Neuroscience, 26*(18), 4729-4739.

Tang, F., Dent, E. W., & Kalil, K. (2003). Spontaneous calcium transients in developing cortical neurons regulate axon outgrowth. *Journal of Neuroscience, 23*(3), 927-936.

Taylor, D. M., Tillery, S. I. H., & Schwartz, A. B. (2002). Direct cortical control of 3D neuroprosthetic devices. *Science, 296*(5574), 1829-1832.

Taylor, H. R., Keeffe, J. E., Vu, H. T. V., Wang, J. J., Rochtchina, E., Pezzullo, M. L., et al. (2005). Vision loss in Australia. *Medical Journal of Australia, 182*(11), 565-568.

Tehovnik, E. J. (1996). Electrical stimulation of neural tissue to evoke behavioral responses. *Journal of Neuroscience Methods, 65*(1), 1-17.

Tetzlaff, W., Okon, E. B., Karimi-Abdolrezaee, S., Hill, C. E., Sparling, J. S., Plemel, J. R., et al. (2011). A systematic review of cellular transplantation therapies for spinal cord injury. *Journal of Neurotrauma, 28*(8), 1611-1682.

Toda, H., Takahashi, J., Iwakami, N., Kimura, T., Hoki, S., Mozumi-Kitamura, K., et al. (2001). Grafting neural stem cells improved the impaired spatial recognition in ischemic rats. *Neuroscience Letters, 316*(1), 9-12.

Todorova, M. G., Soria, B., & Quesada, I. (2008). Gap junctional intercellular communication is required to maintain embryonic stem cells in a non-differentiated and proliferative state. *Journal of Cellular Physiology, 214*(2), 354-362.

Tropea, D., Caleo, M., & Maffei, L. (2003). Synergistic effects of brain-derived neurotrophic factor and chondroitinase ABC on retinal fiber sprouting after denervation of the superior colliculus in adult rats. *Journal of Neuroscience, 23*(18), 7034-7044.

Van Pelt, J., Wolters, P. S., Corner, M. A., Rutten, W. L. C., & Ramakers, G. J. A. (2004). Long-term characterization of firing dynamics of spontaneous bursts in cultured neural networks. *IEEE Transactions on Biomedical Engineering, 51*(11), 2051-2062.

Vaney, D. I. (1991). Many diverse types of retinal neurons show tracer coupling when injected with biocytin or Neurobiotin. *Neuroscience Letters, 125*(2), 187-190.

Vavrek, R., Pearse, D. D., & Fouad, K. (2007). Neuronal populations capable of regeneration following a combined treatment in rats with spinal cord transection. *Journal of Neurotrauma, 24*(10), 1667-1673.

Velliste, M., Perel, S., Spalding, M. C., Whitford, A. S., & Schwartz, A. B. (2008). Cortical control of a prosthetic arm for self-feeding. *Nature, 453*(7198), 1098-1101.

Vorobyov, V., Kwok, J. C. F., Fawcett, J. W., & Sengpiel, F. (2013). Effects of digesting chondroitin sulfate proteoglycans on plasticity in cat primary visual cortex. *Journal of Neuroscience, 33*(1), 234-243.

Wang, D., & Fawcett, J. (2012). The perineuronal net and the control of CNS plasticity. *Cell and Tissue Research, 349*(1), 147-160.

Wang, H., Katagiri, Y., McCann, T. E., Unsworth, E., Goldsmith, P., Yu, Z.-X., et al. (2008). Chondroitin-4-sulfation negatively regulates axonal guidance and growth. *Journal of Cell Science, 121*(18), 3083-3091.

Wang, J., Wang, X., Sun, Z., Yang, H., Shi, S., & Wang, S. (2010). Stem cells from human-exfoliated deciduous teeth can differentiate into dopaminergic neuron-like cells. *Stem Cells Dev, 19*(9), 1375-1383.

Wang, W., Collinger, J. L., Degenhart, A. D., Tyler-Kabara, E. C., Schwartz, A. B., Moran, D. W., et al. (2013). An Electrocorticographic Brain Interface in an Individual with Tetraplegia. *PLoS One, 8*(2).

Ward, M. P., Rajdev, P., Ellison, C., & Irazoqui, P. P. (2009). Toward a comparison of microelectrodes for acute and chronic recordings. *Brain Research, 1282*, 183-200.

Webb, S. E., & Miller, A. L. (2003). Calcium signalling during embryonic development. *Nat Rev Mol Cell Biol, 4*(7), 539-551.

Weber, P., Bartsch, U., Rasband, M. N., Czaniera, R., Lang, Y., Bluethmann, H., et al. (1999). Mice deficient for tenascin-R display alterations of the extracellular matrix and decreased axonal conduction velocities in the CNS. *Journal of Neuroscience, 19*(11), 4245-4262.

Wells, J. E. A., Rice, T. K., Nuttall, R. K., Edwards, D. R., Zekki, H., Rivest, S., et al. (2003). An Adverse Role for Matrix Metalloproteinase 12 after Spinal Cord Injury in Mice. *Journal of Neuroscience, 23*(31), 10107-10115.

White, B. W., Saunders, F. A., Scadden, L., Bach-Y-Rita, P., & Collins, C. C. (1970). Seeing with the skin. *Perception & Psychophysics, 7*(1), 23-27.

Whitten, P. G., Gestos, A. A., Spinks, G. M., Gilmore, K. J., & Wallace, G. G. (2007). Free standing carbon nanotube composite bio-electrodes. *Journal of Biomedical Materials Research - Part B Applied Biomaterials, 82*(1), 37-43.

Widera, D., Grimm, W. D., Moebius, J. M., Mikenberg, I., Piechaczek, C., Gassmann, G., et al. (2007). Highly efficient neural differentiation of human somatic stem cells, isolated by minimally invasive periodontal surgery. *Stem Cells Dev, 16*(3), 447-460.

Wilson, B. S., & Dorman, M. F. (2008). Cochlear implants: Current designs and future possibilities. *Journal of Rehabilitation Research and Development, 45*(5), 695-730.

Wyndaele, M., & Wyndaele, J. J. (2006). Incidence, prevalence and epidemiology of spinal cord injury: What learns a worldwide literature survey? *Spinal Cord, 44*(9), 523-529.

Yamada, H., Fredette, B., Shitara, K., Hagihara, K., Miura, R., Ranscht, B., et al. (1997). The brain chondroitin sulfate proteoglycan brevican associates with astrocytes ensheathing cerebellar glomeruli and inhibits neurite outgrowth from granule neurons. *Journal of Neuroscience, 17*(20), 7784-7795.

Yamaguchi, Y. (2000). Lecticans: Organizers of the brain extracellular matrix. *Cellular and Molecular Life Sciences, 57*(2), 276-289.

Yi, J. H., Katagiri, Y., Susarla, B., Figge, D., Symes, A. J., & Geller, H. M. (2012). Alterations in sulfated chondroitin glycosaminoglycans following controlled cortical impact injury in mice. *Journal of Comparative Neurology, 520*(15), 3295-3313.

Yick, L. W., Cheung, P. T., So, K. F., & Wu, W. (2003). Axonal regeneration of Clarke's neurons beyond the spinal cord injury scar after treatment with chondroitinase ABC. *Experimental Neurology, 182*(1), 160-168.

Ying, Q. L., Stavridis, M., Griffiths, D., Li, M., & Smith, A. (2003). Conversion of embryonic stem cells into neuroectodermal precursors in adherent monoculture. *Nature Biotechnology, 21*(2), 183-186.

Zhang, Y., Dijkhuizen, P. A., Anderson, P. N., Lieberman, A. R., & Verhaagen, J. (1998). NT-3 delivered by an adenoviral vector induces injured dorsal root axons to regenerate into the spinal cord of adult rats. *Journal of Neuroscience Research, 54*(4), 554-562.

Zhang, Y., Klassen, H. J., Tucker, B. A., Perez, M. T. R., & Young, M. J. (2007). CNS progenitor cells promote a permissive environment for neurite outgrowth via a matrix metalloproteinase-2-dependent mechanism. *Journal of Neuroscience, 27*(17), 4499-4506.

Zhang, Z. G., Jiang, Q., Zhang, R., Zhang, L., Wang, L., Arniego, P., et al. (2003). Magnetic resonance imaging and neurosphere therapy of stroke in rat. *Annals of Neurology, 53*(2), 259-263.

Zheng, B., Ho, C., Li, S., Keirstead, H., Steward, O., & Tessier-Lavigne, M. (2003). Lack of enhanced spinal regeneration in Nogo-deficient mice. *Neuron, 38*(2), 213-224.

Zheng, B., Lee, J. K., & Xie, F. (2006). Genetic mouse models for studying inhibitors of spinal axon regeneration. *Trends in Neurosciences, 29*(11), 640-646.

Zhong, Y., & Bellamkonda, R. V. (2007). Dexamethasone-coated neural probes elicit attenuated inflammatory response and neuronal loss compared to uncoated neural probes. *Brain Research, 1148*(1), 15-27.

Zhou, D. M., & Greenberg, R. J. (2003). *Electrochemical Characterization of Titanium Nitride Microelectrode Arrays for Charge-Injection Applications.* Paper presented at the Annual International Conference of the IEEE Engineering in Medicine and Biology - Proceedings.

Zhuang, J., Truccolo, W., Vargas-Irwin, C., & Donoghue, J. P. (2010). Decoding 3-D reach and grasp kinematics from high-frequency local field potentials in primate primary motor cortex. *IEEE Transactions on Biomedical Engineering, 57*(7), 1774-1784.

Zimmermann, D. R., & Dours-Zimmermann, M. T. (2008). Extracellular matrix of the central nervous system: From neglect to challenge. *Histochemistry and Cell Biology, 130*(4), 635-653.